Reversible Activation Dynamics of Tethered Ruthenium(II) Arene Complexes

Memoria para optar al grado de Doctor en Química Aplicada por la Universidad Autónoma de Madrid, presentada por:

Francisco Martínez Peña

Director

Ana M. Pizarro

Madrid, 2018

Agradecimientos

Welcome on board. Con esta frase me daba la bienvenida la que sería mi directora de tesis, iniciando así una de las etapas más importantes de mi vida. Tras años intentando conseguir una tesis doctoral relacionada con el diseño de fármacos, finalmente lo conseguía de la mano de la Dra. Ana M. Pizarro, quien había estado trabajando más de diez años bajo las directrices del Profesor P. J. Sadler. Comenzaban de esta forma unos duros e intensos años de trabajo, a la vez que felices, ya que no todo el mundo tiene la oportunidad de trabajar en algo que le encanta y considera un hobbie. Al contrario de lo esperado, el hecho de ser el primer miembro del grupo de investigación liderado por mi directora, así como tener que poner a punto un laboratorio desde cero, no fue tan duro gracias a todas aquellas personas que desde el punto de vista más altruista han estado dispuestas a ayudarme y tener un buen gesto siempre que lo he necesitado. Con ellas, está tesis a podido ser desarrollada y quiero plasmar aquí mi más sincero agradecimiento. Gracias.

En primer lugar quería agradecer a mi directora de tesis, Ana M. Pizarro, la confianza que puso en mí para desarrollar este proyecto. No tuvo que ser fácil tener la ardua tarea de iniciar un grupo de investigación. Cuantas horas habremos pasado hablando de ciencia, intentado que este proyecto naciera, creciera y se desarrollara de la mejor forma posible. He aprendido muchas cosas a tu lado, tanto científicas como personales. Y desde luego, todas las habilidades que he adquirido durante mi doctorado han sido gracias a ti. No podría haber dado con una mejor mentora. Te agradezco enormemente todo el tiempo que hemos compartido durante estos años, siempre lo recordaré. Te echaré mucho de menos.

Acknowledgements

Sin duda quiero agradecer a Sofi y Tere todos los momentos que hemos vivido juntos en el laboratorio. A pesar de pertenecer a grupos diferentes y llevar líneas de investigación totalmente distintas, siempre nos esforzamos por ayudarnos y entender la química del otro. Será difícil encontrar un lugar con tantas risas y divertidos momentos que amenizaban días interminables esperando obtener el compuesto deseado. Muchas gracias chicas, sin vosotras nada hubiera sido igual.

También quiero dar las gracias a mis recientes compañeras de equipo, Sonia y Ana C., y sobre todo a Abraha, con el que me hubiera encantado coincidir más tiempo, ya que es una persona que desprende gran humanidad y profesionalidad. Agradecer a Vanessa su ayuda en cultivos celulares, y a Adriana por los tan buenos momentos que pasamos en el laboratorio. Agradecer a Mark Davies todos sus consejos sobre química. A Luca Salassa y José Sánchez Costa quiero agradecerles la ayuda que me ofrecieron para enseñarme nuevas líneas de investigación que podrían ser empleadas en este proyecto, sin la cual no hubiera sido posible la realización una parte de esta tesis. Además quiero dar mi agradecimiento a Josefina y Mario porque siempre han estado dispuestos a ayudarme sobre cualquier duda cristalográfica siempre que lo he necesitado.

Como no, a mi amiga Zulay. Muchísimas gracias por ser como eres. Siempre da gusto bajar a resonancia y ver tu sonrisa. No olvidaré lo bien que lo pasábamos mientras cogíamos el lock y de aquellas semanas aprendiendo a patinar. Eres una trabajadora nata y te mereces lo mejor. Sabes que te quiero mucho. A Estefania, por ser tan divertida. Echaré de menos nuestras conversaciones para coger el autobús. A Sara y Warren por tener siempre una sonrisa y transmitir tanta dulzura y paz. Por supuesto, quiero agradecer al personal de administración su ayuda y eficiencia, especialmente a Paloma y Juani. Gracias por haberme dado tan buenos momentos y haberme animado siempre que lo he necesitado. Por todos vuestros besos y abrazos. Por estar ahí. Sin duda, sois muy

especiales para mí. También a Merci, Melania y Vicente, del personal de limpieza. Muchas gracias por apoyarme siempre y por todos los gestos de cariño que me habéis dado.

Un agradecimiento especial quiero dedicárselo a ese grupo de doctorandos que me acogieron cuando llegué a IMDEA. Sara, Patri B., Fer, Elisa y un largo número de personas que ha ido aumentando con el paso de los años. Pero sin duda, los más importantes, aquellos que se convirtieron en mis mejores amigos, Felipe, Irene y Paula. Con ellos he compartido alegrías y penas, es decir, la vida. Sois los mejores. No tengo suficientes palabras para agradeceros todo lo que hemos vivido juntos. Os quiero muchísimo. Muchas gracias por ayudarme, apoyarme y darme fuerzas en todos esos momentos difíciles.

Gracias a mis amigos del CSIC, especialmente a Paula. Pronto volveré a verte. Eres una persona extraordinaria que ama su trabajo y a los demás. A Teresa Quirós, Gonzalo y Carlos, mis amigos de la Complutense. A Maritoñi, por no enfadarse siempre que quedábamos y llegaba tarde por tener que terminar algo en el laboratorio.

También quiero dar las gracias a una gran docente que conocí en Ciudad Real mientras cursaba mi licenciatura, Pilar Prieto. Gracias a ella mi pasión por la química creció todavía más. He conocido muy pocas personas con tal calidad humana, aquí me tienes para siempre. No sólo me inculcaste los principios de las reacciones químicas y la nomenclatura por aquel entonces, sino que me mostraste la integridad moral que cada individuo debe tener. Te quiero mucho.

Gracias a Teresa B., por ti soy quien soy. Me has enseñado que la vida consiste en sentir, a veces cosas buenas y otras no tan buenas, y que la felicidad se encuentra donde

el miedo no llega. Nunca podré agradecerte todo lo que me has ayudado para ser mejor persona y afrontar las adversidades, sin duda siempre te llevaré en mi corazón.

Finalmente quiero agradecer a mi familia todo su cariño. A mi hermana y Juanmi muchas gracias por arroparme cuando voy a Albacete y hacerme sentir el chico más feliz del mundo. Como no, a mis perras, con las que tan buenos ratos paso y me hacen desconectar de cualquier problema. A mi microbiólogo favorito, Edu. Muchas gracias por estar a mi lado. Te agradezco enormemente tu paciencia, apoyo y dedicación todo este tiempo. Gracias a ti la vida siempre se ve desde una perspectiva mucho más bonita. Estos últimos meses tan agitados se han hecho totalmente llevaderos gracias a ti. Me siento privilegiado de estar contigo. Te quiero.

Y a mis padres. Muchísimas gracias por todo lo que me habéis dado, no tengo palabras para agradecéroslo. Siempre que os he necesitado os he encontrado. Muchas gracias por compartir conmigo la dureza del camino, por vuestras palabras y gestos de ánimo en los momentos difíciles. Me siento afortunado de teneros a mi lado. Os quiero muchísimo.

Abstract

Cancer is one of the major causes of death worldwide. There are many types of chemotherapeutic drugs and cisplatin, the first metal-based anticancer agent, is one of the most widely used. Its success to treat several tumours has triggered the investigation of other metal-based agents with cytotoxic activity in cancer research. Ruthenium organometallic complexes have been in the last decade one of the most promising findings due to their inherent anticancer activity and to the possibility of presenting a different cytotoxic profile than that of platinum-based drugs. In fact, some Ru^{III} complexes are currently undergoing clinical trials.

A new family of ruthenium(II) arene compounds of general formula $[Ru(\eta^6{:}\kappa^1\text{-arene:Z})(XY)]^{n+}$, where arene:Z is a hemilabile tethering ligand and XY is a chelating bidentate ligand has recently been reported. The donor group Z offers two reversible functionalities: (i) binding to the Ru^{II} centre to form a closed tether-ring complex (inactive form), or (ii) dissociation from the Ru^{II} centre (as a pendant arm) to afford an open-tether complex (active species). This type of complexes can be useful tools to target selectively the acidic microenvironment of the tumour, exploiting the metabolism of the cancer cell. It is known that cancer metabolism is characterized by the preference, even in the presence of oxygen, for 'aerobic' glycolysis, a phenomenon known as the Warburg effect. As a result, accumulation of lactate influences the acidity of the extracellular pH (values as low as 6.2 vs 7.3 in normal cells). This difference can be advantageous in the design of (pro-)drugs that activate selectively at low pH.

In this context we propose to explore tethered ruthenium(II) arene complexes, of general formula $[Ru(\eta^6{:}\kappa^1\text{-arene:Z})(XY)]^{n+}$, as promising scaffolds to afford reversible pH-dependent activatable metallodrugs. This dissertation focuses in the structural modifications of the building blocks that constitute the ruthenium(II) tether complexes

by varying (i) the hemilabile ligand (arene:Z), and (ii) the chelating ligand (XY), in order to finely tune the Ru–Z bond activation.

Following an introduction to the field of metals in medicine in Chapter 1, Chapter 2 compiles the structure-activation relationship study of ruthenium(II) tether complexes that helped us understand how the tether arm influences the ring-opening process. This provides valuable information about how both length and rigidity of the tethering arm, and nature of the donor atom, are important features that play a crucial role in the activation of the Ru–Z bond to afford the open-tether (activated) species. Compounds bearing 2-aminobiphenyl and phenylacetic acid as hemilabile ligand were chosen as promising activatable platforms for further investigation.

In Chapter 3, we investigated in depth the scaffold $[Ru\{\eta^6{:}\kappa^1\text{-}C_6H_5(C_6H_4)NH_2\}(XY)]^{n+}$ (2-aminobiphenyl as hemilabile arene:Z ligand) bearing different chelating XY ligands. Understanding the dynamics that control the opening of these tether complexes is crucial for rationally designing pro-drugs with controlled activation profiles prior attack of the bond to biological target attack. For this reason, the activation of the ruthenium–nitrogen bond was explored in non-aqueous (dimethylsulfoxide and methanol) and aqueous solvents. Importantly, these complexes were able to afford open species at different pH values in water. Since the open species, $[Ru\{\eta^6\text{-}C_6H_5(C_6H_4)NH_3\}(XY)Cl]^{n+}$, can undergo protonation of the pendant NH_2 rendering the nitrogen unable to coordinate to the Ru^{II}, we studied the reversible protonation and deprotonation phenomena for this type of compounds to better understand the compounds' aqueous dynamics. Also, we investigated the interaction of our switchable system with a model nucleobase.

In Chapter 4, we explored complexes with formula $[Ru(\eta^6\text{-}C_6H_5CH_2COOH)(XY)Cl]^{n+}$, bearing phenylacetic acid as hemilabile ligand. A detailed

study about the speciation in aqueous solution of a series of complexes bearing different XY ligands is described. We also investigated the ring-opening reaction for their analogue closed-tether complexes to prove that κ^1O-dissociation from the ruthenium(II) centre can be tailored under acidic conditions by a reversible pH-mediated activation process. Finally, we explored the capability of these complexes to undergo intracellular hydrogen-transfer reactions.

In Chapter 5, we studied how the tether chelate affects stability and activation of this type of ruthenium(II) arene complexes. In order to do this, we compared the reactivity of the Ru–Z bond in closed-tether versus their un-tether counterparts. In addition, we investigated the possibility of triggering the Ru–Z bond activation of closed-tether complexes at neutral pH upon photo-irradiation. DFT calculations were carried out to support the experimental results.

Finally, in Chapter 6, we studied the possibility to activate the Ru–Z bond in the closed-tether complexes via a solid-state reaction in the presence of vaporous reactants to investigate their potential development as gas sensors. The reversibility of the system was further investigated by different solid state techniques, showing the great versatility that these complexes can offer in the organometallic field.

Resumen

El cáncer es una de las enfermedades que más muertes producen en todo el mundo. Hay muchos tipos de fármacos antitumorales y el cisplatino, el primer fármaco antitumoral basado en un metal de transición, es uno de los más empleados. Su éxito para combatir diferentes tipos de cáncer ha motivado la investigación de otros compuestos metálicos con actividad citotóxica. Los complejos organometálicos de rutenio han despertado un incipiente interés en los últimos años debido a sus propiedades antitumorales y la posibilidad de presentar un diferente mecanismo de acción al de los fármacos basados en platino. De hecho, algunos complejos de Ru^{III} se encuentran bajo ensayos en fase clínica.

Recientemente, se ha publicado una nueva familia de compuestos de rutenio(II) con fórmula general $[Ru(\eta^6{:}\kappa^1\text{-areno:Z})(XY)]^{n+}$, donde areno:Z es un ligando hemilábil y XY es un ligando bidentado. El grupo dador Z ofrece dos funcionalidades reversibles: (i) coordinación al centro de Ru^{II} para formar un complejo cerrado (forma inactiva), o (ii) disociación del centro metálico (como brazo colgante) para generar el correspondiente complejo abierto (forma activa). Este tipo de complejos puede servir como valiosas herramientas para atacar selectivamente el microambiente tumoral, explotando el metabolismo de la célula cancerígena. Se sabe que el metabolismo del cáncer tiene preferencia por la glicolisis 'aerobia', incluso en presencia de oxígeno, fenómeno denominado Efecto Warburg. Como resultado, la acumulación de lactato influye en la acidez del pH extracelular (con valores de 6.2 vs 7.3 en células normales). Esta diferencia puede suponer una ventaja en el diseño de (pro-)fármacos que se activen selectivamente a pH bajo.

En este contexto, nosotros proponemos explorar complejos areno de rutenio(II) 'tethered', de fórmula $[Ru(\eta^6{:}\kappa^1\text{-areno:Z})(XY)]^{n+}$, como prometedoras estructuras para

dar lugar a metalofármacos activables dependientes del pH. Esta Tesis se enfoca en las modificaciones estructurales de los grupos que conforman los complejos 'tethered' mediante la variación de (i) el ligando hemilábil (areno:Z), y (ii) el ligando quelato bidentado (XY), para poder controlar de manera precisa la activación del enlace Ru–Z.

Después de una introducción al área de los metales empleados en medicina en el Capítulo 1, el Capítulo 2 recoge los estudios de relación estructura-activación de complejos de rutenio(II) 'tethered' lo que nos han ayudado a entender cómo el brazo colgante del ligando hemilábil afecta al proceso de apertura. Esto proporciona valiosa información sobre cómo la longitud y rigidez del brazo, así como la naturaleza del átomo dador, son importantes características que juegan un papel crucial en la activación del enlace Ru–Z para generar el complejo abierto (activado). Los compuestos con ligando hemilábil 2-aminobifenilo y ácido fenilacético fueron seleccionados como prometedoras estructuras para una investigación más exhaustiva.

En el Capítulo 3 investigamos en profundidad la estructura $[Ru\{\eta^6:\kappa^1\text{-}C_6H_5(C_6H_4)NH_2\}(XY)]^{n+}$ (donde 2-aminobifenilo es el ligando hemilábil) con distintos ligandos quelatos XY. Entender la dinámica que gobierna la apertura de estos complejos es crucial para el diseño racional de pro-fármacos con perfiles de activación controlada previa a la interacción con la diana terapéutica. Por esta razón, se exploró la activación del enlace Ru–N en disolventes no acuosos (dimetilsulfóxido y metanol) y en disolventes acuosos. El hallazgo más importante fue que estos complejos fueron capaces de producir especies abiertas a diferentes valores de pH en agua. Ya que estas especies abiertas, $[Ru\{\eta^6\text{-}C_6H_5(C_6H_4)NH_3\}(XY)Cl]^{n+}$, pueden dar lugar a la protonación del grupo NH_2 colgante imposibilitando así que el nitrógeno vuelva a coordinarse al centro de Ru^{II}, estudiamos el fenómeno de protonación y desprotonación para este tipo de complejos y de este modo entender mejor la dinámica acuosa de los compuestos.

Además, también investigamos la interacción de estos sistemas con una nucleobase modelo.

En el Capítulo 4 exploramos los complejos con fórmula $[Ru(\eta^6\text{-}C_6H_5CH_2COOH)(XY)Cl]^{n+}$, que contienen ácido fenilacético como ligando hemilábil, y se realizó un estudio detallado sobre la especiación en disolución acuosa de una serie de compuestos que contenían diferentes ligandos XY. También investigamos la reacción de apertura para sus correspondientes complejos cerrados con el objetivo de demostrar que la disociación κ^1O del centro de rutenio(II) puede ser modulada mediante un proceso de activación mediado por el pH. Finalmente, exploramos la capacidad de estos complejos para llevar a cabo reacciones de transferencia de hidrógeno y su posible repercusión dentro de la célula.

En el Capítulo 5 estudiamos como el quelato 'tether' afecta a la estabilidad y la activación de este tipo de complejos areno de rutenio(II). Para ello, comparamos la reactividad del enlace Ru–Z en complejos 'tethered' y sus análogos sin el brazo colgante ('un-tethered'). Además, investigamos la posibilidad de activar el enlace Ru–Z de los compuestos cerrados bajo foto-irradiación a pH neutro. Cálculos DFT fueron realizados para apoyar los resultados experimentales.

Finalmente, en el Capítulo 6 estudiamos la posibilidad de activar el enlace Ru–Z de los complejos cerrados mediante una reacción en estado sólido en presencia de reactivos en fase vapor para investigar su uso potencial como detectores de gases. La reversibilidad del sistema fue explorada a través de técnicas de estado sólido, mostrando la gran versatilidad que estos complejos pueden ofrecer en el campo de la química organometálica.

Notes to the Reader

Structure of the Thesis

Although the chapters of this book could be read independently of one another, they are arranged in a rational sequence of six Chapters. The first Chapter, Introduction, covers the state-of-the-art regarding ruthenium metallodrugs, as well as elementary principles and basic organometallic chemistry related to this dissertation. Chapter 2 deals with a structure-activation relationship study in order to find a suitable scaffold to undergo reversible activation of the Ru–Z bond in ruthenium(II) tether complexes. Chapters 3 and 4 present solution studies on the switchability of two particular systems. Chapters 5 and 6 provide preliminary yet exciting results on using this type of compounds in both photo-irradiation experiments and solid-state reactions, respectively.

Nomenclature for Complexes

The method used for naming the complexes has followed the recommendations by the International Union of Pure and Applied Chemistry (IUPAC) published in Nomenclature of Inorganic Chemistry 2005.

Numbering of Complexes

The numbering of the complexes in this dissertation, all of which are typed in boldface throughout the entire manuscript adhere to the following rules. Generally, complexes synthesised in their closed-tether form, where the donor atom of the pendant arm is coordinated to the ruthenium centre, will be coded with a number, for example, **1**. Complexes synthesised in their open form, with a chlorido ligand coordinated to the ruthenium centre and therefore with the pendant arm dissociated from the metallic centre, will be coded with a number followed by Cl, as in **1Cl**. If the complex is an open

tether but instead of a chlorido ligand bears a dmso molecule, it will be named as the number followed by dmso, this is, **1dmso**. For open-tether chlorido complexes where the pendant arm is in its corresponding protonated form, they will be denoted as the number followed by HCl, as in **1HCl**.

Regarding the counterions of the cationic complexes, unless otherwise indicated, chlorides will be the counterions in the solid state (or sodium for negatively charged complexes), for example, closed tether complex **1**. However, if the complex was not isolated as the chloride salt and a different anion was used to isolate the complex in the solid state, such ion accompanies the number of the complex followed by an interpunct, it will be coded for example, **1·PF_6**.

Abbreviations

Throughout this dissertation the standard abbreviations and acronyms recommended by American Chemical Society for Medicinal Chemistry field, as reviewed in Journal of Medicinal Chemistry on January 2018 (http://pubs.acs.org/paragonplus/submission/jmcmar/jmcmar_authguide.pdf) have been employed. Abbreviations and acronyms which are not present in that Journal are conveniently indicated over the reading.

List of Publications

The present doctoral project has produced the following original publications:

Martínez-Peña, F.; Pizarro, A. M. Control of reversible activation dynamics of $[Ru(\eta^6{:}\kappa^1\text{-}C_6H_5(C_6H_4)NH_2)(XY)]^{n+}$ and the effect of chelate ligand variation. *Chemistry- A European Journal* 2017, *23*, 16231-16241.

Martínez-Peña, F.; Pizarro, A. M. Reversible pH-responsive Behaviour of Ruthenium(II) Arene Complexes with Tethered Carboxylate. *Submmited*

Martínez-Peña, F.; Salassa, L.; Pizarro, A. M. Contrasting activation behaviour of tethered versus un-tethered Ruthenium(II) arene complexes by pH and light irradiation. *Under preparation*

Martínez-Peña, F.; Sanchez Costa J.; Pizarro, A. M. Vapour-Induced Crystalline State Reversible Reactions of Ruthenium(II) Complexes Containing Hemilabile Tethered-Arene Ligands. *Under preparation*

Table of Contents

Chapter 1. Introduction.

Chapter 2. Synthesis, Structure, Characterization and Activation of Tethered Complexes. A SAR Study.

Chapter 4. Reversible pH-responsive Behaviour of Ruthenium(II) Arene Complexes with Tethered Carboxylate.

Chapter 5. Contrasting activation behaviour of tethered versus un-tethered Ru^{II} arene complexes by pH and light irradiation.

Chapter 6. Vapour-Induced Crystalline State Reversible Reactions of Ruthenium(II) Complexes Containing Hemilabile Tethered-Arene Ligands.

1.

Introduction

1.1 Metals in Medicine

Metal ions play important roles in biological processes. In humans, disorders of the metabolism of essential metal ions can have detrimental effects; well-known examples include anaemia caused by low iron levels, growth retardation arising from insufficient dietary zinc, and progressive neurological disorders owing to copper overload.[1]

The use of metals traces dates back to the ancient civilizations of Mesopotamia, Egypt, India, and China, where elements such as arsenic, gold, and iron were used in pharmaceutical potions.[2] One of the first therapeutic metallodrugs was Salvarsan, an arsenic-based antimicrobial agent marketed in 1910. With the addition of mercury and bismuth, Salvarsan remained the standard remedy for syphilis until it was replaced by penicillin after World War II.[3] More recent examples of metals in medicine include the use of platinum drugs like cisplatin (which is now widely used in cancer treatment), lithium salts for neurological disorders, gold drugs for treating rheumatoid arthritis, and vanadium compounds with antidiabetic effects.[2]

All of these examples provide evidence of the potential of metal-based drugs in modern medicine. A key concept is the possibility of structurally tuning the metallodrugs to modulate their properties. The structure can be altered by changing the ligands that surround the metal, or by changing the coordination number/oxidation state of the metal. In this way, we can begin to overcome the toxicity, and control the reactivity and selectivity of the metal complex towards specific targets and diseases.[4]

1.2 Metal-based Anticancer Drugs

Cancer is a major cause of mortality, with 14.1 million new cases and 8.2 million cancer-related deaths in 2012, affecting populations in all countries and all regions. The five most common types of diagnosed cancers are lung, breast, colorectum, prostate, and stomach (Figure 1.1); together, cancers of these five sites constitute half of the overall global cancer problem.[5]

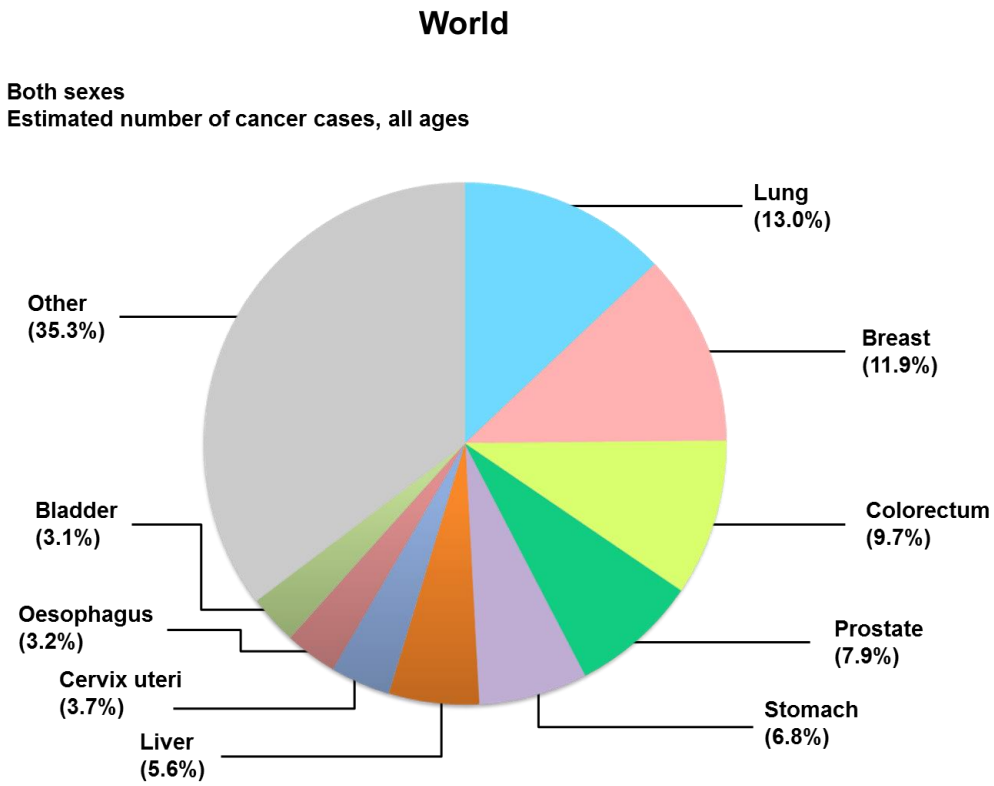

Figure 1.1. Estimated world cancer incidence proportions, in both sexes combined, in 2012. Adapted from ref 5.

Cancer chemotherapy continues to play an increasingly important role in the management of malignancies, either directly or as an adjuvant to surgery and/or radiotherapy. Certain transition metal compounds have been demonstrated to effectively act as anticancer agents. In particular, the inorganic complex cisplatin, *cis*-$[Pt(NH_3)_2Cl_2]$, is currently one of the most widely used chemotherapeutic drug, being active in the treatment of many cancers.[6]

The discovery of cisplatin by Barnett Rosenberg in the 1960s was a milestone in the history of metal-based compounds used in the treatment of cancer. To date, cisplatin and its analogues (Figure 1.2) are some of the most effective chemotherapeutic agents in clinical use, often as the first line of treatment in testicular and ovarian cancers.[7]

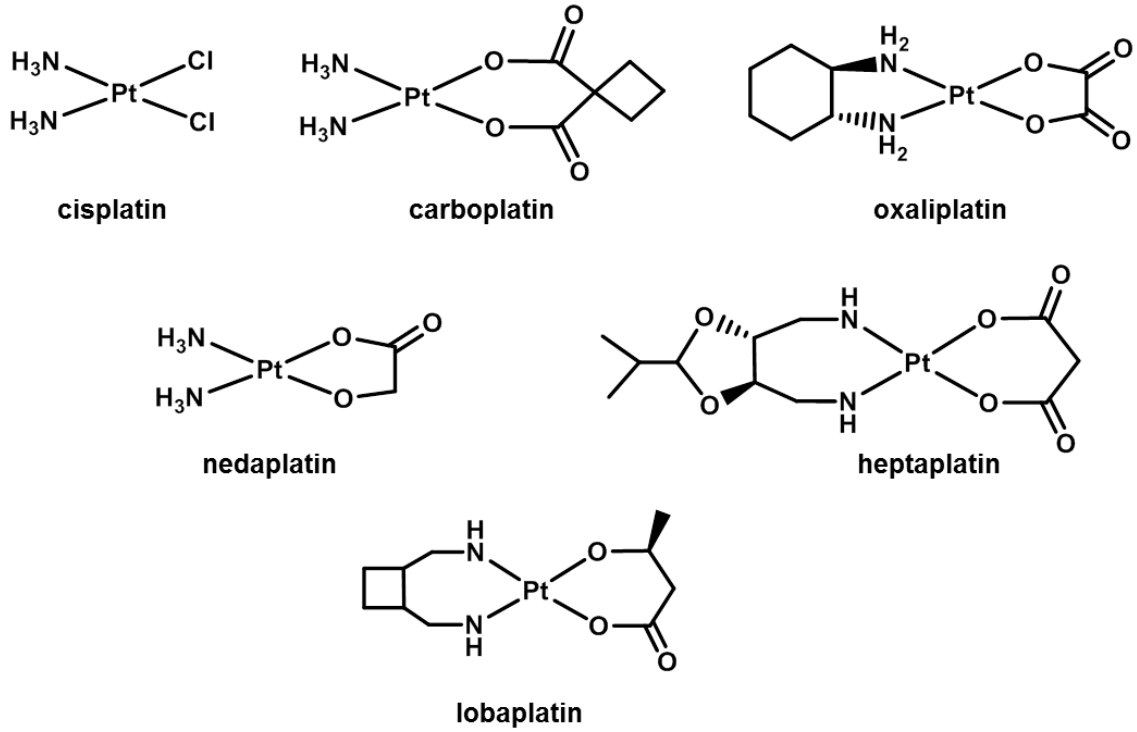

Figure 1.2. Chemical structures of clinically used platinum anticancer drugs.

Investigations into the activity of cisplatin at the biomolecular level indicate that genomic DNA is the primary target.[8] The activity of this drug and of its derivatives is mediated by the formation of DNA lesions that interfere with transcription, resulting in cellular apoptosis.[9] The binding of cisplatin to the DNA is dependent on the hydrolysis (substitution of a leaving group by a water molecule) of its labile chlorido ligands. In the bloodstream, high chloride ion concentration (100 mM) suppresses this process,[10] however once inside the cell, the lower chloride ion concentration (cytosol, 25 mM; nucleus, 4 mM) assists hydrolysis. This gives rise to the formation of the complex $[Pt(NH_3)_2Cl(H_2O)]^+$. The most nucleophilic and accessible site of DNA is the N7 atom

of guanine residues, and these are preferentially platinated.[11] The remaining chloride ligand is substituted for a second water molecule and platinum interacts with an adjacent guanine base, forming a cross-link on the DNA.[12] This chelation of nuclear DNA triggers a specific distortion of the duplex,[13] recognised by the so called High-Mobility Group (HMG) proteins which are believed to strongly bind to platinated DNA,[9, 14] and other some damage-recognition proteins.[15] Finally, the cell undergoes apoptosis following unsuccessful DNA repair (Figure 1.3).[16]

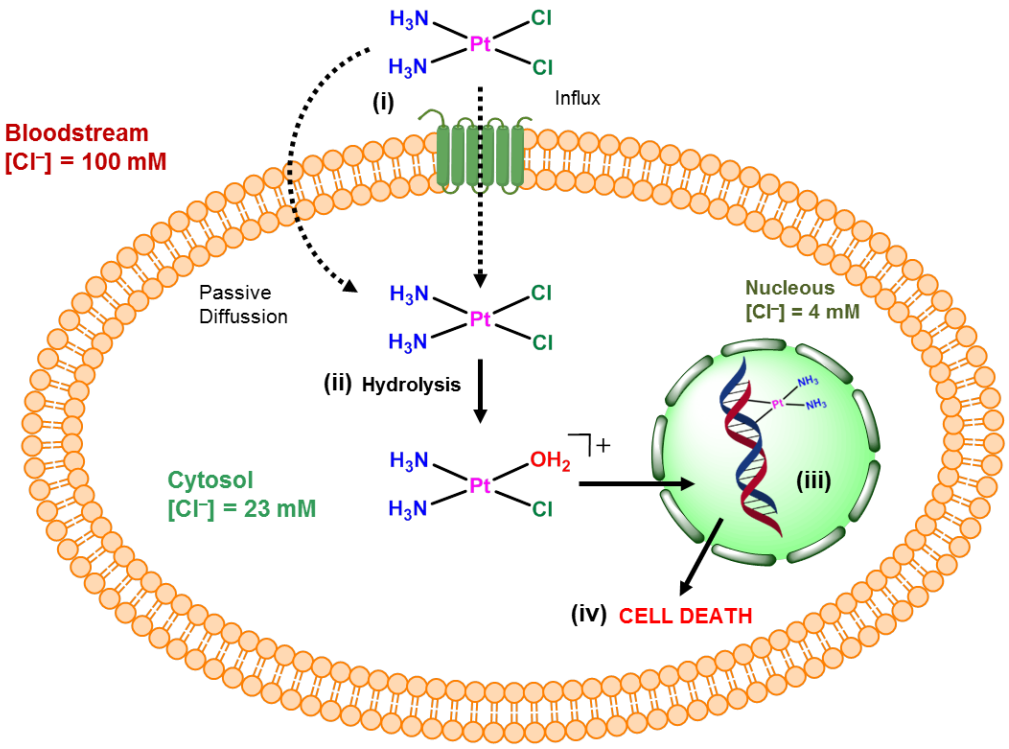

Figure 1.3. The general mechanism of action of cisplatin involves four key steps: (i) cellular uptake, (ii) aquation/activation, (iii) DNA binding, and (iv) cellular processing of DNA lesions leading to cell death.

Regardless of the achievements of current platinum drugs, there are some major drawbacks: they are efficient only for a limited range of cancers and additionally some tumours initially sensitive to cisplatin acquire resistance. Moreover, they often cause severe side-effects, such as nausea, bone marrow suppression and kidney toxicity.[17, 18] One of the goals in the field of anticancer metallodrugs is the development of non-platinum metal anticancer drugs that present activity against tumours that are resistant to

platinum drugs. A secondary goal is that activity should not be accompanied by severe toxicity, that is, that the compounds have a good tolerability and a large therapeutic window.[19] Complexes of transition metals other than platinum may, in principle, exhibit anticancer activity and toxic side-effects significantly different from that of platinum drugs for a number reasons: they are expected to have different chemical behaviour, hydrolysis rates, and mechanism of action.

Compounds of almost all metals of the periodic table have been explored for in vitro cytotoxic activity against cancer cell lines, the most widely used screening.[20] Ruthenium stands out as a particularly attractive alternative to platinum, and occupies a prevalent position among the several metal complexes that have been investigated for anticancer activity.

Jakupec et al.[21] have described the benefits of advantages of exploiting ruthenium in the development of metal-based antitumour drugs: (i) a rich and well-developed preparative coordination chemistry of this transition metal, providing consistent routes to new complexes; (ii) a rate of ligands exchange often comparable to that of platinum or which can be tuned by coordination of appropriate ligands; (iii) octahedral coordination geometry in contrast to the square planar geometry of platinum(II) complexes, implying a reactivity different from cisplatin; (iv) accessibility of oxidation states 2+, 3+, and 4+ under physiological condition; (v) the ability to tune the electron transfer rates and redox potentials; and (vi) the capability of ruthenium to mimic iron in binding to biomolecules such as albumin and transferrin, which makes ruthenium-based agents markedly less toxic than platinum drugs.

These favourable properties have led to two ruthenium compounds that are currently undergoing clinical trials – the anti-primary-tumour imidazolium *trans*-[tetrachloridobis(1*H*-indazole)ruthenate^{III}] (KP1019) and the anti-metastasis

imidazolium *trans*-[tetrachloride(1*H*-imidazole)(S-dimethylsulfoxide)ruthenate^{III}] (NAMI-A) –, opening new perspectives in cancer treatment (Figure 1.4). The most recent representative of this class of compounds is NKP-1339, the corresponding more water soluble sodium salt of KP1019.[22]

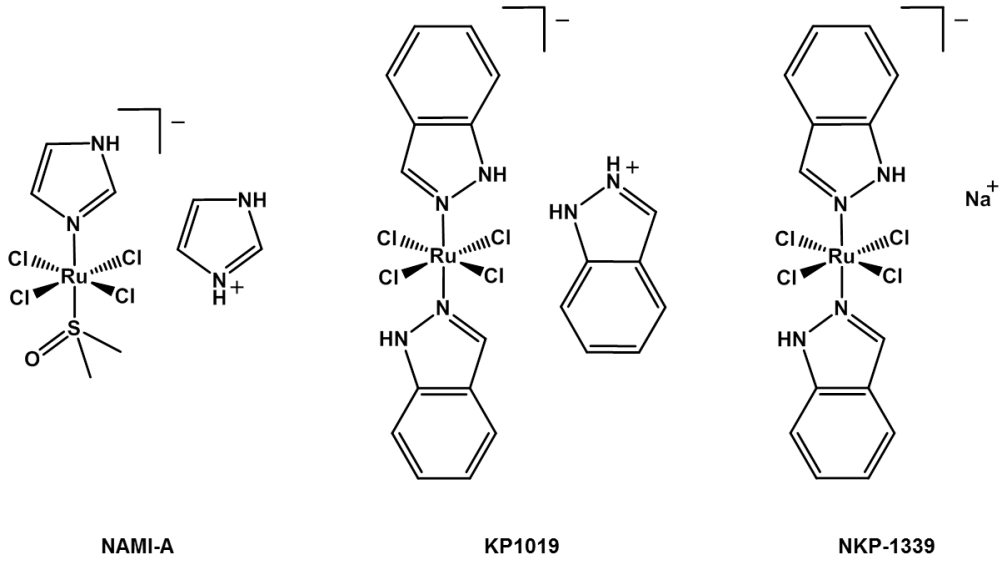

Figure 1.4. The three clinically investigated ruthenium-based anticancer NAMI-A, KP1019, and NKP-1339.

Similar to the clinically used platinum compounds, these Ru^{III} complexes are administered intravenously, and bind rapidly to serum proteins. The protein adduct formation protects the complexes against fast hydrolysis and degradation reactions under physiological conditions. It is hypothesised that they act as a prodrug and are reduced under the hypoxic conditions of the tumour tissue to the reactive Ru^{II} species.[23] This has led to increased interest in pseudo-octahedral organometallic Ru^{II} arene complexes in which the arene stabilizes ruthenium in the 2+ oxidation state.

1.3 Cytotoxic Ruthenium(II) Arene Complexes

Because of the implication of Ru^{II} in the cytotoxic activity of the ruthenium(III) complexes described in the previous section, there is an increased effort in the search of of Ru^{II} complexes with anticancer activity. In recent years, new classes of organometallic Ru^{II}-arene complexes, developed among others by the groups of Sadler and Dyson, have been found to have promising anticancer properties.[24, 25] Representative examples are [Ru(η^6-biphenyl)(en)Cl]PF_6 and [Ru(η^6-*p*-cymene)(pta)Cl_2], with en = ethylenediamine and pta = 1,3,5-triaza-7-phosphaadamantane (Figure 1.5). The piano-stool compounds of formula $[Ru(arene)(XY)Cl]^+$, e.g. where arene = biphenyl, XY = ethylenediamine, show promising activity both in vitro and in vivo [24] and are thought to have a mode of action that is analogous to that of cisplatin, where DNA is the main target. The formation of monofunctional adducts (preferentially at guanine sites) and the non-covalent interactions (i.e. extended arene intercalation and en H-bonding) are believed to be fundamental for DNA recognition and, as a consequence, anticancer activity.[26] However, [Ru(η^6-*p*-cymene)(pta)Cl_2] complexes have low cytotoxic potency towards cancer cell lines but are potent antimetastatic agents. Actually, the major intracellular targets of these compounds appear to be proteins, although DNA binding has been observed.[27]

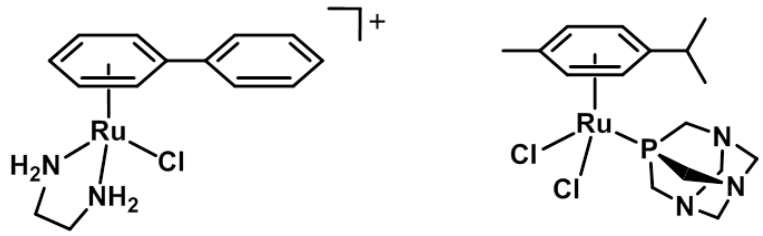

Figure 1.5. Molecular structures corresponding to the cytotoxic complexes [Ru(η^6-biphenyl)(en)Cl]$^+$ and [Ru(η^6-*p*-cymene)(pta)Cl_2].

1.3.1 Structural Features of Ru^{II} Arene Complexes

The general structure of the half-sandwich ruthenium(II) arene complexes developed by Sadler is shown in Figure 1.6. All complexes contain a η^6-arene occupying three coordination sites of the pseudo-octahedral Ru^{II} coordination sphere, a chelating ligand (XY) occupying two positions and a monodentate ligand (Z) occupying the sixth site. This "piano-stool"-type scaffold offers much scope for design, with potential for modifications in the structure, and overall charge of the complex (n+).

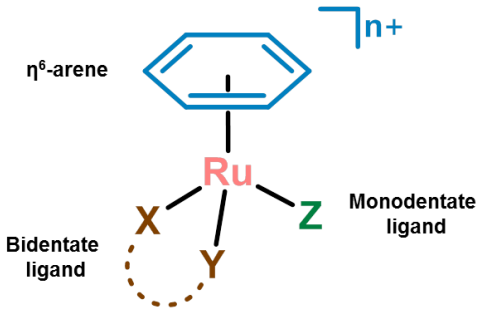

Figure 1.6. General structure of the half-sandwich or piano-stool ruthenium(II) arene complexes.

The arene ligand confers stability to the 2+ oxidation state, binding as a η^6-electron donor and a π-acceptor. The presence of a chelating ligand, XY, offers additional stability to the entire structure and the ability of tuning the electronic properties of the metal centre. The monodentate ligand Z gives the molecule an activation site: if labile, such as halide, it can provide a vacant coordination site for interaction with biomolecules. Such lability can be finely tuned by the variation of both the arene and the XY chelating ligand. These features provide handles for the control of both the thermodynamics and kinetics of this system as well as its overall structural architecture. They also make possible to tailor the chemical reactivity of the complexes, potentially allowing control of important pharmacological properties including cell uptake, distribution, and toxic side effects.

1.3.2 Activation of the Ru–Z Bond

1.3.2.1 Ru–Z Cleavage by Hydrolysis

Metal-ligand bonds (M–L coordination bonds) are much weaker, typically 50–150 kJ mol^{-1}, compared with covalent bonding (the energy of a single C–C bond is 300–400 kJ mol^{-1}).[28] As for cisplatin, activation through hydrolysis of the Ru–Z bond may be important for the mechanism of action of these Ru^{II} arene complexes, making these complexes susceptible to be exploited in medicinal chemistry in a similar way to cisplatin.

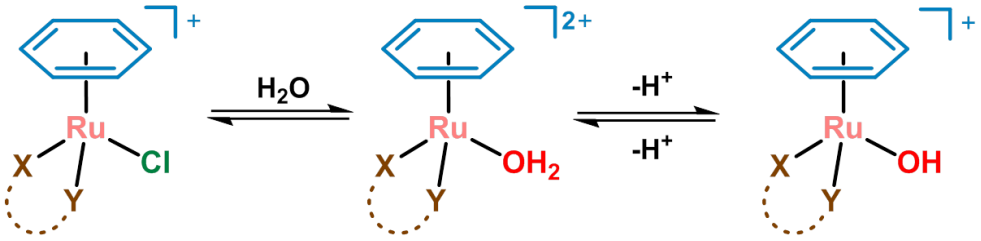

Figure 1.7. Hydrolysis and subsequent acid/base equilibria of ruthenium(II) half-sandwich complexes of general formula $[Ru(\eta^6\text{-arene})(XY)Cl]^+$.

The mechanism of cytotoxic action of Ru^{II} arene complexes is generally thought to involve hydrolysis of the Ru–Z bond, thus generating an active Ru–OH_2 metabolite (Figure 1.7). Aquation is largely suppressed at extracellular chloride concentration ($[Cl^-]$ about 100 mM) but becomes possible inside the cells, where $[Cl^-]$ is much lower (4–20 mM). The aqua species will exist over a range of pH, but above the pK_a value (the pH at which 50% of the species exists as Ru–OH_2 and Ru–OH through deprotonation of the H_2O ligand) the hydroxo Ru–OH species will predominate. The hydroxido complex is usually considered to be a less reactive species due to low lability of the Ru–OH bond. The pK_a values of the $[Ru(\eta^6\text{-arene})(en)(OH_2)]^{2+}$ aqua species are typically between 7 and 8, and thus at physiological pH the Ru–OH_2 species prevails over the less reactive

Ru–OH species. The rate of hydrolysis is also important; if the complex hydrolyses too fast they may not reach the target site.

The speciation of the ruthenium complexes under physiological conditions is therefore rather important. For example, for complex [Ru(η^6-biphenyl)(en)Cl]$^+$,[29] the results indicate that in blood plasma, where the chloride concentration is high, the complexes exist primarily in their chlorido form (> 89%). In contrast, when the chloride concentration is much lower, as in the cell cytoplasm (about 23 mM) and cell nucleus (4 mM), the amount of the more reactive aqua species increases to ca. 30% and 70%, respectively (Figure 1.8).[29] As a result, the extracellular suppression of aquation followed by activation upon entering the cell provides a selective mechanism of activation.

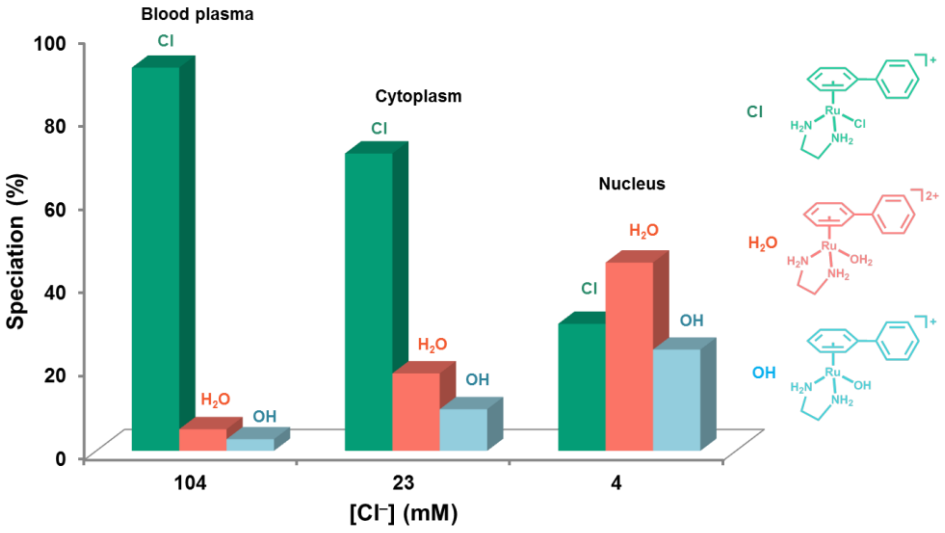

Figure 1.8. Speciation of [Ru(η^6-biphenyl)(en)Cl]$^+$ in blood plasma, cytoplasm and nucleus at equilibrium.

The thermodynamics and kinetics of such activation, as well as the acidity of the water molecule in the aqua adduct, can be finely tuned by appropriate choice of the different building blocks in the general structure [Ru(η^6-arene)(XY)Z]$^+$ and will be further discussed in Section 1.3.4.

1.3.2.2 Ru–Z Cleavage through Irradiation

Since cleavage of the Ru–Z bond appears to be an important step in the mechanism of action of Ru^{II} arene complexes, controlling the activation of these coordination sites can provide a key strategy to increase the potential of $[Ru(\eta^6\text{-arene})(XY)Z]^{n+}$ complexes as anticancer agents. Photochemical activation is an attractive approach for achieving selectively the cleavage by the absorption of light, promoting its release and offering the possibility of controlling the location and timing activity of the therapeutic metal complex. This requires breaking of the coordination bond by the use of high-energy UV-visible light photons. In addition, light is already used to treat certain cancers using the Food and Drug Administration-approved technique of photodynamic therapy (PDT).[30]

Some examples of half-sandwich Ru^{II} arene complexes, $[Ru(\eta^6\text{-}p\text{-cym})(N,N')(Z)]^{2+}$ (where N,N' = bidentate chelated ligand and Z = pyridine o pyridine derivate) have been proved to be activated by UV-visible light to photo-dissociate selectively the monodentate ligand (Z) in aqueous solution and in the presence of a nucleobase (9-ethylguanine or 9-ethyladenine).[31] Irradiation generates the reactive aqua species, able to bind to the DNA base, as depicted in Figure 1.9. Such behaviour represents a promising way to control the hydrolysis reaction and binding of these Ru^{II} complexes to biomolecules such as DNA, controlling therefore the cytotoxic action of the potential anticancer Ru^{II} pro-drug.

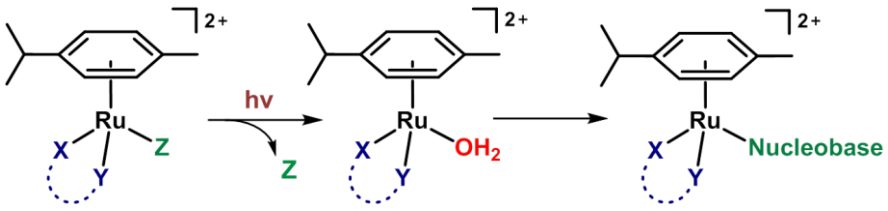

Figure 1.9. Photoactivation of Ru^{II} arene complexes bearing pyridine or pyridine derivate as monodentate ligand Z.

1.3.3 Mechanism of Action

1.3.3.1 Interaction with DNA

The aqua species is then thought to bind to nuclear DNA with a high affinity to the N7 position of guanine bases. Both [Ru(η^6-arene)(en)]–nucleobase and nucleoside adducts have been isolated and characterized by X-ray crystallography where arene = bip (biphenyl), tha (5,8,9,10-tetrahydroanthracene), dha (9,10-dihydroanthracene), and en = ethylenediamine.[32] According to solution and solid-state evidence, the main Ru–N7 (guanine) coordination bond is assisted by stereospecific hydrogen bonding between the C6=O of guanine and the NH of ethylenediamine, and π-π stacking between the aromatic ligand and the nucleobase (Figure 1.10). Also, it has been observed that in cell-free media these adducts distort the DNA duplex.[33]

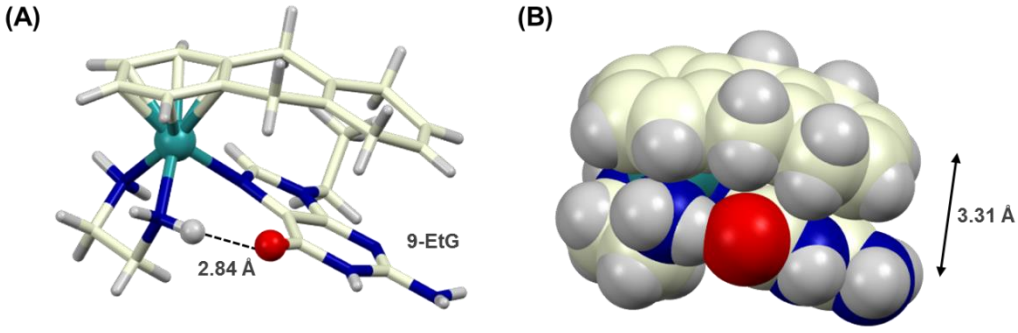

Figure 1.10. X-ray crystallographic structure of [Ru(η^6-dha)(en)(9-EtG)]$^+$ (dha = 9,10-dihydroanthracene , en = ethylenediamine, and 9-EtG = 9-ethylguanine); (A) stereospecific hydrogen bonding interaction of the C6=O carbonyl of 9-EtG with an NH_{en}, (B) π-π arene nucleobase stacking interaction.

Interactions of these complexes of general formula [Ru(η^6-arene)(en)Cl]$^+$ with several biologically relevant molecules and potential targets (e.g. the amino acids histidine, cysteine and methionine, the cytochrome c, and the tripeptide glutathione) have also been explored.[34] Overall, research suggests that DNA is the preferred target.

1.3.3.2 Transfer Hydrogenation Catalysis

Organometallic complexes are well known as catalysts for organic chemical reactions, for example, olefin metathesis by Grubbs' ruthenium carbene complexes,[35, 36] and asymmetric hydrogenation of ketones by Noyori's ruthenium arene complexes.[37, 38]

Ruthenium(II) arene complexes have shown to catalyse regioselectively the reduction of NAD^+ to NADH in the presence of formate as a hydride source under physiologically relevant conditions.[39] In vivo, both NAD^+ and NADH play important roles as cofactors in numerous biocatalyzed processes, and the ratio NAD^+/NADH must be tightly controlled to avoid cell death by oxidative stress.[40] Because eukaryotic cells seem to tolerate high levels of formate,[39] this catalytic pathway can provide a new mechanism of action to increase the cytotoxicity of these Ru^{II} arene metallodrugs.

Recently, the antitumor activity of Ru^{II} arene complexes has been evaluated towards human ovarian cancer cells in the presence of low non-toxic doses of formate,[41] where the cytotoxic activity showed a 50-fold increase. The mechanism of action for this effect is thought to involve the generation of reductive stress instead of apoptosis. The activation of the complex follows the typical substitution of the monodentate ligand by a water molecule which then is replaced by formate to ultimately afford the corresponding hydride complex. The Ru–H complex can reduce NAD^+ to NADH as shown in the proposed mechanism by Cavinet et al. as depicted in Scheme 1.1.[42]

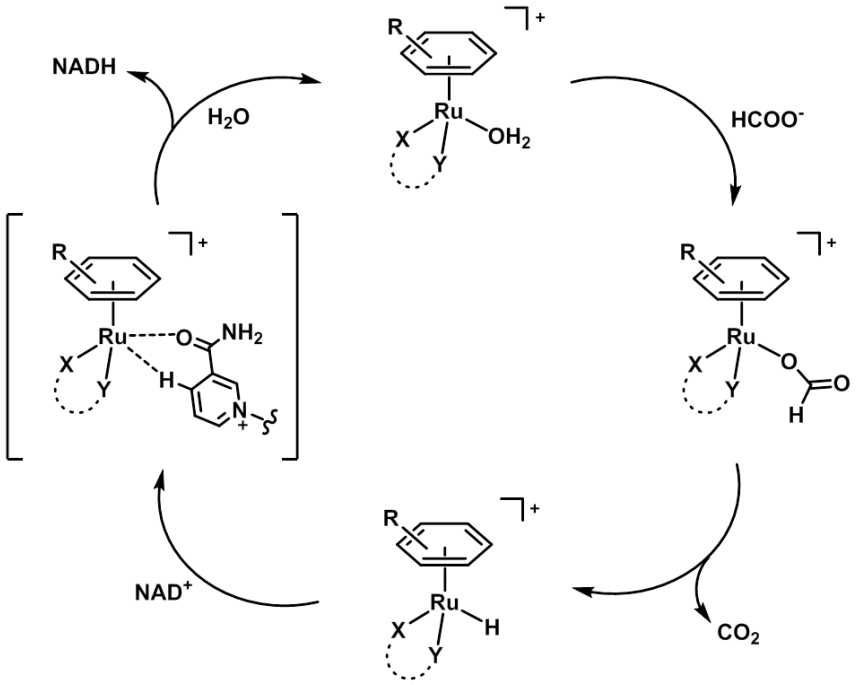

Scheme 1.1

1.3.4 Structure-Activity Relationship. Effect of the Different Building Blocks

From the confluence of the chemical, biochemical and biological studies on this organometallic family of Ru^{II}-arene compounds, valuable pharmacological properties have emerged. The properties may be summarized as: (i) the ruthenium(II) centre is a sustainable metal ion for biological applications when is coordinated to an arene ligand; the stability of the ruthenium arene bond provides an excellent scaffold for chemotherapeutic applications; (ii) bidentate chelating ligands can be used to modulate the pharmacological properties of Ru^{II} arene complexes; and (iii) hydrolysis of the Ru–Z bond allows direct coordination to biomolecular targets, rate of which can be controlled by using different monodentate ligands and by variation of the other building blocks in the structure. The latter will be discussed as follows.

1.3.4.1 The Arene

The arene stabilizes ruthenium in the 2+ oxidation state, but it also provides a hydrophobic face to the complex, which can assist passage across cell membranes and play an important role in biological recognition processes.[43] The biological activity of Ru^{II} arene complexes, $[Ru(\eta^6\text{-arene})(en)Cl]^+$ bearing ethylenediamine as the XY-chelated ligand, has been shown to be highly dependent on the nature of the bound arene, with increasing hydrophobicity correlating lower IC_{50} (drug concentration that inhibit growth of cells by 50% compared to control).[24] Figure 1.11A shows the different IC_{50} values obtained by varying the arene group. The increase in activity with increase in hydrophobicity is primarily thought to be due to the ability of the extended arenes to intercalate into DNA, thus causing further distortion of the DNA structure.[44-46]

1.3.4.2 The XY Chelating Ligand

The reactivity of $[Ru(\eta^6\text{-arene})(XY)Cl]^+$ complexes is highly dependent on the nature of the XY chelating ligand. Variations can be introduced by *N*,*N*-, *N*,*O*- or *O*,*O*-chelates with significant effects depending on the chosen N- and O-group (Figure 1.11B).

Modification of the chelating ligand results in complexes with different cytotoxicities. Aliphatic diamines usually showed good activity when they contain a primary amine, believed to establish stereospecific hydrogen bonding interactions with guanine bases (C6O-HN H-bonding).[47] Bipyridine and phenantroline derivatives are inactive, indicating the importance of NH groups. Replacement of the *N*,*N*-chelating ligand ethylenediamine by *N*,*O*-chelating ligands of some amino acids (amino acidates) showed a high decrease in cytotoxicity.[48] Reactivity studies indicated that fast hydrolysis rates might be responsible for the lack of activity of these derivatives.

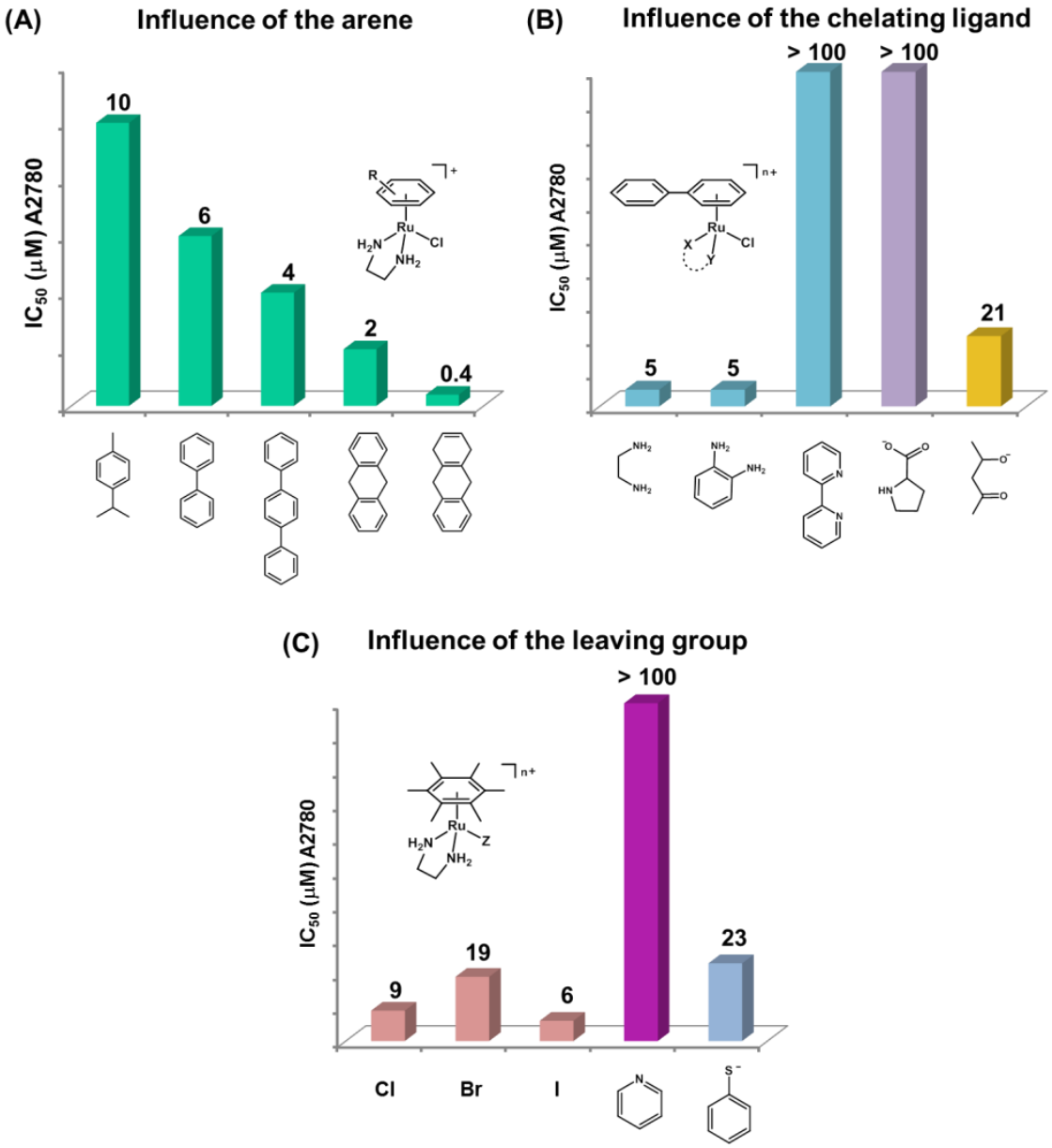

Figure 1.11. General trends that show the influence of (A) the arene, (B) the chelating ligand and (C) the leaving group on the cytotoxicity of Ru^{II} arene complexes. Adapted from ref 49.

Finally, complexes with *O,O*-chelating ligands as acac (acetylacetonate) and its derivates showed good to moderate activity, despite the lack of hydrogen bond donors.[47] Some of these trends can be explained by the general reactivity in aqueous solution of Ru^{II} arene complexes, which will be discussed in more detail below.

1.3.4.3 The Z Leaving Group

The series of $[Ru(\eta^6\text{-hmb})(en)Z]^{n+}$ complexes, varying the monodentate ligand Z shows a correlation between the rate of hydrolysis and the cytotoxicity of the complex towards cancer cells, with high activity for complexes that aquate readily (halides) and inactivity for complexes that do not aquate (pyridine) as shown in Figure 1.11C.[50] An interesting exception to this trend is when the leaving group is thiophenolate. This complex is active towards A2780 human ovarian cancer cells (IC_{50} 23 μM), despite being relatively inert to hydrolysis. The mechanism of action may be different and it has been reported to involve oxidation of the thiolate, followed by hydrolysis of the sulfenate group.[51]

An important next step is then to rationalize the relationships between structure and activity by correlating biological activity to chemical reactivity. Hence, much attention has been given to the study of the reactivity of this family of complexes and their behaviour in aqueous solution.

1.3.4.4 Tunning the Aqueous Solution Reactivity

The rate and extent of hydrolysis of the Ru–Z bond are highly dependent on the nature of Z, more labile leaving groups affording faster hydrolysis.[50] Good correlations between hydrolysis rates, hydrolysis equilibrium and cytotoxicity have been observed for the ruthenium complexes of general formula $[Ru(\eta^6\text{-hmb})(en)Z]^+$, where hmb is hexamethylbenzene (Figure 1.12). In general, a faster hydrolysis rate and a high percentage of aqua species at equilibrium correlated with good cytotoxicity towards the A2780 human ovarian cancer cell line. For the halidos, the aquation rate was found to decrease in the order Cl ≈ Br > I. Replacement of the chlorido ligand with the pseudohalide N_3 slowed down the hydrolysis rate even by 40-fold. Substituting halides

by leaving groups such as pyridines or pyridine derivates caused a further decrease in the hydrolysis process and even block it almost completely at biologically-relevant time scales. Such complexes were not active against cancer cells.[50]

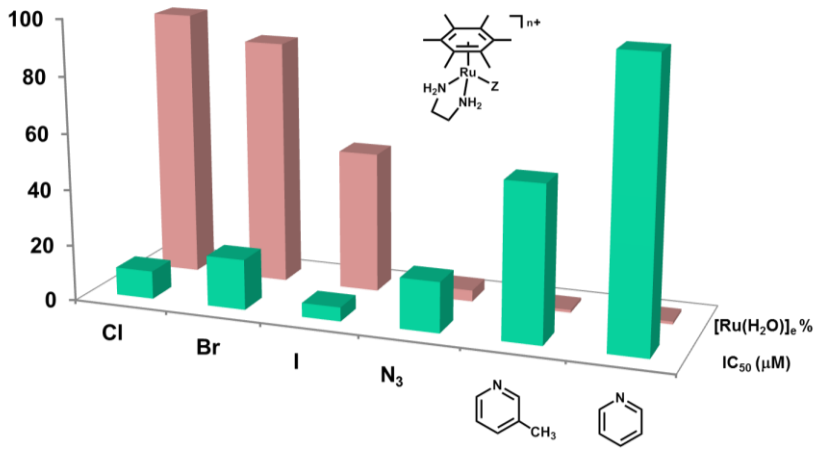

Figure 1.12. Correlation of hydrolysis with cytotoxicity. Equilibrium percentage of total Ru^{II} as $[Ru(\eta^6\text{-hmb(en)}(H_2O)]^{2+}$ (% $[Ru(H_2O)]_e$), and A2780 human ovarian cancer cell IC_{50} values for $[Ru(\eta^6\text{-hmb(en)(Z)}]^{n+}$ complexes with several leaving groups Z. Adapted from ref 50.

The chelating ligand also influences the hydrolysis rate and equilibrium constant. In general, the effect on substitution reactions depends on the nature of the chelate, suggesting that electronic and steric effects are responsible for this behaviour. Replacement of the neutral *N,N*- en by the anionic *O,O*- acac as the chelating ligand increases the rate and extent of hydrolysis.[52] However, the presence of π-acceptor ligands as bipyrimidines derivates slows down the hydrolysis reactions.[53] The nature of the arene also affects both the rate and extent of hydrolysis. The hydrolysis reactions of three $[Ru(\eta^6\text{-arene)(en)Cl)}]^+$ complexes (arene = bip, dha, and tha) showed that the rates of aquation increased in the order tha ≈ dha > bip.[29]

As important as the rate and extent of hydrolysis for drug activation is the pK_a of the coordinated water molecule of the activated aqua complex. As discussed in Section 1.3.2.1, the pK_a value determines whether the active species containing the more labile

Ru–OH_2 bond or the less reactive deprotonated form Ru–OH prevails in solution at a given pH.[54]

Table 1.1. pK_a data for Ru^{II} organometallic complexes with different arenes and chelating ligands.

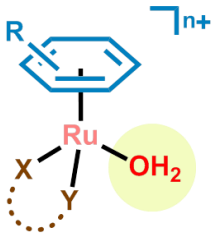

Arene	Chelating Ligand (XY)	pK_a	Ref.
p-cym	azpyz-NMe_2	4.60	47
p-cym	bpm	6.96	53
p-cym	phen	7.32	53
Bip	en	7.71	29
Dha	en	7.89	29
Bz	en	7.90	55
Tha	en	8.01	29
p-cym	en	8.25	54
p-cym	trop	9.12	56
p-cym	maltol	9.23	57
p-cym	acac	9.41	52

p-cym, *p*-cymene; bip, biphenyl; dha, 9,10-dihydroanthracene; bz, benzene; tha, 5,8,9,10-tetrahydroanthracene; azpyz-NMe_2, phenylazopyrazole derivative; bpm, 2,2'-bipyrimidine; phen, phenantroline; en, ethylenediamine; trop, tropolone; acac, acetylacetonate.

The pK_a values of the coordinated water molecule in $[Ru(\eta^6\text{-arene})(en)(OH_2)]^+$ was found to be 7.71, 7.89 and 8.01 when the arene was an extended π-system bip, dha, and tha, respectively.[29] This relatively low acidity of the water ligand is important, since under physiological conditions large amounts of the most reactive aqua complexes (Ru–OH_2) are predicted to exist. Changing the XY-chelated ligand to monoanionic oxygen

O,O-chelates such as tropolone or acetylacetonate results in a further pK_a to 9.12 for $[Ru(\eta^6\text{-}p\text{-cym})(trop)(OH_2)]^+$ [56] and 9.41 for $[Ru(\eta^6\text{-}p\text{-cym})(acac)(OH_2)]^+$,[52] most likely as a consequence of electronic effects exerted by the chelating ligand on the metal centre. In contrast, the pK_a of the aqua adduct in $[Ru(\eta^6\text{-}p\text{-cym})(azpyz\text{-}NMe_2)(OH_2)]^+$ (azpyz-NMe_2 = 4-(1H-pyrazol-3-ylazo)-N,N-dimethylaniline) is 4.60,[47] indicating the low electron density at ruthenium centre and consistent with the π-acidic nature of the ligand. Indeed, the complex has allow affinity for DNA bases as it would predominately exists in the more inert hydroxido form at physiological pH.

These results clearly show that the hydrolysis reaction (and with that drug activation) and the pK_a of the aqua adduct, can be finely tuned by the choice of the appropriate arene, chelating and monodentate ligands. This opens up the possibility of designing drugs with tailor-made properties which can be exploited in cancer therapy.

1.4 Targeting the Cancer Cell Metabolism

Cancer is the name given to a collection of related diseases characterised by abnormal cell growth through which cells may acquire the potential to disperse (metastasise) from the site of origin (primary tumour) to other sites in the body (secondary tumour).[58] The understanding of cancer has changed dramatically over the past three decades, due in large part to the revolution in molecular biology that has altered the face of all biomedical research. That research has revealed a number of molecular, biochemical, and cellular traits – acquired capabilities– shared by most and perhaps all types of human cancer. These rules that govern the transformation of normal human cells into malignant cancers are classified in the so-called Hallmarks of Cancer.[59]

1.4.1 Hallmarks of Cancer

The hallmarks of cancer involve a number of biological acquired capabilities during the multistep development of human tumours, described by Hanahan and Weinberg, which allows cancer cells to survive, proliferate, and disseminate. They were originally classified as follows: (1) sustaining proliferative signalling, (2) evading growth suppressors, (3) activating invasion and metastasis, (4) enabling replicative immortality, (5) inducing angiogenesis, and (6) resisting cell death.[59]

The hallmarks constitute an organizing principle for rationalizing the complexities of neoplastic disease. Moreover, in last decades an increasing body of research has suggested that four additional hallmarks of cancer are involved in the pathogenesis of some cancers:[60] (7) deregulating cellular energetics, (8) avoiding immune destruction, (9) genome instability and mutation, and (10) tumour-promoting inflammation.

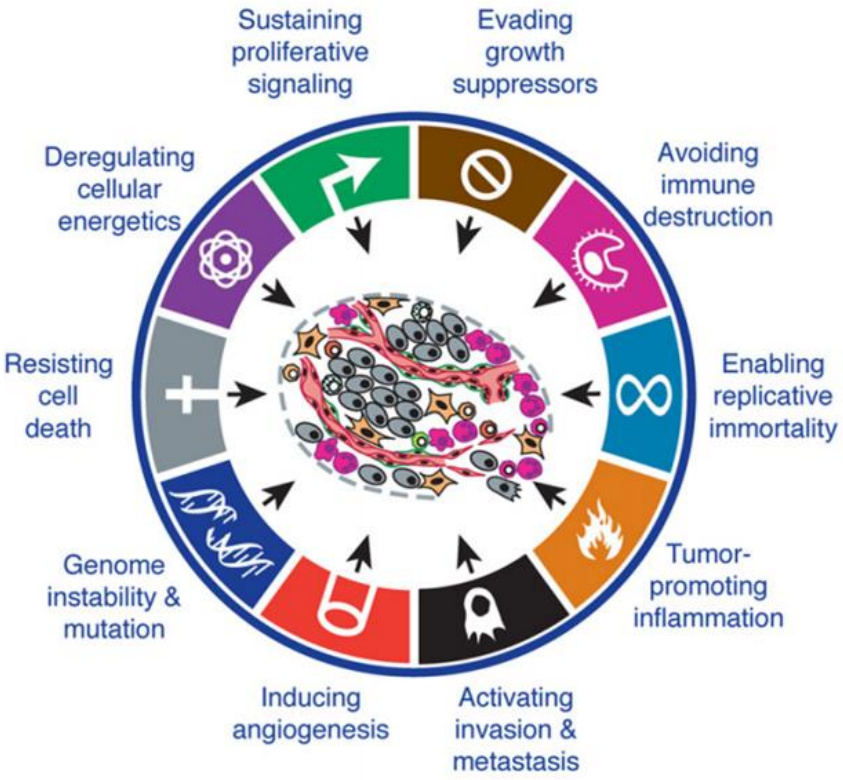

Figure 1.13. Hallmarks of cancer. This illustration shows the ten acquired capabilities of cancer. Reproduced from ref 59.

This section will be focused on the *deregulation of the cellular energy* of the tumour cell, because is a plausible niche where ruthenium(II) arene complexes might present unique advantages in chemotherapy research.

1.4.2 Deregulating Cellular Energy. *The Warburg Effect*

The chronic and often uncontrolled cell proliferation that represents the essence of neoplastic disease involves not only deregulated control of cell proliferation but also corresponding adjustments of energy metabolism in order to fuel cell growth and division.[60]

The alterations of metabolism and energetics, within which glucose and adenosine triphosphate (ATP) are prominent players, have been recognized in recent years as an emerging hallmark of cancer.[60] Actually, the importance of metabolic alterations in

cancer cells was recognized long ago. In the 1920s, Otto Warburg, a German biochemist, demonstrated that unlike normal tissues, cancer cells predominantly undergo fermentation instead of oxidative phosphorylation even when oxygen is abundant.[61-63] This phenomenon of so-called aerobic glycolysis became known as the Warburg effect.[64] In the presence of oxygen, most normal tissues metabolize glucose to pyruvate through glycolysis, and then completely oxidize a large fraction of the generated pyruvate to carbon dioxide in the mitochondria through oxidative phosphorylation. Under anaerobic conditions, normal cells redirect glycolytic pyruvate away from mitochondrial oxidation and instead largely reduce it to lactate in the cytosol.[65] The fundamental paradigm stemming from Warburg's studies was that in contrast to normal cells, rapidly proliferating tumours metabolized glucose to lactate even under aerobic conditions despite this process being far less efficient (18-fold) in terms of net ATP production per molecule of glucose (Figure 1.14).[65] Because of the upregulated metabolism in cancer cells, it is necessary a compromise to balance the need of energy and anabolites to create biomass. Oxidative phosphorylation is not ideal for this purpose because produces a large amount of energy as ATP but inefficient carbon sources.[65] However, through aerobic glycolysis enough lactate is generated to supply nutrients to the cell growth and division of the proliferating cells. Additionally, the energy requirements are also supported due to the high glucose levels found in the tumour cells.[66] This phenomenon has since been observed across several tumour types and often occurs in parallel with a marked increase in glucose uptake and consumption, as visualized, and clinically exploited, through the use of 18F-deoxyglucose-positron emission tomography.[67]

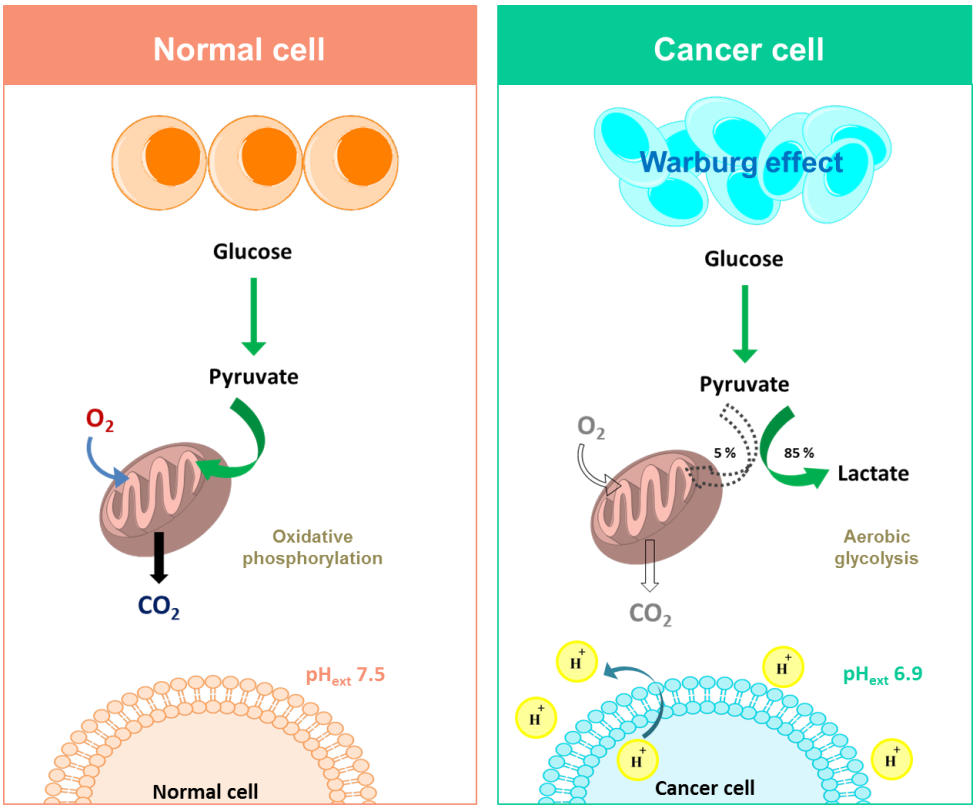

Figure 1.14. Schematic representation of the different metabolism of normal versus cancer cells and its ultimate effect in the final extracellular pH.

The high conversion rate of pyruvate to lactate via the aerobic glycolysis (Warburg effect), and its accumulation in tumour cells, has been observed to be critical in the development and progression of cancer.[68] Actually, the accumulation of lactate in cancer has been demonstrated to possess clinical relevance as a prognostic marker.[69] Following production, lactic acid is transported out of the cancer cell and across the plasma membrane by carboxylate transporter (MCT) family proteins.[68] The MCTs are essential components of cellular metabolism and provide an important contribution to the regulation of tumour intracellular pH (pH_{int}) by coupling H^+ export with monocarboxylates such as lactate. This lactate production/release is commonly considered to be the primary acidification mechanism of the metabolic microenvironment providing additional extracellular acidification (pH_{ext}).[70-73] For this reason, tumour cells present slightly acidic pH_{ext} values (6.2–6.9 vs 7.3–7.4 in normal

cells) while producing slight alkaline pH_{int} values (7.1–7.7 vs 6.9–7.1 in normal cells).[74] This creates a reversed pH gradient across the cell membrane that increases as the tumour progresses. The development and maintenance of this gradient is directly due to the ability of the tumour cells to secrete protons (H^+) and acidify their extracellular environment.[75] Cancer cells have an acid-base balance that is completely different than that observed in normal tissues and that increases with increasing neoplastic state: an alkaline intracellular pH (pH_{int}) linked to a "malignant" extracellular acid microenvironment (pH_{ext}).

Exploting the peculiar cancer H^+ dynamics (both pH_{ext} and pH_{int}) coupled with intracellular metabolic disruption could provide a new strategy for anticancer therapeutics,[76] for example those that activate selectively at low pH.

1.5 Ruthenium(II) Tether Complexes

1.5.1 General Objective of this Thesis

Taking into account the more acidic extracellular pH predominating in cancer cells I will explore ruthenium(II) arene complexes that would undergo activation under low pH.

The general structure described above for typical half-sandwich complexes might provide complexes whose reactivity is pH-dependent by using a pH-activatable monodentate ligand, i.e., by protonation of a suitable Z following cleavage of the Ru–Z bond (Figure 1.15).

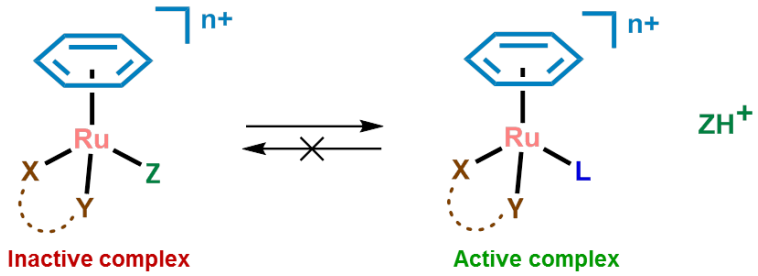

Figure 1.15. Activation of a typical Ru^{II} arene complex. This process is non-reversible because the Z ligand is released and a solvent molecule, L, (or biomolecule) occupies the vacant site.

However, tethering the monodentate ligand (Z) to the Ru^{II}–arene structure may provide an attractive strategy to create not only pH-dependent complexes but also switchable compounds which "turn-on" in a reversible manner. These "tether" complexes contain the π-coordinated neutral arene group from which the σ-coordinated ligand (Z) is tethered. The donor group offers two reversible functionalities: (i) binding to the Ru^{II} centre to form a tether-ring-closed (inactivated) complex, or (ii) dissociation of the donor group from the Ru^{II} centre (as a dangling arm) to afford an open-tether complex with a pendant free Z group (Figure 1.16).[77] Protonation of the labile group Z would impair reversible metal coordination (active complex), while a decrease in proton

concentration enables coordination to the metal centre. These features make complex activation pH-dependent and reversible.

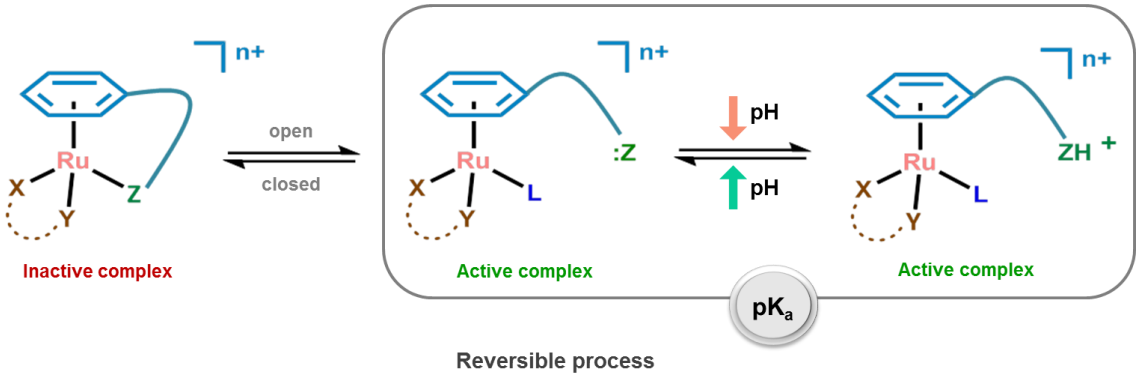

Figure 1.16. Schematic representation of the pH activation of tether complexes. First, the closed complex can undergoes the ring-opening process by the dissociation of the donor atom Z from the Ru^{II} centre. If pH drops, the donor atom is susceptible to be protonated impairing the reversible coordination to the metal centre. However, if the pH increases, deprotonation of Z can reversibly trigger the ring closure reaction.

1.5.2 State-of-the-Art of Ru^{II}-Tether Complexes

1.5.2.1 Synthesis

Ruthenium(II) η^6-arene complexes with tethered carboxylic,[78] amine[79, 80], alcohol,[81, 82] phosphorous[83, 84] or carbene[85] group functions have been reported. Side chains containing a coordinating moiety such as these donor groups result in hemilabile tether η^6:κ^1-arene ligands.

Such ligand provides a group that binds strongly to the metal centre (through the η^6-arene), and a relatively weak donor which may protect a vacant site on the metal centre until it is displaced by an incoming ligand.[86] This displacement can be a reversible process as shown in Figure 1.17.

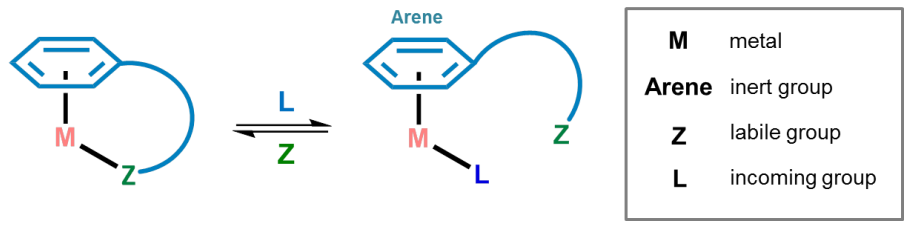

Figure 1.17. General properties of hemilabile tethering ligands coordinated to transition metals.

The preparative procedures for tether arene complexes can be organised in three different classes, which are represented in Figure 1.18 and described below:

1) A labile arene is displaced by a second arene, which is attached by a tether arm to the already coordinated donor atom.
2) A η^6-coordinated functionalized arene is connected by a tether arm to a donor group. The tether is formed by displacement of the monodentate ligand (L) and coordination of the Z donor atom to the metal centre.
3) Intramolecular condensation reaction between a substituent on the η^6-arene (Y) and a functional group on the monodentate ligand (X).

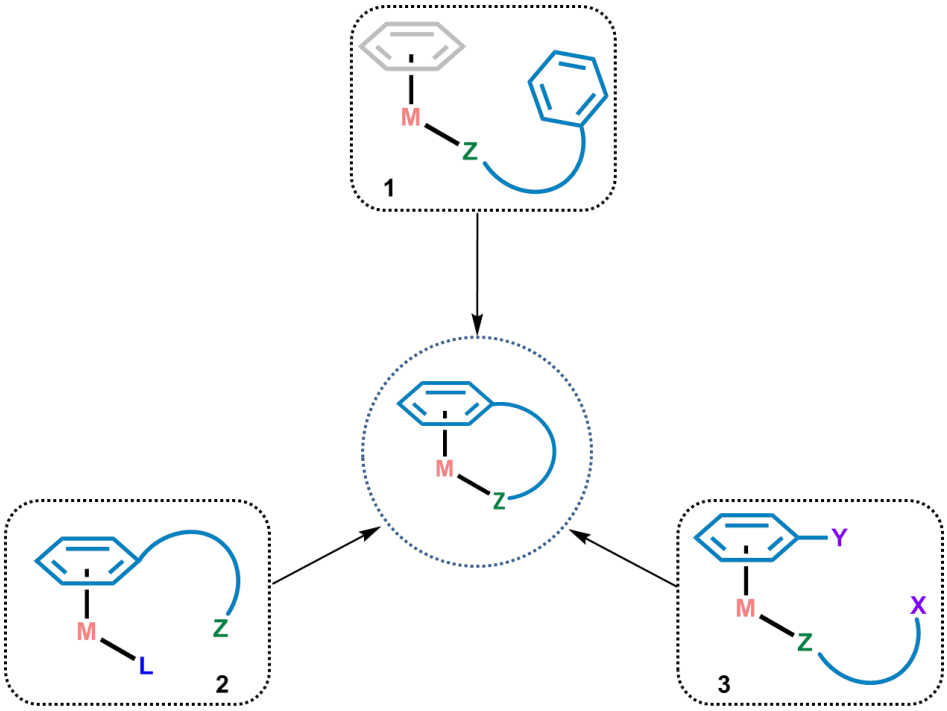

Figure 1.18. Schematic representation of the different experimental procedures for the synthesis of Ru^{II} tether complexes.

Synthetic path 1

This is the most widely used synthetic method for obtaining Ru^{II} tether complexes. Smith and Wright reported the first η^6-arene tether complexes using this methodology in the second half of the 1990s. As shown in Figure 1.19A, the complex [Ru{η^6:κ^1-$C_6H_5(CH_2)_3PPh_2$}Cl_2] was obtained by thermolysis of [Ru(η^6-*p*-cym){κ^1-$PPh_2(CH_2)_3Ph$}Cl_2] at high temperature.[87] In the same year, Therrien et al. hoped that the chelating effect may force the arene to displace the coordinated *p*-cymene in [Ru(η^6-*p*-cymene){κ^1-P-*o*-$C_6H_4(CH_2OH)(CH_2CH_2PPh_2)$}$Cl_2$]. Having failed, they sought to synthesize a more labile ruthenium arene dimer as the precursor for the arene exchanging reaction. Since electron-poor arenes gave the lowest yields in displacement reactions with [Ru(η^6-*p*-cymene)Cl_2]$_2$, they reasoned that [Ru(η^6-etb)Cl_2]$_2$ (etb = ethyl benzoate) would may be a good starting material for the synthesis of [Ru{η^6:κ^1-$C_6H_4(CH_2OH)(CH_2CH_2PPh_2)$}]$Cl_2$]. Birch reduction of ethyl benzoate yielded ethyl-1,4-cyclohexadiene-3-carboxylate.[88-90] Reaction of the cyclohexadiene with $RuCl_3$ in ethanol afforded [Ru(η^6-etb)Cl_2]$_2$ in high yield. This dimer was a promising starting material for arene-exchange reactions. Treatment of dimer [Ru(η^6-etb)Cl_2]$_2$ with the phosphine alcohol {*o*-$C_6H_4(CH_2OH)(CH_2CH_2PPh_2)$} afforded [Ru($\eta^6$-etb){$\kappa^1$-P-*o*-$C_6H_4(CH_2OH)(CH_2CH_2PPh_2)$}$Cl_2$]. The intramolecular arene exchange was effectively carried out in a sealed tube leading to the corresponding tether complex (Figure 1.19B).[91] Nowadays, in addition to ethyl benzoate dimers, methyl benzoates complexes are used as general precursors since they undergo the tether reaction much faster than *p*-cymene counterparts because the former fragment is a much better leaving group as it was observed by Navarro et al.[84]

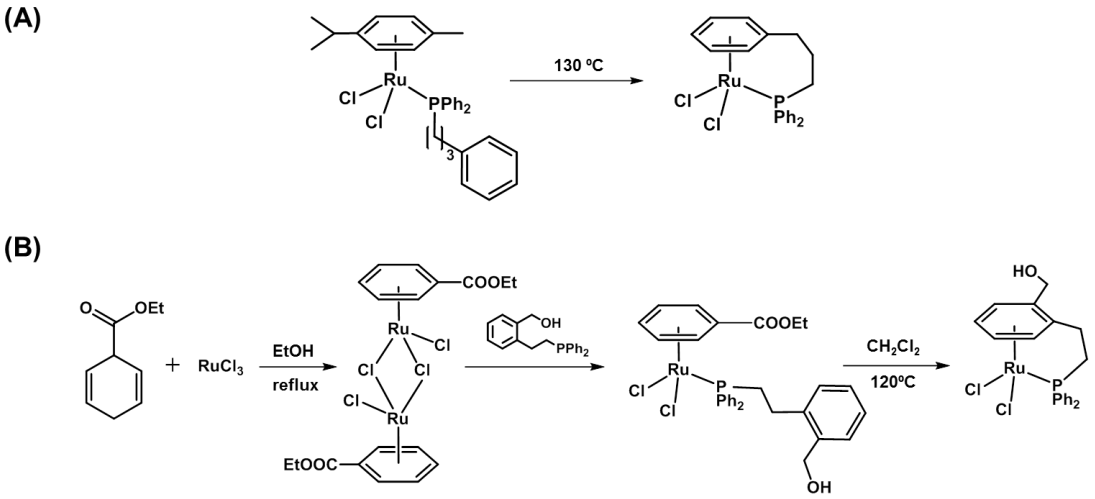

Figure 1.19. Synthetic method of Ru^{II} tether complexes by arene displacement through intramolecular exchange. (A) $[Ru(\eta^6{:}\kappa^1\text{-}C_6H_5(CH_2)_3PPh_2)Cl_2]$, (B) $[Ru(\eta^6{:}\kappa^1\text{-}o\text{-}C_6H_4(CH_2OH)(CH_2CH_2PPh_2))]Cl_2]$.

Synthetic path 2

Ruthenium(II) tether complexes with oxygen as the donor atom have been synthesized from the starting dimer $[Ru\{\eta^6\text{-}C_6H_5(CH_2)_3OH\}Cl_2]_2$, prepared through the reaction between the corresponding cyclohexadiene derivative $C_6H_7(CH_2)_3OH$ (obtained by the Birch reduction of $C_6H_5(CH_2)_3OH$) and $RuCl_3$. Subsequent reaction with bipyridine afforded the complex $[Ru\{\eta^6\text{-}C_6H_5(CH_2)_3OH\}(bip)Cl]BF_4$, which on treatment with $AgBF_4$ loses the chlorido ligand generating the alcohol tether $[Ru\{\eta^6{:}\kappa^1O\text{-}C_6H_5(CH_2)_3OH\}(bip)](BF_4)_2$.[81]

Similarly, complex $[Ru\{\eta^6\text{-}C_6H_5(CH_2)_3NH_3\}(PPh_3)Cl_2]Cl$ was susceptible to afford its corresponding closed tether counterpart $[Ru\{\eta^6{:}\kappa^1N\text{-}C_6H_5(CH_2)_3NH_2\}(PPh_3)Cl]BF_4$ upon treatment with sodium hydroxide (to deprotonate the ammonium group and subsequently free the nitrogen for metal binding) and $NaBF_4$.[81]

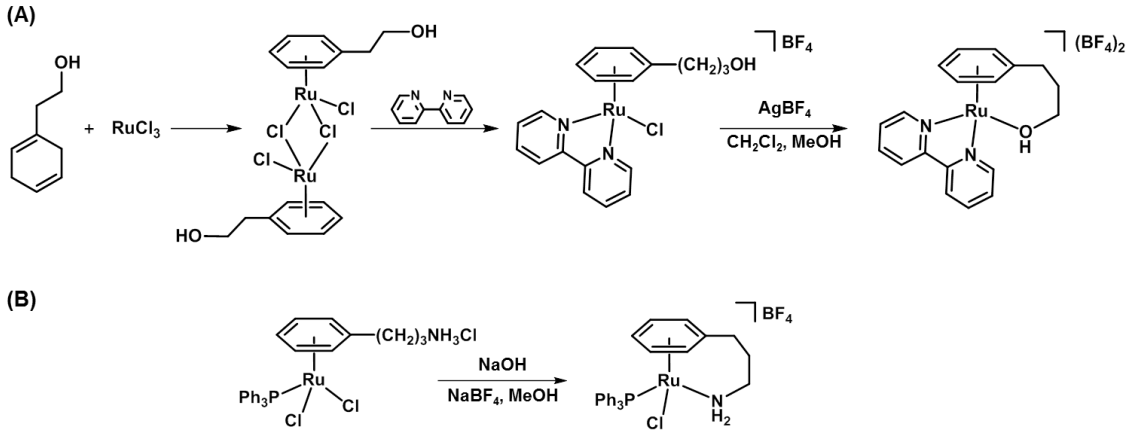

Figure 1.20. Synthesis of Ru^{II} tether complexes via coordination of the donor atom from the arene to the ruthenium centre.

Synthetic path 3

Several examples are known of ruthenium(II) tether complexes having either sulphur or phosphorous as the donor atom in which the tether results from an intramolecular condensation between a substituent on the arene and a functional group on the monodentate ligand. A typical example is shown in Figure 1.21. The treatment of the vinyldiphenylphosphine complex with KO^tBu in refluxing acetonitrile gave the corresponding tethered complex $[Ru\{\eta^6{:}\kappa^1\text{-}p\text{-}Me_2CH\text{-}C_6H_4(CH_2)_3PPh_2\}Cl_2]$ where only the methyl group on the *p*-cymene arene has been deprotonated.[92] This procedure provides an alternative approach to the synthesis of new tethered complexes.

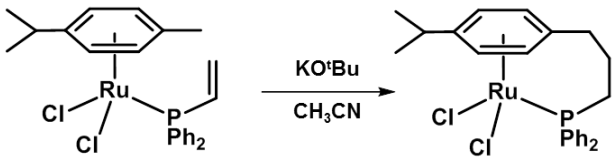

Figure 1.21. Synthesis of Ru^{II} tethered complexes via intramolecular condensation.

1.5.2.2 Applications

The introduction of a hemilabile group on the metal centre not only allows for the modulation of steric and electronic properties of the resulting complexes but also

confers other interesting features for their use as metallodrugs. As an example, it has been reported that bischelated P,N aminophosphene Pt^{II} complexes binds to the model DNA base 5'-dTMP through a chelate ring-opening mechanism,[93] showing that the activation could be controlled by the substituents on the N atom, the size of the chelate ring, the pH, and the concentration of an external reagent such as the Cl^- ion.[94] Moreover, in a recent report, Molas et al. have described platinum(II) square planar complexes with intricate solvent-mediated interconversion of open and closed chelates with varying cytotoxic action against different cancer cell lines.[95] Hemilabile coordination complexes have also encountered success with applications in catalysis and small molecule sensing.[96, 97]

The length of a tether and its composition (heteroatom, branching, or multiple bonds) are anticipated to affect the tether ring properties, including the rate of tether ring formation, ring strain, and orientation of the tethering functional group. Thus, a molecular switch can be design to work by selective ring-opening of the tether under certain conditions. Control over the opening and closure of the tether ring as a function of pH might provide a Ru-arene complex which is specifically activated in cancer cells.

Last but not least, tether complexes are commonly used for asymmetric transfer hydrogenation and asymmetric hydrogenation of ketones and imines, in which the suitable carbon chain length of the tether arm has an important role. Thus, this type of complexes can undergo the transfer hydrogenation of the biological cofactor NAD^+ to NADH providing a new mechanism of activation to trigger the cytotoxicity of Ru^{II} tether complexes.

1.6 References

(1) Mawani, Y.; Orvig, C. In *Bioinorganic Medicinal Chemistry*; Eds; Wiley-VCH Verlag GmbH & Co. KGaA: 2011; pp 307-350.

(2) Mjos, K. D.; Orvig, C. Metallodrugs in Medicinal Inorganic Chemistry. *Chem. Rev.* **2014**, *114*, 4540-4563.

(3) Parascandola, J. *History of Salvarsan (Arsphenamine)*; John Wiley & Sons, Ltd: Chichester, 2001.

(4) Thompson, K. H.; Orvig, C. Metal Complexes in Medicinal Chemistry: New Vistas and Challenges in Drug Design. *Dalton Trans.* **2006**, 10.1039/B513476E.761-764.

(5) WHO. *World Cancer Report 2014*; 2014.

(6) Dasari, S.; Bernard Tchounwou, P. Cisplatin in Cancer Therapy: Molecular Mechanisms of Action. *Eur. J. Pharmacol.* **2014**, *740*, 364-378.

(7) Suss-Fink, G. Arene Ruthenium Complexes as Anticancer Agents. *Dalton Trans.* **2010**, *39*, 1673-1688.

(8) Kelland, L. The Resurgence of Platinum-Based Cancer Chemotherapy. *Nat. Rev. Cancer* **2007**, *7*, 573-584.

(9) Johnstone, T. C.; Suntharalingam, K.; Lippard, S. J. The Next Generation of Platinum Drugs: Targeted Pt(II) Agents, Nanoparticle Delivery, and Pt(IV) Prodrugs. *Chem. Rev.* **2016**, *116*, 3436-3486.

(10) Jennerwein, M.; Andrews, P. A. Effect of Intracellular Chloride on the Cellular Pharmacodynamics of cis-Diamminedichloroplatinum(II). *Drug Metab. Disposition* **1995**, *23*, 178-184.

(11) Fichtinger-Schepman, A. M. J.; Van der Veer, J. L.; Den Hartog, J. H. J.; Lohman, P. H. M.; Reedijk, J. Adducts of the Antitumor Drug cis-Diamminedichloroplatinum(II) with DNA: Formation, Identification, and Quantitation. *Biochemistry* **1985**, *24*, 707-713.

(12) Caradonna, J. P.; Lippard, S. J.; Gait, M. J.; Singh, M. The Antitumor Drug cis-Dichlorodiammineplatinum Forms an Intrastrand d(GpG) Crosslink Upon Reaction with [d(ApGpGpCpCpT)]2. *J. Am. Chem. Soc.* **1982**, *104*, 5793-5795.

(13) Gelasco, A.; Lippard, S. J. NMR Solution Structure of a DNA Dodecamer Duplex Containing a cis-Diammineplatinum(II) d(GpG) Intrastrand Cross-Link, the Major Adduct of the Anticancer Drug Cisplatin. *Biochemistry* **1998**, *37*, 9230-9239.

(14) Bianchi, M.; Beltrame, M.; Paonessa, G. Specific Recognition of Cruciform DNA by Nuclear Protein HMG1. *Science* **1989**, *243*, 1056-1059.

(15) Wang, D.; Lippard, S. J. Cellular Processing of Platinum Anticancer Drugs. *Nat. Rev. Drug Discov.* **2005**, *4*, 307.

(16) Ohndorf, U.-M.; Rould, M. A.; He, Q.; Pabo, C. O.; Lippard, S. J. Basis for Recognition of Cisplatin-Modified DNA by High-Mobility-Group Proteins. *Nature* **1999**, *399*, 708-712.

(17) Zhang, J.-G.; Lindup, W. E. Cisplatin Nephrotoxicity: Decreases in Mitochondrial Protein Sulphydryl Concentration and Calcium Uptake by Mitochondria from Rat Renal Cortical Slices. *Biochem. Pharmacol.* **1994**, *47*, 1127-1135.

(18) Barabas, K.; Milner, R.; Lurie, D.; Adin, C. Cisplatin: a Review of Toxicities and Therapeutic Applications. *Vet. Comp. Oncol.* **2008**, *6*, 1-18.

(19) Bratsos, I.; Gianferrara, T.; Alessio, E.; Hartinger, C. G.; Jakupec, M. A.; Keppler, B. K. In *Bioinorganic Medicinal Chemistry*; Eds; Wiley-VCH Verlag GmbH & Co. KGaA: 2011; pp 151-174.

(20) Ndagi, U.; Mhlongo, N.; Soliman, M. E. Metal Complexes in Cancer Therapy – an Update from Drug Design Perspective. *Drug Des. Devel. Ther.* **2017**, *11*, 599-616.

(21) Jakupec, M. A.; Galanski, M.; Arion, V. B.; Hartinger, C. G.; Keppler, B. K. Antitumour Metal Compounds: More than Theme and Variations. *Dalton Trans.* **2008**, 10.1039/B712656P.183-194.

(22) Trondl, R.; Heffeter, P.; Kowol, C. R.; Jakupec, M. A.; Berger, W.; Keppler, B. K. NKP-1339, the First Ruthenium-Based Anticancer Drug on the Edge to Clinical Application. *Chem. Sci.* **2014**, *5*, 2925-2932.

(23) Kuhn, P. S.; Pichler, V.; Roller, A.; Hejl, M.; Jakupec, M. A.; Kandioller, W.; Keppler, B. K. Improved Reaction Conditions for the Synthesis of new NKP-1339 Derivatives and Preliminary Investigations on their Anticancer Potential. *Dalton Trans.* **2015**, *44*, 659-668.

(24) Aird, R. E.; Cummings, J.; Ritchie, A. A.; Muir, M.; Morris, R. E.; Chen, H.; Sadler, P. J.; Jodrell, D. I. In Vitro and In Vivo Activity and Cross Resistance Profiles of Novel Ruthenium(II) Organometallic Arene Complexes in Human Ovarian Cancer. *Br. J. Cancer* **2002**, *86*, 1652.

(25) Scolaro, C.; Bergamo, A.; Brescacin, L.; Delfino, R.; Cocchietto, M.; Laurenczy, G.; Geldbach, T. J.; Sava, G.; Dyson, P. J. In Vitro and In Vivo Evaluation of Ruthenium(II)−Arene PTA Complexes. *J. Med. Chem.* **2005**, *48*, 4161-4171.

(26) Noffke, A. L.; Habtemariam, A.; Pizarro, A. M.; Sadler, P. J. Designing Organometallic Compounds for Catalysis and Therapy. *Chem. Commun.* **2012**, *48*, 5219-5246.

(27) Adhireksan, Z., et al. Ligand Substitutions Between Ruthenium–Cymene Compounds Can Control Protein Versus DNA Targeting and Anticancer Activity. *Nat. Commun.* **2014**, *5*, 3462.

(28) Reedijk, J. Metal-Ligand Exchange Kinetics in Platinum and Ruthenium Complexes. *Platinum Met. Rev.* **2008**, *52*, 2.

(29) Wang, F.; Chen, H.; Parsons, S.; Oswald, I. D. H.; Davidson, J. E.; Sadler, P. J. Kinetics of Aquation and Anation of Ruthenium(II) Arene Anticancer Complexes, Acidity and X-ray Structures of Aqua Adducts. *Chem. Eur. J.* **2003**, *9*, 5810-5820.

(30) Dolmans, D. E. J. G. J.; Fukumura, D.; Jain, R. K. Photodynamic Therapy for Cancer. *Nat. Rev. Cancer* **2003**, *3*, 380-387.

(31) Betanzos-Lara, S.; Salassa, L.; Habtemariam, A.; Novakova, O.; Pizarro, A. M.; Clarkson, G. J.; Liskova, B.; Brabec, V.; Sadler, P. J. Photoactivatable Organometallic Pyridyl Ruthenium(II) Arene Complexes. *Organometallics* **2012**, *31*, 3466-3479.

(32) Chen, H.; Parkinson, J. A.; Parsons, S.; Coxall, R. A.; Gould, R. O.; Sadler, P. J. Organometallic Ruthenium(II) Diamine Anticancer Complexes: Arene-Nucleobase Stacking and Stereospecific Hydrogen-Bonding in Guanine Adducts. *J. Am. Chem. Soc.* **2002**, *124*, 3064-3082.

(33) Novakova, O.; Chen, H.; Vrana, O.; Rodger, A.; Sadler, P. J.; Brabec, V. DNA Interactions of Monofunctional Organometallic Ruthenium(II) Antitumor Complexes in Cell-Free Media. *Biochemistry* **2003**, *42*, 11544-11554.

(34) Dougan, S. J.; Sadler, P. J. The Design of Organometallic Ruthenium Arene Anticancer Agents. *CHIMIA Journal* **2007**, *61*, 704-715.

(35) Schwab, P.; France, M. B.; Ziller, J. W.; Grubbs, R. H. A series of Well-Defined Metathesis Catalysts–Synthesis of [RuCl2(CHR′)(PR3)2] and Its Reactions. *Angew. Chem. Int. Ed.* **1995**, *34*, 2039-2041.

(36) Schwab, P.; Grubbs, R. H.; Ziller, J. W. Synthesis and Applications of RuCl2(CHR‘)(PR3)2: the Influence of the Alkylidene Moiety on Metathesis Activity. *J. Am. Chem. Soc.* **1996**, *118*, 100-110.

(37) Haack, K.-J.; Hashiguchi, S.; Fujii, A.; Ikariya, T.; Noyori, R. The Catalyst Precursor, Catalyst, and Intermediate in the Ru(II)-Promoted Asymmetric Hydrogen Transfer Between Alcohols and Ketones. *Angew. Chem. Int. Ed.* **1997**, *36*, 285-288.

(38) Hashiguchi, S.; Fujii, A.; Haack, K.-J.; Matsumura, K.; Ikariya, T.; Noyori, R. Kinetic Resolution of Racemic Secondary Alcohols by RuII-Catalyzed Hydrogen Transfer. *Angew. Chem. Int. Ed.* **1997**, *36*, 288-290.

(39) Yan, Y. K.; Melchart, M.; Habtemariam, A.; Peacock, A. F. A.; Sadler, P. J. Catalysis of Regioselective Reduction of NAD+ by Ruthenium(II) Arene Complexes Under Biologically Relevant Conditions. *J. Biol. Inorg. Chem.* **2006**, *11*, 483-488.

(40) Ying, W. NAD+/NADH and NADP+/NADPH in Cellular Functions and Cell Death: Regulation and Biological Consequences. *Antioxid. Redox Signal.* **2007**, *10*, 179-206.

(41) Soldevila-Barreda, J. J.; Romero-Canelón, I.; Habtemariam, A.; Sadler, P. J. Transfer Hydrogenation Catalysis in Cells as a New Approach to Anticancer Drug Design. *Nat Commun* **2015**, *6*,

(42) Canivet, J.; Süss-Fink, G.; Štěpnička, P. Water-Soluble Phenanthroline Complexes of Rhodium, Iridium and Ruthenium for the Regeneration of NADH in the Enzymatic Reduction of Ketones. *Eur. J. Inorg. Chem.* **2007**, *2007*, 4736-4742.

(43) Peacock, A. F. A.; Sadler, P. J. Medicinal Organometallic Chemistry: Designing Metal Arene Complexes as Anticancer Agents. *Chem. Asian J.* **2008**, *3*, 1890-1899.

(44) Liu, H.-K.; Berners-Price, S. J.; Wang, F.; Parkinson, J. A.; Xu, J.; Bella, J.; Sadler, P. J. Diversity in Guanine-Selective DNA Binding Modes for an Organometallic Ruthenium Arene Complex. *Angew. Chem. Int. Ed.* **2006**, *45*, 8153-8156.

(45) Liu, H.-K.; Wang, F.; Parkinson, J. A.; Bella, J.; Sadler, P. J. Ruthenation of Duplex and Single-Stranded d(CGGCCG) by Organometallic Anticancer Complexes. *Chem. Eur. J.* **2006**, *12*, 6151-6165.

(46) Novakova, O.; Kasparkova, J.; Bursova, V.; Hofr, C.; Vojtiskova, M.; Chen, H.; Sadler, P. J.; Brabec, V. Conformation of DNA Modified by Monofunctional Ru(II) Arene Complexes: Recognition by DNA Binding Proteins and Repair. Relationship to Cytotoxicity. *Chem. Biol.* **2005**, *12*, 121-129.

(47) Dougan, S. J.; Melchart, M.; Habtemariam, A.; Parsons, S.; Sadler, P. J. Phenylazo-pyridine and Phenylazo-pyrazole Chlorido Ruthenium(II) Arene Complexes: Arene Loss, Aquation, and Cancer Cell Cytotoxicity. *Inorg. Chem.* **2006**, *45*, 10882-10894.

(48) Peacock, A. F. A.; Parsons, S.; Sadler, P. J. Tuning the Hydrolytic Aqueous Chemistry of Osmium Arene Complexes with N,O-Chelating Ligands to Achieve Cancer Cell Cytotoxicity. *J. Am. Chem. Soc.* **2007**, *129*, 3348-3357.

(49) Bruijnincx, P. C. A.; Sadler, P. J. Controlling Platinum, Ruthenium and Osmium Reactivity for Anticancer Drug Design. *Adv. Inorg. Chem.* **2009**, *61*, 1-62.

(50) Wang, F., et al. Controlling Ligand Substitution Reactions of Organometallic Complexes: Tuning Cancer Cell Cytotoxicity. *Proc. Natl. Acad. Sci. U. S. A.* **2005**, *102*, 18269-18274.

(51) Petzold, H.; Xu, J.; Sadler, P. J. Metal and Ligand Control of Sulfenate Reactivity: Arene Ruthenium Thiolato-Mono-S-Oxides. *Angew. Chem. Int. Ed.* **2008**, *47*, 3008-3011.

(52) Fernández, R.; Melchart, M.; Habtemariam, A.; Parsons, S.; Sadler, P. J. Use of Chelating Ligands to Tune the Reactive Site of Half-Sandwich Ruthenium(II)–Arene Anticancer Complexes. *Chem. Eur. J.* **2004**, *10*, 5173-5179.

(53) Betanzos-Lara, S.; Novakova, O.; Deeth, R.; Pizarro, A.; Clarkson, G.; Liskova, B.; Brabec, V.; Sadler, P.; Habtemariam, A. Bipyrimidine Ruthenium(II) Arene Complexes: Structure, Reactivity and Cytotoxicity. *J. Biol. Inorg. Chem.* **2012**, *17*, 1033-1051.

(54) Chen, H.; Parkinson, J. A.; Morris, R. E.; Sadler, P. J. Highly Selective Binding of Organometallic Ruthenium Ethylenediamine Complexes to Nucleic Acids: Novel Recognition Mechanisms. *J. Am. Chem. Soc.* **2003**, *125*, 173-186.

(55) Peacock, A. F. A.; Habtemariam, A.; Fernández, R.; Walland, V.; Fabbiani, F. P. A.; Parsons, S.; Aird, R. E.; Jodrell, D. I.; Sadler, P. J. Tuning the Reactivity of Osmium(II) and Ruthenium(II) Arene Complexes under Physiological Conditions. *J. Am. Chem. Soc.* **2006**, *128*, 1739-1748.

(56) Melchart, M.; Habtemariam, A.; Parsons, S.; Moggach, S. A.; Sadler, P. J. Ruthenium(II) Arene Complexes Containing Four- and Five-Membered Monoanionic O,O-Chelate Rings. *Inorg. Chim. Acta* **2006**, *359*, 3020-3028.

(57) Peacock, A. F. A.; Melchart, M.; Deeth, R. J.; Habtemariam, A.; Parsons, S.; Sadler, P. J. Osmium(II) and Ruthenium(II) Arene Maltolato Complexes: Rapid Hydrolysis and Nucleobase Binding. *Chem. Eur. J.* **2007**, *13*, 2601-2613.

(58) Hesketh, R. *Introduction to Cancer Biology*; Cambridge University Press: Cambridge, 2012.

(59) Hanahan, D.; Weinberg, R. A. The Hallmarks of Cancer. *Cell* **2000**, *100*, 57-70.

(60) Hanahan, D.; Weinberg, Robert A. Hallmarks of Cancer: The Next Generation. *Cell* **2011**, *144*, 646-674.

(61) Warburg, O.; Wind, F.; Negelein, E. The Metabolism of Tumors in the Body. *J. Gen. Physiol.* **1927**, *8*, 519-530.

(62) Warburg, O. The Chemical Constitution of Respiration Ferment. *Science* **1928**, *68*, 437-443.

(63) Warburg, O. On the Origin of Cancer Cells. *Science* **1956**, *123*, 309-314.

(64) Chen, X.; Qian, Y.; Wu, S. The Warburg Effect: Evolving Interpretations of an Established Concept. *Free Radical Biol. Med.* **2015**, *79*, 253-263.

(65) Vander Heiden, M. G.; Cantley, L. C.; Thompson, C. B. Understanding the Warburg Effect: The Metabolic Requirements of Cell Proliferation. *Science* **2009**, *324*, 1029-1033.

(66) Ngo, H.; Tortorella, S.; Ververis, K.; Karagiannis, T. The Warburg Effect: Molecular Aspects and Therapeutic Possibilities. *Mol. Biol. Rep.* **2015**, *42*, 825-834.

(67) Cantor, J. R.; Sabatini, D. M. Cancer Cell Metabolism: One Hallmark, Many Faces. *Cancer Discov.* **2012**, *2*, 881-898.

(68) Luc, R.; Tortorella, S.; Ververis, K.; Karagiannis, T. Lactate as an Insidious Metabolite due to the Warburg Effect. *Mol. Biol. Rep.* **2015**, *42*, 835-840.

(69) Hirschhaeuser, F.; Sattler, U. G. A.; Mueller-Klieser, W. Lactate: A Metabolic Key Player in Cancer. *Cancer Res.* **2011**, *71*, 6921-6925.

(70) Gillies, R. J.; Raghunand, N.; Karczmar, G. S.; Bhujwalla, Z. M. MRI of the Tumor Microenvironment. *J. Magn. Reson. Imaging* **2002**, *16*, 430-450.

(71) Gatenby, R. A.; Gillies, R. J. Why Do Cancers Have High Aerobic Glycolysis? *Nat. Rev. Cancer* **2004**, *4*, 891-899.

(72) Xu, X. D.; Shao, S. X.; Jiang, H. P.; Cao, Y. W.; Wang, Y. H.; Yang, X. C.; Wang, Y. L.; Wang, X. S.; Niu, H. T. Warburg Effect or Reverse Warburg Effect? A Review of Cancer Metabolism. *Oncol. Res. Treat.* **2015**, *38*, 117-122.

(73) Parks, S. K.; Chiche, J.; Pouyssegur, J. pH Control Mechanisms of Tumor Survival and Growth. *J. Cell. Physiol.* **2011**, *226*, 299-308.

(74) Stephan, J. R.; Rosa, A. C.; Salvador, H. Na+-H+ Exchanger, pH Regulation and Cancer. *Recent Pat. Anticancer Drug Discov.* **2013**, *8*, 85-99.

(75) Cardone, R. A.; Casavola, V.; Reshkin, S. J. The Role of Disturbed pH Dynamics and the Na+/H+ Exchanger in Metastasis. *Nat. Rev. Cancer* **2005**, *5*, 786-795.

(76) Huber, V., et al. Proton Dynamics in Cancer. *J. Transl. Med.* **2010**, *8*, 57.

(77) Pizarro, A. M.; Melchart, M.; Habtemariam, A.; Salassa, L.; Fabbiani, F. P. A.; Parsons, S.; Sadler, P. J. Controlling the Reactivity of Ruthenium(II) Arene Complexes by Tether Ring-Opening. *Inorg. Chem.* **2010**, *49*, 3310-3319.

(78) Stodt, R.; Gencaslan, S.; Müller, Iris M.; Sheldrick, William S. Preparation, Reactivity and Peptide Labelling Properties of (η6-Arene)ruthenium(II) Complexes with Pendant Carboxylate Groups. *Eur. J. Inorg. Chem.* **2003**, *2003*, 1873-1882.

(79) Melchart, M.; Habtemariam, A.; Novakova, O.; Moggach, S. A.; Fabbiani, F. P. A.; Parsons, S.; Brabec, V.; Sadler, P. J. Bifunctional Amine-Tethered Ruthenium(II) Arene Complexes Form Monofunctional Adducts on DNA. *Inorg. Chem.* **2007**, *46*, 8950-8962.

(80) Reiner, T.; Jantke, D.; Miao, X.-H.; Marziale, A. N.; Kiefer, F. J.; Eppinger, J. Phenylalanine - a Biogenic Ligand with Flexible η6- and η6:κ1-Coordination at Ruthenium(II) Centres. *Dalton Trans.* **2013**, *42*, 8692-8703.

(81) Miyaki, Y.; Onishi, T.; Kurosawa, H. Synthesis and Reaction of Ruthenium(II) Complexes Containing Heteroatom Donor (O, N, and P) Tethered to η6-Arene Ring. *Inorg. Chim. Acta* **2000**, *300–302*, 369-377.

(82) Lastra-Barreira, B.; Diez, J.; Crochet, P.; Fernandez, I. Functionalized Arene-Ruthenium(II) Complexes: Dangling vs. Tethering Side Chain. *Dalton Trans.* **2013**, *42*, 5412-5420.

(83) Bennett, M. A.; Edwards, A. J.; Harper, J. R.; Khimyak, T.; Willis, A. C. Synthesis, Structure and Redox Behaviour of Tethered Arene–Ruthenium(II) Complexes. *J. Organomet. Chem.* **2001**, *629*, 7-18.

(84) Navarro, M.; Vidal, D.; Clavero, P.; Grabulosa, A.; Muller, G. Mild Photochemical Tethering of [RuCl2(η6-arene)P*] Complexes with P-Stereogenic 2-Biphenylylphosphines. *Organometallics* **2015**, *34*, 973-994.

(85) Çetinkaya, B.; Demir, S.; Özdemir, I.; Toupet, L.; Sémeril, D.; Bruneau, C.; Dixneuf, P. H. η6-Mesityl,η1-Imidazolinylidene–Carbene–Ruthenium(II) Complexes: Catalytic Activity of their Allenylidene Derivatives in Alkene Metathesis and Cycloisomerisation Reactions. *Chem. Eur. J.* **2003**, *9*, 2323-2330.

(86) Adams, J. R.; Bennett, M. A. Transition Metal Complexes of Tethered Arenes. *Adv. Organomet. Chem.* **2006**, *54*, 293-331.

(87) Smith, P. D.; Wright, A. H. Synthesis and Structure of a Chelating Arene–Ruthenium Complex [RuCl2(PPh2(CH2)3-η6-C6H5)]. *J. Organomet. Chem.* **1998**, *559*, 141-147.

(88) Rabideau, P. W.; Wetzel, D. M.; Young, D. M. Metal-Ammonia Ring Reduction of Aromatic Carboxylic Acid Esters. *J. Org. Chem.* **1984**, *49*, 1544-1549.

(89) Pertici, P.; Bertozzi, S.; Lazzaroni, R.; Vitulli, G.; Bennett, M. A. A Simple Method of Regenerating Arene Ruthenium Dichloride Dimers, [RuCl2(η6-arene)]2, From their Monomeric Adducts with Amines or Tertiary Phosphines, RuCl2(η6-arene)L. *J. Organomet. Chem.* **1988**, *354*, 117-121.

(90) Mashima, K.; Kusano, K.-h.; Sato, N.; Matsumura, Y.-i.; Nozaki, K.; Kumobayashi, H.; Sayo, N.; Hori, Y.; Ishizaki, T. Cationic BINAP-Ru(II) Halide Complexes: Highly Efficient Catalysts for Stereoselective Asymmetric Hydrogenation of α- and β-Functionalized Ketones. *J. Org. Chem.* **1994**, *59*, 3064-3076.

(91) Therrien, B.; Ward, T. R.; Pilkington, M.; Hoffmann, C.; Gilardoni, F.; Weber, J. Synthesis and Reactivity of Tethered η1:η6-(Phosphinoarene)ruthenium Dichlorides. *Organometallics* **1998**, *17*, 330-337.

(92) Ghebreyessus, K. Y.; Nelson, J. H. Base-Promoted Hydroalkylation Reactions of 1,3,5-Me3C6H3, p-MeC6H4CHMe2, C6Me6, p-MeC6H4Me, and MeC6H5 Ligands Coordinated to Ruthenium(II). *Organometallics* **2000**, *19*, 3387-3392.

(93) Margiotta, N.; Habtemariam, A.; Sadler, P. J. Strong, Rapid Binding of a Platinum Complex to Thymine and Uracil Under Physiological Conditions. *Angew. Chem. Int. Ed.* **1997**, *36*, 1185-1187.

(94) Abraha Habtemarian, S. B.-L., and Peter J. Sadler. *Ruthenium Complexes, in Inorganic Syntheses*; John Wiley & Sons: 2010.

(95) Molas Saborit, J.; Caubet, A.; Brissos, R. F.; Korrodi-Gregorio, L.; Perez-Tomas, R.; Martinez, M.; Gamez, P. pH-Driven Preparation of Two Related Platinum(II) Complexes Exhibiting Distinct Cytotoxic Properties. *Dalton Trans.* **2017**, *46*, 11214-11222.

(96) Lindner, R.; van den Bosch, B.; Lutz, M.; Reek, J. N. H.; van der Vlugt, J. I. Tunable Hemilabile Ligands for Adaptive Transition Metal Complexes. *Organometallics* **2011**, *30*, 499-510.

(97) Angell, S. E.; Rogers, C. W.; Zhang, Y.; Wolf, M. O.; Jones, W. E. Hemilabile Coordination Complexes for Sensing Applications. *Coord. Chem. Rev.* **2006**, *250*, 1829-1841.

2.

Synthesis, Structure, Characterization and Activation of Tethered Complexes. A SAR Study.

2.1 Introduction

The first part of this Chapter is devoted to an introduction towards the rational design of the hemilabile ligand, which plays a crucial role triggering the activation of Ru^{II} tethered complexes. Different structural modifications on this ligand were proposed in an attempt to control the Ru–Z bond activation. In the second part of the Chapter, the synthesis and structural characterization of Ru^{II} tethered complexes after complexation with different hemilabile and/or XY chelating ligands is presented and discussed. Moreover, acidic activation of a series of complexes was investigated by means of ^{1}H NMR to develop a structure-activation relationship of a variety Ru^{II}-tether scaffolds retaining ethylenediamine as the XY chelate on the metal.

2.1.2 The Hemilabile Arene:Z Ligand

The term "hemilabile ligand" was first introduced in synthetic chemistry in 1979 by Jeffrey and Rauchfuss.[1] Since then, a broad range of coordinating groups of different reactivity has been synthesized and complexed to various metal centres, and several reviews have highlighted the versatile coordination chemistry with various types of scaffolds.[2, 3] This hemilabile ligand, that contains both substitutionally inert and labile groups, forms a chelate with the metal centre (Figure 2.1).

The reason behind studying hemilabile ligands relates to their ability to provide open coordination sites at the metal through a weak and reversible bonding interaction of specific donor groups. In fact, the small energy differences (often in the order of 50 kJ mol^{-1}) involved in the dynamic reversible process of bond breaking and bond making forms the basis of hemilabity conferring to these systems interesting properties.[2]

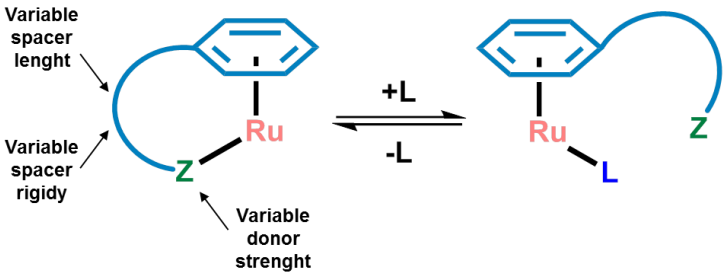

Figure 2.1. Representation of a hemilabile ligand in a Ru^{II} complex. The arene group binds strongly to the metal centre while the Z atom is labile, offering the possibility of dissociation of the metal in a reversible way. The hemilability of the Ru–Z bond can be tuned by varying the spacer length, the spacer rigidity, and the donor binding strength. Sustituents of different nature on the arene as well as the remaining ligands will also swift the lability of the Ru–Z bond (vide infra).

Although such aspects will not be discussed here, it is interesting to note that some metalloenzymes operate through a mechanism of activation similar to hemilability; for example, the opening of a zinc-cysteine bond allowing coordination of a water molecule occurs when going from an inactive to an active form of the metalloenzyme.[4, 5]

The modification of both steric and electronic effects of the tether arm (spacer) provides an important modulation approach for a rational design of hemilabile ligands. Since we are developing these complexes for aqueous-based reactivity, we have focused on the modulation of the pK_a of the labile donor group Z (ZH^+/Z), to provide complexes whose hemilabile chelate allows protonation and depronation upon dissociation from the metal depending on the surrounding pH. This requirement is key to produce complexes susceptible to undergo activation of a coordination site in order to further interact with a biomolecule (or solvent molecule) taking into account the biological context of the cancer cell, this is, the slight acidic extracellular pH.

2.1.3 Acid-Base Properties of Z in the Hemilabile Ligand

2.1.3.1 The Acid-Base Equilibrium. The pK_a

The main feature of the hemilabile ligand is the presence of the two distinguished groups, one of them weakly bound (Z) to the metal centre offering the possibility to de-coordinate from the metal atom. This dissociation can be followed (and perhaps controlled) by a protonation/deprotonation process in the labile group, this is, an acid-base reaction. The possibility of controlling Ru–Z activation by the acidity of Z has brought us to investigate which would be good candidates for our switchable system. Three functional groups appear most appropriate for our system (because of other functional groups are too weak to behave as acids or bases in aqueous solution): amines ($pK_a \approx 11$), phenols ($pK_a \approx 10$) and carboxylic acids ($pK_a \approx 5$).

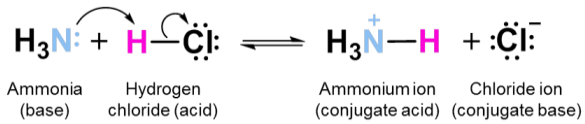

Figure 2.2. Acid-base reaction between ammonia and hydrogen chloride.

As the typical example of Brønsted-Lowry acid-base reactions shown in Figure 2.2, hydrogen chloride (HCl), the acid, donates a proton to ammonia ($:NH_3$), the base. The chloride ion is the *conjugate base* and ammonium ion is the *conjugate acid*.

Acids differ in their ability to donate H^+. Stronger acids, such as HCl, react almost completely with water, whereas weaker acids, such as acetic acid (CH_3CO_2H), react only slightly. The strength of an acid HA dissolved in water is measured by its acidity constant (K_a) for the acid-dissociation equilibrium (equation 2.1).[6]

$$HA + H_2O \rightleftharpoons A^- + H_3O^+$$

$$K_a = \frac{[H_3O^+]\ [A^-]}{[HA]}$$

Equation 2.1

A large value of K_a means the acid is a strong acid, and a small value of K_a means the acid is a weak acid. A convenient way to express the strength of an acid is by its pK_a defined in equation 2.2.[6] A stronger acid (larger K_a) has a smaller pK_a, and a weaker acid (smaller K_a) has a larger pK_a.

$$pK_a = -\log K_a$$

Equation 2.2

Table 2.1 lists the pK_a values of some common acids in order of their strength. As shown in the table the stronger the acid, the weaker its conjugate base. The stronger the base, the weaker its conjugate acid.

Table 2.1. Relative strengths of some common acids and their conjugate bases.[7]

	Acid	Name	pK_a	Conjugate Base	Name	
Weaker acid	CH_3CH_2OH	Ethanol	16.00	$CH_3CH_2O^-$	Ethoxide ion	Stronger base
	H_2O	Water	14.00	HO^-	Hydroxide ion	
	HCN	Hydrocyanic acid	9.31	CN^-	Cyanide ion	
	H_2PO^{4-}	Dihydrogen phosphate ion	7.21	HPO_4^{2-}	Acetate ion	
	CH_3CO_2H	Acetic acid	4.76	$CH_3CO_2^-$	Hydrogen phosphate ion	
	H_3PO_4	Phosphoric acid	2.16	H_2PO^{4-}	Dihydrogen phosphate ion	
	HNO_3	Nitric acid	-1.30	NO_3^-	Nitrate ion	
Stronger acid	HCl	Hydrochloric acid	-7.00	Cl^-	Chloride ion	Weaker base

2.1.3.2 Amines

Amines are driven to equilibrium in aqueous solution, where water acts as an acid and transfers a proton to the amine. The basic strength of an amine can be measured by the basicity constant K_b (Equation 2.3). The larger the value of K_b, the smaller the value of pK_b. Thus, the more favorable the proton-transfer equilibrium, the stronger the base.

$$RNH_2 + H_2O \rightleftharpoons RNH_3^+ + HO^-$$

$$K_b = \frac{[RNH_3^+][HO^-]}{[RNH_2]}$$

$$pK_b = -\log K_b$$

Equation 2.3

In practice, K_b values are not often used. Instead, the most convenient way to measure the basicity of an amine (RNH_2) is to look at the acidity of the corresponding ammonium ion (RNH_3^+) as represented in Equation 2.4. The more acidic the ammonium ion, the less tightly the proton is held and the weaker the corresponding base. That is, a weaker base has an ammonium ion with a smaller pK_a and a stronger base has an ammonium ion with a larger pK_a.

$$RNH_3^+ + H_2O \rightleftharpoons RNH_2 + H_3O^+$$

$$K_a = \frac{[RNH_2][H_3O^+]}{[RNH_3^+]}$$

$$pK_a = -\log K_a$$

Equation 2.4.

Table 2.2 lists pK_a values of the ammonium ions of a variety of amines and indicates that there is a substantial range of amine basicities. It is shown that arylamines are considerably less basic that alkylamines.[7]

Table 2.2. Basicity of some common amines.

	Name	Structure	pK_a of the ammonium cation	
Aromatic Amines	Aniline	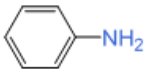	4.63	Weaker base
	Piridine		5.25	
Aliphatic Amines	Ammonia	NH_3	9.26	
	Methylamine	CH_3NH_2	10.64	
	Triethylamine	$(CH_3CH_2)_3N$	10.76	
	Diethylamine	$(CH_3CH_2)_2NH$	10.98	Stronger base

2.1.3.3 Alcohols and Carboxylic Acids

The acidity of alcohols vary widely, from alcohols that are about as acidic as water to some that are orders of magnitud less acidic, as displayed in Table 2.3. Phenols are about 10^6 times more acidic than alcohols because the phenoxide anion is resonance-stabilized. Both alcohols and phenols may dissociate in aqueous solution by donating a proton to water, generating H_3O^+ and an alkoxide ion, RO^-, and phenoxide ion, ArO^-, respectively.

With pK_a values of ca. 5, carboxylic acids are much stronger acids than water and alcohols. Like other Brønsted-Lowry acids, carboxylic acids dissociate in aqueous solutions to give H_3O^+ and the corresponding carboxylate anions, RCO_2^-. The extent of dissociation is given again by the acidity constant, K_a. Table 2.3 represents the acidity of some carboxylic acids in comparison with alcohols.[7]

Table 2.3. Acidity of some alcohols and carboxylic acids.

	Structure	pK_a	
Alcohols	CH_3CH_2OH	16	Weaker acid
	CH_3OH	15.54	
	H_2O	14	
	CF_3CH_2OH	12.43	
	Phenol	9.89	
	p-Nitrophenol	7.15	
Carboxylic Acids	$CH_3CH_2CO_2H$	4.87	
	CH_3CO_2H	4.76	
	$C_6H_5CO_2H$	4.19	
	HCO_2H	3.75	Stronger acid

2.1.4 Scope of This Chapter

We have selected a number of hemilabile ligands to bind ruthenium(II) to explore the effect of the formerly discussed considerations for Ru–Z bond activation, namely, length and rigidity of the spacer, nature of the donor atom that closes the tether, and the acidity of its protonated form. In order to fully investigate such an effect and its tuneability we have studied variation of another crucial building block in this structure, i.e. the XY ligand. This serves as starting point for the exploration of the effect of the XY in the Ru–Z bond activation and will be expanded later in this Thesis.

2.2 Results and Discussion

2.2.2 Selection of Hemilabile Ligands

A series of hemilabile ligands (Table 2.4) were chosen considering several structural features. First, donor atoms (Z) were preferred to be nitrogen and oxygen according to their reported affinity for Ru^{II}. Second, ligands with a wide range of pK_a (3.8–15.2) were selected to investigate the influence of the acidity of ZH^+ in the ring opening mechanism. For nitrogen-based ligands the pK_a corresponds to the cation ZH^+ (e.g. RNH_3^+ and pyH^+), while for alcohols and carboxylic acids the pK_a correspond to the ROH and RCOOH species, respectively. Finally, different length size and rigidity of the tether arm were considered to study their relationship with the lability of the Ru–Z bond. The Ru^{II} tether complexes synthesized with these hemilabile ligands were classified in three groups attending to the type of functional group (Z) coordinated to the metallic centre, i.e. amines, alcohols and carboxylic acids.

Table 2.4. Proposed hemilabile ligands to be studied in this Thesis ordered by increasing pK_a. The indicated pK_a for the amines corresponds to the pK_a of their conjugated acid.

Molecule	pK_a	Molecule	pK_a
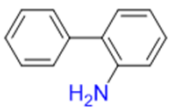	3.8	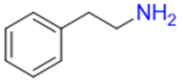	9.9
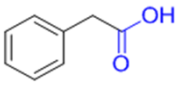	4.3	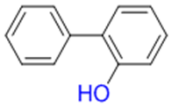	10.0
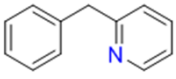	4.9	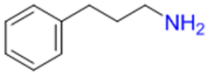	10.3
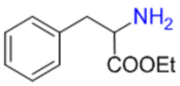	7.3	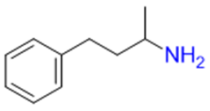	10.6
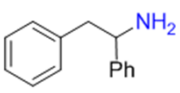	8.8	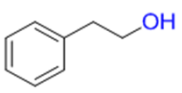	15.2

2.2.3 Tethering Amines

2.2.3.1 Synthesis and Characterization

Fourteen Ru^{II} tethered complexes of the type $[Ru(\eta^6{:}\kappa^1\text{-arene:N})(XY)]^{0/+2}$ (Figure 2.4 and Table 2.5), where the hemilabile ligand or arene:N is 1-methyl-3-phenylpropylamine (**1**–**3**), 3-phenyl-1-propylamine (**4**–**6**), 2-phenylethylamine (**7**), 1,2-diphenylethylamine (**8**), 2-benzylpyridine (**9**–**12**) or 2-aminobiphenyl (**13**–**14**), and XY is the chelating ligand ethylenediamine (en), 1,3-diaminopropane (dap), *N*,*N*-diethylethylenediamine (deen), 1,10-phenantroline (phen), *o*-phenylendiamine (*o*-pda) or oxalate (oxo) were synthesized in good yields by reaction of different chelating ligands with the appropriate dichlorido complex $[Ru(\eta^6\text{-arene:N})Cl_2]$. This precursor dichlorido complex was synthesized according to the route employed by Melchart et al.,[8] and indicated in Scheme 2.1, which involves the thermal displacement of ethyl benzoate (etb) from $[Ru(\eta^6\text{-etb})Cl_2]_2$ by the convenient nitrogen-donor derivative (synthetic path 1, Chapter 1). Subsequent reaction with the corresponding XY chelating ligand afforded closed complexes **1**–**14**. Detailed synthetic procedures are explained in the Experimental Section at the end of this Chapter. Complexes were characterized by elemental analysis, ^{1}H NMR spectroscopy and/or ESI-MS spectroscopy. The molecular structures of **5**–**7**, **9**, **12** and **13** were determined by single crystal X-ray diffraction (vide infra).

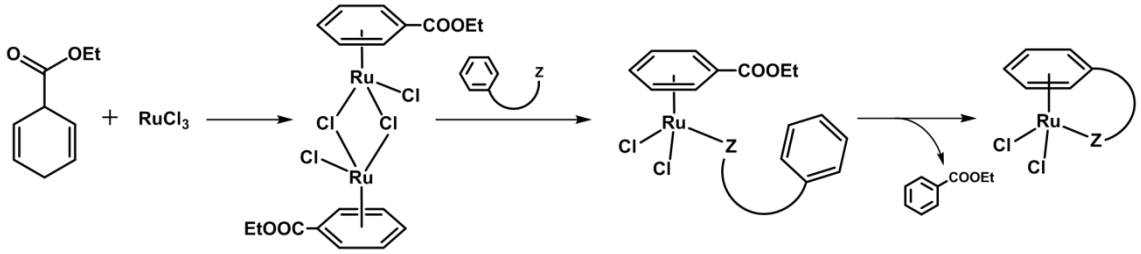

Scheme 2.1

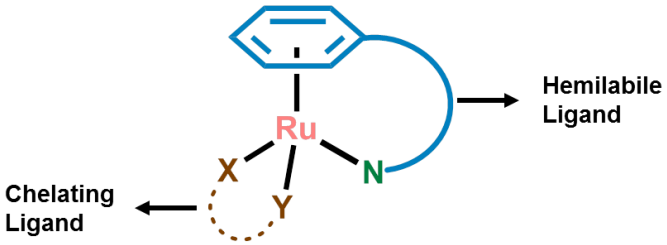

Figure 2.4. General structure for closed tethered complexes of formula [Ru(η^6:κ^1-arene:N)(XY)]$^{0/+2}$.

Table 2.5. Hemilabile ligands and XY-chelating ligands used in this Chapter for the synthesis of tethered complexes **1**–**14**.

Complex	Hemilabile Ligand	XY Chelating Ligand	Complex	Hemilabile Ligand	XY Chelating Ligand
1	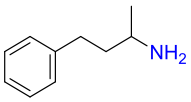	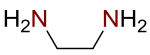	**8**	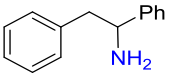	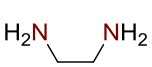
2	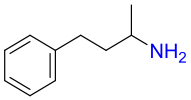	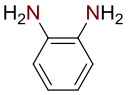	**9**	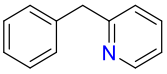	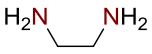
3	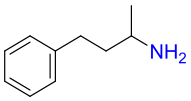	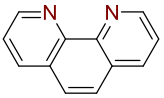	**10**	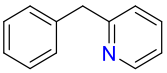	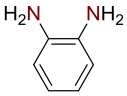
4	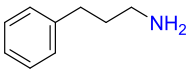	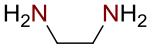	**11**	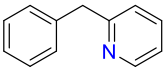	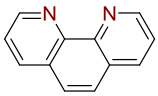
5	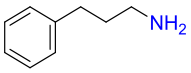	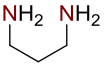	**12**	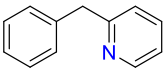	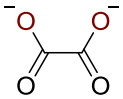
6	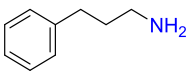	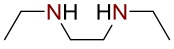	**13**	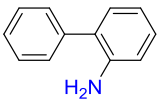	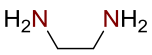
7	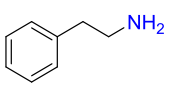	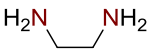	**14**	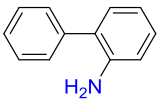	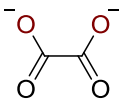

The ^{1}H NMR spectra of the tethered complexes in D_2O at 298 K proved η^6-coordination of the corresponding arene ligand to the metal. Coordination of the amine to the metal centre was verified by a typical NMR pattern of the η^6-bound arene resonances in the aromatic region. Three characteristic peaks (triplet:doublet:triplet in a

ratio 2:2:1) were assigned to these η^6-coordinated arene ring protons. These characteristic signals for the η^6-bound arene in the complexes were upfield-shifted (ca. 1.8 ppm) in all cases with regard to those of the free ligands. Moreover, the large distance between the most deshielded and most shielded η^6-bound arene signals (ca. 0.8 ppm) evidenced coordination of Z to the metal centre. Crystallographic structures confirmed unequivocally the structure of these complexes.

2.2.3.2 X-Ray Crystallography

Suitable crystals for X-ray diffraction studies were obtained from slow diffusion of diethyl ether into methanol solutions or slow evaporation of water solutions. The crystal structures of complexes [Ru{η^6:κ^1-$C_6H_5(CH_2)_3NH_2$}(dap)]Cl_2 (**5**), [Ru{η^6:κ^1-$C_6H_5(CH_2)_3NH_2$}(deen)]Cl_2 (**6**), [Ru{η^6:κ^1-$C_6H_5(CH_2)_2NH_2$}(en)]Cl_2 (**7**), [Ru{η^6:κ^1-$C_6H_5CH_2(C_5H_4N)$}(en)]Cl_2 (**9**), [Ru{η^6:κ^1-$C_6H_5(CH_2)C_5H_4N$}(oxo)] (**12**) and [Ru{η^6:κ^1-$C_6H_5(C_6H_4)NH_2$}(en)]Cl_2 (**13**) were determined by X-ray diffraction. Their molecular structures and numbering schemes are shown in Figure 2.5. The crystallographic structure of complex [Ru{η^6:κ^1-$C_6H_5(C_6H_4)NH_2$}(oxo)] (**14**) has been published previously and its crystallographic data have been used here for comparative reasons.[9] Selected bond lengths and angles are given in Table 2.6, and the crystallographic data are listed in Appendix II.

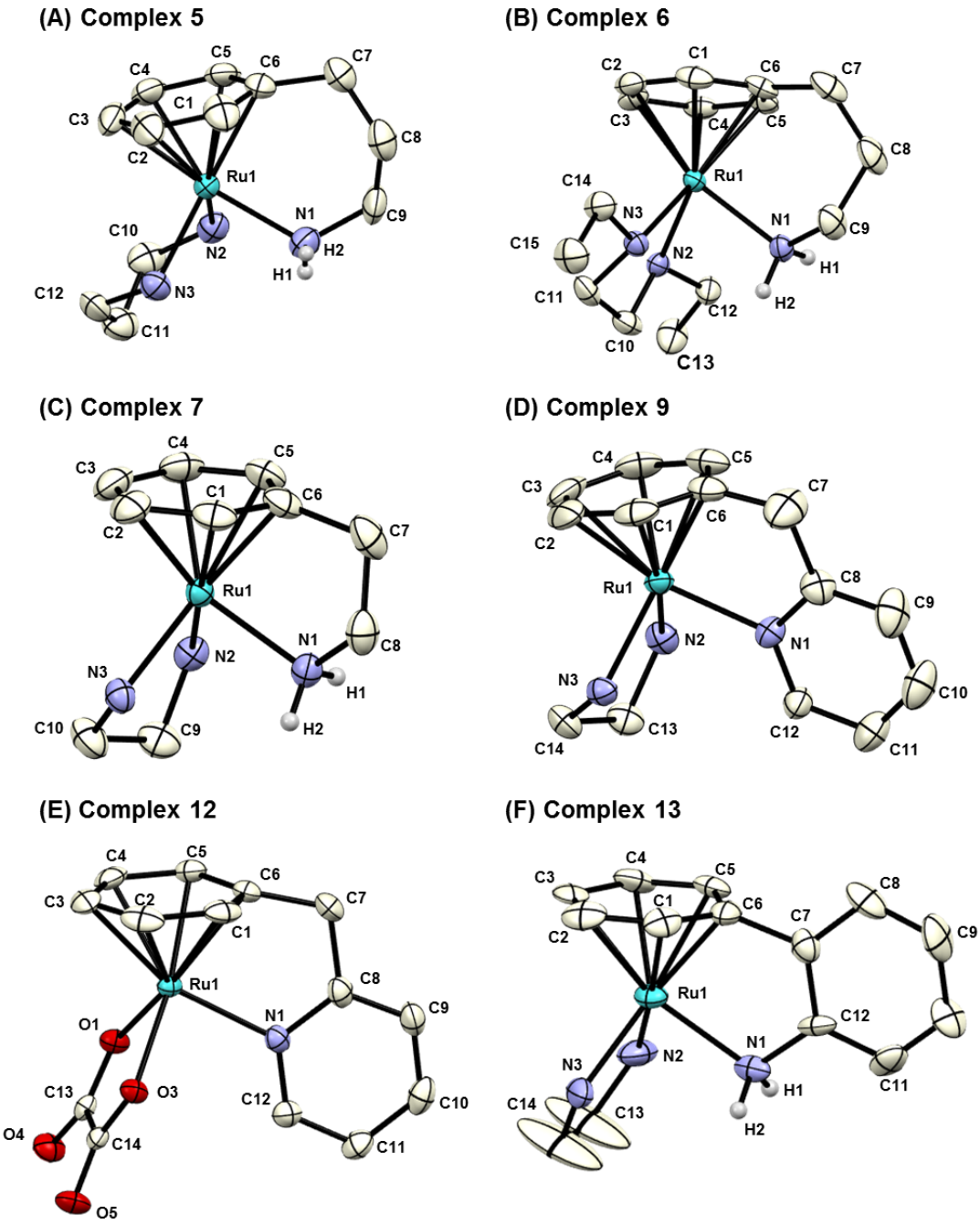

Figure 2.5. X-ray structures and atom numbering schemes for complexes (A) [Ru{η^6:κ^1-$C_6H_5(CH_2)_3NH_2$}(dap)]Cl_2 (**5**), (B) [Ru{η^6:κ^1-$C_6H_5(CH_2)_3NH_2$}(deen)]Cl_2 (**6**), (C) [Ru{η^6:κ^1-$C_6H_5(CH_2)_2NH_2$}(en)]Cl_2 (**7**), (D) [Ru{η^6:κ^1-$C_6H_5CH_2(C_5H_4N)$}(en)]Cl_2 (**9**), (E) [Ru{η^6:κ^1-$C_6H_5CH_2(C_5H_4N)$}(oxo)] (**12**) and (F) [Ru{η^6:κ^1-$C_6H_5(C_6H_4)NH_2$}(en)]Cl_2 (**13**). The hydrogen atoms and counterions have been omitted for clarity (except on the nitrogen of the tether arm).

Table 2.6. Selected bond lenghts (Å) and angles (deg) for complexes **5**–**6**, **7**, **9** and **12**–**14**.

Bond / angle	5	6	7	9	12	13	14[14]
Ru-C6	2.202(2)	2.188(7)	2.125(2)	2.117(5)	2.165(5)	2.115(13)	2.104(2)
Ru-C5	2.186(2)	2.178(7)	2.175(2)	2.182(5)	2.157(5)	2.184(13)	2.160(2)
Ru-C4	2.181(2)	2.194(7)	2.186(2)	2.176(4)	2.168(5)	2.207(14)	2.174(3)
Ru-C3	2.197(2)	2.187(7)	2.203(2)	2.195(5)	2.197(5)	2.221(15)	2.214(2)
Ru-C2	2.192(2)	2.194(7)	2.183(2)	2.175(5)	2.163(5)	2.198(13)	2.192(2)
Ru-C1	2.197(2)	2.194(7)	2.176(2)	2.163(5)	2.111(4)	2.191(13)	2.159(2)
Ru-centroid	1.679	1.679	1.651	1.652	1.637	1.659	1.635
Ru-X	2.1433(18)	2.136(5)	2.1238(17)	2.143(3)	2.092(3)	2.144(11)	2.081(1)
Ru-Y	2.1470(19)	2.122(5)	2.1258(19)	2.116(3)	2.096(3)	2.148(11)	2.076(1)
Ru-N1	2.1372(18)	2.138(7)	2.1269(17)	2.121(4)	2.136(4)	2.161(11)	2.131(2)
X-Ru-Y	80.32(7)	85.5(2)	79.49(7)	78.83(13)	77.81(11)	80.4(4)	78.42(6)
X-Ru-N1	87.56(7)	85.2(2)	86.61(8)	91.65(13)	90.23(13)	88.2(4)	86.19(6)
Y-Ru-N1	84.19(7)	87.1(3)	89.51(7)	90.19(14)	89.29(13)	88.0(4)	86.63(7)
Ru-C6-C7	126.41	126.41	114.49	114.44	115.37	112.82	112.19
C7-offset[a]	0.147 (+)	0.112 (+)	0.446 (+)	0.436 (+)	0.423 (+)	0.488 (+)	0.481 (+)

[a] Offset of C7 with respect to the plane formed by the bound arene (carbons C1–C6); (+) toward ruthenium

The structures are similar, and all the complexes adopt the "piano stool" type of geometry common to several other ruthenium(II) arene compounds.[10, 11] The arene ligands display the usual π-bonded η^6-coordination mode, whereas the XY chelating ligand assumes a bidentate-chelate coordination mode, occupying two coordination positions. The last place in the coordination sphere is occupied by the nitrogen atom pendant from the tethered arene. This resulted in an additional chelate (5-membered) in the structure. Complexes **5**, **6**, **7** and **9** crystallized with four independent molecules in the unit cell, while complex **13** crystallized with six molecules. The structure of **12** showed dimer formation between equivalent molecules. The Cl^- counterions in the crystal structures of **5**–**7** and **13** were extensively involved in H-bonding to the N_{tether} hydrogen atoms (N–H···Cl distances of 2.310–2.854 Å) and to the hydrogens atoms on the nitrogen of the chelating ligands (N–H···Cl distances in the range 2.325–2.575 Å). Only the crystal structure of complex **12** showed intermolecular π-π interaction between the pyridines of adjacent molecules with a distance between pyridine centroids of 3.544 Å.

The Ru–C_{arene} bond lengths were in the range of 2.104(2)–2.221(15) Å. The Ru–centroid distances for the different complexes fell into a narrow interval (1.635–1.679 Å) and were comparable with similar tethered complexes (e.g. [Ru{η^6:κ^1-$C_6H_5(CH_2)_3NH_2$}Cl_2],[12] [Ru{η^6:κ^1-$C_6H_5(CH_2)_2NH_2$}Cl_2][8] and [Ru{η^6:κ^1-$C_6H_5(C_6H_6N)$}Cl_2],[13] for comparison with complex **5**, **7** and **9**, respectively). Longer distances between the bound arene and the ruthenium centre have been observed when the N_{tether} is replaced by a phosphine group (ranging from 1.682 to 1.794 for literature).[14, 15] The Ru–X/Y distances were ranged between 2.076(1)–2.148(11) Å, and the Ru–N1 distances with values between 2.121(4)–2.161(11) Å.

No significant structural differences were observed between the complexes, however, some variations were appreciated regarding to the Ru-C6-C7 angle (112.19–126.41º). This angle, where C6 is the arene carbon connected to the tether and C7 is the first carbon atom on the tether arm, is an important geometrical parameter which correlates with the strain imposed on the tether ring. It is interesting to note that the non-strained Ru-C6-C7 angle is ca. 130º. However, for these tethered complexes this value was smaller. The observed trend followed as: **5**, **6** >> **7**, **9**, **12** > **13**, **14**, with complex **14**[9] bearing the most strained tether chelate. Additional tether-ring strain was defined by the offset of C7 with regard to the plane that contains the η^6-bound arene (from 0.112 Å towards ruthenium for **6** and 0.488 Å for **13**).

Complexes **5** and **6** exhibited the largest Ru-C6-C7 angle (126.41º). These results are in accordance with the published analogue complex [Ru{η^6:κ^1-$C_6H_5(CH_2)_3NH_2$}Cl_2][8] with an angle of 127.17º, near to the non-strained angle 130º. This suggests that the three-atom spacer in the tether of **5** and **6** present a lower strain when compared to the rest two-atom spacers in complexes **7**, **9**, **12**, **13** and **14**. Complexes containing 2-aminobiphenyl (**13** and **14**) presented, however, the highest constrain in the molecule

(ca. 112º). Finally, when we compared complex **13** with its open-tether analogue [Ru{η^6-$C_6H_5(C_6H_4)NH_2$}(en)Cl]Cl,[16] the tether chelate strain disappeared due to the free rotation of the tether arm, and the latter complex presents a Ru-C6-C7 angle of 133.17º.

2.2.4 Alcohols and Carboxylic Acid as Hemilabile Ligands

2.2.4.1 Synthesis and Characterization

Six ruthenium(II) complexes of general formula [Ru(η^6-arene)(XY)Cl]$^{0/+1}$ (Figure 2.6 and Table 2.7) were synthesised bearing as hemilabile ligand 2-phenylethyl alcohol (**15Cl**–**19Cl**) and phenylacetic acid (**20Cl**), and containing as XY-chelating ligand ethylenediamine (en), *N,N,N',N'*-tetramethylethylendiamine (tmen), *N*,*N*-dimethyl-4-(2-pyridylazo)aniline (azpy-NMe_2), 2,2'-bipyridine (bip) and sodium oxalate (oxo). These open tether complexes are interesting because they could potentially afford the typical closed tethered complexes through the synthetic path 2 detailed in the Chapter 1.

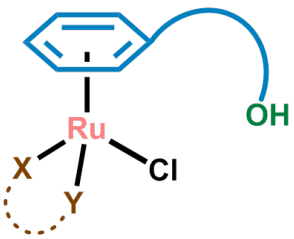

Figure 2.6. General structure for open tethered complexes of formula [Ru(η^6-arene)(XY)Cl]$^{0/+1}$, which can potentially afford the closed tethered counterpart by synthetic path 2, as indicated in Chapter 1.

Table 2.7. Hemilabile ligands and XY-chelating ligands used in this Chapter for the synthesis of complexes **15Cl**–**20Cl**.

Complex	Hemilabile Ligand	XY Chelating Ligand	Complex	Hemilabile Ligand	XY Chelating Ligand
15Cl	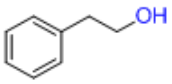		**18Cl**	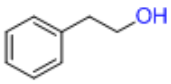	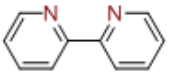
16Cl	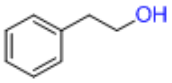		**19Cl**	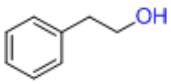	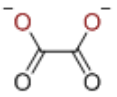
17Cl	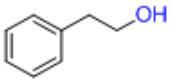	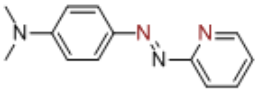	**20Cl**	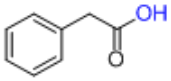	

Synthesis of alcohols derivatives was carried out as follows. First, cyclohexa-2,5-dienecarboxylic acid was prepared by Birch reduction of commercially available benzoic acid,[17] followed by esterification.[18] Treatment of $RuCl_3$ with the diene afforded the dimer complex $[Ru(\eta^6\text{-etb})(\mu\text{-Cl})Cl]_2$ in high yield (Scheme 2.1). This was converted to the corresponding 2-phenylethyl alcohol dimer $[Ru\{\eta^6\text{-}C_6H_5(CH_2)_2OH\}(\mu\text{-Cl})Cl]_2$ when treated with a high excess of 2-phenylethyl alcohol in a closed vessel under pressure, rising as a novel and effective procedure for obtaining that dimer (Scheme 2.2). The resulting red crystals were reacted with the appropriate X,Y-chelating ligand in methanol to afford complexes **15Cl**–**19Cl**.

Complex **20Cl** containing phenylacetic acid as hemilabile ligand was also synthesized as an open tether complex with the carboxylic group dissociated from the ruthenium(II) centre. In contrast to the preparation of alcohol complexes, a different method was used for the synthesis of complex **20Cl**.

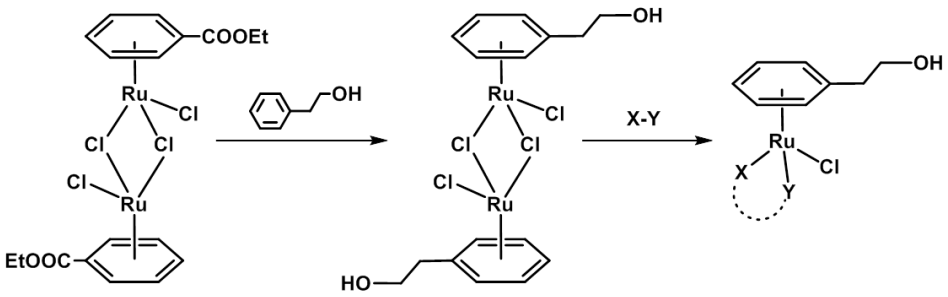

Scheme 2.2

Birch reduction of commercial phenylacetic acid afforded 2,5-dihydrophenylacetic acid, which was reacted with $RuCl_3$ to obtain the dimer $[Ru(\eta^6\text{-}C_6H_5CH_2COOH)(\mu\text{-}Cl)Cl]_2$.[19] Cleavage of the chloro bridges of the dinuclear dimer with two equivalents of ethylenediamine (en) in methanol afforded the monomeric complex **20Cl** (Scheme 2.3).

Several attempts to obtain complexes bearing 2-phenylphenol as hemilabile ligand were unsuccessful since decomposition or starting material was invariably found. The lack of success was found upon varying the solvent, the temperature and/or the reaction time.

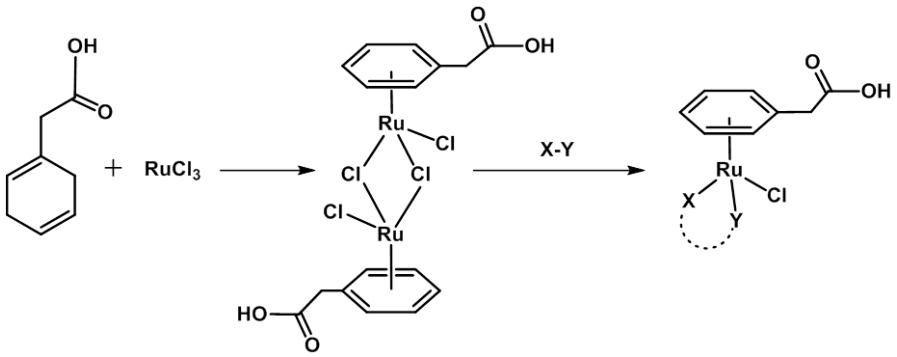

Scheme 2.3

All complexes were characterized by CHN elemental analysis, ^{1}H NMR spectroscopy and single crystal X-ray diffraction analysis for complexes **15Cl**–**18Cl** and **20Cl**. Complexes **15Cl** and **20Cl** were also confirmed by ESI-MS. The mass spectra recorded in positive ion mode featured peaks at m/z values in close agreement with the expected

values for $[M–Cl–H]^+$ ions, after cleavage of the labile chlorido ligand from the metal complex during the ionization process.

The ^{1}H NMR spectra show five CH resonances in the coordinated η^6-arene region for all complexes **15Cl**–**20Cl**, in addition to the peaks in the aliphatic spectral region. The presence of three signals attributed to the coupling between *para*, *meta* and *ortho* positions gives two triplets and one doublet of relative intensities 2:1:2, respectively. The distance between the most deshielded and shielded η^6-bound arene signals are ca. 0.1 ppm, in contrast to values observed for complexes **1**–**14** (ca. 0.8 ppm). This suggests a bigger nuclear equivalence of the arene protons due to the free rotation of the η^6-bound arene in contrast to no rotation in the buckled closed tethered structure. Figure 2.7 illustrates the above mentioned differences in the ^{1}H NMR between closed and open tether complexes.

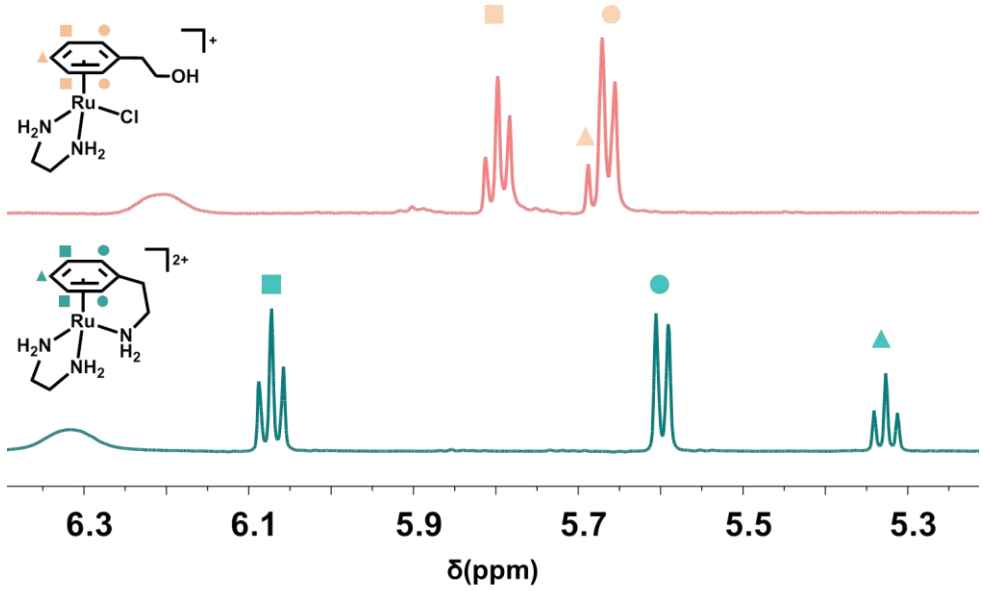

Figure 2.7. ^{1}H NMR spectrum (D_2O) showing the η^6-arene region of the open complex $[Ru\{(\eta^6\text{-}C_6H_5(CH_2)_2OH\}(en)Cl]^{+1}$ (**15Cl**) and its related closed tether complex $[Ru\{\eta^6{:}\kappa^1\text{-}C_6H_5(CH_2)_2NH_2\}(en)]^{+2}$ (**7**). Pendant arm (de)coordination from the metal centre can be related to the splitting of the coordinated η^6-arene proton signals.

In accordance with literature reports,[20] the treatment of open tether complexes **15Cl**–**20Cl** with silver salts should afford the closed tethered derivatives $[Ru\{\eta^6{:}\kappa^1\text{-}$

arene:O}(XY)]$^{+2}$, which results from the elimination of the chlorido ligand and subsequent coordination of the pendant arm to the ruthenium(II) centre. However, only compound **20Cl** afforded the corresponding closed tethered complex **20**, of formula [Ru{η^6:κ^1-$C_6H_5(CH_2)COO$}(en)]$^+$, via a method explained in detail in Chapter 4. The impossibility of the –CH_2CH_2OH side arm of compounds **15Cl**–**19Cl** to form a tethered chelate (closed species) was somehow unexpected since related derivatives readily generated tethered η^6:κ^1arene-O complexes under similar reaction conditions.[21, 22] Explorative work by our research group has shown that in the case of **15Cl**–**19Cl** derivatives, where the alcohol oxygen is only weakly nucleophilic, a larger side tether arm (more than two-carbon spacer) is necessary for coordination to the metal and to afford a sufficiently stable closed tether η^6:κ^1arene-O complex to be isolated.[23]

2.2.4.2 X-Ray Crystallography

Crystals of complexes **15Cl**–**18Cl** and **20Cl** suitable for X-ray analysis were obtained from methanol solutions layered with diethyl ether. Once again, the ORTEP views showed the classical pseudo-octahedral "three-legged piano-stool" geometry around the metal centre, with Ru^{II} π-bonded to the arene ligand (1.666–1.711 Å), σ-bonded to a chloride (2.390(2)–2.4172(15) Å) and a chelating ligand (2.057(7)–2.209(11) Å) which constituted the three "legs" of the piano stool. The structures along with their atom numbering schemes are shown in Figure 2.8. Selected bond lengths and angles are listed in Table 2.8.

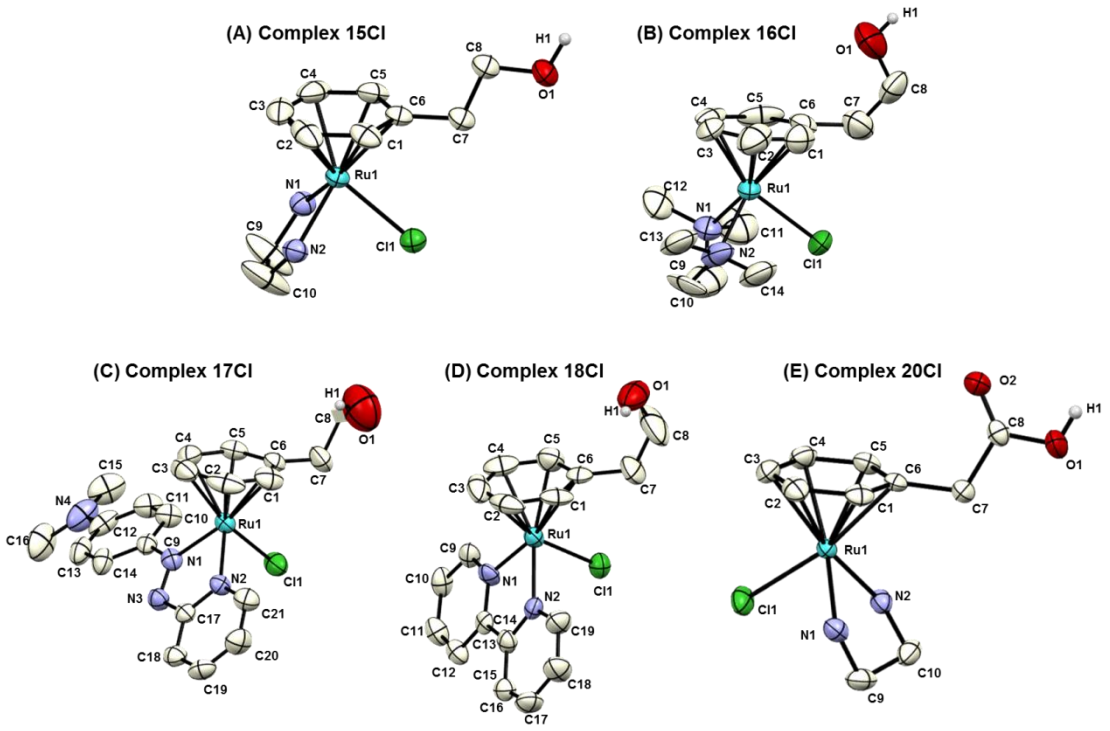

Figure 2.8. X-ray structures and atom numbering schemes for complexes (A) [Ru{η^6-$C_6H_5(CH_2)_2OH$}(en)Cl]Cl (**15Cl**), (B) [Ru{η^6-$C_6H_5(CH_2)_2OH$}(tmen)Cl]Cl (**16Cl**), (C) [Ru{η^6-$C_6H_5(CH_2)_2OH$}(azpy-NMe_2)Cl]Cl (**17CL**), (D) [Ru{η^6-$C_6H_5(CH_2)_2OH$}(bip)Cl]Cl (**18Cl**) and (E) [Ru{η^6-$C_6H_5(CH_2COOH$}(en)Cl]Cl (**20Cl**). The hydrogen atoms and counterions have been omitted for clarity (except on the oxygen pendant from the tether arm).

Table 2.8. Selected bond lenghts (Å) and angles (deg) for complexes **15Cl–18Cl** and **20Cl**.

Bond / angle	15Cl	16Cl	17Cl	18Cl	20Cl
Ru-C6	2.220(5)	2.234(12)	2.250(8)	2.252(18)	2.1819(19)
Ru-C5	2.207(4)	2.155(14)	2.226(9)	2.181(17)	2.182(2)
Ru-C4	2.154(4)	2.164(10)	2.185(10)	2.182(18)	2.202(2)
Ru-C3	2.171(6)	2.188(11)	2.214(10)	2.184(19)	2.180(2)
Ru-C2	2.154(4)	2.177(16)	2.173(9)	2.17(2)	2.186(2)
Ru-C1	2.207(4)	2.210(14)	2.203(10)	2.219(17)	2.158(2)
Ru-centroid	1.667	1.701	1.711	1.710	1.666
Ru-X	2.117(3)	2.209(11)	2.070(7)	2.102(13)	2.1255(17)
Ru-Y	2.117(3)	2.177(11)	2.057(7)	2.091(13)	2.1229(16)
Ru-Cl	2.4172(15)	2.415(3)	2.390(2)	2.411(4)	2.4114(5)
X-Ru-Y	79.40(19)	79.3(5)	75.0(3)	77.6(5)	78.84(7)
X-Ru-Cl	84.47(10)	88.1(3)	85.44(19)	84.3(3)	83.95(5)
Y-Ru-Cl	84.47(10)	85.5(3)	86.1(2)	84.6(4)	85.10(5)
Ru-C6-C7	130.33	126.50	127.06	128.39	127.71
C7-offset	0.034 (+)	0.008 (+)	0.071 (+)	0.065 (+)	0.069 (+)

Complexes **15Cl** and **20Cl** crystallized with four independent molecules in the unit cell, while complex **16Cl** crystallized with two molecules, and **17Cl** and **19Cl** with eight molecules in the unit cell. The Cl^- counterions in the crystal structures of **15Cl** and **20Cl** were extensively involved in H-bonding to the O_{tether} hydrogen atoms (O–H···Cl distance of 2.029–2.202 Å) and to the hydrogen atoms on the nitrogen of the chelating ligands (N–H···Cl distances in the range 2.389–2.590 Å). As expected for open-tether complexes, the Ru-C6-C7 angles fall within the range 126.5–130.3º. Structures of **16Cl** and **19Cl** showed H-bonding interactions between Cl^- counterions and the O_{tether} hydrogen atoms (O–H···Cl distance in the range 2.164–2.467 Å). Only the crystal structure of complex **18Cl** showed evidence for intermolecular π-π interactions between the pyridine rings of adjacent molecules with a distance between centroids of 3.581 Å.

2.2.5 Structure-Activation Relationship

In this part of the Chapter we illustrate the activation (opening) of the Ru–Z bond of closed tethered complexes under acidic conditions (Figure 1.15). To establish a structure-activation relationship regarding the effect of the arene:Z hemilabile ligand, we selected closed-tethered complexes bearing ethylenediamine (en) as XY chelating ligand.

Complexes of formula $[Ru(\eta^6{:}\kappa^1\text{-arene:Z})(en)]^{n+}$, i.e.; **1**, **4**, **7**, **8**, **9**, **13** and **20**, were dissolved in D_2O at pH 7.0 at 298 K. Then, the pH of the solutions was adjusted to ca. 0. Their ^1H NMR spectra were recorded at 298 K immediately after the pH adjustment (ca. 15 min) and after 24 h. Figure 2.9 shows the different extents of activation. The amount of activated open-tether complexes was determined by integration of the η^6-bound arene ring signals. The ^1H NMR spectra for complexes **1** and **4** did not show any new signals overtime after 24 h. At t = 15 min only complexes **9**, **13** and **20** showed

activation by the presence of new set of ^{1}H NMR signals corresponding to the open protonated species (**9HCl**, **13HCl** and **20HCl**), of general formula [Ru(η^6-arene:ZH)(en)Cl]$^{n+}$, whose characterization will be described in detail in Chapters 3 and 4. Percentages of the open protonated species were 10, 79 and 100% for complexes **9HCl**, **13HCl** and **20HCl**, respectively. Over 24 h, all tethered complexes containing two-carbon tether in the pendant arm underwent activation of the Ru–Z bond at different extents. At this point, when equilibrium is reached, intensity of peaks assigned to **9HCl** and **13HCl** increased up to 100%, while peaks of very little intensity attributed to **7HCl** and **8HCl** were also observed (3 and 2%, respectively). Since pH 0 < pK_a for all complexes, the pendant arm of the tether must be protonated (ZH^+). Despite the important role of Z protonation in bloking the complex in its (open) active form, the data clearly shows that the pK_a of the hemilabile ligands is not the only factor driving in the opening process.

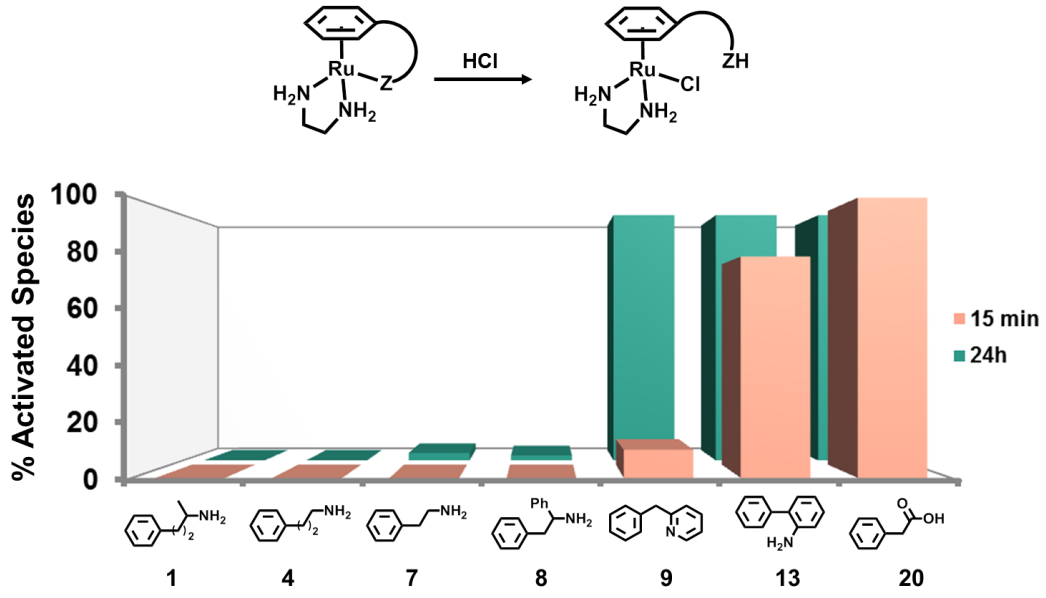

Figure 2.9. Extents of open protonated species through acidic activation (pH ca. 0) of [Ru(η^6:κ^1-arene:Z)(en)]$^{n+}$ complexes bearing different hemilabile ligands and fixed chelating ligand (en).

We could highlight two features affecting the ring-opening process: i) appropriate ring constrain, including length and flexibility of the pendant arm, and ii) the nature of

the donor tether atom (functional group and pK_a). All complexes with η^6-bound arene bearing two-carbon atoms in the side arm (**7–9**, **13** and **20**) showed acidic activation after 24 h at different extents. However, complexes **1** and **4** bearing three-carbon atoms in the spacer of the pendant arm showed no activation overtime. This observation can be explained by discussing the representatives crystal structures of $[Ru\{\eta^6:\kappa^1\text{-}C_6H_5(CH_2)_3NH_2\}(dap)]Cl_2$ (**5**, three-atom tether) and $[Ru\{\eta^6:\kappa^1\text{-}C_6H_5(CH_2)_2NH_2\}(en)]Cl_2$ (**7**, two-atom tether). As mentioned in the X-ray Crystallography Section, the Ru-C6-C7 angle in **5** is closer to 130º (126.41º) than the angle observed for **7** (114.5º), showing that **5** appears to accommodate a non-strained tether chelate, while **7** presents a forced chelate. In this manner, more strained (short) tether arms favours tether-ring opening.

Complexes **7–9** and **13** (hemilabile ligand containing amines with two-atom tethers) all showed acidic activation after 24 h. However, the percentage of the open activated forms of complexes **7** and **8** (where Z is an aliphatic amine) was only of ca. 3% while the total activation was observed for complexes **9** and **13** (where Z is an aromatic amine) over 24 h. These results reveal that aromatic amines as pendant arms show a substantial increase of activation compared with aliphatic amines. This could be explained on the basis that the unshared electron pair on nitrogen in aliphatic amines occupies a sp^3-hybridized orbital. This lone pair is involved in the coordination to the ruthenium(II) center. However, the unshared electron pair on the nitrogen in 2-aminobiphenyl is delocalized into the π-system of the ring and 2-benzylpyridine presents a sp^2-hybridization. This feature makes aromatic amines less basic and less nucleophilic than aliphatic amines, regarding their coordination to ruthenium(II) providing complexes with weaker Ru–Z bond and thus more prone to activation.

A significant difference in the rate of activation is observed between complexes **9** and **13** (at time 15 min, 10 vs 79%, respectively). This observation is consistent with a high ring constrain imposed by a sp^2-hybridization on the C7 atom in complex **13** versus the sp^3-hybridization in complex **9**, proving the importance on the rigidity of the side arm or spacer in the tether opening process.

Complex **20**, bearing a carboxylate group from the η^6-bound arene underwent the fastest activation which was complete in the first 15 min of reaction in acidic water. This suggests that κ^1O-coordination is weaker than κ^1N-coordination. This demonstrates the crucial role of the donor atoms nature in the activation of the Ru–Z bond.

2.3 Conclusions

When designing a new molecule for a certain purpose always the structure and the stereo-electronic properties should be taken into account and modified and modulated accordingly. We consider that it is rather important to study in detail the structural aspects of hemilabile ligands and their influence on the Ru–Z bond activation in order to design Ru^{II} tether switchable complexes. It is crucial to have a clear overall picture of what the structural and stereo-electronic properties affecting the κ^1Z dissociation/association from the ruthenium(II) centre, since dissociation (inactivation) will provide a site for coordinative interactions with intracellular targets. The novel structure-activation relationship established between the new tethered complexes **1**, **4**, **7**–**9**, **13** and **20** of formula $[Ru(\eta^6{:}\kappa^1\text{-arene:Z})(en)]^{n+}$ displayed essential information about the hemilabile ligand structural features and how they affect the susceptibility of Ru–Z activation.

Complexes containing hemilabile ligands with nitrogen as donor atom (**1**, **4**, **7**–**9** and **13**) only underwent activation if the side arm is short (two-atom tether) in different extents in an acidified environment. In that case, only complexes bearing aromatic amines as the coordinating group (**9** and **13**) showed total activation after 24 h. Complex $[Ru\{\eta^6{:}\kappa^1\text{-}C_6H_5(C_6H_4)NH_2\}(en)]Cl_2$ (**13**) bearing 2-aminobiphenyl (two-carbon atoms with sp^2-hybridization) exhibited the fastest tether activation. For this reason, a detailed study of ruthenium(II) complexes containing 2-aminobiphenyl as hemilabile ligand will be presented in Chapter 3.

Our results demonstrated that κ^1O-coordination is weaker than κ^1N-coordination. On the one hand, complexes containing 2-phenylethyl alcohols could not be isolated as closed tethered counterparts, and an elongation of the tether arm was necessary to achieve the κ^1O-coordination.[23] On the other hand, the total conversion of complex **20**

towards the open protonated species was observed after 15 min following acidification. The interesting features observed for complex **20** led us to develop a new family of ruthenium(II) complexes containing 2-phenylacetic acid as hemilabile group, which will be presented in Chapter 4.

2.4 Experimental Section

2.4.2 Instrumentation

NMR Spectroscopy. ^{1}H NMR spectra were acquired in 5 mm NMR tubes using a Bruker DPX 400 MHz spectrometer. ^{1}H NMR chemical shifts were internally referenced to 1,4-dioxane (3.75 ppm) for aqueous solutions, (C*H*D$_2$)(CD$_3$)SO (2.50 ppm) for DMSO-d_6 and CD$_2$*H*OD (3.34 ppm) for methanol-d_4. Data processing was carried out using MestreNova, version 6.0 (Mestrelab Research, S.L.).

Single Crystal X-ray Diffraction. Suitable crystals of compounds **5–7**, **9**, **12–13**, **15Cl–18Cl** and **20Cl**, were coated with mineral oil and mounted on Mitegen MicroMounts. The samples were measured in a Bruker D8 KAPPA APEX II diffractometer with CCD area-detector, equipped with graphite-monochromated Mo Kα radiation (λ = 0.71073 Å). The substantial redundancy in data allowed empirical absorption corrections (SADABS)[24] to be applied using multiple measurements of symmetry-equivalent reflections. Raw intensity data frames were integrated with the SAINT program, which also applied corrections for Lorentz and polarization effects. The Bruker SHELXTL Software Package was used for space group determination, structure solution, and refinement.[25] The space group determination was based on a check of the Laue symmetry, and systematic absences were confirmed using the structure solution. The structures were solved by direct methods (SHELXL-2014/7),[26, 27] completed with different Fourier syntheses, and refined with full-matrix least-squares using SHELXS minimizing $\omega(F_o^2 - F_c^2)^2$. Weighted R factors (R_w) and goodness of fit (S) are based on F^2; conventional R factors (R) are based on F. All non-hydrogen atoms were refined with anisotropic displacement parameters. Hydrogen atom positions were geometrically calculated and allowed to ride on their parent carbon or nitrogen atoms

with fixed isotropic U. All scattering factors and anomalous dispersion factors are contained in the SHELXTL 6.10 program library. The data were processed by the modelling program Mercury version 3.9 (CSD System).

Mass Spectrometry. Electrospray ionization mass spectra (ESI-MS) were obtained by infusing the samples into an Agilent 6120 Single Quadrupole LC/MS. The cone voltage was varied between 40 and 200 V depending on sensitivity. The mass spectra were recorded with a scan range of m/z 50–500 for positive ions.

Elemental Analysis. Elemental analysis was carried out using a Leco analytical elemental analyzer CHNS-932.

pH Measurements. The pH* values (pH meter readings in D_2O solutions) of NMR samples in D_2O were measured at 298 K directly in the NMR tube, using a FiveEasy pH meter equipped with a Crison micro-electrode calibrated with Crison buffer solutions at pH 4 and 7. The pH* values can be converted to pH values by use of the equation pH = 0.929 pH* + 0.42, suggested by Krezel and Bal,[28] for comparison with related values in the literature.

2.4.3 Methods

Acidic Activation. The ring-opening process of closed tethered complexes **1**, **4**, **7**, **8**, **9**, **13** and **20** was monitored by ^{1}H NMR in aqueous solutions at 298 K. After dissolving complexes (6–7 mM) in D_2O at pH 7.0, DCl was used to adjust the pH close to ca. 0. The relative percentages of closed- and open-tether species were quantified at different time points (15 min and 24 h) by integration of peaks in the ^{1}H NMR spectra.

2.4.4 Synthesis

MATERIALS

$RuCl_3 \cdot 3H_2O$ was acquired from Precious Metals Online. Benzoic acid, ethylendiamine (en), 1,3-diaminopropane (dap), *N,N,N′,N′*-tetramethylethylenediamine (tmen), sodium oxalate (oxo), 2,2'-bipyridyl (bipy), 1-methyl-3-phenylpropylamine, 3-phenylpropylamine, phenylethylamine, 1,2-diphenylethylamine, 2-benzylpydirine phenylacetic acid and deuterium chloride were purchased from Sigma-Aldrich. *N,N′*-diethylethylenediamine (deen), *N,N*, dimethyl-4-(2-pyridylazo)aniline (azpi-NMe_2) and 2-phenylphenol were acquired from Cymit. Dichloroethane and magnesium were acquired from Acros Organics, and 2-aminobiphenyl, phenylethyl alcohol, iodine, molecular sieves of 3Å and silver hexafluorophosphate from Fisher. Ethanol, dry methanol, diethyl ether, tetrahydrofuran, sodium metal, and sodium chloride were purchased from Sharlau. For NMR spectroscopy, the solvents used were MeOD-d_4, dimethyl-d_6 sulfoxide, deuterium oxide and 1,4-dioxane obtained from VWR International.

PREPARATION OF PRECURSORS

Dichlorido complexes of general formula $[Ru(\eta^6{:}\kappa^1\text{-arene:N})Cl_2]$ were prepared by previously reported procedures.[16, 19] Typically, dimer $[RuCl_2(\eta^6\text{-etb})]_2$ and the corresponding hemilabile ligand were suspended in 1,2-dichloroethane. The mixture was stirred for 45 min at ambient temperature giving a dark red solution. THF (1 mL) was added, and the mixture degassed with argon for 30 min. The vessel was closed, and the reaction mixture heated under pressure at 393 K (5–16 h depending on the target product). The air stable microcrystalline material was collected by filtration, washed

with acetone and diethyl ether, and dried in air. Details of the amounts of reactants, volume of solvents, stirring times, and the aspect of the product are described below for the individual reactions, as well as any variation in the synthetic procedure.

[Ru(η^6-etb)(μ-Cl)Cl]$_2$. **Benzoate dimer**. Birch reduction of benzoic acid was carried out following the experimental procedure described by Habtemariam et al.[1] to afford cyclohexa-2,5-dienecarboxylic acid. However, the esterification step to obtain ethyl cyclohexa-2,5-dienecarboxylate was performed according to the experimental conditions published by Butters et al.[2] Ethyl cyclohexa-2,5-dienecarboxylate (628 mg, 4.13 mmol) and $RuCl_3 \cdot 3H_2O$ (216 mg, 0.83 mmol) were stired under reflux in dry EtOH (25 mL) overnight. The solvent was concentrated and the orange precipitate was filtered off, washed with cold ethanol and diethyl ether, and dried in vacuum. Yield: 264 mg (99%). ^{1}H NMR (400 MHz, $CDCl_3$, δ): 6.47 (d, *J* = 6.3 Hz, Ar H, 2H), 5.97 (dd, *J* = 8.2, 3.0 Hz, Ar H, 1H), 5.78 (t, *J* = 5.8 Hz, Ar H, 2H), 4.47 (q, *J* = 7.2 Hz, –C*H*$_2$CH$_3$, 2H), 1.42 (t, *J* = 7.1 Hz, –CH$_2$C*H*$_3$, 3H).

[Ru{η^6:κ^1-C_6H_5(C_3H_5Me)NH_2}Cl_2]. **Precursor of complexes 1–3**. [$RuCl_2(\eta^6$-etb)]$_2$ (200 mg, 0.31 mmol) and 1-methyl-3-phenylpropylamine (100 μL, 0.62 mmol) were suspended in 1,2-dichloroethane (20 mL). The reaction mixture was heated under pressure at 393 K for 16 h. The red-brown, air stable microcrystalline material was collected by filtration, washed with acetone and diethyl ether, and dried in air. Yield: 173 mg (87%). Elemental analysis: Cald for $C_{10}H_{15}Cl_2NRu$ (321.21): C, 37.39; H, 4.71; N, 4.36. Found: C, 37.55; H, 4.61; N, 4.61. ^{1}H NMR (400 MHz, $CDCl_3$-*d*$_1$, δ): 5.88 (t, *J* = 5.6 Hz, Ar H, 1H), 5.81 (t, *J* = 5.6 Hz, Ar H, 1H), 5.69 (t, *J* = 5.6 Hz, Ar H, 1H), 5.25 (d, *J* = 5.7 Hz, Ar H, 1H), 5.09 (t, *J* = 5.4 Hz, Ar H, 1H), 3.37–3.27 (m, 1H), 3.03 (br s,

NH_2, 2H), 2.82–2.78 (m, 1H), 2.28–2.17 (m, 2H), 2.08–2.03 (m, 1H), 1.39 (t, *J* = 5.8 Hz, –C*H*$_3$, 3H).

[Ru{η^6:κ^1-C$_6$H$_5$(CH$_2$)$_3$NH$_2$}Cl$_2$] . **Precursor of complexes 4–6**. [$RuCl_2$(η^6-etb)]$_2$ (250 mg, 0.388 mmol) and 3-phenyl-1-propylamine (113 mg, 0.775 mmol) were suspended in 1,2-dichloroethane (20 mL). The reaction mixture was heated under pressure at 393 K for 16 h. A red-brown, air stable microcrystalline material was collected by filtration, washed with acetone and diethyl ether, and dried in air. Yield: 164 mg (69%). Elemental analysis: Cald for $C_9H_{13}Cl_2NRu$ (307.18): C, 35.19; H, 4.27; N, 4.56. Found: C, 35.44; H, 4.18; N, 4.44. ^{1}H NMR (400 MHz, $CDCl_3$-*d$_1$*, δ): 5.87 (t, *J* = 5.7 Hz, Ar H, 2H), 5.72 (t, *J* = 5.6 Hz, Ar H, 1H), 5.15 (d, *J* = 5.7 Hz, Ar H, 2H), 3.21 (br s, NH_2, 2H), 2.96–2.91 (m, 2H), 2.49–2.46 (m, 2H), 2.22–2.16 (m, 2H).

[Ru{η^6:κ^1-C$_6$H$_5$(CH$_2$)$_2$NH$_2$}Cl$_2$]. **Precursor of complex 7**. [$RuCl_2$(η^6-etb)]$_2$ (187 mg, 0.289 mmol) and 2-phenylethylamine (77 μL, 0.61 mmol) were suspended in 1,2-dichloroethane (20 mL). The reaction mixture was heated under pressure at 393 K for 18 h. The red, air stable microcrystalline material was collected by filtration, washed with acetone and diethyl ether, and dried in air. Yield: 107 mg (63%). Elemental analysis: Cald for $C_8H_{11}Cl_2NRu$ (293.15): C, 32.78; H, 3.78; N, 4.78. Found: C, 33.14; H, 3.70; N, 4.66. ^{1}H NMR (400 MHz, $CDCl_3$-*d$_1$*, δ): 5.93 (t, *J* = 5.8 Hz, Ar H, 2H), 5.52 (t, *J* = 5.6 Hz, Ar H, 1H), 5.21 (d, *J* = 5.8 Hz, Ar H, 2H), 3.91–3.88 (m, 2H), 3.62 (br s, NH_2, 2H), 2.83 (t, *J* = 6.7 Hz, –C*H*$_2$–, 2H).

[Ru{η^6:κ^1-C$_6$H$_5$(C$_8$H$_8$)NH$_2$}Cl$_2$]. **Precursor of complex 8**. [$RuCl_2$(η^6-etb)]$_2$ (50 mg, 0.078 mmol) and 1,2-diphenylethylamine (15 μL, 0.078 mmol) were suspended in 1,2-

dichloroethane (7 mL). The reaction mixture was heated under pressure at 393 K for 18 h. The yellow material was collected by filtration, washed with diethyl ether, and dried in air. Yield: 21 mg (72%). Elemental analysis: Cald for $C_{14}H_{15}Cl_2NRu$ (369.25): C, 45.54; H, 4.09; N, 3.79. Found: C, 45.42; H, 4.12; N, 3.47. ^{1}H NMR (400 MHz, $CDCl_3$-d_1, δ): 7.50–7.41 (m, Ar H, 5H), 6.04 (t, *J* = 5.5 Hz, Ar H, 1H), 5.89–5.84 (m, Ar H, 1H), 5.54 (t, *J* = 5.3 Hz, Ar H, 1H), 5.43–5.42 (m, Ar H, 1H), 5.33 (d, *J* = 5.6 Hz, Ar H, 1H), 5.18–5.09 (m, 1H), 3.21 (dd, *J* = 13.7, 5.2 Hz, –C*H*$_2$–, 1H), 3.04 (t, *J* = 13.3 Hz, –C*H*$_2$–, 1H). ESI-MS (m/z): $[M–Cl]^+$ calcd. for $C_{14}H_{15}Cl_2NRu$, 334.0; found, 334.0.

[Ru{η^6:κ^1-C$_6$H$_5$(C$_5$H$_8$O$_2$)NH$_2$}Cl$_2$]. $[RuCl_2(\eta^6\text{-etb})]_2$ (100 mg, 0.155 mmol) and L-phenylalanine ethyl ester (60 mL, 0.310 mmol) were suspended in 1,2-dichloroethane (20 mL). The reaction mixture was heated under pressure at 393 K for 16 h. The brown solid was collected by filtration, washed with diethyl ether, and dried in air. Yield: 67 mg (59%). ^{1}H NMR (400 MHz, $CDCl_3$-d_1, δ): 6.03 (t, *J* = 5.6 Hz, Ar H, 1H), 5.92 (t, *J* = 5.6 Hz, Ar H, 1H), 5.51 (t, *J* = 5.6 Hz, Ar H, 1H), 5.38 (d, *J* = 5.6 Hz, Ar H, 1H), 5.27 (d, *J* = 5.7 Hz, Ar H, 1H), 4.72–4.55 (m, 2H), 4.34–4.28 (m, 2H), 3.29 (dd, *J* = 14.1, 6.1 Hz, 1H), 2.97(dd, *J* = 14.1, 11.3 Hz, 1H), 1.34 (t, *J* = 7.1 Hz, 3H). This dichlorido precursor did not afford the subsequent reaction with ethylenediamine.

[Ru{η^6:κ^1-C$_6$H$_5$CH$_2$(C$_5$H$_4$N)}Cl$_2$]. **Precursor of complexes 9–12**. $[RuCl_2(\eta^6\text{-etb})]_2$ (117 mg, 0.182 mmol) and 2-benzylpyridine (58 μL, 0.364 mmol) were suspended in 1,2-dichloroethane (12 mL). The reaction mixture was heated under pressure at 393 K for 16 h. A pale green powder was collected by filtration, washed with acetone and diethyl ether, and dried in air. Yield: 92 mg (75%). Elemental analysis: Cald for $C_{12}H_{11}Cl_2NRu$ (341.20): C, 42.24; H, 3.25; N, 4.11. Found: C, 42.45; H, 3.26; N, 3.95.

^{1}H NMR (400 MHz, DMSO-d_6, δ): 7.95 (td, *J* = 7.7, 1.7 Hz, Ar H, 1H), 7.76 (dd, *J* = 5.8, 1.4 Hz, Ar H, 1H), 7.50 (d, *J* = 7.9 Hz, Ar H, 1H), 7.36 (t, *J* = 6.7 Hz, Ar H, 1H), 5.99 (t, *J* = 5.8 Hz, Ar H, 2H), 5.79 (d, *J* = 5.8 Hz, Ar H, 2H), 5.56 (t, *J* = 5.6 Hz, Ar H, 1H), 4.43 (s, –C*H*$_2$–, 2H).

[Ru{η^6:κ^1-C$_6$H$_5$(C$_6$H$_4$)NH$_2$}Cl$_2$]. **Precursor of complexes 13 and 14**. [RuCl$_2$(η^6-etb)]$_2$ (200 mg, 0.31 mmol) and 2-aminobiphenyl (105 mg, 0.62 mmol) were suspended in 1,2-dichloroethane (25 mL). The reaction mixture was heated under pressure at 393 K for 5 h. The red crystals were collected by filtration, washed with acetone and diethyl ether, and dried in air. Yield: 202 mg (95%). Elemental analysis: Cald for $C_{12}H_{11}Cl_2NRu$ (341.20): C, 42.24; H, 3.25; N, 4.11. Found: C, 42.11; H, 3.22; N, 3.97. ^{1}H NMR (400 MHz, DMSO-d_6, δ): 7.38 (d, *J* = 7.7 Hz, Ar H, 1H), 7.16 (t, *J* = 7.4 Hz, Ar H, 1H), 6.80 (d, *J* = 8.0 Hz, Ar H, 1H), 6.67 (t, *J* = 7.4 Hz, Ar H, 1H), 6.22 (d, *J* = 6.0 Hz, Ar H, 2H), 6.13 (t, *J* = 5.5 Hz, Ar H, 1H), 5.95 (t, *J* = 5.9 Hz, Ar H, 2H), 5.42 (br s, NH$_2$, 2H).

[Ru{η^6-C$_6$H$_5$(CH$_2$)$_2$OH}(μ-Cl)Cl]$_2$. **Precursor for complexes 15Cl–19Cl**. A suspension of [Ru(η^6-etb)(μ-Cl)Cl]$_2$ (50 mg, 0.078 mmol) in 2-phenylethyl alcohol (1 mL, 8.3 mmol) and DCE (1 mL) was fluxed with argon for 15 min. The vessel was closed, and the reaction mixture heated under pressure at 393 K for 12 h. The red precipitate was filtered off, washed with cold ethanol and diethyl ether, and dried in vacuum. Yield: 39 mg, 85%. Elemental analysis: Cald for $C_{16}H_{20}Cl_4O_2Ru_2$ (588.27): C, 32.67; H, 3.45. Found: C, 33.45; H, 3.45. ^{1}H NMR (400 MHz, DMSO-d_6, δ): 5.98 (t, *J* = 5.9 Hz, Ar H, 2H), 5.78 (d, *J* = 6.1 Hz, Ar H, 2H), 5.75 (t, *J* = 5.7 Hz, Ar H, 1H), 3.69 (t, *J* = 6.1 Hz, –C*H*$_2$–, 2H), 2.57 (t, *J* = 6.1 Hz, –C*H*$_2$–, 2H).

[Ru{η^6-C$_6$H$_5$CH$_2$COOH}(μ-Cl)Cl]$_2$. **Precursor for complex 20Cl**. Birch reduction of phenylacetic acid following a previously reported procedure[19] afforded 2,5-dihydrophenylacetic acid. The cyclic diene (400 mg, 2.9 mmol) and $RuCl_3 \cdot 3H_2O$ (473 mg, 1.810 mmol) were suspended in 10 mL of 1:4 (v/v) water/acetone in a closed pressure tube. The reaction mixture was heated at 100 ºC for 3 h. The red precipitate was filtered off, washed with cold ethanol and diethyl ether, and dried in vacuum. Yield: 445 mg, 80%. Elemental analysis: Cald for $C_{16}H_{16}Cl_4O_4Ru_2$ (616.24): C, 31.19; H, 2.62. Found: C, 31.66; H, 2.55. ^{1}H NMR (400 MHz, DMSO-d_6, δ): 12.79 (br s, OH, 1H), 6.01 (t, *J* = 5.9 Hz, Ar H, 2H), 5.91 (d, *J* = 6.1 Hz, Ar H, 2H), 5.83 (t, *J* = 5.6 Hz, Ar H, 1H), 3.49 (s, C*H*$_2$, 2H).

PREPARATION OF CLOSED TETHERED COMPLEXES 1–14

[Ru{η^6:κ^1-C$_6$H$_5$(C$_3$H$_5$Me)NH$_2$}(en)]Cl$_2$ (1). Ethylenediamine (15 μL, 0.23 mmol) was added to a suspension of [Ru{η^6:κ^1-C$_6$H$_5$(C$_3$H$_5$Me)NH$_2$}Cl$_2$] (63 mg, 0.19 mmol) in dry methanol (3 mL). The reaction mixture was stirred at ambient temperature for 2 h. The solvent was removed under reduced pressure to give a solid, which was redissolved in the minimum volume of ethanol. Addition of diethyl ether afforded the precipitation of a yellow solid, which was collected by filtration, and dried in vacuum. Yield: 40 mg (67%). ^{1}H NMR (400 MHz, D_2O, δ): 6.03 (t, *J* = 5.8 Hz, Ar H, 1H), 5.94 (t, *J* = 5.8 Hz, Ar H, 1H), 6.61 (d, *J* = 6.0 Hz, Ar H, 1H), 5.54 (d, *J* = 5.7 Hz, Ar H, 1H), 5.46 (t, *J* = 5.7 Hz, Ar H, 1H), 2.89–2.82 (m, 2H), 2.65–2.51 (m, 3H), 2.44–2.28 (m, 2H), 2.14–2.08 (m, 1H), 1.97–1.87 (m, 1H), 1.30 (d, *J* = 6.5 Hz, –C*H*$_3$, 3H). ESI-MS (m/z): [M–H]$^+$ calcd. for $C_{12}H_{23}Cl_2N_3Ru$, 310.0; found, 310.1.

[Ru{η^6:κ^1-$C_6H_5(C_3H_5Me)NH_2$}(*o*-pda)]Cl_2 (2). To a suspension of [Ru(η^6:κ^1-$C_6H_5(C_4H_8)NH_2)Cl_2$] (25 mg, 0.078 mmol) in methanol was added *o*-phenyldiamine (8.42 mg, 0.078 mmol). The reaction mixture was stirred for 16 h. Solvent was removed in the rotary evaporator to give a yellow solid, which was washed with acetone and dried in air. Yield: 21 mg (64%). Elemental analysis: Cald for $C_{16}H_{23}Cl_2N_3Ru$ (429.35): C, 44.76; H, 5.40; N, 9.79. Found: C, 43.51; H, 5.38; N, 9.44. ^{1}H NMR (400 MHz, D_2O, δ): 7.41–7.29 (m, Ar H, 4H), 6.17 (t, *J* = 5.8 Hz, Ar H, 1H), 6.07 (t, *J* = 5.7 Hz, Ar H, 1H), 5.71 (d, *J* = 6.0 Hz, Ar H, 1H), 5.63 (d, *J* = 5.6 Hz, Ar H, 1H), 5.52 (t, *J* = 5.8 Hz, Ar H, 1H), 2.95–2.86 (m, 2H), 2.41–2.31 (m, 1H), 2.02–1.92 (m, 1H), 1.21 (d, *J* = 6.5 Hz, –C*H*$_3$, 3H). ESI-MS (m/z): [M–H]$^+$ calcd. for $C_{16}H_{23}N_3Ru$, 358.1; found, 358.1.

[Ru{η^6:κ^1-$C_6H_5(C_3H_5Me)NH_2$}(phen)]Cl_2 (3). 1,10-phenantroline (10 mg, 0.056 mmol) was added to a suspension of [Ru(η^6:κ^1-$C_6H_5(C_3H_5Me)NH_2)Cl_2$] (18 mg, 0.056 mmol) in methanol (1 mL). The reaction mixture was stirred for 16 h. Solvent was removed in the rotary evaporator to give a pale yellow solid, which was washed with acetone and dried in air. Yield: 16 mg (57%). Elemental analysis: Cald for $C_{22}H_{23}Cl_2N_3Ru$ (501.42): C, 52.70; H, 4.62; N, 8.38. Found: C, 51.81; H, 4.69; N, 8.10. ^{1}H NMR (400 MHz, D_2O, δ): 9.68 (d, *J* = 5.3 Hz, Ar H, 1H), 9.65 (d, *J* = 5.2 Hz, Ar H, 1H), 8.83 (m, Ar H, 2H), 8.19 (s, Ar H, 2H), 8.06 (m, Ar H, 2H), 6.44 (t, *J* = 6.0 Hz, Ar H, 1H), 6.28 (t, *J* = 6.0 Hz, Ar H, 1H), 6.14 (d, *J* = 6.2 Hz, Ar H, 1H), 6.03 (d, *J* = 6.0 Hz, Ar H, 1H), 5.52 (t, *J* = 5.9 Hz, Ar H, 1H), 3.07–2.92 (m, 2H), 2.75–2.67 (m, 1H), 2.29–2.13 (m, 2H), 1.03 (d, *J* = 6.6 Hz, –C*H*$_3$, 3H). ESI-MS (m/z): [M–H]$^+$ calcd. for $C_{22}H_{23}N_3Ru$, 430.1; found, 430.1.

[Ru{η^6:κ^1-C$_6$H$_5$(CH$_2$)$_3$NH$_2$}(en)]Cl$_2$ (4). Ethylenediamine (15 μL, 0.22 mmol) was added to a suspension of [Ru{η^6:κ^1-C$_6$H$_5$(CH$_2$)$_3$NH$_2$}Cl$_2$] (57 mg, 0.18 mmol) in dry methanol (2 mL). The reaction mixture was stirred at ambient temperature for 2 h. The solvent was removed in the rotary evaporator to give a yellow solid, which was redissolved in the minimum volume of ethanol. Addition of diethyl ether aided precipitation of a yellow solid, which was collected by filtration, and dried in vacuum. Yield: 40 mg (61%). ^{1}H NMR (400 MHz, D$_2$O, δ): 6.01 (t, *J* = 5.9 Hz, Ar H, 2H), 5.60 (d, *J* = 5.9 Hz, Ar H, 2H), 5.54 (t, *J* = 5.7 Hz, Ar H, 1H), 2.83–2.81 (m, –C*H*$_2$–, 2H), 2.66–2.61 (m, –C*H*$_2$–, 2H), 2.57 (t, *J* = 6.1 Hz, –C*H*$_2$–, 2H), 2.51–2.45 (m, –C*H*$_2$–, 2H), 2.14–2.08 (m, –C*H*$_2$–, 2H). ESI-MS (m/z): [M–H]$^+$ calcd. for C$_{11}$H$_{21}$N$_3$Ru, 296.1; found, 296.1.

[Ru{η^6:κ^1-C$_6$H$_5$(CH$_2$)$_3$NH$_2$}(dap)]Cl$_2$ (5). Complex [Ru{η^6:κ^1-C$_6$H$_5$(CH$_2$)$_3$NH$_2$}Cl$_2$] (10 mg, 0.03 mmol) was suspended in methanol (1 mL). 1,3-diaminopropane (3 μL, 0.03 mmol) was added and the reaction mixture was stirred for 1 h at room temperature. The solvent was removed, and addition of diethyl ether afforded a yellow solid which was dried at vacuum. Yield: 10 mg (87%). ^{1}H NMR (400 MHz, DMSO-*d*$_6$, δ): 5.96 (t, *J* = 5.6 Hz, Ar H, 2H), 5.63 (t, *J* = 5.9 Hz, Ar H, 1H), 5.39 (d, *J* = 5.6 Hz, Ar H, 2H), 2.67–2.33 (m, –C*H*$_2$–, 8H), 2.04–1.97 (m, –C*H*$_2$–, 2H), 1.75–1.72 (m, –C*H*$_2$–, 1H), 1.60–1.50 (m, –C*H*$_2$–, 1H). Crystals suitable for X-ray diffraction were obtained by slow evaporation of a methanol/diethyl ether solution at ambient temperature

[Ru{η^6:κ^1-C$_6$H$_5$(CH$_2$)$_3$NH$_2$}(deen)]Cl$_2$ (6). Complex [Ru(η^6:κ^1-C$_6$H$_5$(CH$_2$)$_3$NH$_2$)Cl$_2$] (10 mg, 0.03 mmol) was suspended in methanol (1 mL). 1,3-diaminopropane (4 μL, 0.03 mmol) was added and the reaction mixture was stirred for 1 h at room temperature.

The solvent was removed in the rotary evaporator, and addition of diethyl ether afforded a yellow solid, which was dried in vacuum. Yield: 11 mg (90%). ^{1}H NMR (400 MHz, D_2O, δ): 6.01–5.92 (m, Ar H, 2H), 5.65 (t, *J* = 5.6 Hz, Ar H, 1H), 5.54–5.46 (m, Ar H, 2H), 4.03–3.94 (m, –C*H*$_2$–, 1H), 3.61–3.52 (m, –C*H*$_2$–, 1H), 3.35–3.27 (m, –C*H*$_2$–, 1H), 3.11–3.00 (m, –C*H*$_2$–, 2H), 2.85–2.36 (m, –C*H*$_2$–, 6H), 2.14–2.10 (m, –C*H*$_2$–, 2H), 1.75–1.66 (m, –C*H*$_2$–, 1H), 1.24–1.17 (m, –C*H*$_3$, 6H). Crystals suitable for X-ray diffraction were obtained by slow evaporation of a methanol/tert-butyl methyl ether solution at ambient temperature.

[Ru{η^6:κ^1-C$_6$H$_5$(CH$_2$)$_2$NH$_2$}(en)]Cl$_2$ (7). Ethylenediamine (17 μL, 0.26 mmol) was added to a suspension of [Ru{η^6:κ^1-C$_6$H$_5$(CH$_2$)$_2$NH$_2$}Cl$_2$] (64 mg, 0.22 mmol) in dry methanol (2 mL). The reaction mixture was stirred at ambient temperature for 2 h. The solvent was removed in the rotary evaporator to give a yellow solid, which was redissolved in the minimum volume of ethanol. Addition of diethyl ether afforded the precipitation of a yellow solid, which was collected by filtration, and dried in vacuum. Yield: 61 mg (78%). ^{1}H NMR (400 MHz, D_2O, δ): 6.07 (t, *J* = 6.0 Hz, Ar H, 2H), 5.60 (d, *J* = 5.9 Hz, Ar H, 2H), 5.33 (t, *J* = 5.7 Hz, Ar H, 1H), 3.82–3.77 (m, –C*H*$_2$–, 2H), 2.73 (t, *J* = 6.7 Hz, –C*H*$_2$–, 2H), 2.62–2.59 (m, –C*H*$_2$–, 2H), 2.41–2.37 (m, –C*H*$_2$–, 2H). ESI-MS (m/z): [M–H]$^+$ calcd. for $C_{11}H_{21}N_3Ru$, 282.1; found, 282.1. Crystals suitable for X-ray diffraction were obtained by slow evaporation of a methanol solution at ambient temperature.

[Ru{η^6:κ^1-C$_6$H$_5$(C$_8$H$_8$)NH$_2$}(en)]Cl$_2$ (8). Ethylenediamine (3.7 μL, 0.055 mmol) was added to a solution of [Ru(η^6:κ^1-C$_6$H$_5$(C$_8$H$_8$)NH$_2$)Cl$_2$] (20 mg, 0.055 mmol) in dry methanol (3 mL). The reaction mixture was stirred at ambient temperature for 30 min.

The solvent was removed in the rotary evaporator to give a yellow solid, which was redissolved in the minimum volume of ethanol. Addition of diethyl ether afforded a yellow solid, which was collected by filtration, and dried in vacuum. Yield: 12 mg (51%). ^{1}H NMR (400 MHz, D_2O, δ): 7.58–7.42 (m, Ar H, 5H), 6.24 (t, *J* = 5.9 Hz, Ar H, 1H), 6.12 (t, *J* = 5.9 Hz, Ar H, 1H), 5.79 (t, *J* = 5.9 Hz, Ar H, 1H), 5.70 (t, *J* = 5.6 Hz, Ar H, 1H), 5.39 (t, *J* = 5.9 Hz, Ar H, 1H), 5.11 (dd, *J* = 12.5, 5.5 Hz, –C*H*–, 1H), 3.23 (dd, *J* = 14.1, 5.7 Hz, –CH_2–, 1H), 2.91 (t, *J* = 13.3 Hz, –CH_2–, 1H), 2.66–2.56 (m, –CH_2–, 2H), 2.49–2.27 (m, –CH_2–, 2H).

[Ru{η^6:κ^1-$C_6H_5CH_2(C_5H_4N)$}(en)]Cl_2 (9). Ethylenediamine (8 μL, 0.193 mmol) was added to a suspension of [Ru{η^6:κ^1-$C_6H_5CH_2(C_5H_4N)$}Cl_2] (60 mg, 0.176 mmol) in dry methanol (5 mL). The reaction mixture was stirred at ambient temperature for 2 h. The solvent was removed in the rotary evaporator to give a yellow solid, which was redissolved in the minimum volume of ethanol. Addition of diethyl ether afforded the precipitation of a yellow solid, which was collected by filtration, and dried in vacuum. Yield: 61 mg (87 %). Cald for $C_{14}H_{19}Cl_2N_3Ru$ (401.30): C, 41.9; H, 4.77; N, 10.47. Found: C, 39.79; H, 5.29; N, 9.70. ^{1}H NMR (400 MHz, D_2O, δ): 8.00 (td, *J* = 7.8, 1.6 Hz, Ar H, 1H), 7.56 (d, *J* = 8.0 Hz, Ar H, 1H), 7.46 (d, *J* = 4.8 Hz, Ar H, 1H), 7.41 (t, *J* = 7.0 Hz, Ar H, 1H), 6.26 (t, *J* = 6.0 Hz, Ar H, 2H), 5.95 (d, *J* = 6.2 Hz, Ar H, 2H), 5.44 (t, *J* = 5.7 Hz, Ar H, 1H), 4.43 (s, 2H), 2.90-2.81 (m, 4H). ESI-MS (m/z): $[M–H]^+$ calcd. for $C_{14}H_{19}N_3Ru$, 330.1; found, 330.0. Crystals suitable for X-ray diffraction were obtained by slow evaporation from a water solution at ambient temperature.

[Ru{η^6:κ^1-$C_6H_5CH_2(C_5H_4N)$}(*o*-pda)]Cl_2 (10). *o*-phenyldiamine (3 mg, 0.029 mmol) was added to a suspension of [Ru{η^6:κ^1-$C_6H_5CH_2(C_5H_4N)$}Cl_2] (10 mg, 0.029 mmol) in

dry methanol (2 mL). The reaction mixture was stirred at ambient temperature for 2 h. The solvent was removed in the rotary evaporator to give a yellow solid, which was redissolved in the minimum volume of ethanol. Addition of diethyl ether afforded the precipitation of a yellow solid, which was collected by filtration, and dried in vacuum. Yield: 6 mg (48 %). Cald for $C_{18}H_{19}Cl_2N_3Ru$ (449.34): C, 48.11; H, 4.26; N, 8.48. Found: C, 46.09; H, 4.62; N, 8.48. ^{1}H NMR (400 MHz, D_2O, δ): 7.94 (td, *J* = 7.8, 1.3 Hz, Ar H, 1H), 7.56 (d, *J* = 8.0 Hz, Ar H, 1H), 7.49–7.41 (m, Ar H, 4H), 7.09 (td, *J* = 6.9, 1.2 Hz, Ar H, 1H), 6.56 (d, *J* = 6.0 Hz, Ar H, 1H), 6.41 (t, *J* = 5.9 Hz, Ar H, 2H), 6.08 (t, *J* = 6.4 Hz, Ar H, 2H), 5.46 (td, *J* = 5.8 Hz, Ar H, 1H), 4.52 (s, –C*H*$_2$–, 2H).). ESI-MS (m/z): $[M–H]^+$ calcd. for $C_{18}H_{19}N_3Ru$, 378.1; found, 378.0.

[Ru{η^6:κ^1-C$_6$H$_5$CH$_2$(C$_5$H$_4$N)}(phen)](PF$_6$)$_2$ (11). $AgPF_6$ (18 mg, 0.07 mmol) was added to a methanolic solution containing [Ru{η^6:κ^1-$C_6H_5CH_2(C_5H_4N)$}Cl_2] (12 mg, 0.035 mmol). The reaction mixture was stirred for 2 h. Then, the precipitated AgCl was removed by filtration and phenantroline (6 mg, 0.035 mmol) was added stepwise to the remaining solution. The solvent was removed in the rotary evaporator after 2 h of reaction to give a yellowish solid, which was re-dissolved in the minimum volume of ethanol, which washed with ethanol and diethyl ether, and dried in vacuum. Yield: 16 mg (62 %). Cald for $C_{24}H_{19}F_{12}N_3P_2Ru$ (740.44): C, 38.93; H, 2.59; N, 5.68. Found: C, 39.46; H, 2.68; N, 5.77. ^{1}H NMR (400 MHz, D_2O, δ): 9.70 (d, *J* = 5.3 Hz, Ar H, 2H), 8.89 (d, *J* = 8.1 Hz, Ar H, 2H), 8.28 (s, Ar H, 2H), 8.05 (dd, *J* = 8.2, 5.3 Hz, Ar H, 2H), 7.81 (t, *J* = 7.8 Hz, Ar H, 1H), 7.56 (d, *J* = 8.1 Hz, Ar H, 1H), 6.65 (m, Ar H, 3H), 6.52 (d, *J* = 6.2 Hz, Ar H, 2H), 5.56 (d, *J* = 6.1 Hz, –C*H*$_2$–, 1H), 5.39 (t, –C*H*$_2$–, 1H).

[Ru{η^6:κ^1-C$_6$H$_5$CH$_2$(C$_5$H$_4$N)}(oxo)] (12). $AgPF_6$ (14 mg, 0.058 mmol) was added to a water (2 mL) solution containing [Ru{η^6:κ^1-$C_6H_5CH_2(C_5H_4N)$}Cl_2] (10 mg, 0.029 mmol). The reaction mixture was stirred for 2 h. Then, the precipitated AgCl was removed by filtration and sodium oxalate (4 mg, 0.029 mmol) was added to the remaining solution. The solvent was removed in the rotary evaporator after 2 h of reaction to give a yellowish solid, which was re-dissolved in the minimum volume of ethanol, which washed several times with ethanol and diethyl ether, and dried in vacuum. Yield: 6 mg (56 %). Cald for $C_{14}H_{11}NO_4Ru$ (358.32): C, 46.93; H, 3.09; N, 3.91. Found: C, 46.18; H, 3.23; N, 3.73. ^{1}H NMR (400 MHz, D_2O, δ): 8.04 (td, *J* = 7.8, 1.5 Hz, Ar H, 1H), 7.63 (d, *J* = 8.0 Hz, Ar H, 1H), 7.36 (t, *J* = 6.7 Hz, Ar H, 1H), 6.63 (d, *J* = 6.7 Hz, Ar H, 1H), 6.19 (t, *J* = 6.1 Hz, Ar H, 2H), 5.80 (d, *J* = 6.0 Hz, Ar H, 2H), 5.71 (d, *J* = 5.8 Hz, Ar H, 1H), 4.58 (s, –C*H*$_2$–, 1H). ESI-MS (m/z): $[M+H]^-$ calcd. for $C_{14}H_{11}NO_4Ru$, 360.0; found, 360.0. Crystals suitable for X-ray diffraction were obtained by slow evaporation from a water solution at ambient temperature.

[Ru{η^6:κ^1-C$_6$H$_5$(C$_6$H$_4$)NH$_2$}(en)]Cl$_2$ (13). [Ru(η^6:κ^1-$C_6H_5(C_6H_4)NH_2$)Cl_2] (25 mg, 0.073 mmol) was suspended in 95% aqueous methanol (5 mL). Ethylenediamine (4.9 µL, 0.073 mmol) was added, and the mixture was stirred for 2 h at room temperature. The solvent was removed on a rotary evaporator, and the product was re-dissolved in 3 mL of ethanol. The resultant yellow solution was filtered through a 0.45 µm syringe filter. The solvent was reduced to ca. 5% of its original volume, and diethyl ether (4 mL) was added. The sticky solid was sonicated to give a yellowish precipitate, centrifuged, washed with diethyl ether and dried in vacuum. Water (11 mL) was added and the solution was left to stand overnight. Lyophilization afforded a yellow solid. Yield: 36 mg (98 %). Cald for $C_{14}H_{19}Cl_2N_3Ru$ (401.30): C, 41.90; H, 4.77; N, 10.47.

Found: C, 37.3; H, 5.45; N, 9.91.^{1}H NMR (400 MHz, D_2O, δ): 7.67–7.65 (m, Ar H, 1H), 7.57–7.50 (m, Ar H, 2H), 7.41–7.38 (m, Ar H, 1H), 6.50 (br s, NH_2, 1H), 6.22 (t, *J* = 6.1 Hz, Ar H, 2H), 5.67 (d, *J* = 5.8 Hz, Ar H, 2H), 5.53 (t, *J* = 5.8 Hz, Ar H, 1H), 2.69 (m, –C*H*$_2$–, 2H), 2.49 (m, –C*H*$_2$–, 2H). Orange single crystals of **13** suitable for X-ray diffraction were obtained by evaporation of water solution at ambient temperature.

[Ru{η^6:κ^1-$C_6H_5(C_6H_4)NH_2$}(ox)] (**14**). [Ru(η^6:κ^1-$C_6H_5(C_6H_4)NH_2$)Cl_2] (5 mg, 0.015 mmol) was suspended in water (2 mL). Silver oxalate (18 mg, 0.059 mmol) was added, and the mixture was stirred for 6 h at room temperature. The solvent was removed on the rotary evaporator and the product was re-dissolved in 3 mL of ethanol. The resultant yellow solution was filtered through a 0.45 μm syringe filter. The solvent was reduced to ca. 5% of its original volume, and diethyl ether (3 mL) was added. The sticky solid was sonicated to give a pale yellow precipitate, which was washed with diethyl ether and dried in vacuum. Yield: 8 mg (57 %). Elemental analysis: Cald for $C_{14}H_{11}NO_4Ru$ (358.31): C, 46.93; H, 3.09; N, 3.91. Found: C, 32.56; H, 2.59; N, 2.39. ^{1}H NMR (400 MHz, D_2O, δ): 7.68–7.66 (m, Ar H, 1H), 7.58–7.50 (m, Ar H, 2H), 7.39–7.37 (m, Ar H, 1H), 6.14 (t, *J* = 5.9 Hz, Ar H, 2H), 5.75 (t, *J* = 6.0 Hz, Ar H, 1H), 5.53 (d, *J* = 6.2 Hz, Ar H, 2H).

PREPARATION OF OPEN-TETHER COMPLEXES 15Cl–20 Cl

[Ru{η^6-$C_6H_5(CH_2)_2OH$}(en)Cl]Cl (15Cl). Ethylenediamine (7 μL, 0.101 mmol) was added to a suspension of [Ru{η^6-$C_6H_5(CH_2)_2OH$}(μ-Cl)Cl]$_2$ (30 mg, 0.051 mmol) in dry methanol (2 mL). The reaction mixture was stirred at ambient temperature for 2 h. The solvent was removed in the rotary evaporator to give a yellow solid, which was redissolved in the minimum volume of ethanol. Addition of diethyl ether afforded the

precipitation of a yellow solid, which was collected by filtration, and dried in vacuum. Yield: 27 mg (75%). Elemental analysis: Cald for $C_{10}H_{18}Cl_2N_2ORu$ (354.24): C, 33.91; H, 5.12; N, 7.91. Found: C, 33.90; H, 5.09; N, 8.17. ^{1}H NMR (400 MHz, D_2O, δ): 5.80 (t, *J* = 5.9 Hz, Ar H, 2H), 5.69–5.66 (m, Ar H, 3H), 3.89 (t, *J* = 6.1 Hz, –C*H*$_2$–, 2H), 2.70 (t, *J* = 6.1 Hz, –C*H*$_2$–, 2H), 2.50–2.45 (m, –C*H*$_2$–, 4H). ESI-MS (m/z): $[M–Cl–H]^+$ calcd. for $C_{10}H_{17}N_2ORu$, 283.0; found, 283.0. Crystals suitable for X-ray diffraction were obtained by slow evaporation of a methanol/diethyl ether solution at ambient temperature.

[Ru{η^6-C$_6$H$_5$(CH$_2$)$_2$OH}(tmen)Cl]Cl (16Cl). *N,N,N',N'*-tetramethylethylenediamine (5 μL, 0.034 mmol) was added to a suspension of [Ru(η^6-C$_6$H$_5$(CH$_2$)$_2$OH)(μ-Cl)Cl]$_2$ (10 mg, 0.017 mmol) in dry methanol (2 mL). The reaction mixture was stirred at ambient temperature for 3 h. The solvent was removed in the rotary evaporator to give an orange solid, which was redissolved in the minimum volume of ethanol. Addition of diethyl ether afforded the precipitation of a yellow solid, which was collected by filtration, and dried in vacuum. Yield: 11 mg (79%). ^{1}H NMR (400 MHz, D_2O, δ): 5.90–5.87 (m, Ar H, 3H), 5.74–5.72 (m, Ar H, 2H), 3.83 (t, *J* = 6.2 Hz, –C*H*$_2$–, 2H), 3.36 (s, –C*H*$_3$, 6H), 2.78 (s, –C*H*$_3$, 6H), 2.68 (t, *J* = 6.1 Hz, –C*H*$_2$–, 2H), 2.49 (m, –C*H*$_2$–, 4H). Crystals suitable for X-ray diffraction were obtained by slow evaporation of a methanol/diethyl ether solution at ambient temperature.

[Ru{η^6-C$_6$H$_5$(CH$_2$)$_2$OH}(azpy-NMe$_2$)Cl]Cl (17Cl). Ethylenediamine (7.7 μL, 0.034 mmol) was added to a suspension of [Ru(η^6-C$_6$H$_5$(CH$_2$)$_2$OH)(μ-Cl)Cl]$_2$ (10 mg, 0.017 mmol) in dry methanol (2 mL). The reaction mixture was stirred at ambient temperature for 3 h. The solvent was removed in the rotary evaporator to give a blue solid, which

was redissolved in the minimum volume of ethanol. Addition of diethyl ether precipitated a purple solid, which was collected by filtration, and dried in vacuum. Yield: 9 mg (48%). Elemental analysis: Cald. for $C_{21}H_{25}Cl_2N_4ORu$ (521.43): C, 48.37; H, 4.83; N, 10.75. Found: C, 47.41; H, 5.10; N, 9.72. ^{1}H NMR (400 MHz, D_2O, δ): 9.23 (d, *J* = 5.7 Hz, Ar H, 1H), 8.22–8.17 (m, Ar H, 4H), 7.58 (td, *J* = 5.8, 3.0 Hz, Ar H, 1H), 6.94 (d, *J* = 9.6 Hz, Ar H, 2H), 6.23 (t, *J* = 6.0 Hz, Ar H, 1H), 6.19 (t, *J* = 6.1 Hz, Ar H, 1H), 6.02 (d, *J* = 6.2 Hz, Ar H, 1H), 5.98 (d, *J* = 6.2 Hz, Ar H, 1H), 5.85 (t, *J* = 5.9 Hz, Ar H, 1H), 3.81 (t, *J* = 6.0 Hz, –C*H*$_2$–, 2H), 3.29 (s, –C*H*$_3$, 6H), 2.66–2.48 (m, –C*H*$_2$–, 2H). Crystals suitable for X-ray diffraction were obtained by slow evaporation of a methanol/diethyl ether solution at ambient temperature.

[Ru{η^6-$C_6H_5(CH_2)_2OH$}(bip)Cl]Cl (18Cl). A solution of 2,2'-bipyridine (7 μL, 0.101 mmol) in methanol (1 mL) was added dropwise to a suspension of [Ru(η^6-$C_6H_5(CH_2)_2OH$)(μ-Cl)Cl]$_2$ (30 mg, 0.051 mmol) in methanol (2 mL). The reaction mixture was stirred at ambient temperature overnight. The resultant solution was filtered through a 0.45 μm syringe filter. The solvent was removed in the rotary evaporator to give a yellow solid, which was redissolved in the minimum volume of ethanol. Addition of diethyl ether afforded the precipitation of a yellow solid, which was collected by filtration, and dried in vacuum. Yield: 34 mg (75%). Elemental analysis: Cald for $C_{18}H_{18}Cl_2N_2ORu$ (450.33): C, 48.01; H, 4.03; N, 6.22. Found: C, 47.17; H, 4.08; N, 6.08. ^{1}H NMR (400 MHz, D_2O, δ): 9.44 (d, *J* = 5.0 Hz, Ar H, 2H), 8.38 (d, *J* = 8.1 Hz, Ar H, 2H), 8.21 (t, *J* = 7.9 Hz, Ar H, 2H), 7.75 (t, *J* = 7.9 Hz, Ar H, 2H), 6.22 (t, *J* = 6.1 Hz, Ar H, 2H), 6.04 (d, *J* = 6.3 Hz, Ar H, 2H), 5.91 (t, *J* = 5.8 Hz, Ar H, 1H), 3.86 (t, *J* = 6.1 Hz, –C*H*$_2$–, 2H), 2.67 (t, *J* = 6.1 Hz, –C*H*$_2$–, 2H). Crystals

suitable for X-ray diffraction were obtained by slow evaporation of a methanol/diethyl ether solution at ambient temperature.

[Ru{η^6-C$_6$H$_5$(CH$_2$)$_2$OH}(oxo)Cl]Na (19Cl). A solution of sodium oxalate (5 mg, 0.034 mmol) in 1 mL of 1:1 (v/v) water/acetone was added to a suspension of [Ru(η^6-C$_6$H$_5$(CH$_2$)$_2$OH)(μ-Cl)Cl]$_2$ (10 mg, 0.017 mmol) in dry methanol (2 mL). The resultant solution was filtered through a 0.45 μm syringe filter. The solvent was removed in the rotary evaporator to give an orange solid, which was redissolved in the minimum volume of ethanol. Addition of diethyl ether afforded the precipitation of a yellow solid, which was collected by filtration, and dried in vacuum. Yield: 5 mg (36%). ^{1}H NMR (400 MHz, D$_2$O, δ): 5.98 (t, *J* = 6.1 Hz, , Ar H, 2H), 5.83 (t, *J* = 5.9 Hz, , Ar H, 1H), 5.73 (d, *J* = 5.9 Hz, , Ar H, 2H), 3.94 (t, *J* = 6.0 Hz, –C*H*$_2$–, 2H), 2.78 (t, *J* = 6.1 Hz, –C*H*$_2$–, 2H).

[Ru{η^6-C$_6$H$_5$CH$_2$COOH}(en)Cl]Cl (20Cl). [Ru(η^6-C$_6$H$_5$CH$_2$COOH)Cl$_2$]$_2$ (100 mg, 0.162 mmol) was suspended in anhydrous ethanol (5 mL). Ethylenediamine (22 μL, 0.324 mmol) was added, and the mixture was stirred for 2 h at reflux. The resultant yellow solution was filtered through a 0.45 μm syringe filter. The solvent was reduced to ca. 5% of its original volume, and diethyl ether (4 mL) was added. The sticky solid was sonicated to give a yellow precipitate, centrifuged, washed with diethyl ether and dried in vacuum. Yield: 96 mg (80%). Elemental analysis: Cald. for C$_{10}$H$_{16}$Cl$_2$N$_2$O$_2$Ru (368.22): C, 31.10; H, 4.70; N, 7.25. Found: C, 32.54; H, 4.87; N, 7.83. ^{1}H NMR (400 MHz, MeOD-*d*$_4$, δ): 6.43 (br s, NH$_2$, 2H), 5.75 (t, *J* = 5.7 Hz, Ar H, 2H), 5.67 (d, *J* = 5.7 Hz, Ar H, 2H), 5.64 (t, *J* = 5.5 Hz, Ar H, 1H), 4.04 (br s, N*H*$_2$, 2H), 3.57 (s, –C*H*$_2$–, 2H), 2.54–2.50 (m, –C*H*$_2$–, 2H), 2.46–2.41 (m, –C*H*$_2$–, 2H). ESI-MS (m/z): [M–Cl–H]$^+$

calcd. for $C_{10}H_{15}N_2O_2Ru$, 297.0; found, 297.0. Crystals suitable for X-ray diffraction were obtained by slow evaporation of a methanol/diethyl ether solution at ambient temperature.

2.5 References

(1) Jeffrey, J. C.; Rauchfuss, T. B. Metal Complexes of Hemilabile Ligands. Reactivity and Structure of Dichlorobis(o-(diphenylphosphino)anisole)Ruthenium(II). *Inorg. Chem.* **1979**, *18*, 2658-2666.

(2) Braunstein, P.; Naud, F. Hemilability of Hybrid Ligands and the Coordination Chemistry of Oxazoline-Based Systems. *Angew. Chem. Int. Ed.* **2001**, *40*, 680-699.

(3) Braunstein, P. Functional Ligands and Complexes for New Structures, Homogeneous Catalysts and Nanomaterials. *J. Organomet. Chem.* **2004**, *689*, 3953-3967.

(4) Springman, E. B.; Angleton, E. L.; Birkedal-Hansen, H.; Van Wart, H. E. Multiple Modes of Activation of Latent Human Fibroblast Collagenase: Evidence for the Role of a Cys73 Active-Site Zinc Complex in Latency and a "Cysteine Switch" Mechanism for Activation. *Proc. Natl. Acad. Sci.* **1990**, *87*, 364-368.

(5) Van Wart, H. E.; Birkedal-Hansen, H. The Cysteine Switch: a Principle of Regulation of Metalloproteinase Activity with Potential Applicability to the Entire Matrix Metalloproteinase Gene Family. *Proc. Natl. Acad. Sci. U. S. A.* **1990**, *87*, 5578-5582.

(6) Carey, F. A. *Organic Chemistry*; McGraw-Hill: New York, NY, 2000.

(7) McMurry, J. *Organic Chemistry*; Cengage Learning: Boston, MA, 2015.

(8) Melchart, M.; Habtemariam, A.; Novakova, O.; Moggach, S. A.; Fabbiani, F. P. A.; Parsons, S.; Brabec, V.; Sadler, P. J. Bifunctional Amine-Tethered Ruthenium(II) Arene Complexes Form Monofunctional Adducts on DNA. *Inorg. Chem.* **2007**, *46*, 8950-8962.

(9) Melchart, M.; Parsons, S.; Sadler, P. Experimental Crystal Structure Determination. **2015**, 10.5517/cc1jf9bl.

(10) Morris, R. E., et al. Inhibition of Cancer Cell Growth by Ruthenium(II) Arene Complexes. *J. Med. Chem.* **2001**, *44*, 3616-3621.

(11) Chen, H.; Parkinson, J. A.; Parsons, S.; Coxall, R. A.; Gould, R. O.; Sadler, P. J. Organometallic Ruthenium(II) Diamine Anticancer Complexes: Arene-Nucleobase Stacking and Stereospecific Hydrogen-Bonding in Guanine Adducts. *J. Am. Chem. Soc.* **2002**, *124*, 3064-3082.

(12) Ito, M.; Komatsu, H.; Endo, Y.; Ikariya, T. Synthesis and Structure of Novel (η1:η6-Aminoalkylarene)Ru(II) Complexes. *Chem. Lett.* **2009**, *38*, 98-99.

(13) Zheng, C.; Kim, K.; Matsumoto, T.; Ogo, S. The Useful Properties of H2O as a Ligand of a Hydrogenase Mimic. *Dalton Trans.* **2010**, *39*, 2218-2225.

(14) Navarro, M.; Vidal, D.; Clavero, P.; Grabulosa, A.; Muller, G. Mild Photochemical Tethering of [RuCl2(η6-arene)P*] Complexes with P-Stereogenic 2-Biphenylylphosphines. *Organometallics* **2015**, *34*, 973-994.

(15) Geldbach, T. J.; Breher, F.; Gramlich, V.; Anil Kumar, P. G.; Pregosin, P. S. X-ray Diffraction and NMR Studies on a Series of Binap-Based Ru(II) Hydroxyphosphine π-Arene Complexes. *Inorg. Chem.* **2004**, *43*, 1920-1928.

(16) Pizarro, A. M.; Melchart, M.; Habtemariam, A.; Salassa, L.; Fabbiani, F. P. A.; Parsons, S.; Sadler, P. J. Controlling the Reactivity of Ruthenium(II) Arene Complexes by Tether Ring-Opening. *Inorg. Chem.* **2010**, *49*, 3310-3319.

(17) Abraha Habtemarian, S. B.-L., and Peter J. Sadler. *Ruthenium Complexes, in Inorganic Syntheses*; John Wiley & Sons: 2010.

(18) Butters, M. E., M. C.; Hill-Cousins, J. T. An Unexpected Prins Desymmetrisation Reaction Driven by Silyl Migration. *ARKIVOC* **2012**, *7*, 114-126.

(19) Stodt, R.; Gencaslan, S.; Müller, Iris M.; Sheldrick, William S. Preparation, Reactivity and Peptide Labelling Properties of (η6-Arene)ruthenium(II) Complexes with Pendant Carboxylate Groups. *Eur. J. Inorg. Chem.* **2003**, *2003*, 1873-1882.

(20) Miyaki, Y.; Onishi, T.; Kurosawa, H. Synthesis and Reaction of Ruthenium(II) Complexes Containing Heteroatom Donor (O, N, and P) Tethered to η6-Arene Ring. *Inorg. Chim. Acta* **2000**, *300–302*, 369-377.

(21) Takafumi, O.; Yoshiharu, M.; Hideo, A.; Hideo, K. Coordination Behavior of Ruthenium(II) Complexes with Alcohol Ligand Tethered to η6-Arene Donor. *Chem. Lett.* **1999**, *28*, 809-810.

(22) Lastra-Barreira, B.; Diez, J.; Crochet, P.; Fernandez, I. Functionalized Arene-Ruthenium(II) Complexes: Dangling vs. Tethering Side Chain. *Dalton Trans.* **2013**, *42*, 5412-5420.

(23) Bocos, F. Master Thesis. 2017.

(24) Bruker. In *APEX2,SAINT and SADABS*; Eds; Bruker AXS Inc.: Madison, WI, 2008; pp

(25) AXS, B. In *SHELXTL Version 6.10, Structure Determination Package*; Eds; Bruker Analytical X-ray Instruments: 2000; pp

(26) Sheldrick, G. M. A Short History of SHELX. *Acta Crystallogr. Sect. A* **2008**, *64*, 112-122.

(27) Sheldrick, G. M. Crystal Structure Refinement with SHELXL. *Acta Crystallogr. Sect. C* **2015**, *71*, 3-8.

(28) Krężel, A.; Bal, W. A Formula for Correlating pKa Values Determined in D2O and H2O. *J. Inorg. Biochem.* **2004**, *98*, 161-166.

3.

Control of Reversible Activation Dynamics of $[Ru\{\eta^6:\kappa^1\text{-}C_6H_5(C_6H_4)NH_2\}(XY)]^{n+}$ and the Effect of Chelate Ligand Variation

3.1 Introduction

As demonstrated in Chapter 2, when the hemilabile ligand contained a nitrogen atom as the monodentate ligand Z, the ethylenediamine derivative [Ru{η^6:κ^1-$C_6H_5(C_6H_4)NH_2$}(en)]Cl_2 (**13**) presented the highest activation of the Ru–Z bond under acidic conditions. In this Chapter we have investigated the activation of a series of analogues Ru^{II} closed tethered complexes of general formula [Ru{η^6:κ^1-$C_6H_5(C_6H_4)NH_2$}(XY)]$^{n+}$, where XY is a bidentate chelating ligand, in non-aqueous solutions, and in water, within the acidic pH range.

We demonstrate that pH-activation (cleavage of the Ru–N_{tether} bond) is not only possible in the acidic pH scale but, most importantly, tuneable by using chelating ligands with different electronic and steric properties. The pH is a major factor that governs the activation and its associated kinetic parameters. Since this type of organometallic compounds has been reported to interact with DNA,[1, 2] we also have investigated the interaction of our switchable system with a model nucleobase, guanosine monophosphate (GMP). Finally, and most importantly, we prove total reversibility, forcing the activated form of the compound to reverse to its inactive form (closed-tether), again showing pH-dependent inactivation dynamics. We set the parameters that control the ruthenium arene (in)activation to further the design of pH-responsive switchable anticancer metallodrugs.

3.2 Results and Discussion

3.2.1 Synthesis and Characterization

Eleven closed-tether ruthenium(II) arene complexes, **13** and **21**–**30**, of general formula $[Ru\{\eta^6:\kappa^1\text{-}C_6H_5(C_6H_4)NH_2\}(XY)]^{n+}$ containing primary, secondary and tertiary aliphatic amines, *ortho*-phenylenediamine, and oxalato as chelating ligands (Table 3.1) were prepared following the synthesis described by Pizarro et al.,[3] in good yields. The complexes were fully characterized by ^{1}H NMR spectroscopy, and CHN analysis for **13**, **21**–**24** and **27**–**30**. Complexes **25** and **26** were characterized in the solution state by ^{1}H NMR spectroscopy and mass spectrometry. The $[Ru(\eta^6\text{-etb})Cl_2]_2$ dimer was used for the arene exchange reaction leading to the precursor complex $[Ru\{\eta^6:\kappa^1\text{-}C_6H_5(C_6H_4)NH_2\}Cl_2]$.

Upon reaction of $[Ru\{\eta^6:\kappa^1\text{-}C_6H_5(C_6H_4)NH_2\}Cl_2]$ with the appropriate chelating ligand (details in the Experimental Section) a mixture of two structural isomers, closed and open-tether Ru^{II} complexes (Figure 3.1), was obtained for complexes **13** and **21**–**27**, while complexes **28**–**30** were obtained as closed-tether isomers only. Usually both isomers, closed- and open-tether species, showed a typical set of three resonances attributable to the η^6-bound arene protons in the range ca. 5.20–6.20 ppm. The characteristic chemical shift difference between the most deshielded and most shielded η^6-bound arene resonances are ca. 0.70 ppm and 0.20 ppm for closed- and open- tether complexes, respectively. Analysis of the ^{1}H NMR spectra in all solvents used in this Chapter proved an instant and reliable evidence for the open- versus closed-tether ring status in Ru^{II} arene complexes in solution. Both closed- and open-tether structures were confirmed by X-ray crystal structure analysis.

Table 3.1. Tether ruthenium(II) arene complexes of general formula [Ru{η^6:κ^1-$C_6H_5(C_6H_4)NH_2$}(XY)]Cl_n (n = 0, 2) studied in this Chapter, containing different XY chelating ligands.

Complex	X-Y Ligand		Complex	X-Y Ligand	
13	en	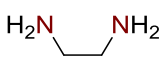	**27**	dpip	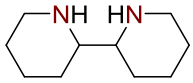
21	dap	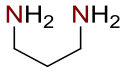	**28**	tmen	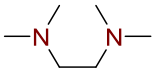
22	dab	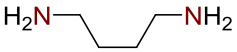	**29**	*o*-pda	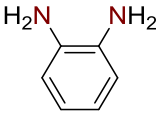
23	dach	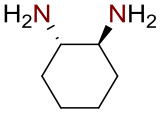	**30**	oxo	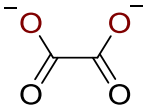
24	pipma	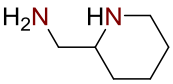	**31Cl**	dmphe	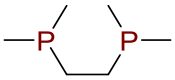
25	dmen	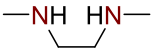	**32Cl**	dtben	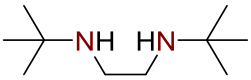
26	deen	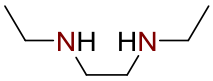	**33Cl**	bipy	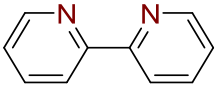

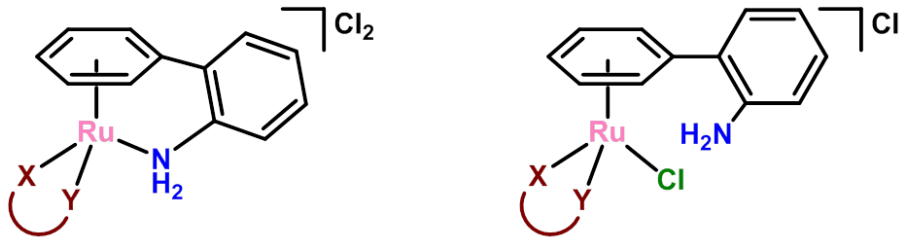

closed-tether **open-tether**

Figure 3.1. Ruthenium(II) arene tether isomers of general formula [Ru{η^6:κ^1-$C_6H_5(C_6H_4)NH_2$}(XY)]Cl_2, closed-tethered complex (left), and [Ru{η^6-$C_6H_5(C_6H_4)NH_2$}(XY)Cl]Cl, open-tether complex (right). Ru^{II} arene closed-tether complex **30**, where XY is oxalato, is neutral, and no chloride ions are present in its structure; for the open tether obtained in solution, the vacant site would be occupied by a solvent molecule, and the complex remains neutral.

Observation of open-to-closed tether conversion in aqueous solution, overnight at ambient temperature, allowed for the separation of the closed-tether Ru^{II} complexes **13** and **21**–**27**. The crude product was re-dissolved in water, left to stand overnight at ambient temperature and subsequently lyophilized, affording quantitatively the closed-tether complexes **13** and **21**–**27** in good yields (over 95%). Tether-ring-opened analogues **13Cl** and **21Cl–29Cl**, of general structure [Ru{η^6-$C_6H_5(C_6H_4)NH_2$}(XY)Cl]Cl, where the κ^1-bound N_{tether} is released from the first coordination sphere of the metal to allow a chloride ligand bind the ruthenium centre, were characterized in solution by ^{1}H NMR and LC/MS. While attempts to isolate complexes **31** and **32** were unsuccessful, it was possible to isolate pure open tether analogues **31Cl** and **32Cl** (characterized by CHN and NMR analysis). Complex **30Cl** was not observed in methanol, solvent in which **30** was insoluble. Dissolution of **30** in HCl afforded the dichlorido precursor [Ru{η^6:κ^1-$C_6H_5(C_6H_4)NH_2$}Cl_2]. Complex **33Cl** could be dissolved in DMSO-d_6, yet instability towards arene loss afforded complex $[Ru(bipy)_3]^{2+}$.[4] X-crystal structures of complexes **13**, **23**, **27**, **29**, **26Cl**, **28Cl**, and **28HCl**, were essential to unequivocally assign the open- and closed-tether ring structures. Solution experiments with complexes **30**–**33** were not performed due to their instability and/or insolubility under the conditions used in this Chapter.

3.2.2 X-Ray Crystal Structures

We determined the X-ray crystal structure of the closed-tether complexes **13**, **23**, **27** and **29** (Figure 3.2), and open-tether complexes **26Cl**, **28Cl** and **28HCl** (Figure 3.3).

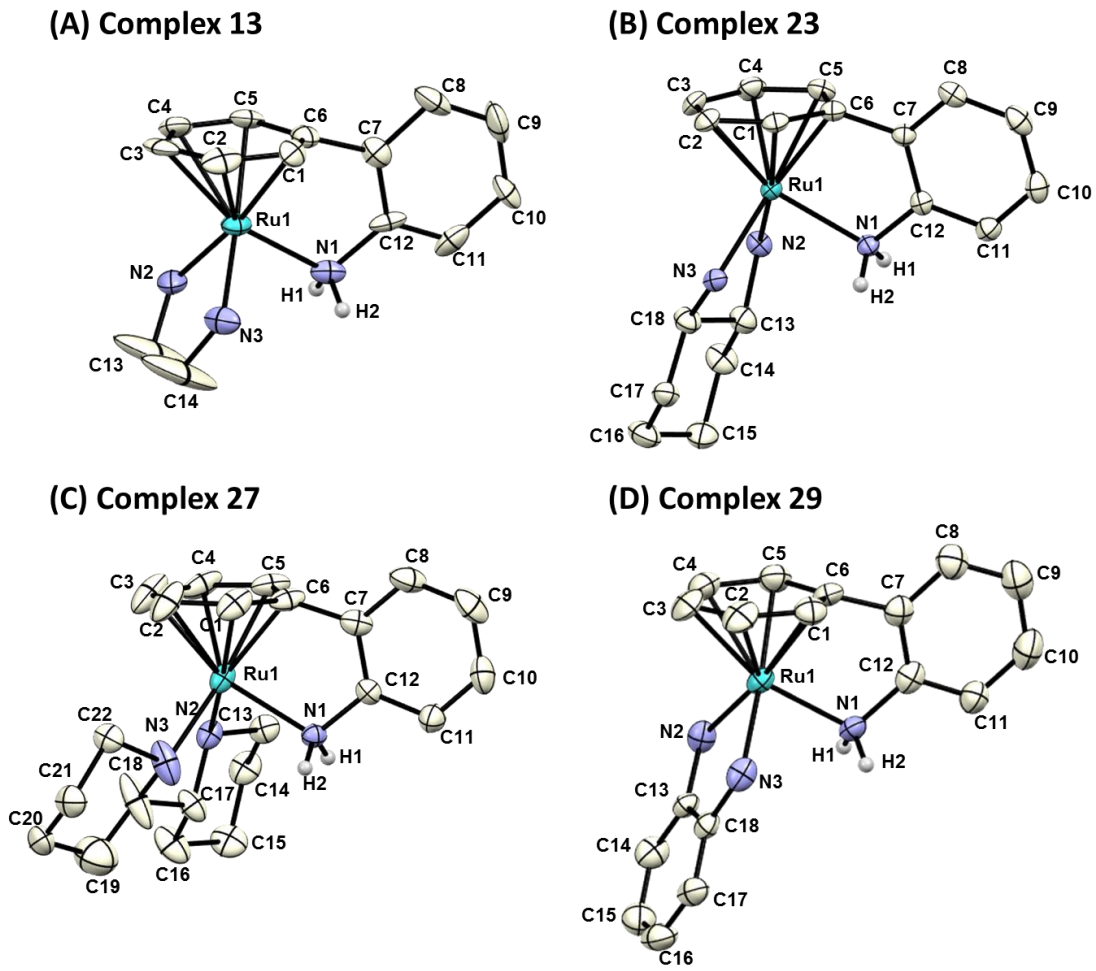

Figure 3.2. ORTEP diagrams and atom numbering for X-ray structures for (A) [Ru{η^6:κ^1-$C_6H_5(C_6H_4)NH_2$}(en)]Cl_2 (**13**), (B) [Ru{η^6:κ^1-$C_6H_5(C_6H_4)NH_2$}(dach)]Cl_2 (**23**), (C) [Ru{η^6:κ^1-$C_6H_5(C_6H_4)NH_2$}(dpip)]Cl_2 (**27**) and (D) [Ru{η^6:κ^1-$C_6H_5(C_6H_4)NH_2$}(*o*-pda)]Cl_2 (**29**), with thermal ellipsoids drawn at 50% probability. The H atoms (except those on the nitrogen pendant from the tether), chloride counterions and solvent molecules have been omitted for clarity.

X-ray diffraction data of suitable crystals corresponding to closed-tether complexes were collected for [Ru{η^6:κ^1-$C_6H_5(C_6H_4)NH_2$}(en)]Cl_2 (**13**), [Ru{η^6:κ^1-$C_6H_5(C_6H_4)NH_2$}(dach)]Cl_2 (**23**) and [Ru{η^6:κ^1-$C_6H_5(C_6H_4)NH_2$}(*o*-pda)]Cl_2 (**29**) from aqueous solutions. Single crystals of [Ru{η^6:κ^1-$C_6H_5(C_6H_4)NH_2$}(dpip)]Cl_2 (**27**) were obtained from the reaction mixture. Crystals suitable for X-ray analysis of complexes [Ru{η^6:κ^1-$C_6H_5(C_6H_4)NH_2$}(deen)Cl]Cl (**26Cl**) and [Ru{η^6:κ^1-$C_6H_5(C_6H_4)NH_2$}(tmen)Cl]Cl (**28Cl**) were obtained by crystallization from methanol.

Single crystals of protonated-open-tether complex [Ru{η^6-$C_6H_5(C_6H_4)NH_3$}(tmen)Cl]Cl_2 (**28HCl)** were obtained from a 1 M HCl solution.

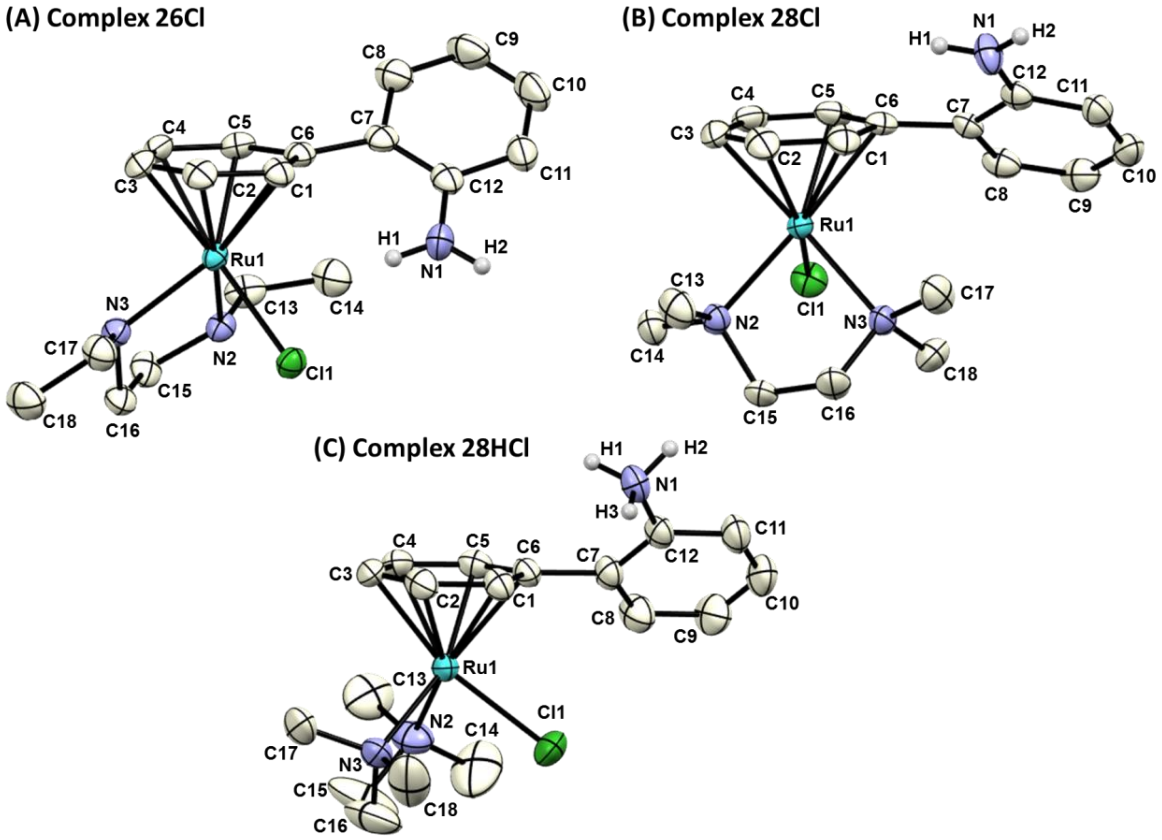

Figure 3.3. ORTEP diagrams and atom numbering schemes for (A) [Ru{η^6-$C_6H_5(C_6H_4)NH_2$}(deen)Cl]Cl (**26Cl**), (B) [Ru{η^6-$C_6H_5(C_6H_4)NH_2$}(tmen)Cl]Cl (**28Cl**), and (C) [Ru{η^6-$C_6H_5(C_6H_4)NH_3$}(tmen)Cl]Cl_2 (**28HCl**), with thermal ellipsoids drawn at 50% probability. The hydrogen atoms (with the exception of the tether NH_2/NH_3 protons), chloride counterions and solvent molecules have been omitted for clarity.

The complexes adopted the expected pseudo-octahedral "three-legged piano-stool" geometry with the ruthenium η^6-bonded to the arene ligand occupying three of the six octahedral positions. The other three positions in the first coordination sphere were occupied by a bidentate chelating ligand and either a NH_2 group (pendant from the η^6-bound arene) for **13**, **23**, **27** and **29**, or a chlorido ligand for **26Cl**, **28Cl**, and **28HCl**. Closed-tether complexes **13**, **27** and **29** crystallized with two molecules, and **23** with eight molecules, in the unit cell. Structures corresponding to open-tether complexes

7Cl, **28Cl** and **28HCl** crystallized with four, two and four molecules in the cell unit, respectively.

Selected bond lengths and angles of closed-tether complexes **13**, **23**, **27** and **29** are shown in Table 3.2. The Ru–C_{arene} bond lengths are in the range of 2.108–2.221 Å. The Ru–N1 distances are 2.148–2.166 Å, and the distances ruthenium-to-centroid are 1.631–1.669 Å. The propeller twist of the pendant ring with respect to the coordinated phenyl of 2-aminobiphenyl ranges from 82.6º in **23** to 89.9º in **29**.

Table 3.2. Selected bond lengths (Å) and angles (deg) for complexes **13**, **23**, **27** and **29**.

Bond / angle	13	23	27	29
Ru-C6	2.115(13)	2.113(6)	2.114(4)	2.108(7)
Ru-C5	2.184(13)	2.180(6)	2.188(5)	2.163(8)
Ru-C4	2.207(14)	2.185(6)	2.179(5)	2.175(8)
Ru-C3	2.221(15)	2.219(6)	2.211(5)	2.189(7)
Ru-C2	2.198(13)	2.199(6)	2.218(5)	2.192(7)
Ru-C1	2.191(13)	2.190(6)	2.203(4)	2.170(8)
Ru-centroid	1.659	1.656	1.669	1.643
Ru-X	2.144(11)	2.124(5)	2.128(3)	2.128(6)
Ru-Y	2.148(11)	2.147(5)	2.131(4)	2.126(6)
Ru-N1	2.161(11)	2.156(4)	2.167(3)	2.147(5)
X-Ru-Y	80.4(4)	79.17(18)	79.45(14)	79.6(2)
X-Ru-N1	88.2(4)	86.89(18)	89.45(13)	88.5(2)
Y-Ru-N1	88.0(4)	89.72(18)	88.15(16)	87.7(2)
Propeller twist	89.7	82.6	88.9	89.9
C7–offset[a]	0.488 (+)	0.460 (+)	0.460 (+)	0.475 (+)

[a] Offset of C7 with respect to the plane formed by the bound arene (carbons C1–C6); (+) toward ruthenium

Coordination of the NH_2 group of the pendant arm to the ruthenium centre results in different Ru–centroid distances, appearing to be shorter in **13** (1.659 Å), than the reported open-tether analogue **13Cl** (1.666 Å).[3] Additional differences are observed in C7–offset distances (0.488 Å towards ruthenium for **13** and 0.055 Å for the corresponding open-tether counterpart **13Cl**).

Importantly, the size of the tether arm may influence the strain on the structure as indicated by bond lengths and angles. In order to demonstrate the contribution of tether-ring size to cause such strain we compare complex **13** with X-ray crystallographic data of structurally related complexes, containing a five-member and a six-member ring with a tethering aliphatic amine. For example, in complex **13** and its analogue **13Cl**,[5] both with two carbon atoms between the η^6-bound arene and the N_{tether}, centroid distances are similar (1.659 vs 1.651 Å), and Ru-C6-C7 angles are in the same range 113–115º. However, when the number of carbon atoms in the tether arm is three, as in [Ru{η^6:κ^1-$C_6H_5(CH_2)_3NH_2$}(deen)]Cl_2,[5] Ru–centroid distance increases to 1.679 Å and the Ru-C6-C7 angle to 126º. This suggests that the shorter the pendant arm, the higher the ring constraint, since the non-strained Ru-C6-C7 angle in open-tether complexes is ca. 130º.

As expected, open-tether complexes **26Cl**, **28Cl** and **28HCl** showed longer ruthenium-centroid distances (1.684–1.688 Å), in agreement with a non-strained structure. Selected bond lengths and angles are shown in Table 3.3. Detailed crystallographic data are shown in Annex 2. The propeller twist of the pendant ring with respect to the coordinated phenyl of 2-aminobiphenyl is significantly smaller, ranging from 41 to 46º. The Ru–C_{arene} bond lengths are accordingly significantly higher (2.168–2.273 Å) for the open tether complexes, and the Ru–Cl distances are 2.400–2.410 Å.

The structural analysis shows a pronounced tilt in the η^6-bound arene for closed-tethers in comparison to open-tether complexes, as indicated by the differences in the Ru–C3 versus Ru–C6 bond lengths. Additional tether-ring strain is defined by the offset of C7 with regard to the plane that contains the η^6-bound arene. Comparison between the propeller twist in closed complexes (83–90º) versus open tether structures (40–46º) furthers the evidence of the constraint that the tether ring holds, which has been related to instability of the complexes towards arene loss.[6]

Table 3.3. Selected bond lengths (Å) and angles (deg) for complexes **26Cl**, **28Cl** and **28HCl**.

Bond / angle	26Cl	28Cl	28HCl
Ru–C6	2.274(4)	2.245(3)	2.235(3)
Ru–C5	2.193(4)	2.195(3)	2.210(3)
Ru–C4	2.181(4)	2.182(3)	2.195(3)
Ru–C3	2.170(4)	2.174(3)	2.193(3)
Ru–C2	2.204(4)	2.191(3)	2.169(3)
Ru–C1	2.198(4)	2.185(3)	2.168(3)
Ru–centroid	1.688	1.686	1.684
Ru–X	2.163(3)	2.198(2)	2.229(3)
Ru–Y	2.148(3)	2.258(2)	2.200(3)
Ru–Cl	2.4096(9)	2.406(7)	2.4006(9)
X-Ru-Y	79.46(11)	80.03(8)	80.12(11)
X-Ru-Cl	82.62(8)	87.56(6)	89.83(9)
Y-Ru-Cl	85.66(9)	88.74(6)	86.86(8)
Propeller twist	40.43	40.54	45.75
C7–offset	0.228 (-)	0.121 (+)	0.017(-)

No significant differences are observed between the open-tether **28Cl** and its corresponding protonated species **28HCl**. However, a longer distance for the N1–C12 bond is observed in **28HCl** versus **28Cl**, indicating nitrogen protonation and subsequent loss of conjugation of the amine group (1.378 vs 1.462 Å).

In all complexes the chloride counterions were involved in weak bonding interactions with the N(tether) hydrogen atoms and the hydrogen atoms on the N(XY-chelate ligand) (Table 3.4). No intermolecular π-π stacking interactions were observed.

Table 3.4. Selected hydrogen-bonding interactions with the N_{tether} [N(t)] hydrogen atoms, and the hydrogen atoms on the $N_{XY\text{-chelating ligand}}$ [N(l)] for complexes **13**, **23**, **27**, **29**, **26Cl**, **28Cl**, and **28HCl**.

Closed	D–H···A	d(H···A)	d(D···A)	∠ DHA
13	N(t)–H···Cl	2.268	3.180	176
	N(l)–H···Cl	2.430	3.286	155
23	N(t)–H···Cl	2.288	3.194	168
	N(l)–H···Cl	2.357	3.286	176
	N(l)–H···Cl	2.310	3.234	171
27	N(t)–H···Cl	2.575	3.403	150
	N(t)–H···Cl	2.288	3.194	168
	N(l)–H···Cl	2.357	3.286	176
	N(l)–H···Cl	2.310	3.234	171
29	N(t)–H···Cl	2.242	3.155	171
	N(t)–H···Cl	2.247	3.165	176
Open	**D–H···A**	**d(H···A)**	**d(D···A)**	**∠ DHA**
26Cl	N(t)–H···Cl	2.505	3.279	147
	N(l)–H…Cl	2.265	3.193	175
28Cl	O–H···Cl	2.389	3.240	175
	O–H···Cl	2.423	3.269	175
	N(t)–H···Cl	2.169	3.000	162
Protonated	**D–H···A**	**d(H···A)**	**d(D···A)**	**∠ DHA**
28HCl	N(t)–H···Cl	2.467	3.217	142
	N(t)–H···Cl	2.246	3.133	174
	N(t)–H···Cl	2.230	3.113	172

3.2.3 Solution Studies in Non-aqueous Solvents

It has been reported that when the tether pendant group is poorly coordinating, such as alcohol or amine, coordination/dissociation can occur depending on the experimental conditions.[3, 6-9] We have investigated here the effects of varying the XY chelating ligand in $[Ru\{\eta^6{:}\kappa^1\text{-}C_6H_5(C_6H_4)NH_2\}(XY)]^{2+}$ on the tether ring opening in different solvents (methanol and dimethyl sulfoxide) with the aim of exploiting these systems as activatable organometallic switches, in drug design or otherwise.

^{1}H NMR or UV-visible spectroscopy were used to study the lability of the Ru–N_{tether} bond of closed-tether Ru^{II} complexes in different solvents over 24 h. All

quantification data (extent of open-tether species versus closed-tether complex at equilibrium) were generated by NMR spectroscopy, while kinetic data were obtained by UV-vis spectroscopy in the case of methanol, and by NMR for DMSO.

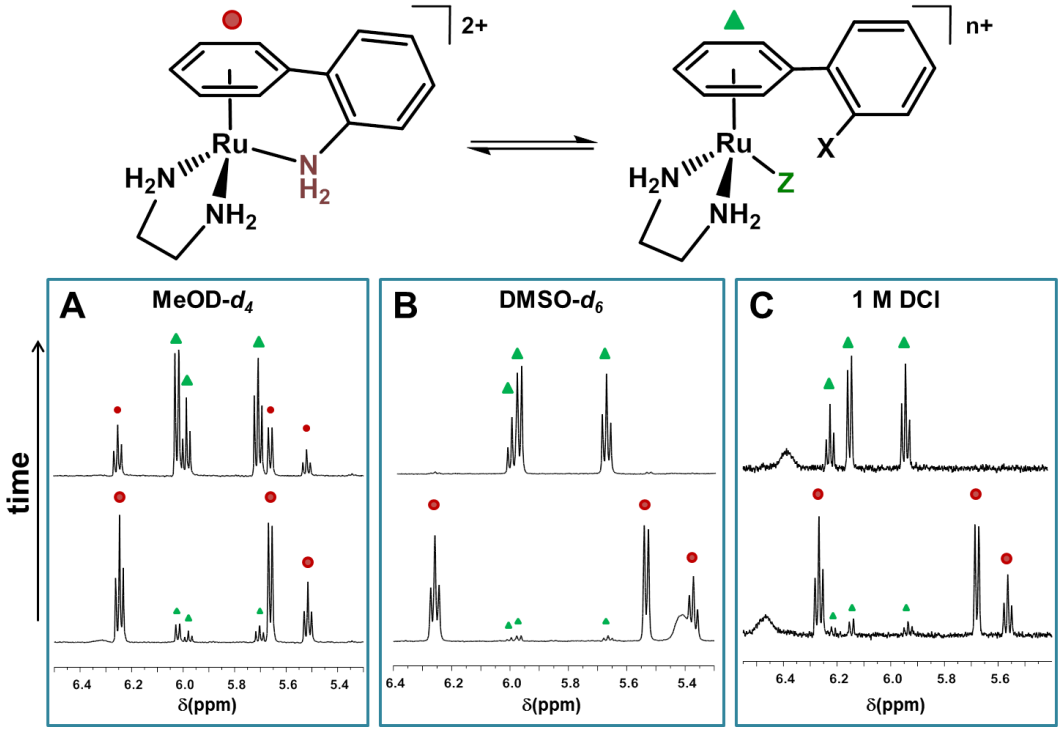

Figure 3.4. ^{1}H NMR low-field spectral region of 6 mM solutions of [Ru{η^6:κ^1-$C_6H_5(C_6H_4)NH_2$}(en)]$^{2+}$ (**13**, ●) showing resonances of the η^6-bounded arene ligand at various times in (A) MeOD-d_4 at 298 K (Z = Cl, X = NH_2), (B) DMSO-d_6 at 298 K (Z = DMSO, X = NH_2), and (C) 1 M DCl solution at 310 K (Z = Cl, X = NH_3^+). New sets of peaks appear (▲), corresponding to an open-tether species, in all solvents over 24 h.

Activation in methanol of the Ru–N_{tether} bond can provide important information about the tuneability of the ring-opening process since methanol readily dissolves our complexes and appears to be non-coordinating. Ring-opening dynamics were followed with complexes **13** and **21**–**29** by ^{1}H NMR spectroscopy. ^{1}H NMR data of freshly prepared 6–7 mM solutions of complexes **13** and **21**–**29** were recorded directly after the complex was dissolved ($t \leq 10$ min) and at 24 h, at 298 K in MeOD-d_4. The ^{1}H NMR spectra initially contained one major set of peaks attributable to the closed-ring form. A second set of peaks appeared over time (Figure 3.4A), increasing in intensity until

reaching equilibrium (2–24 h). The new set of peaks were assigned to the open-tether counterparts, **13Cl** and **21Cl–29Cl**, of general formula $[Ru\{\eta^6\text{-}C_6H_5(C_6H_4)NH_2\}(XY)Cl]^+$, formed to different extents at equilibrium. The crystallographic structures of **26Cl** and **28Cl** were obtained from methanol and unequivocally confirmed the chlorido open-tether complexes. The extent of the conversion of closed-to-open-tether at equilibrium varied depending on the chelating ligand (Figure 3.5).

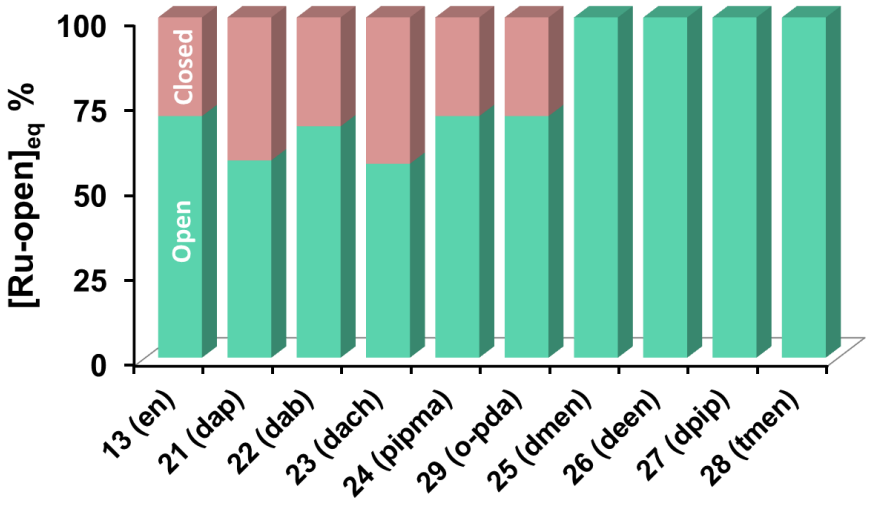

Figure 3.5. Percentage of Ru^{II} open species at equilibrium, corresponding to the activation of the complexes **13** and **21–29** in MeOD-d_4.

Only complexes bearing a secondary or tertiary aliphatic diamines as chelating ligand XY (**25–28**) underwent full conversion over 24 h at 298 K. Chelating ligands binding through primary amines RNH_2 (**13**, **21–24** and **29**) showed percentages of the open-tether complex at equilibrium in the range of 57–71%. Since the basicity of the chelating amines is similar and seems not to govern this trend (Table 3.5), we suggest that this effect might be attributable to a higher steric hindrance effect by the secondary and tertiary XY amines.

Table 3.5. Theoretical pK_a values corresponding to the free XY ligand.

XY in	**13**	**21**	**22**	**23**	**24**	**25**	**26**	**27**	**28**	**29**	**30**	**31**	**32**
pK_a	8.9	10.4	9.9	10.7	10.4	10.5	11.2	10.8	8.9	4.5	1.7	8.6	10.5

In order to determine the ring opening rate constants in methanol, 0.2 mM solutions of the Ru^{II} complexes were monitored over 24 h by UV-visible spectroscopy (Table 3.6 and Figure 3.6). The rate of tether-ring opening for complexes **21**, **22**, **25**, **26**, **28** and **29** was too fast to be determined by this method (equilibrium reached in < 5 min).

Table 3.6. Opening-tether kinetic data for complexes **13** and **21–30** in methanol, dimethylsulfoxide and 1 M HCl.

Complex	**Ligand**	**$k \times 10^{-4}$ (s^{-1})**			**$t_{1/2}$ (min)**		
		Methanol[a]	**DMSO[b]**	**1 M HCl[a]**	**Methanol[a]**	**DMSO[b]**	**1 M HCl[a]**
13	**en**	1.1	0.70	2.65	107	168	44
21	**dap**	n.d.	n.d.	3.48	< 5	< 5	33
22	**dab**	n.d.	n.d.	3.62	< 5	< 5	32
23	**dach**	0.61	0.68	1.63	191	170	71
24	**pipma**	0.81	0.86	0.73	142	135	158
25	**dmen**	n.d.	n.d.	n.d.	< 5	< 5	< 5
26	**deen**	n.d.	n.d.	n.d.	< 5	< 5	< 5
27	**dpip**	8.8	1.7	1.10	13	67	105
28	**tmen**	n.d.	n.d.	27.80	< 5	< 5	4
29	***o*-pda**	n.d.	n.d.	2.48	< 5	< 5	47
30	**oxo**	-	n.d.	-	-	< 5	-

[a] Determined by UV-visible spectroscopy
[b] Determined by ^1H NMR spectroscopy
n.d., too rapid to be determined

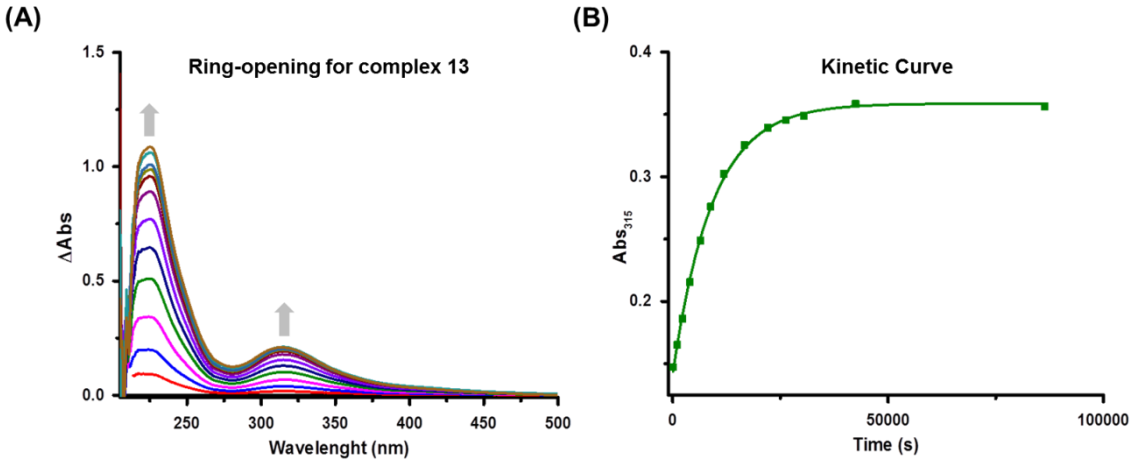

Figure 3.6. (A) UV-visible difference spectra of complex **13** in methanol showing that the largest changes in absorbance occurs at 225 and 315 nm. (B) Change in absorbance at 315 nm over 24 h during the opening of complex **13**, from which the kinetic data ($t_{1/2}$ and k) were determined.

In DMSO, the high coordinating nature of the solvent results in total tether-opening for all complexes in the series, following nucleophilic attack by dimethyl sulfoxide and subsequent formation of the DMSO adduct within 12 h. ^{1}H NMR data of freshly prepared 6–7 mM solutions of complexes **13** and **21**–**30** were recorded directly after the complex was dissolved ($t \leq 10$ min) and at 24 h, at 298 K in DMSO-d_6. The initial ^{1}H NMR spectra of complexes **13** and **21**–**30** after sample preparation (ca. 10 min) showed peaks corresponding to the intact closed-tethered species, as well as some low-intensity peaks assignable to Ru^{II} open-tether complexes (5–65%). After 24 h at 298 K, the peaks corresponding to the closed-tether precursor $[Ru\{\eta^6{:}\kappa_1\text{-}C_6H_5(C_6H_4)NH_2\}(XY)]^{2+}$ disappeared while the intensity of the signals corresponding to the open ring-tether complex reached 100% (Figure 3.4B) in all cases. The new open-tether Ru^{II} arene species were identified as $[Ru\{\eta^6\text{-}C_6H_5(C_6H_4)NH_2\}(XY)(DMSO)]^{n+}$, **13dmso** and **21dmso**–**30dmso**. The conversion of closed-tether Ru^{II} complexes into the open-tether dmso-adducts occurred at different rates, and the rate constants were determined based

on data obtained by ^{1}H NMR (Table 3.6 and Figure 3.7). For complexes **21**, **22**, **25**– **26** and **28**–**30** the tether opening rates in DMSO were too rapid to be determined.

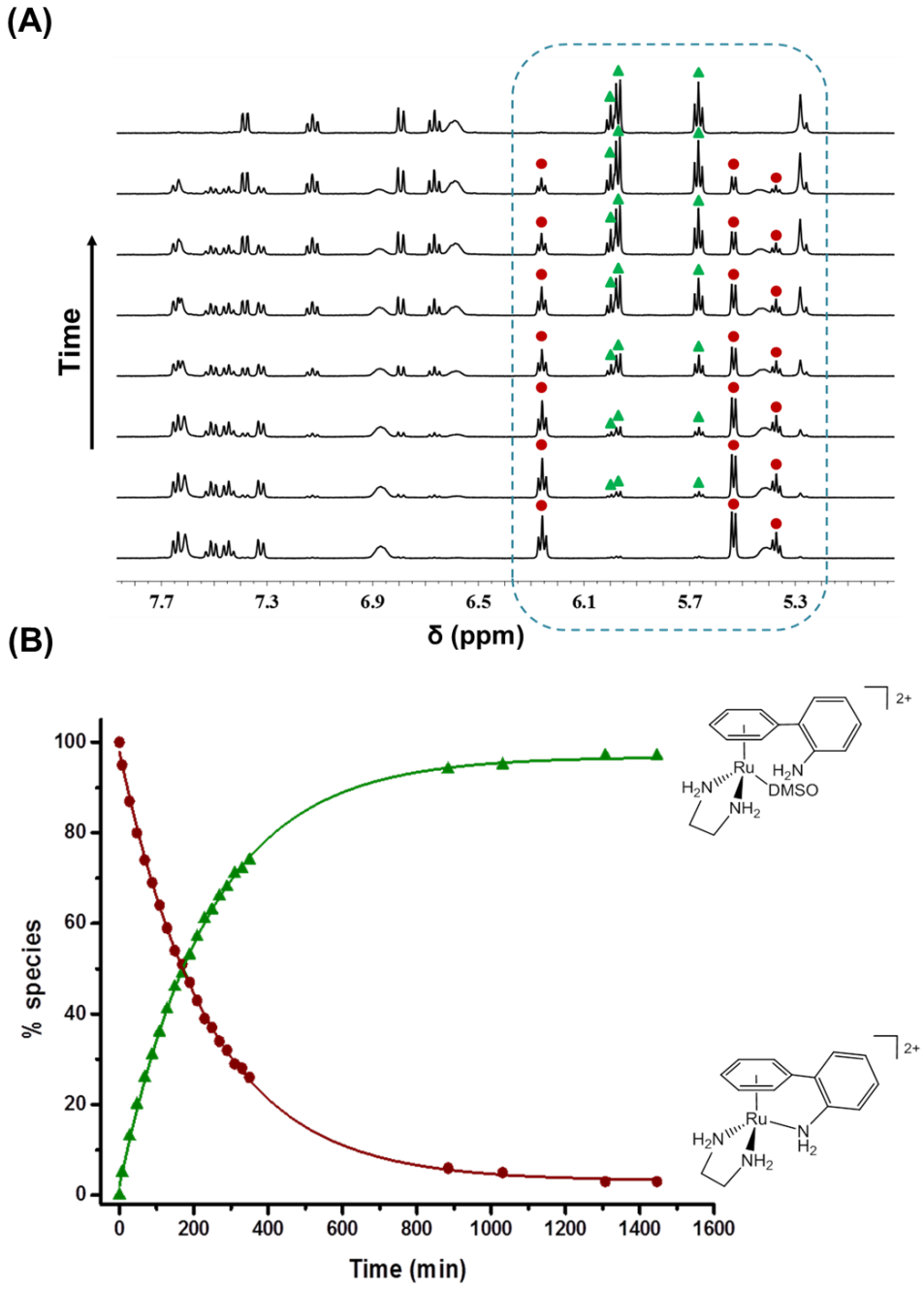

Figure 3.7. (A) Time evolution of the signals corresponding to the low-field arene region of the ^{1}H NMR spectra of $[Ru\{\eta^{6}:\kappa^{1}\text{-}C_6H_5(C_6H_4)NH_2\}(en)]^{2+}$ (**13**) in DMSO-d_6 at 298 K (6 mM Ru). (B) Plot of the concentration of open (▲) and closed-tether (●) complexes versus time for the conversion of $[Ru\{\eta^{6}:\kappa^{1}\text{-}C_6H_5(C_6H_4\}NH_2)(en)]^{2+}$ (**13**) into $[Ru\{\eta^{6}\text{-}C_6H_5(C_6H_4)NH_2\}(en)(DMSO)]^{2+}$ (**13dmso**) in DMSO-d_6 at 298 K.

The observed trend for the tether-ring opening process in DMSO is similar to that of methanol throughout the entire series (Table 3.6). We observed rapid reactivity in complexes **25**, **26** and **28**, which bear sterically demanding XY diamines of the type $RR'NCH_2CH_2NRR'$, where at least one of the R substituents is a carbon chain (methyl or ethyl) with free 360° rotation along the N–C(R) bond. This observation would be in agreement with an associative mechanism[10] for the substitution reaction. According to this mechanism, a molecule of solvent enters the ruthenium coordination sphere before the tether unbuckles from the Ru^{II} center, and therefore a more crowded intermediate would favor rapid dissociation of the N_{tether} from the ruthenium. Complex **23** shows - in both solvents - the slowest *k* and the longest half-life times of the series, which is in contrast with the rapid ring-opening rate of its aromatized counterpart, complex **29**, demonstrating how the tether ring dynamics can be finely tailored by the nature of XY. In their crystal structure a longer $Ru–N_{tether}$ bond (2.156 Å) in **23** is observed, as opposed to a shorter (2.148 Å) bond in **29**. This is in agreement with electron back donation by phenylenediamine in **29**, thus rendering the ruthenium center more electrophilic and subsequently more prone to nucleophilic attack.[11] Such attack could be enhanced in **29** due to the less sterically demanding sp^2 ligand phenylenediamine in comparison to sp^3 diaminocyclohexane.

3.2.4 Activation Under Acidic Conditions

Since our aim was to prove the pH-dependent on-and-off switching capability and tuneability of our system, we investigated the possibility of activating the $Ru–N_{tether}$ bond in aqueous solution at 310 K.

Very few studies where protonation of the binding functional group in the tether plays an important role in the dynamics of metal–tether bond in aqueous solution have

been reported.[9, 12-14] Pizarro et al. reported the synthesis of [Ru{η^6-$C_6H_5(C_6H_4)NH_3$}Cl_3] from its closed-tether counterpart, [Ru{η^6:η^1-$C_6H_5(C_6H_4)NH_2$}Cl_2], by suspending the former in concentrated HCl (ca. 12 M) at ambient temperature for 18 h. The tethered nitrogen dissociated from the ruthenium upon protonation.[3] Activation of a Ru–N_{tether} bond was also proved in the Ru^{II} tether complex [Ru{η^6:κ^1-$C_6H_5(C_6H_4)NH_2$}(en)]Cl_2 in 12 M HCl for 18 h, yielding [Ru{η^6:κ^1-$C_6H_5(C_6H_4)NH_3$}(en)Cl]$^{2+}$. Acidic activation had been deemed unsuccessful at pH as low as 2.

Complexes **13HCl** and **21HCl–29HCl** were dissolved in 1 M DCl and their ^{1}H NMR spectra were recorded at 310 K over 24 h (Figure 3.4C). In all cases the open-ring tethered cation [Ru{η^6-$C_6H_5(C_6H_4)NH_3$}(XY)Cl]$^{2+}$, **13HCl** and **21HCl–29HCl**, was identified as the only species at equilibrium. The ^{1}H NMR data showed that complexes **13HCl** and **21HCl–29HCl** were fully converted into the corresponding open-tether ruthenium arene hydrochloride salt upon dissociation of the NH_2(tether) group from the ruthenium center, position now occupied by a chlorido ligand. Under these acidic conditions, the NH_2 is protonated to become NH_3^+. X-ray crystallographic structure of complex **28HCl** allowed the unequivocal assignment of these complexes (Figure 3.3C). The conversion of closed-tethered species into the protonated open-tether Ru^{II} complexes occurred at different rates as determined by UV-visible spectroscopy (shown in Table 3.6 and Figure 3.8 for **13**).

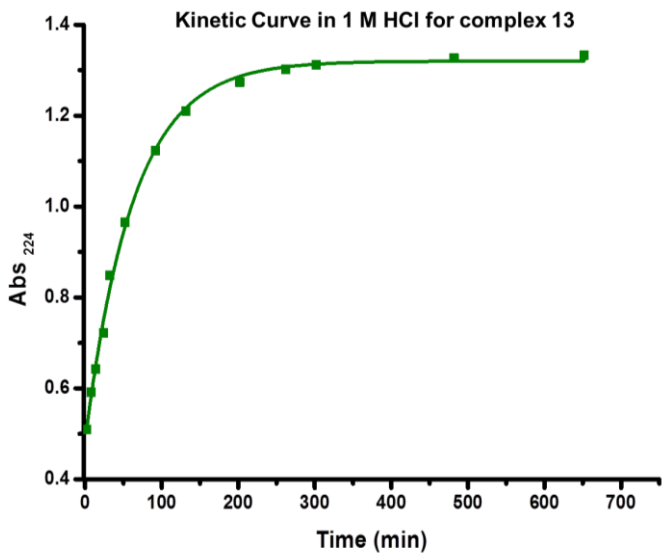

Figure 3.8. Time dependency (min) of the absorbance at 224 nm for the opening process of 0.2 mM $[Ru\{\eta^6{:}\kappa^1\text{-}C_6H_5(C_6H_4)NH_2\}(en)]^{2+}$ (**13**) in 1 M HCl solution at 310 K. The full line represents computer fit giving the first order rate constant.

The trend of the rates of activation for the series **13** and **21**–**28** shared similarities with those in methanol and DMSO. Complex **28**, bearing tetramethylethylenediamine as a chelating ligand, showed the highest rate constant for the pH-dependent tether-opening process. Complexes **25** and **26** were converted too rapidly into their protonated open-tether form (fully opened within 5 min), so their rate constants could not be determined by ^{1}H NMR nor UV-visible spectroscopy. The slowest rates of ring-opening in strong acidic conditions were for complexes **13**, **23**, **24**, **27**, and **29**, where the XY chelating ligand forms a 5-member chelating ring, which bears no freely rotating substituents in the N,N-chelating diamines. As observed for the tether/opening dynamics in non/aqueous solvents, this is in agreement with an associative mechanism for the substitution reaction (vide supra). Complexes **24** and **27**, bearing secondary amines with restricted rotation of the N–C bond in the chelating ligand, present the slowest rate constants, perhaps due to a more stable intermediate in the substitution reaction. This rational would explain why **25**, **26** and **28** show the most rapid tether-ring

opening, attributable to the high steric hindrance imposed by the methyl or ethyl groups, freely rotating along the N–C(R) axes in the chelating RR'NCH$_2$CH$_2$NRR' ligand.

In order to investigate the behavior of the Ru–NH$_2$(tether) bond under milder acidic conditions, complexes **13** and **21**–**29** in 0.1 M DCl solutions were followed over time at 310 K by ^{1}H NMR. A mixture of closed- and protonated open-tether Ru^{II} complexes, $[Ru(\eta^6{:}\kappa^1\text{-}C_6H_5(C_6H_4)NH_2)(XY)]^{2+}$ and $[Ru(\eta^6\text{-}C_6H_5(C_6H_4)NH_3)(XY)Cl]^{2+}$, was observed for all complexes at equilibrium. In general, higher percentages of open-tether Ru^{II} species are observed with increasing steric hindrance on the nitrogen atoms of the N,N-chelating diamine (Figure 3.9). Strikingly, complex **28** (XY = tetramethylethylenediamine, tmen), with the highest rate constant for the opening process of the series, showed the least percentage of open species at equilibrium, perhaps attributable to the lack of H-bond formation capability by tmen.[15]

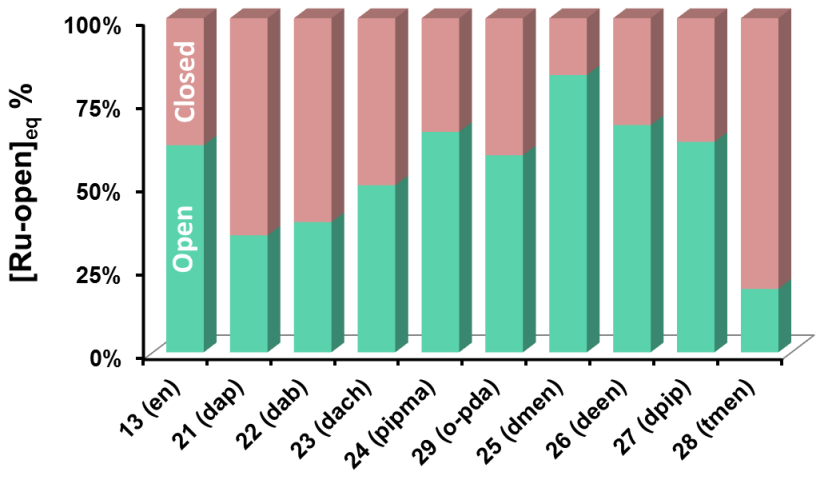

Figure 3.9. Percentage of Ru^{II} open species at equilibrium, corresponding to the activation of the complexes **13** and **21**–**29** in 0.1 M DCl.

A decrease in the concentration of DCl (0.01 M) resulted in a modest extent of activation of the Ru–N$_{tether}$ bond (ca. 2–5% of open-tether species at equilibrium). Further dilutions of DCl did not lead to the activation of the Ru–NH$_2$(tether) bond as observed by NMR spectroscopy.

^{1}H NMR experiments of complexes **13**, **25**, **26** and **28** in $DClO_4$ (0.1 M) were also carried out in presence and absence of 0.1 M NaCl, in order to investigate the role of the chloride ions in the opening process in acidic conditions. In the absence of NaCl, the percentage of protonated open species **13HCl**, **25HCl**, **26HCl** and **28HCl** were 17, 77, 50 and 3%, respectively, significantly lower than in the presence of sodium chloride (56, 79, 65 and 18%, respectively) as seen in Figure 3.10. Complex **25** and **26** showed the lowest activation dependency to the presence of excess chloride ions. The importance of the pH was demonstrated when complex **25** afforded merely 15% of the open tether complex **25Cl** when exposed to a 2 M NaCl solution for 24 h at 298 K. When experiments of tether ring activation of **13**, **25**, **26** and **28**, using a mixture of 0.1 M $DClO_4$ and 0.1 M NaCl were carried out, identical extent of activation to that of 0.1 M DCl solutions was obtained after 24 h.

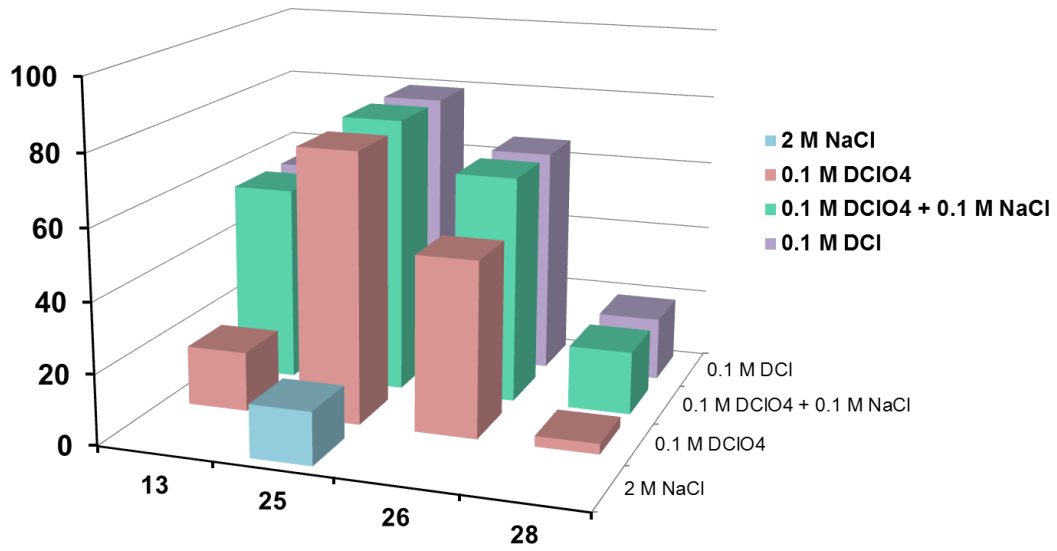

Figure 3.10. Percentage of Ru^{II} open species at equilibrium, corresponding to the activation of the complexes **13**, **25**, **26** and **28** in aqueous solutions of different proton and chloride concentrations.

3.2.5 pK_a Values and Reversibility of the Activation Process

The activation (opening) and deactivation (closing) of the ruthenium complex can be understood as the unbuckling and buckling of the pendant NH_2(tether) to Ru^{II}. For this reason, control over the availability of this group to bind to the metal center through its acid/base equilibrium (unavailable NH_3^+ versus available for metal coordination NH_2) appears as an elegant way of controlling compound activation. For this purpose we have determined the acid/base equilibrium (pK_a values) of the pendant tether-nitrogen for complexes **25HCl** and **28HCl**.

The pH dependency of the ^1H NMR chemical shifts of the η^6-bound arene of $[Ru\{\eta^6\text{-}C_6H_5(C_6H_4)NH_3\}(dmen)Cl]^{2+}$ (**25HCl**) and $[Ru\{\eta^6\text{-}C_6H_5(C_6H_4)NH_3\}(tmen)Cl]^{2+}$ (**28HCl**) was probed over the pH range 0–10 and the pK_a of the amine group of the pendant arm was determined. Complexes **25** and **28** were dissolved in 1 M DCl to obtain **25HCl** and **28HCl**. At pH 0, the species in solution was identified as $[Ru\{\eta^6\text{-}C_6H_5(C_6H_4)NH_3\}(dmen/tmen)Cl]^{2+}$. With increasing pH, the ^1H NMR triplet resonance corresponding to H_m (*meta*- proton of the η^6-bound arene) shifted to high-field accompanied with a decrease in intensity (see Figure 3.11 for **28HCl**). A plot of the change in chemical shift of the H_m(**25HCl**) and H_m(**28HCl**) versus pH is shown in Figure 3.12. The data were fitted to the Henderson-Hasselbach equation which yielded pK_a values of 2.51 and 2.64 for **25HCl** and **28HCl**, respectively. These values are ca. 1.5 units lower than that of the free ligand (pK_a 3.81). This suggests that electron density from the aniline pendant ring is more readily delocalized when 2-aminobiphenyl is η^6-coordinated to Ru^{II}. The higher pK_a for **28HCl** versus **25HCl** may be understood on the basis of the more electron rich tmen in comparison

with dmen, perhaps ultimately conferring more basicity to the tether NH_2 through the arene ligand on the Ru^{II}.

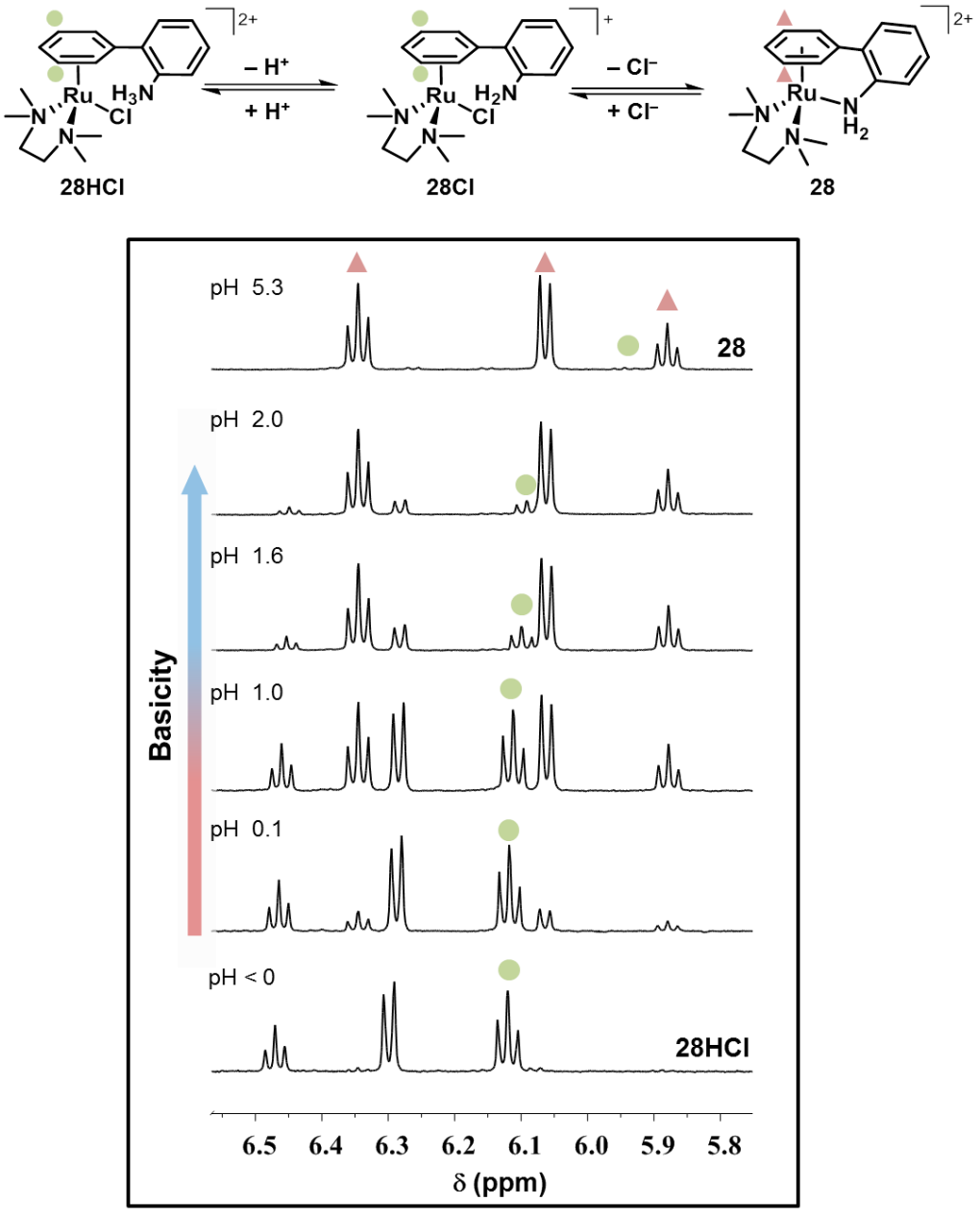

Figure 3.11. pH-dependence of the signals corresponding to the η^6-bound arene spectral region of $[Ru\{\eta^6\text{-}CH_5(C_6H_4)NH_3\}(tmen)Cl]^{2+}$ (●) in DCl/D_2O. Note that a new species (▲), the closed tether counterpart $[Ru\{\eta^6\text{-}CH_5(C_6H_4)NH_2\}(tmen)]^{2+}$, appears over time to finally dominate the spectrum at pH 5.3.

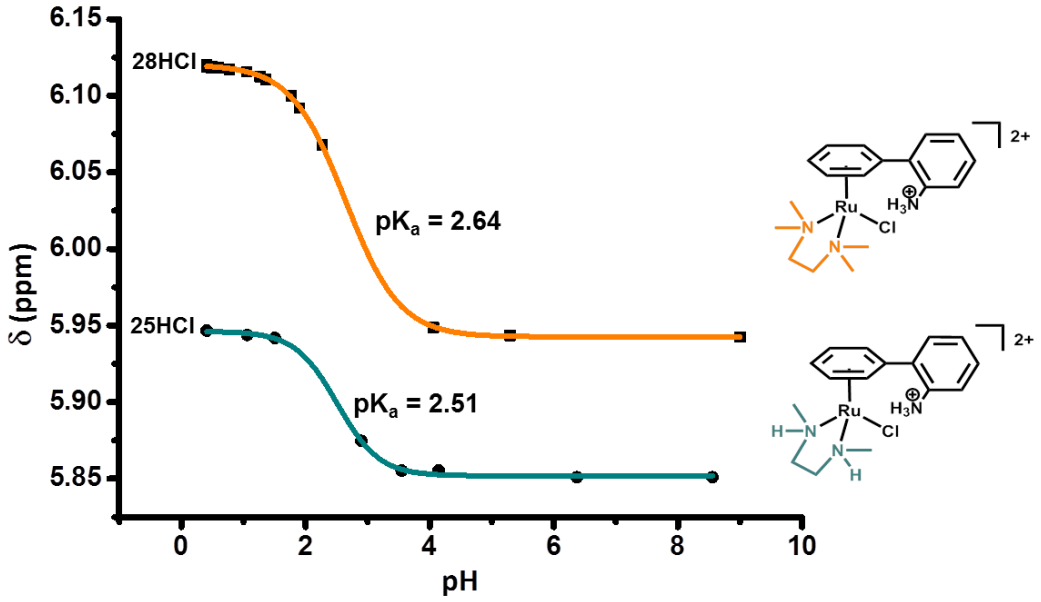

Figure 3.12. ^{1}H NMR chemical shift dependency of the H_m proton of the η^6-bound arene on pH of the protonated open-tether complexes $[Ru\{\eta^6\text{-}C_6H_5(C_6H_4)NH_3\}(dmen)Cl]^{2+}$ (**25HCl**) and $[Ru\{\eta^6\text{-}C_6H_5(C_6H_4)NH_3\}(tmen)Cl]^{2+}$ (**28HCl**). The curve represents the best fit to the Henderson-Hasselbalch equation and corresponds to pK_a value of 2.51 and 2.64, respectively.

Since our aim is to design systems capable of reversible switching, we investigated the pH effect in the reverse tether-ring closure. This process, to our understanding mediated by hydrolysis,[3] was followed for complex **25Cl** in water at different pH values above the pK_a of the amine tether group. Open-tether complex **25Cl** (6 mM) was dissolved in different pH buffered aqueous solutions at 310 K. The closure rate to form **25** in these solutions was monitored by ^{1}H NMR spectroscopy. Data were fitted to the Henderson-Hasselbach equation which yielded half-life values of 84, 75, 63 and 15 min for pH 3.4, 4.3, 5.8 and 7.2, respectively. The rate constants were calculated as 8.2, 9.3, 11.0 and 50.8 × 10^{-3} min^{-1}. The data revealed that inactivation (ring closure) of the Ru^{II} complex is slower at the more acidic pH. The results, shown in Figure 3.13, clearly illustrate that tether-ring fastening is governed by pH.

Proton concentration plays a key role both in the activation and in the deactivation process, as protons appear to compete with the electrophilic ruthenium center for the nucleophilic free dangling amine.

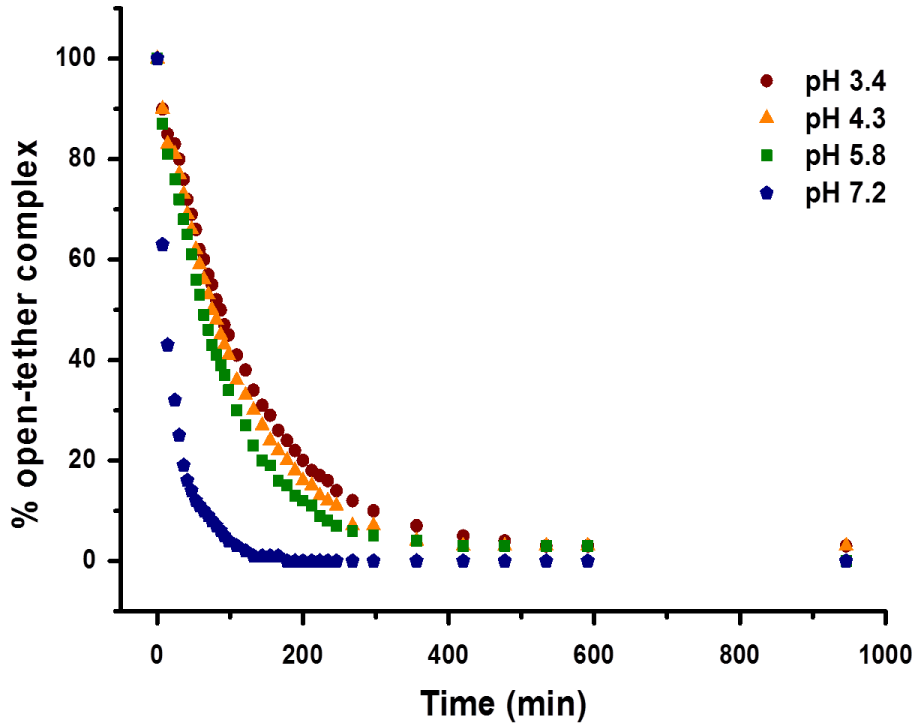

Figure 3.13. The rate of reversion of the open-tether species [Ru{η^6-$C_6H_5(C_6H_4)NH_2$}(dmen)Cl]Cl (**25Cl**), to [Ru{η^6:κ^1-$C_6H_5(C_6H_4)NH_2$}(dmen)]$^{2+}$ (**25**) in four different citrate/phosphate buffered solutions over time at 310 K.

3.2.6 Interaction with Nucleobases and Biological Activity

Irreversible DNA damage is often believed to be the mechanism of action of metal-based anticancer complexes, with guanine N7 nitrogen being the preferred metal binding site on DNA.[2, 16-18] We propose that open (activated) tether Ru^{II} complexes are prone to nucleobase interaction, while the corresponding closed tether complex, with no vacant site in the first coordination sphere around the ruthenium centre, should not interact with the model nucleobase.

We were interested in knowing if closed-to-open tether Ru^{II} arene activation could lead to DNA interaction, hence the reaction of **25Cl** with guanosine monophosphate (GMP) was investigated. The binding of the open-tether complex **25Cl**, $[Ru\{\eta^6\text{-}C_6H_5(C_6H_4)NH_2\}(dmen)Cl]^+$, to 5'-GMP in either water or methanol was monitored by ^1H NMR spectroscopy. Upon mixing **25Cl** with 5'-GMP (1:5 metal:nucleobase ratio, 5 mM Ru^{II}) in deuterated methanol, total disappearance of the peaks corresponding to complex **25Cl** and the appearance of new peaks assignable to Ru-guanine adducts, including three new peaks in the H8 region of guanine, was observed in the ^1H NMR spectra at 298 K over 24 h (equilibrium).

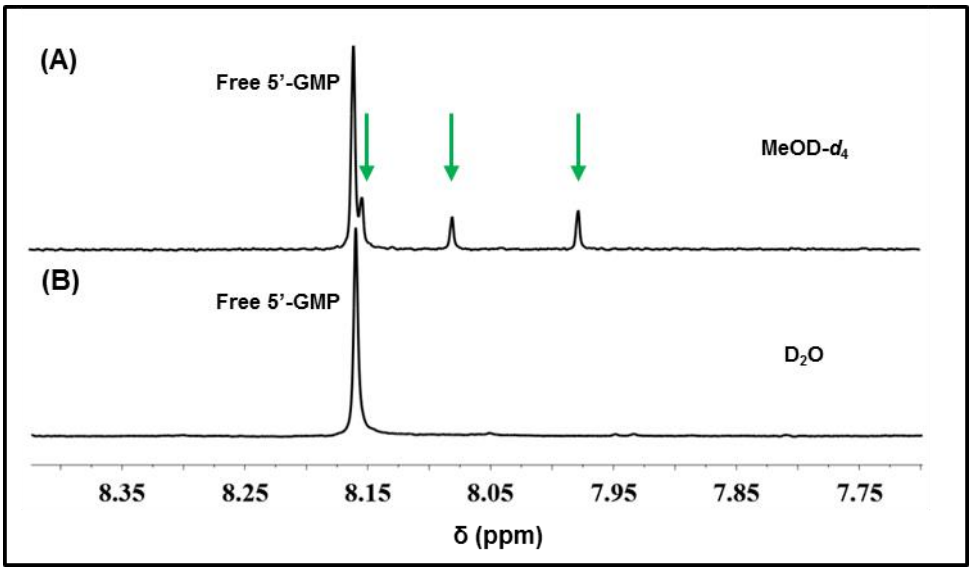

Figure 3.14. Region of H8-guanine in the ^1H NMR spectrum. (A) Three new peaks assignable to Ru-guanine adducts are observed upon mixing open complex **25Cl** and 5'-GMP in methanol for 24 h. (B) No new signals corresponding to guanine adducts are observed in the reaction of closed complex **25** and 5'-GMP in water over 24 h at 310 K.

The three new peaks (Figure 3.14) were tentatively assigned to the Ru–*N7*GMP, Ru–*O*(PO_3)GMP and Ru–*N1*GMP adducts, according to literature.[19, 20] We hoped to investigate the pH-dependency of the binding of complex **25Cl** to nucleobases. However, the pK_a of the tether NH_3^+ (ca. 2.5) is inconveniently close to that of the N7 of guanine (pK_a 2.57).[19, 21] This implies that prevention of $Ru–N_{tether}$ bond formation by

carrying out the reaction at pH < $pK_a(NH_3^+{}_{tether})$ would also render the guanine unable for interaction with the ruthenium.

Reaction of closed-tether **25** with 5 mol equiv of 5'-GMP in D_2O at 310 K did not afford any new H8-guanine signals over 24 h (Figure 3.14) as observed by ^1H NMR. These results support that opening of the tether-ring equals Ru^{II} complex activation, while a closed tether Ru^{II} complex is rendered unreactive towards nucleobases. These results are in agreement with the lack of cytotoxic activity in our cell viability experiments in the human ovarian cancer cell line A2780 for complexes **13** and **21**–**30** (Table 3.7). At the maximum concentration tested (100 μM), well within the range of cytotoxic activity for the type of drugs of general structure [Ru(η^6-arene)(XY)Cl]Cl as reported in literature,[22] no significant inhibition of cell growth was observed (with the exception of complex **29**, perhaps attributable to redox-active *o*-pda ligand) and thus the complexes were deemed inactive. This demonstrates the inactivated state of the compounds at physiological pH, and represents the first step towards rational design of a pH-responsive organometallic pro-drug.

Table 3.7. Percentage of viable A2780 cells (human ovarian cancer) exposed to 100 μM of Ru complex as determined by the sulforhodamine B (SRB) assay,[5] following a reported protocol.[6] Cisplatin was used as the positive control, with an IC_{50} value of 1.0±0.3 μM. The SD (±7%) of the values is determined based on the negative control (100% of cell survival of drug-free cells).

Complex	% cell viability	complex	% cell viability
13	78	**26**	100
21	100	**27**	100
22	100	**28**	80
23	100	**29**	63*
24	100	**30**	100
25	100	**cisplatin**	0

* This value was not reproduced in subsequent experiments, which upon further investigation was attributed to lack of stability of **29** in aqueous solution over 24 h.

3.3 Conclusions

In this Chapter we have presented a series of Ru^{II} arene complexes capable of on-and-off switching in a pH-dependent manner. The complexes have a general structure of $[Ru(\eta^6{:}\kappa^1\text{-}C_6H_5(C_6H_4)NH_2)(XY)]Cl_n$, and show structural stability in solution. We have used this ruthenium platform to understand the chelate-based ring-opening and ring-closing reactions in view of the development of new pH-activatable inorganic drugs.

The complexes bear a $\eta^6{:}\kappa^1$-arene:N tether-ring capable of locking and unlocking by the $Ru–N_{tether}$ bond. We have demonstrated that once activated (tether-ring open) the Ru^{II} complexes are prone to interaction with nucleophiles, such as chloride ions, as well as with model DNA nucleobases. The activation kinetics and thermodynamic equilibria of the $Ru–N_{tether}$ bond can be finely tuned in methanol, dimethylsulfoxide and, more importantly, in acidic water by varying the N,N-chelating ligand. In general, both electronic and steric effects play a role in $Ru–N_{tether}$ activation in a substitution reaction that appears to occur via an associative mechanism.

We have demonstrated that organometallic drug activation via dissociation of the $Ru–N_{tether}$ bond in acidic water solution is possible within the pH scale. Importantly, protonation of the tethering group locks the complex in its activated form. Reversibly, deprotonation triggers metal binding thus rendering the complex unsuited for biomolecule interaction, conveniently inactivating the drug. The dynamics of tether ring opening (activation) and closure (inactivation) are both pH dependent. The process is fully reversible, and the system robust to such reversibility.

3.4 Experimental Section

3.4.1 Instrumentation

NMR Spectroscopy, Mass Spectrometry, Elemental Analysis and **pH Measurements** have been described in Chapter 2.

Single Crystal X-ray Diffraction. Suitable crystals of compounds **13**, **23**, **26Cl**, **27**, **28Cl**, **28HCl**, and **29**, were coated with mineral oil and mounted on Mitegen MicroMounts. The samples were measured in a Bruker D8 KAPPA APEX II diffractometer with CCD area-detector, equipped with graphite-monochromated Mo Kα radiation (λ = 0.71073 Å). The substantial redundancy in data allowed empirical absorption corrections (SADABS)[23] to be applied using multiple measurements of symmetry-equivalent reflections. Raw intensity data frames were integrated with the SAINT program, which also applied corrections for Lorentz and polarization effects. The Bruker SHELXTL Software Package was used for space group determination, structure solution, and refinement.[24] The space group determination was based on a check of the Laue symmetry, and systematic absences were confirmed using the structure solution. The structures were solved by direct methods (SHELXL-2014/7),[25, 26] completed with different Fourier syntheses, and refined with full-matrix least-squares using SHELXS minimizing $\omega(F_o^2 - F_c^2)^2$. Weighted R factors (R_w) and goodness of fit (S) are based on F^2; conventional R factors (R) are based on F. All non-hydrogen atoms were refined with anisotropic displacement parameters. Hydrogen atom positions were geometrically calculated and allowed to ride on their parent carbon or nitrogen atoms with fixed isotropic U. All scattering factors and anomalous dispersion factors are contained in the SHELXTL 6.10 program library.

UV-visible Spectroscopy. A Cary 5000 UV-Vis-NIR spectrophotometer (Agilent Technologies, CA), was used with 1 cm path length cuvettes (850 μL) provided with a Temperature Controller. Spectra (500–200 nm) were recorded at 310 K when the samples were in water and at 298 K for methanol samples. The data were processed using OriginPro version 9.0 (OriginLab, Northampton, MA).

3.4.2 Methods

Solution Studies. The tether ring-opening process of closed-tether complexes was monitored by ^{1}H NMR or UV-visible spectroscopy in methanol, dimethylsulfoxide and acidic aqueous solutions. The concentration of Ru^{II} for the NMR studies was 6–7 mM, and 0.2 mM for UV-visible spectroscopy, unless otherwise stated. The relative amounts of closed- and open-tether species in DMSO-d_6, MeOD-d_4 (298 K) and DCl solutions (1, 0.1, and 0.01 M DCl) at 310 K at equilibrium (1–8 h) were quantified by integration of peaks in the ^{1}H NMR spectra. The extent of the ring opening process by ^{1}H NMR spectroscopy in acidic conditions at equilibrium was also determined in 1 M $DClO_4/D_2O$ and 0.1 M $DClO_4/D_2O$ (with and without 0.1 M NaCl) at 310 K in ca. 6 mM Ru^{II} solutions for selected complexes of the series.

In order to determine the rate of the ring-opening process in DMSO-d_6, ^{1}H NMR spectra were acquired at 10 minutes intervals over 12 h at 298 K. The data following time-course dynamics of the DMSO-adduct formation, based on peak integrals, were fitted to a pseudo-first-order kinetic equation. OriginPro was used to fit the exponential decay and to obtain the rate constant (k, min^{-1}). Experiments with **25** and **26** were performed by adding a 10 μL aliquot of a 15 mM heavy water solution to 690 μL of DMSO-d_6. In methanol and 1 M HCl ($[Ru^{II}]$ = 200 μM), the rate constants were calculated from the time-course data obtained by following the opening process by UV-visible

spectroscopy. Experiments with complexes **25** and **26** were performed by adding an aliquot of a Ru^{II} 6 mM water solution to either methanol or 1 M HCl for a final Ru^{II} concentration of ca. 100 μM. The absorbance was recorded at several time intervals over 24 h at 298 K for methanol and at 310 K for 1 M HCl. A plot of the change in absorbance with time was fitted to the appropriate equation for pseudo-first-order kinetics using OriginPro to give the half-lives ($t_{1/2}$, min) and rate constants (k, min^{-1}). The tether ring-closure of open tether complex **25Cl** was monitored by ^1H NMR using different buffered aqueous solutions. Citric acid/Na_2HPO_4 buffer was used to prepare pH 3.4, 4.3, 5.8 and 7.2 D_2O solutions and chosen based on the weak coordinating properties of the anions. Complex **25Cl** was dissolved (ca. 6 mM) in each buffered solution and the spectra were acquired at 10 min intervals over 12 h at 310 K. The data of the time-course dynamics to form the closed-tether complex (**25**) was determined by integration of the ^1H NMR peaks and data were fitted to the equation for pseudo-first-order kinetics.

Calculation of pK_a Values. In order to determine the pK_a values of the pendant NH_2 group in open tether complexes, the pH of aqueous solutions of complexes **25HCl** and **28HCl** was varied from pH 0 to 10 by the addition of dilute aliquots of NaOD and DCl, measuring the solution pH before and after recording the ^1H NMR spectra. The chemical shifts of the bound-arene ring protons were plotted against pH. The pH titration curves were fitted to the Henderson-Hasselbach equation using the program OriginPro, with the assumption that the observed chemical shifts are weighted averages according to the populations of the protonated (**25HCl** and **28HCl**) and the deprotonated (**25Cl** and **28Cl**) species, i.e., the NH_3^+/NH_2 equilibrium on the pendant NH_2 tether arm.

Interaction with Nucleobases. 25Cl was allowed to react with 5'-GMP (9 mol equiv) in methanol-d_4 at 298 K. The reaction was monitored by ^{1}H NMR over 24 h, when equilibrium had been reached. In addition, reaction of closed-tether complex **25** with 5'-GMP (5 mol equiv) was followed in D_2O at 310 K for 24 h. Their ^{1}H NMR spectra were recorded at various time intervals.

3.4.3 Synthesis

MATERIALS

$RuCl_3 \cdot 3H_2O$ was acquired from Precious Metals Online. Ethylendiamine (en), 1,3-diaminopropane (dap), *trans*-1,2-diaminocyclohexane (dach), 2-piperidinemethanamine (pipma), *N,N,N′,N′*-tetramethylethylenediamine (tmen), sodium oxalate (oxo), 2,2'-bipyridyl (bipy), ethyl benzoate, and 5'-guanosine monophosphate were purchased from Sigma-Aldrich. *N,N′*-dimethylethylenediamine (dmen), *N,N′*-diethylethylenediamine (deen), and 1,2-bis(dimethylphosphino)ethane (dmphe) were acquired from Alfa Aesar. 1,4-Diaminobutane (dab), 2,2'-bipiperidine (dpip), and *N,N′*-di-*tert*-butylethylenediamine (dtben) were purchased from TCI Europe. Dichloroethane, magnesium, 2-aminobiphenyl, and *o*-phenylenediamine (*o*-pda) were acquired from Acros Organics, and iodine from Fisher. Ethanol, dry methanol, diethyl ether, tetrahydrofuran, dimethylsulfoxide, sodium metal, and sodium chloride were purchased from Sharlau. The solvents used for UV-visible absorption spectroscopy were dry methanol, and deionized water. For NMR spectroscopy, the solvents used were MeOD-d_4, DMSO-d_6, DCl, $DClO_4$ and D_2O obtained from VWR International.

PREPARATION OF COMPLEXES

The Ru^{II} dimer $[Ru(\eta^6\text{-etb})Cl_2]_2$ where etb is ethyl benzoate was synthesized following the reported synthesis by Habtemariam et al.[27] The dichlorido complex $[Ru\{\eta^6{:}\kappa^1\text{-}C_6H_5(C_6H_4)NH_2\}Cl_2]$ was synthesized via thermal displacement of ethyl benzoate in the Ru^{II} dimer $[Ru(\eta^6\text{-etb})Cl_2]_2$ by 2-aminobiphenyl in 1,2-dichloroethane under pressure overnight as reported by Pizarro et al.[3] Complexes **13** and **21**–**30**, **31Cl** and **32Cl** (Table 3.1) were isolated as chloride salts using slight variations of a reported procedure.[3] Typically, 1 mole equivalent of the bidentate chelating ligand (XY) was added to a suspension of the dichlorido ruthenium complex $[Ru\{\eta^6{:}\kappa^1\text{-}C_6H_5(C_6H_4)NH_2\}Cl_2]$ in methanol or methanol/water to afford $[Ru\{\eta^6{:}\kappa^1\text{-}C_6H_5(C_6H_4)NH_2\}(XY)]^{2+}$. Complexes **13Cl** and **21**–**29Cl**, **31**, **32** and **33Cl** were characterized in solution. Details of the amount of reactants, volume of solvents, color changes, stirring times, and nature of the product are given below for the individual reactions, as well as any variation in the synthetic procedure.

The experimental procedures for the synthesis of complexes $[Ru(\eta^6\text{-etb})Cl_2]_2$, $[Ru\{\eta^6{:}\kappa^1\text{-}C_6H_5(C_6H_4)NH_2\}Cl_2]$ and $[Ru\{\eta^6{:}\kappa^1\text{-}C_6H_5(C_6H_4)NH_2\}(en)]Cl_2$ (**13**) have been described in Chapter 2.

$[Ru\{\eta^6{:}\kappa^1\text{-}C_6H_5(C_6H_4)NH_2\}(dap)]Cl_2$ (**21**). $[Ru\{\eta^6{:}\kappa^1\text{-}C_6H_5(C_6H_4)NH_2\}Cl_2]$ (22 mg, 0.059 mmol) was suspended in methanol (3 mL). 1,3-diaminopropane (4.9 μL, 0.059 mmol) was added, and the mixture was stirred for 6 h at room temperature. The solvent was removed under vacuum, and the product was re-dissolved in 2 mL of ethanol. The resultant yellow solution was filtered through a 0.45 μm syringe filter. The solvent was

reduced to ca. 5% of its original volume, and diethyl ether (3 mL) was added. The sticky solid was sonicated to give a yellowish precipitate, which was washed with diethyl ether and dried in vacuum. Water (7 mL) was added and the solution was left to stand overnight. Lyophilization afforded a dark solid. Yield: 22 mg (90%). Elemental analysis: Cald for $C_{15}H_{21}Cl_2N_3Ru$ (415.32): C, 43.38; H, 5.10; N, 10.12. Found: C, 41.17; H, 5.84; N,9.21. ^{1}H NMR (400 MHz, D_2O, δ): 7.64 (dd, *J* = 7.4, 1.8 Hz, Ar H, 1H), 7.56–7.48 (m, Ar H, 2H), 7.39 (dd, *J* = 7.4, 1.8 Hz, Ar H, 1H), 6.29 (t, *J* = 5.9 Hz, Ar H, 2H), 5.60 (t, *J* = 5.8 Hz, Ar H, 1H), 5.53 (d, *J* = 5.8 Hz, Ar H, 2H), 3.15–3.09 (m, 2H), 2.93 (td, *J* = 11.0, 2.6 Hz, 2H), 1.97–1.90 (m, 1H), 1.67–1.57 (m, 1H).

[Ru{η^6:κ^1-C$_6$H$_5$(C$_6$H$_4$)NH$_2$}(dab)]Cl$_2$ (**22**). [Ru{η^6:κ^1-$C_6H_5(C_6H_4)NH_2$}Cl_2] (20 mg, 0.059 mmol) was suspended in methanol (3 mL). 1,4-diaminobutane (5.8 μL, 0.059 mmol) was added, and the mixture was stirred for 3 h at room temperature. The solvent was removed on a rotary evaporator, and the product was re-dissolved in 3 mL of ethanol. The resultant yellow solution was filtered through a 0.45 μm syringe filter. The solvent was reduced to ca. 5% of its original volume, and diethyl ether (3 mL) was added. The sticky solid was sonicated to give a pale yellow precipitate, which was washed with diethyl ether and dried in vacuum. Water (7 mL) was added and the solution was left to stand overnight. Lyophilization afforded a pale yellow solid. Yield: 24 mg (95%). Elemental analysis: Cald for $C_{16}H_{23}Cl_2N_3Ru$ (429.35): C, 44.76; H, 5.40; N, 9.79. Found: C, 41.96; H, 6.04; N, 9.29. ^{1}H NMR (400 MHz, D_2O, δ): 7.64 (dd, *J* = 6.9, 1.9 Hz, Ar H, 1H), 7.53 (td, *J* = 7.3, 2.1 Hz, Ar H, 2H), 7.38 (dd, *J* = 6.8, 1.5 Hz, Ar H, 1H), 6.34 (t, *J* = 4.9 Hz, Ar H, 2H), 5.71 (t, *J* = 4.8 Hz, Ar H, 1H), 5.56 (d, *J* = 5.8 Hz, Ar H, 2H), 3.15–3.09 (m, 2H), 3.05–2.98 (m, 2H), 1.96–1.89 (m, 2H), 1.70–1.63 (m, 2H).

[Ru{η^6:κ^1-C$_6$H$_5$(C$_6$H$_4$)NH$_2$}(dach)]Cl$_2$ (23). [Ru{η^6:κ^1-C$_6$H$_5$(C$_6$H$_4$)NH$_2$}Cl$_2$] (30 mg, 0.088 mmol) was suspended in methanol (4 mL). Trans-1,2-diaminocyclohexane (10.5 μL, 0.088 mmol) was added, and the mixture was stirred for 6 h at room temperature. The solvent was removed in vacuo, and the product was re-dissolved in 4 mL of ethanol. The resultant yellow solution was filtered through a 0.45 μm syringe filter. The solvent was reduced to ca. 5% of its original volume, and diethyl ether (3 mL) was added. The sticky solid was sonicated to give a pale yellow precipitate, which was centrifuged, washed with diethyl ether and dried in vacuum. Water (10 mL) was added and the solution was left to stand overnight. Lyophilization afforded a yellow solid. Yield: 34 mg (85%). Elemental analysis: Cald for $C_{18}H_{25}Cl_2N_3Ru$ (455.39): C, 47.47; H, 5.53; N, 9.23. Found: C, 45.19; H, 5.96; N, 8.92. ^{1}H NMR (400 MHz, D_2O, δ): 7.66 (dd, *J* = 7.2, 1.9 Hz, Ar H, 1H), 7.54 (td, *J* = 7.3, 1.9 Hz, Ar H, 2H), 7.41 (dd, *J* = 7.1, 1.9 Hz, Ar H, 1H), 6.23 (t, *J* = 5.8 Hz, Ar H, 1H), 6.18 (t, *J* = 5.8 Hz, Ar H, 1H), 5.67 (d, *J* = 5.9 Hz, Ar H, 1H), 5.65 (d, *J* = 5.9 Hz, Ar H, 1H), 5.51 (t, *J* = 5.8 Hz, Ar H, 1H), 2.31–2.22 (m, 1H), 2.15–2.07 (m, 2H), 1.69–1.63 (m,3H), 1.35–1.07 (m, 4H). The yellow single crystals grown from a water solution (298 K) were suitable for X-ray diffraction.

[Ru{η^6:κ^1-C$_6$H$_5$(C$_6$H$_4$)NH$_2$}(pipma)]Cl$_2$ (24). [Ru{η^6:κ^1-C$_6$H$_5$(C$_6$H$_4$)NH$_2$}Cl$_2$] (40 mg, 0.120 mmol) was suspended in methanol (4 mL). 2-piperidinemethanamine (14.2 μL, 0.120 mmol) was added, and the mixture was stirred for 4 h at room temperature. The solvent was removed in vacuo, and the product was re-dissolved in 3 mL of ethanol. The resultant yellow solution was filtered through a 0.45 μm syringe filter. The solvent was reduced to ca. 5% of its original volume, and diethyl ether (3 mL) was added. The

sticky solid was sonicated to give a pale yellow precipitate, which was centrifuged, washed with diethyl ether and dried in vacuum. Water (14 mL) was added and the solution was left to stand overnight. Lyophilization afforded a yellow solid. Yield: 51 mg (93%). Elemental analysis: Cald for $C_{18}H_{25}Cl_2N_3Ru$ (455.39): C, 47.47; H, 5.53; N, 9.23. Found: C, 44.16; H, 6.04; N, 8.84. ^{1}H NMR (400 MHz, D_2O, δ): 7.66–7.63 (m, Ar H, 1H), 7.57–7.49 (m, Ar H, 2H), 7.45–7.40 (m, Ar H, 1H), 6.25–6.15 (m, Ar H, 2H), 5.70–5.53 (m, Ar H, 3H), 3.87–3.48 (m, 1H), 2.95–2.77 (m, 2H), 2.33–2.03 (m, 1H), 1.93–1.58 (m,5H), 1.57–1.44 (m, 1H), 1.28–1.24 (m, 1H).

[Ru{η^6:κ^1-C$_6$H$_5$(C$_6$H$_4$)NH$_2$}(dmen)]Cl$_2$ (25). [Ru{η^6:κ^1-$C_6H_5(C_6H_4)NH_2$}Cl_2] (60 mg, 0.180 mmol) was suspended in methanol (6 mL). Dimethylethylendiamine (18.9 μL, 0.180 mmol) was added, and the mixture was stirred for 7 h at room temperature. The solvent was removed in vacuo, and the product was re-dissolved in 3 mL of ethanol. The resultant yellow solution was filtered through a 0.45 μm syringe filter. The solvent was reduced to ca. 5% of its original volume, and diethyl ether (4 mL) was added. The sticky solid was sonicated to give a yellow precipitate, which was centrifuged, washed with diethyl ether and dried in vacuo. Water (21 mL) was added and the solution left to stand in water for 24 h to afford closed complex **25** in aqueous solution. ^{1}H NMR (400 MHz, D_2O, δ): 7.67–7.65 (m, Ar H, 1H), 7.58–7.50 (m, Ar H, 2H), 7.44-7.41 (m, Ar H, 1H), 6.29 (t, *J* = 5.9 Hz, Ar H, 1H), 6.22 (t, *J* = 5.9 Hz, Ar H, 1H), 5.77 (d, *J* = 6 Hz, Ar H, 1H), 5.72 (t, *J* = 5.8 Hz, Ar H, 1H), 5.65 (d, *J* = 5.9 Hz, Ar H, 1H), 3.19 (s, CH_3, 3H), 2.98 (dd, *J* = 12.7, 3.0 Hz, C*H*H, 1H), 2.92 (dd, *J* = 13.1, 3.7 Hz, C*H*H, 1H), 2.80 (s, CH_3, 3H), 2.49 (td, *J* = 13.4, 3.8 Hz, C*H*H, 1H), 1.98 (td, *J* = 13.3, 3.8 Hz, C*H*H, 1H). ESI-MS (m/z): $[M–H]^+$ calcd for $C_{16}H_{23}N_3Ru$, 358.1; found, 358.0.

[Ru{η^6:κ^1-C$_6$H$_5$(C$_6$H$_4$)NH$_2$}(deen)]Cl$_2$ (26). [Ru{η^6:κ^1-C$_6$H$_5$(C$_6$H$_4$)NH$_2$}Cl$_2$] (10 mg, 0.029 mmol) was suspended in methanol (4 mL). Diethylethylendiamine (4.2 μL, 0.029 mmol) was added, and the mixture was stirred for 6 h at room temperature. The solvent was removed on the rotary evaporator, and the product was re-dissolved in 0.2 mL of ethanol. The resultant yellow solution was filtered through a 0.45 μm syringe filter. The solvent was reduced to ca. 5% of its original volume, and diethyl ether (4 mL) was added. The sticky solid was sonicated to give a yellow precipitate, which was centrifuged, washed with diethyl ether and dried in vacuum. Water (4 mL) was added and the solution was left to stand in water for 24 h to afford closed complex **26** in aqueous solution. ^{1}H NMR (400 MHz, D_2O, δ): 7.67–7.65 (m, Ar H, 1H), 7.58–7.50 (m, Ar H, 2H), 7.43–7.41 (m, Ar H, 1H), 6.28 (t, *J* = 5.8 Hz, Ar H, 1H), 6.19 (t, *J* = 5.9 Hz, Ar H, 1H), 5.74 (d, *J* = 5.4 Hz, Ar H, 1H), 5.72 (t, *J* = 5.85 Hz, Ar H, 1H), 5.62 (d, *J* = 5.9 Hz, Ar H, 1H), 3.69 (m, 1H), 3.42–3.32 (m, 2H), 3.21 (dd, *J* = 9.3, 3.6 Hz, 1H), 3.18 (dd, *J* = 9.7, 3.6 Hz, 1H), 2.93–2.84 (m, 1H), 2.40 (td, *J* = 13.3, 3.7 Hz, 1H), 1.82 (td, *J* = 13.4, 3.8 Hz, 1H), 1.27 (m, 6H). ESI-MS (m/z): $[M–H]^+$ calcd for $C_{18}H_{27}N_3Ru$, 386.1; found, 386.1.

[Ru{η^6:κ^1-C$_6$H$_5$(C$_6$H$_4$)NH$_2$}(dpip)]Cl$_2$ (27). [Ru{η^6:κ^1-C$_6$H$_5$(C$_6$H$_4$)NH$_2$}Cl$_2$] (20 mg, 0.059 mmol) was suspended in methanol (3 mL). Bis-piperidine (9.9 μL, 0.059 mmol) was added, and the mixture was stirred for 6 h at room temperature. The solvent was removed in vacuo, and the product was re-dissolved in 2 mL of ethanol. The resultant yellow solution was filtered through a 0.45 mm syringe filter. The solvent was reduced to ca. 5% of its original volume, and diethyl ether (3 mL) was added. The sticky solid was sonicated to give a brown precipitate, which was washed with diethyl ether and dried in vacuum. Water (5 mL) was added and the solution was left to stand in water for

24 h to afford the closed complex. Lyophilization afforded a brown solid. Yield: 20 mg (67%). Elemental analysis: Cald for $C_{22}H_{31}Cl_2N_3Ru$ (509.48): C, 51.86; H, 6.13; N, 8.25. Found: C, 48.92; H, 6.35; N, 7.66. ^{1}H NMR (400 MHz, D_2O, δ): 7.67–7.64 (m, Ar H, 1H), 7.59–7.49 (m, Ar H, 2H), 7.48–7.44 (m, Ar H, 1H), 6.33–6.16 (m, Ar H, 2H), 5.96–5.53 (m, Ar H, 3H), 3.84–2.04 (m, 6H), 1.98–1.19 (m, 12H). Single crystals of **27** suitable for X-ray diffraction were obtained from the reaction mixture.

[Ru{η^6:κ^1-C$_6$H$_5$(C$_6$H$_4$)NH$_2$}(tmen)]Cl$_2$ (28). [Ru{η^6:κ^1-$C_6H_5(C_6H_4)NH_2$}Cl_2] (30 mg, 0.088 mmol) was suspended in 12 mL of 1:1 (v/v) methanol/water. Tetramethylethylendiamine (13.2 μL, 0.088 mmol) was added, and the mixture was stirred for 3 h at room temperature. The solvent was removed in vacuo, and the product was re-dissolved in 3 mL of ethanol. The resultant brown solution was filtered through a 0.45 μm syringe filter. The solvent was reduced to ca. 5% of its original volume, and diethyl ether (4 mL) was added. The sticky solid was sonicated to give a yellow precipitate, which was washed with diethyl ether and dried in vacuum. Yield: 38 mg (94 %). Elemental analysis: Cald for $C_{18}H_{27}Cl_2N_3Ru$ (457.4): C, 47.27; H, 5.95; N, 9.19. Found: C, 45.82; H, 6.23; N, 8.24. ^{1}H NMR (400 MHz, D_2O, δ): 7.68–7.66 (m, Ar H, 1H), 7.57–7.49 (m, Ar H, 2H), 7.44–7.42 (m, Ar H, 1H), 6.34 (t, J = 6.3 Hz, Ar H, 2H), 6.03 (d, J = 6.0 Hz, Ar H, 2H), 5.86 (t, J = 6.0 Hz, Ar H, 1H), 3.53 (s, 2CH_3, 6H), 2.93–2.86 (m, 2H), 2.66 (s, 2CH_3, 6H), 2.59–2.52 (m, 2H).

[Ru{η^6:κ^1-C$_6$H$_5$(C$_6$H$_4$)NH$_2$}(*o*-pda)]Cl$_2$ (29). [Ru{η^6:κ^1-$C_6H_5(C_6H_4)NH_2$}Cl_2] (60 mg, 0.176 mmol) was suspended in 10 mL of 1:1 (v/v) methanol/water. *o*-Phenylenediamine (17.9 μL, 0.165 mmol) was added, and the mixture was stirred for 6 h at room temperature. The solvent was removed in vacuo, and the product was re-dissolved in 4

mL of ethanol. The resultant dark solution was filtered through a 0.45 μm syringe filter. The solvent was reduced to ca. 5% of its original volume, and diethyl ether (4 mL) was added. The sticky solid was sonicated to give a violet precipitate, which was washed with diethyl ether and dried in vacuum. Yield: 45 mg (57 %). Elemental analysis: Cald for $C_{18}H_{19}Cl_2N_3Ru$ (449.34): C, 48.11; H, 4.26; N, 9.35. Found: C, 46.73; H, 4.98; N, 9.10. ^{1}H NMR (400 MHz, D_2O, δ): 7.70–7.68 (m, Ar H, 1H), 7.53–7.51 (m, Ar H, 2H), 7.41–7.38 (m, Ar H, 2H), 7.34–7.31 (m, Ar H, 2H), 7.27–7.25 (m, Ar H, 1H), 6.38 (t, *J* = 5.9 Hz, Ar H, 2H), 5.76 (d, *J* = 5.8 Hz, Ar H, 2H), 5.63 (t, *J* = 5.8 Hz, Ar H, 1H). Dark single crystals of **29** suitable for X-ray diffraction were obtained by evaporation of water solution at ambient temperature.

[Ru{η^6:κ^1-$C_6H_5(C_6H_4)NH_2$}(oxo)] (**30**). [Ru{η^6:κ^1-$C_6H_5(C_6H_4)NH_2$}Cl_2] (5 mg, 0.015 mmol) was suspended in water (2 mL). Silver oxalate (18 mg, 0.059 mmol) was added, and the mixture was stirred for 6 h at room temperature. The solvent was removed on the rotary evaporator and the product was re-dissolved in 3 mL of ethanol. The resultant yellow solution was filtered through a 0.45 μm syringe filter. The solvent was reduced to ca. 5% of its original volume, and diethyl ether (3 mL) was added. The sticky solid was sonicated to give a pale yellow precipitate, which was washed with diethyl ether and dried in vacuum. Yield: 8 mg (57 %). Elemental analysis: Cald for $C_{14}H_{11}NO_4Ru$ (358.31): C, 46.93; H, 3.09; N, 3.91. Found: C, 32.56; H, 2.59; N, 2.39. ^{1}H NMR (400 MHz, D_2O, δ): 7.68–7.66 (m, Ar H, 1H), 7.58–7.50 (m, Ar H, 2H), 7.39–7.37 (m, Ar H, 1H), 6.14 (t, *J* = 5.9 Hz, Ar H, 2H), 5.75 (t, *J* = 6.0 Hz, Ar H, 1H), 5.53 (d, *J* = 6.2 Hz, Ar H, 2H).

[Ru{η^6:κ^1-C$_6$H$_5$(C$_6$H$_4$)NH$_2$}(en)Cl]Cl (13Cl). [Ru{η^6:κ^1-C$_6$H$_5$(C$_6$H$_4$)NH$_2$}(en)]Cl$_2$ (2 mg, 0.005 mmol) was dissolved in methanol (0.6 mL). The solution was left to stand overnight to afford a mixture of complex **1** and the open-tether complex **1Cl**. ^{1}H NMR (400 MHz, MeOD-d_4, δ): 7.44 (dd, J = 7.7, 1.5 Hz, Ar H, 1H), 7.23 (ddd, J = 8.2, 7.3, 1.6 Hz, Ar H, 1H), 6.89 (dd, J = 8.1, 1.0 Hz, Ar H, 1H), 6.83 (td, J = 7.6, 1.2 Hz, Ar H, 1H), 6.05 (d, J = 5.9 Hz, Ar H, 2H), 6.02 (t, J = 5.6 Hz, Ar H, 1H), 5.74 (t, J = 6.1 Hz, Ar H, 2H), 2.59–2.53 (m, 2H), 2.46–2.40 (m, 2H). Crystallographic data of complex **13Cl** have been published previously.[3]

[Ru{η^6:κ^1-C$_6$H$_5$(C$_6$H$_4$)NH$_2$}(dap)Cl]Cl (21Cl). [Ru{η^6:κ^1-C$_6$H$_5$(C$_6$H$_4$)NH$_2$}(dap)]Cl$_2$ (3 mg, 0.007 mmol) was dissolved in methanol (0.6 mL). The solution was left to stand overnight to afford a mixture of complex **21** and the open-tether complex **21Cl**. ^{1}H NMR (400 MHz, MeOD-d_4, δ): 7.45 (dd, J = 7.8, 1.5 Hz, Ar H, 1H), 7.24 (td, J = 7.4, 1.6 Hz, Ar H, 1H), 6.89 (dd, J = 8.1, 1.0 Hz, Ar H, 1H), 6.83 (td, J = 7.6, 1.2 Hz, Ar H, 1H), 6.09 (d, J = 5.9 Hz, Ar H, 2H), 6.01 (t, J = 5.6 Hz, Ar H, 1H), 5.79 (t, J = 5.7 Hz, Ar H, 2H), 3.11–3.06 (m, 2H), 2.72–2.66 (m, 2H), 1.84–1.78 (m, 1H), 1.55–1.45 (m, 1H).

[Ru{η^6:κ^1-C$_6$H$_5$(C$_6$H$_4$)NH$_2$}(dab)Cl]Cl (22Cl). [Ru{η^6:κ^1-C$_6$H$_5$(C$_6$H$_4$)NH$_2$}(dab)]Cl$_2$ (3 mg, 0.007 mmol) was dissolved in methanol (0.6 mL). The solution was left to stand overnight to afford a mixture of complex **22** and the open-tether complex **22Cl**. ^{1}H NMR (400 MHz, MeOD-d_4, δ): 7.47 (dd, J = 7.7, 1.5 Hz, Ar H, 1H), 7.25 (ddd, J = 8.2, 7.3, 1.5 Hz, Ar H, 1H), 6.91 (dd, J = 8.2, 1.0 Hz, Ar H, 1H), 6.85 (td, J = 7.7, 1.2 Hz, Ar H, 1H), 6.12 (d, J = 5.9 Hz, Ar H, 2H), 6.03 (t, J = 5.6 Hz, Ar H, 1H), 5.85 (t, J = 5.7 Hz, Ar H, 2H), 2.97–2.81 (m, 4H), 1.89–1.77(m, 2H), 1.67–1.56 (m, 2H).

[Ru{η^6:κ^1-C$_6$H$_5$(C$_6$H$_4$)NH$_2$}(dach)Cl]Cl (**23Cl**). [Ru{η^6:κ^1-C$_6$H$_5$(C$_6$H$_4$)NH$_2$}(dach)]Cl$_2$ (3 mg, 0.007 mmol) was dissolved in methanol (0.6 mL). The solution was left to stand overnight to afford a mixture of complex **23** and the open-tether complex **23Cl**. ^{1}H NMR (400 MHz, MeOD-d_4, δ): 7.44 (dd, J = 7.7, 1.5 Hz, Ar H, 1H), 7.22 (td, J = 7.4, 1.5 Hz, Ar H, 1H), 6.88 (dd, J = 8.1, 1.0 Hz, Ar H, 1H), 6.82 (td, J = 7.6, 1.2 Hz, Ar H, 1H), 6.10 (d, J = 5.8 Hz, Ar H, 1H), 6.07 (d, J = 5.8 Hz, Ar H, 1H), 6.01 (t, J = 5.8 Hz, Ar H, 1H), 5.73–5.68 (m, Ar H, 2H), 2.12–1.99 (m, 3H), 1.71–1.65(m, 2H), 1.46–1.10 (m, 5H).

[Ru{η^6:κ^1-C$_6$H$_5$(C$_6$H$_4$)NH$_2$}(pipma)Cl]Cl (**24Cl**). [Ru{η^6:κ^1-C$_6$H$_5$(C$_6$H$_4$)NH$_2$}(pipma)]Cl$_2$ (3 mg, 0.007 mmol) was dissolved in methanol (0.6 mL). The solution was left to stand overnight to afford a mixture of complex **24** and the open-tether complex **24Cl**. ^{1}H NMR (400 MHz, MeOD-d_4, δ): 7.46–7.41 (m, Ar H, 1H), 7.25–7.20 (m, Ar H, 1H), 6.89–6.79 (m, Ar H, 2H), 6.26–6.00 (m, Ar H, 3H), 5.83–5.71 (m, Ar H, 2H), 3.72–1.20 (m, 11H).

[Ru{η^6:κ^1-C$_6$H$_5$(C$_6$H$_4$)NH$_2$}(dmen)Cl]Cl (**25Cl**). [Ru{η^6:κ^1-C$_6$H$_5$(C$_6$H$_4$)NH$_2$}(dmen)]Cl$_2$ (3 mg, 0.007 mmol) was dissolved in methanol (0.6 mL). The solution was left to stand overnight to quantitatively afford open-tether complex **25Cl**. Elemental analysis: Cald for C$_{16}$H$_{23}$Cl$_2$N$_3$Ru (429.35): C, 44.76; H, 5.40; N, 9.79. Found: C, 43.15; H, 5.73; N, 9.07. ^{1}H NMR (400 MHz, MeOD-d_4, δ): 7.48 (dd, J = 7.8, 1.4 Hz, Ar H, 1H), 7.24 (td, J = 7.3, 1.6 Hz, Ar H, 1H), 6.88 (dd, J = 8.2, 1.0 Hz, Ar H, 1H), 6.81 (td, J = 7.8, 1.2 Hz, Ar H, 1H), 6.30–6.12 (m, Ar H, 2H), 6.18 (t, J = 5.7 Hz, Ar H, 1H), 5.83–5.70 (m, Ar H, 2H), 2.91–2.89 (m, 3H), 2.80–2.79 (m, 3H), 2.76–2.69

(m, C*H*H, 1H), 2.54–2.49 (m, C*H*H, 1H), 2.37–2.27 (m, C*H*H, 1H), 2.21–2.11 (m, C*H*H, 1H).

[Ru{η^6:κ^1-C$_6$H$_5$(C$_6$H$_4$)NH$_2$}(deen)Cl]Cl (**26Cl**). [Ru{η^6:κ^1-C$_6$H$_5$(C$_6$H$_4$)NH$_2$}(deen)]Cl$_2$ (3 mg, 0.007 mmol) was dissolved in methanol (0.6 mL). The solution was left to stand overnight to quantitatively afford open-tether complex **26Cl**. Elemental analysis: Cald for $C_{18}H_{27}Cl_2N_3Ru$ (457.40): C, 47.27; H, 5.95; N, 9.19. Found: C, 46.08; H, 6.07; N, 8.85. ^{1}H NMR (400 MHz, MeOD-d_4, δ): 7.48 (dd, *J* = 7.8, 1.4 Hz, Ar H, 1H), 7.21 (td, *J* = 7.3, 1.5 Hz, Ar H, 1H), 6.86 (dd, *J* = 8.1, 1.0 Hz, Ar H, 1H), 6.77 (td, *J* = 7.8, 1.2 Hz, Ar H, 1H), 6.27 (d, *J* = 6.0 Hz, Ar H, 1H), 6.24 (d, *J* = 6.1 Hz, Ar H, 1H), 6.08 (t, *J* = 5.7 Hz, Ar H, 1H), 5.77 (t, *J* = 5.8 Hz, Ar H, 1H), 5.72 (t, *J* = 5.9 Hz, Ar H, 1H), 3.48–3.39 (m, 1H), 3.22–3.05 (3H, m), 3.00 (dd, *J* = 12.0, 2.7 Hz, 1H), 2.78 (dd, *J* = 12.4, 3.2 Hz, 1H), 2.27 (td, *J* = 12.1, 4.1 Hz, 1H), 1.98 (td, *J* = 13.0, 3.7 Hz, 1H), 1.22 (m, 6H). Yellow crystals were obtained from a methanol solution affording the structure of complex 7Cl.

[Ru{η^6:κ^1-C$_6$H$_5$(C$_6$H$_4$)NH$_2$}(dpip)Cl]Cl (**27Cl**). [Ru{η^6:κ^1-C$_6$H$_5$(C$_6$H$_4$)NH$_2$}(dpip)]Cl$_2$ (3 mg, 0.005 mmol) was dissolved in methanol (0.6 mL). The solution was left to stand overnight to quantitatively afford open-tether complex **27Cl**. Elemental analysis: Cald for $C_{22}H_{31}Cl_2N_3Ru$ (509.48): C, 51.86; H, 6.13; N, 8.25. Found: C, 50.04; H, 6.38; N, 7.5. ^{1}H NMR (400 MHz, MeOD-d_4, δ): 7.59–7.48 (m, 1H), 7.24–7.20 (m, 1H), 6.89–6.79 (m, 2H), 6.43–6.40 (m, 1H), 6.27–6.14 (m, 2H), 5.80–5.69 (m, 2H), 3.58–1.13 (m, 18H).

[Ru{η^6:κ^1-C$_6$H$_5$(C$_6$H$_4$)NH$_2$}(tmen)Cl]Cl (**28Cl**). [Ru{η^6:κ^1-C$_6$H$_5$(C$_6$H$_4$)NH$_2$}(tmen)]Cl$_2$ (10 mg, 0.022 mmol) was dissolved in methanol (0.6 mL). The solution was left to stand overnight to quantitatively afford open-tether complex **28Cl**. ^{1}H NMR (400 MHz, MeOD-d_4, δ): 7.54 (dd, J = 7.9, 1.5 Hz, Ar H, 1H), 7.25 (td, J = 7.2, 1.5 Hz, Ar H, 2H), 6.89 (dd, J = 8.2, 1.1 Hz, Ar H, 1H), 6.82 (td, J = 7.3, 1.2 Hz, Ar H, 2H), 6.45 (d, J = 6.5 Hz, Ar H, 2H), 6.45 (t, J = 5.7 Hz, Ar H, 1H), 5.77 (t, J = 5.8 Hz, Ar H, 2H), 3.25 (s, 6H), 2.77 (s, 6H), 2.47 (br s, 4H). Yellow crystals were obtained from a methanol solution affording the structure of complex **28Cl**.

[Ru{η^6:κ^1-C$_6$H$_5$(C$_6$H$_4$)NH$_2$}(*o*-pda)Cl]Cl (**29Cl**). [Ru{η^6:κ^1-C$_6$H$_5$(C$_6$H$_4$)NH$_2$}(*o*-pda)]Cl$_2$ (3 mg, 0.007 mmol) was dissolved in methanol (0.6 mL). The solution was left to stand overnight to afford a mixture of complex **29** and the open-tether complex **29Cl**. ^{1}H NMR (400 MHz, MeOD-d_4, δ): 7.47-7.43 (m, Ar H, 6H), 6.91 (dd, J = 8.1, 1.1 Hz, Ar H, 1H), 6.82 (t, J = 7.7, 1.2 Hz, Ar H, 1H), 6.23 (d, J = 5.9 Hz, Ar H, 2H), 6.10 (t, J = 5.7 Hz, Ar H, 1H), 5.82 (t, J = 5.7 Hz, Ar H, 2H).

[Ru{η^6:κ^1-C$_6$H$_5$(C$_6$H$_4$)NH$_2$}(dmphe)Cl]Cl (**31Cl**). [Ru{η^6:κ^1-C$_6$H$_5$(C$_6$H$_4$)NH$_2$}Cl$_2$] (10 mg, 0.029 mmol) was suspended in dry methanol (2 mL). 1,2-bis(dimethylphosphino)ethane (4.9 μL, 0.029 mmol) was added, and the mixture was stirred for 2 h under argon at room temperature. The solvent was removed on the rotary evaporator and the product was re-dissolved in 3 mL of ethanol. The resultant solution was filtered through a 0.45 μm syringe filter. The solvent was reduced to ca. 5% of its original volume, and diethyl ether (3 mL) was added. The sticky solid was sonicated to give a pale yellow precipitate, which was washed with diethyl ether and dried in vacuum. Yield: 7 mg (49 %). Elemental analysis: Cald for C$_{18}$H$_{27}$Cl$_2$N$_3$Ru (491.34): C,

44.00; H, 5.54; N, 2.85. Found: C, 41.2; H, 6.04; N, 2.17. ^{1}H NMR (400 MHz, D_2O, δ): 7.40–7.33 (m, 2H), 7.00 (d, *J* = 7.9 Hz, Ar H, 2H), 6.89 (t, *J* = 6.3 Hz, Ar H, 1H), 6.36 (d, *J* = 6.2 Hz, Ar H, 2H), 6.14 (t, *J* = 5.7 Hz, Ar H, 1H), 5.84 (t, *J* = 5.9 Hz, Ar H, 2H), 2.05–1.17 (m, 16H).

[Ru{η^6:κ^1-C$_6$H$_5$(C$_6$H$_4$)NH$_2$}(tben)Cl]Cl (32Cl). [Ru{η^6:κ^1-$C_6H_5(C_6H_4)NH_2$}Cl_2] (19 mg, 0.056 mmol) was suspended in 4 mL of 1:1 (v/v) methanol/water. *N,N′*-di-tert-butylethylenediamine (12.2 µL, 0.057 mmol) was added, and the mixture was stirred for 6 h at room temperature. The solvent was removed on the rotary evaporator and the product was re-dissolved in 3 mL of ethanol. The resultant solution was filtered through a 0.45 µm syringe filter. The solvent was reduced to ca. 5% of its original volume, and diethyl ether (3 mL) was added. The sticky solid was sonicated to give a brown precipitate, which was washed with diethyl ether and dried in vacuum. Yield: 21 mg (72 %). Elemental analysis: Cald for $C_{22}H_{35}Cl_2N_3Ru$ (513.51): C, 51.46; H, 6.87; N, 8.18. Found: C, 46.84; H, 6.47; N, 6.57. ^{1}H NMR (400 MHz, D_2O, δ): 7.58 (dd, *J* = 7.7, 1.5 Hz, Ar H, 2H), 7.34 (td, *J* = 7.7, 1.6 Hz, Ar H, 2H), 7.01 (td, *J* = 7.6, 1.1 Hz, Ar H, 2H), 6.95 (dd, *J* = 8.1, 1.0 Hz, Ar H, 2H), 5.70–5.68 (m, 2H), 5.61–5.57 (m, 3H), 3.27 (s, 4H), 1.36 (s, 18H).

[Ru{η^6:κ^1-C$_6$H$_5$(C$_6$H$_4$)NH$_2$}(bipy)Cl]Cl (33Cl). [Ru{η^6:κ^1-$C_6H_5(C_6H_4)NH_2$}Cl_2] (25 mg, 0.073 mmol) was suspended in 2 mL of methanol. 2,2'-bipyridyl (25 mg, 0.160 mmol) was added dropwise, and the mixture was stirred for 2 h at 55 ºC. The solution turned dark red. The solvent was removed on the rotary evaporator and the product was re-dissolved in 2 mL of ethanol. The resultant solution was filtered through a 0.45 µm syringe filter. The solvent was reduced to ca. 5% of its original volume, and diethyl

ether (3 mL) was added. The sticky solid was sonicated to give a red precipitate, which was washed with diethyl ether and dried in vacuum. ^{1}H NMR (400 MHz, MeOD-d_4, δ): 9.28 (d, J = 5.0 Hz, Ar H, 2H), 8.50 (d, J = 8.0 Hz, Ar H, 2H), 8.20 (td, J = 7.9, 1.4 Hz, Ar H, 2H), 7.63 (ddd, J = 7.3, 5.7, 1.3 Hz, Ar H, 2H), 7.19 (td, J = 1.5, 7.3, 5.9 Hz, Ar H, 1H), 7.03 (dd, J = 7.8, 1.4 Hz, Ar H, 1H), 6.87 (d, J = 7.3, 0.8 Hz, Ar H, 1H), 6.62 (m, Ar H, 1H), 6.50 (d, J = 6.1 Hz, Ar H, 2H), 6.33 (t, J = 5.8 Hz, Ar H, 1H), 6.19 (t, J = 6.1 Hz, Ar H, 2H).

NOTE: Isolation of complexes **25** and **26** as chloride salts proved difficult. Although they are readily obtained pure in water (full characterization was carried out in solution state, vide supra), removal of the solvent causes tether ring opening to afford **25Cl** and **26Cl** up to ca. 50% as observed by ^{1}H NMR. We suggest that an increase in the chloride concentration (present in solution as counterions of the Ru^{II} complexes) following solvent removal triggers the chloride nucleophilic attack on the ruthenium centre and subsequent opening of the tether ring. Isolation of pure **25** and **26** was possible as PF_6^- salts.

3.5 References

(1) Liu, H.-K.; Wang, F.; Parkinson, J. A.; Bella, J.; Sadler, P. J. Ruthenation of Duplex and Single-Stranded d(CGGCCG) by Organometallic Anticancer Complexes. *Chem. Eur. J.* **2006**, *12*, 6151-6165.

(2) Pizarro, A. M.; Sadler, P. J. Unusual DNA Binding Modes for Metal Anticancer Complexes. *Biochimie* **2009**, *91*, 1198-1211.

(3) Pizarro, A. M.; Melchart, M.; Habtemariam, A.; Salassa, L.; Fabbiani, F. P. A.; Parsons, S.; Sadler, P. J. Controlling the Reactivity of Ruthenium(II) Arene Complexes by Tether Ring-Opening. *Inorg. Chem.* **2010**, *49*, 3310-3319.

(4) Ruhlmann, L.; Costa-Coquelard, C.; Hao, J.; Jiang, S.; He, C.; Sun, L.; Lampre, I. Association of Ruthenium Complexes [Ru(bpy)3]2+ or [Ru(bpy)2(Mebpy-py)]2+ with Dawson Polyanions α-[P2W18O62]6– or α2-[FeIII(H2O)P2W17O61]7–. *Can. J. Chem.* **2008**, *86*, 1034-1043.

(5) Martínez-Peña, F.; Pizarro, A. M. *Unpublished results*

(6) Reiner, T.; Jantke, D.; Miao, X.-H.; Marziale, A. N.; Kiefer, F. J.; Eppinger, J. Phenylalanine - a Biogenic Ligand with Flexible η6- and η6:κ1-Coordination at Ruthenium(II) Centres. *Dalton Trans.* **2013**, *42*, 8692-8703.

(7) Miyaki, Y.; Onishi, T.; Kurosawa, H. Synthesis and Reaction of Ruthenium(II) Complexes Containing Heteroatom Donor (O, N, and P) Tethered to η6-Arene Ring. *Inorg. Chim. Acta* **2000**, *300–302*, 369-377.

(8) Amarasekera, J.; Rauchfuss, T. B. Interconversion of Persulfido, Sulfur Hydride, and Hydride Ligands Coordinated to CpRu(PPh3)2+. *Inorg. Chem.* **1989**, *28*, 3875-3883.

(9) Stodt, R.; Gencaslan, S.; Müller, Iris M.; Sheldrick, William S. Preparation, Reactivity and Peptide Labelling Properties of (η6-Arene)ruthenium(II) Complexes with Pendant Carboxylate Groups. *Eur. J. Inorg. Chem.* **2003**, *2003*, 1873-1882.

(10) Wang, F.; Chen, H.; Parsons, S.; Oswald, I. D. H.; Davidson, J. E.; Sadler, P. J. Kinetics of Aquation and Anation of Ruthenium(II) Arene Anticancer Complexes, Acidity and X-ray Structures of Aqua Adducts. *Chem. Eur. J.* **2003**, *9*, 5810-5820.

(11) Bugarcic, T.; Habtemariam, A.; Deeth, R. J.; Fabbiani, F. P. A.; Parsons, S.; Sadler, P. J. Ruthenium(II) Arene Anticancer Complexes with Redox-Active Diamine Ligands. *Inorg. Chem.* **2009**, *48*, 9444-9453.

(12) Habtemariam, A.; Watchman, B.; Potter, B. S.; Palmer, R.; Parsons, S.; Parkin, A.; Sadler, P. J. Control of Aminophosphine Chelate Ring-Opening in Pt(II) and Pd(II) Complexes: Potential Dual-Mode Anticancer Agents. *Dalton Trans.* **2001**, 10.1039/B009117K.1306-1318.

(13) Scrase, T. G.; O'Neill, M. J.; Peel, A. J.; Senior, P. W.; Matthews, P. D.; Shi, H.; Boss, S. R.; Barker, P. D. Selective Lability of Ruthenium(II) Arene Amino Acid Complexes. *Inorg. Chem.* **2015**, *54*, 3118-3124.

(14) Molas Saborit, J.; Caubet, A.; Brissos, R. F.; Korrodi-Gregorio, L.; Perez-Tomas, R.; Martinez, M.; Gamez, P. pH-Driven Preparation of Two Related Platinum(II) Complexes Exhibiting Distinct Cytotoxic Properties. *Dalton Trans.* **2017**, *46*, 11214-11222.

(15) Ito, M.; Endo, Y.; Ikariya, T. Well-Defined Triflylamide-Tethered Arene−Ru(Tsdpen) Complexes for Catalytic Asymmetric Hydrogenation of Ketones. *Organometallics* **2008**, *27*, 6053-6055.

(16) Todd, R. C.; Lippard, S. J. Inhibition of Transcription by Platinum Antitumor Compounds. *Metallomics* **2009**, *1*, 280-291.

(17) Dougan, S. J.; Sadler, P. J. The Design of Organometallic Ruthenium Arene Anticancer Agents. *Chimia* **2007**, *61*, 704-715.

(18) Pizarro, A. M.; Barry, N. P. E.; Sadler, P. J. In *Comprehensive Inorganic Chemistry II (Second Edition)*; Poeppelmeier, K., Eds; Elsevier: Amsterdam, 2013; pp 751-784.

(19) Chen, H.; Parkinson, J. A.; Morris, R. E.; Sadler, P. J. Highly Selective Binding of Organometallic Ruthenium Ethylenediamine Complexes to Nucleic Acids: Novel Recognition Mechanisms. *J. Am. Chem. Soc.* **2003**, *125*, 173-186.

(20) Peacock, A. F. A.; Habtemariam, A.; Moggach, S. A.; Prescimone, A.; Parsons, S.; Sadler, P. J. Chloro Half-Sandwich Osmium(II) Complexes: Influence of Chelated N,N-Ligands on Hydrolysis, Guanine Binding, and Cytotoxicity. *Inorg. Chem.* **2007**, *46*, 4049-4059.

(21) Lippert, B. In *Prog. Inorg. Chem.*; Eds; John Wiley & Sons, Inc.: 2007; pp 1-97.

(22) Aird, R. E.; Cummings, J.; Ritchie, A. A.; Muir, M.; Morris, R. E.; Chen, H.; Sadler, P. J.; Jodrell, D. I. In Vitro and In Vivo Activity and Cross Resistance Profiles of Novel Ruthenium(II) Organometallic Arene Complexes in Human Ovarian Cancer. *Br. J. Cancer* **2002**, *86*, 1652.

(23) Bruker. In *APEX2,SAINT and SADABS*; Eds; Bruker AXS Inc.: Madison, WI, 2008; pp

(24) AXS, B. In *SHELXTL Version 6.10, Structure Determination Package*; Eds; Bruker Analytical X-ray Instruments: 2000; pp

(25) Sheldrick, G. M. A Short History of SHELX. *Acta Crystallogr. Sect. A* **2008**, *64*, 112-122.

(26) Sheldrick, G. M. Crystal Structure Refinement with SHELXL. *Acta Crystallogr. Sect. C* **2015**, *71*, 3-8.

(27) Habtemarian, A.; Betanzos-Lara, S.; Sadler, P. J. In *Inorg. Synth.*; Rauchfuss, T. B., Eds; John Wiley & Sons: Hoboken, NJ, 2010; pp 160-163.

4.

Reversible pH-responsive Behaviour of Ruthenium(II) Arene Complexes with Tethered Carboxylate

4.1 Introduction

In Chapter 3, we have presented the effect of chelating-ligand (XY) variation on the activation dynamics of $[Ru\{\eta^6:\kappa^1\text{-}C_6H_5(C_6H_4)NH_2\}(XY)]^{n+}$ and showed how this activation is fully reversible and can be controlled by the choice of solvent. Additionally, in water the closure process is mediated by the aqua adduct, and reversibly controlled by the pH. However, the 2-aminobiphenyl system presents some limitations: (i) structurally π-acceptor XY ligands compromise the stability of the Ru-arene binding by withdrawing the electron density from the metal centre, (ii) the pH of activation regarding activation in water is very low, and (iii) the opening and closing processes in aqueous solution are so fast that the aqua intermediate, which is the active species, is not stable in solution, providing a narrow reactivity window.

In this Chapter we present a family of tethered Ru^{II}-arene complexes with a pendant carboxylic acid functionality. These tethered complexes form 5-member tether rings when closed, and the labile bond is $Ru–O_{carboxylate}$. We have investigated the intricate aqueous behaviour of the system regarding the interconversion of the open and closed species in the pH scale 1–12. We have tested the cytotoxic activity of these complexes and since some appear to possess some cytotoxic activity even under conditions where the closed tether should predominate (inactive towards macromolecule interaction), we have tried to explain such activity on the basis of their capability as mediators in transfer hydrogenation reactions.

4.2 Results and Discussion

4.2.1 Synthesis and Characterization

Ruthenium(II) arene complexes with typical half-sandwich structure synthesized for this Chapter are shown in Chart 4.1. Complexes **20Cl** and **35Cl–37Cl**, containing ethylenediamine (en), *o*-phenylenediamine (*o*-pda), 1,10-phenanthroline (phen) and oxalate (oxo) as chelating ligands were synthesized as open-tether complexes, where the carboxylate group pendant from the η^6-bound arene is protonated in its carboxylic acid form. These complexes bear a Ru–Cl bond susceptible to hydrolysis. The Scheme 2.3 displayed in Chapter 2 shows the synthetic route for obtaining these complexes, using dimer $[Ru(\eta^6\text{-}C_6H_5CH_2COOH)(\mu\text{-}Cl)Cl]_2$ (**34dimer**) as precursor. Complex **38**, with *N*,*N*,*N'*,*N'*-tetramethylethylenediamine (tmen) as chelating bidentate ligand, was however isolated and characterized as the closed-tether ruthenium(II) isomer, even following the similar synthetic procedure than for the open tether counterparts. In this complex the pendant carboxylate group has lost its proton and the negatively charged O^- of the carboxylate group is bound to the Ru^{II} centre, occupying one of the pseudo-octahedral positions of the three-legged piano-stool structure.

All complexes were prepared as chloride (or sodium in **37Cl**) salts in good yields (57–91%) via the Cl-bridged dimer $[Ru(\eta^6\text{-}C_6H_5CH_2COOH)(\mu\text{-}Cl)Cl]_2$. The complexes exhibited good solubility in aqueous solution (up to 2 mM). They were characterized by elemental analysis, LC-MS, ^{1}H NMR spectroscopy and/or X-ray crystallography.

As a general feature, the ^{1}H NMR spectra of open-tether complexes (**20Cl** and **35Cl–37Cl**) displayed distinct patterns for the resonances of the η^6-bound arene protons in comparison to the equivalent protons in the closed-tether counterparts (**37**). The distance between the most deshielded and most shielded η^6-bound arene signals spaned ca. 0.1–0.4 ppm for open (**20Cl** and **35Cl–37Cl**) and 0.9 ppm for the closed-tether (**38**)

complexes (Figure 4.1). We have observed similar features in the NMR spectra of complexes synthesized in Chapter 3 of general formula $[Ru\{\eta^6:\kappa^1\text{-}C_6H_5(C_6H_4)NH_2\}(XY)]^{n+}$ (XY = aliphatic diamine, *o*-phenylenediamine, oxalato, bis(phosphino)ethane). X-ray crystallographic data of these complexes confirmed unequivocally their structure.

Chart 4.1. Ruthenium(II) arene complexes synthesized in this Chapter. The formal charge of the organometallic complexes is not specified for clarity.

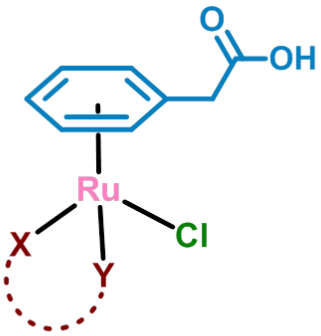

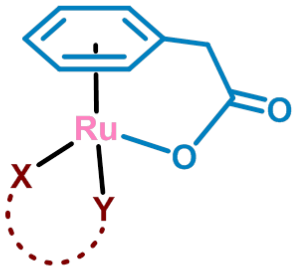

Compound	X–Y
20Cl	en
35Cl	*o*-pda
36Cl	phen
37Cl	oxo

Compound	X–Y
38	tmen

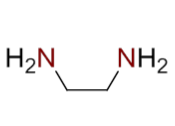

en

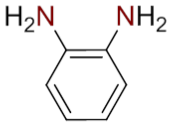

***o*-pda**

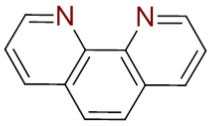

phen

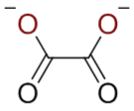

oxo

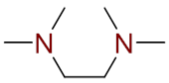

tmen

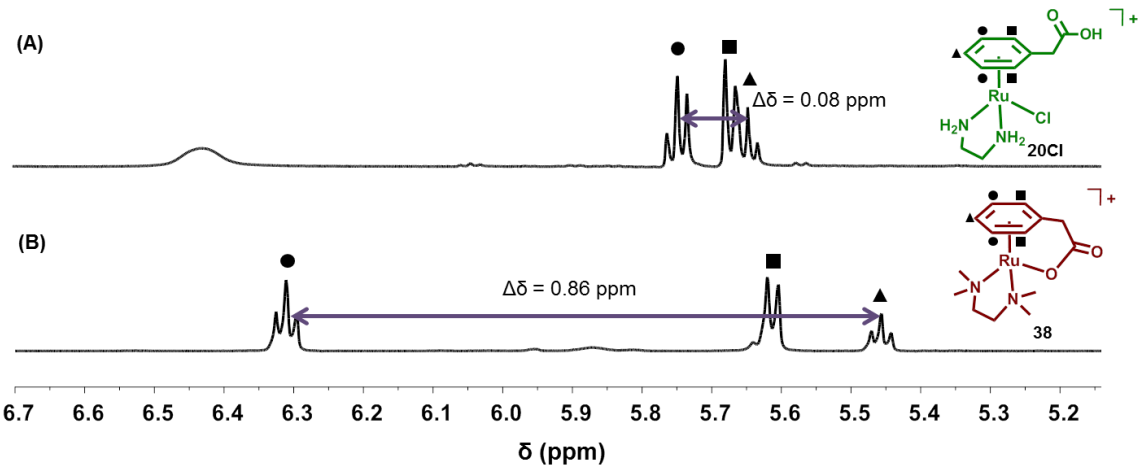

Figure 4.1. ^{1}H NMR spectra of complexes **20Cl** and **38** in MeOD-d_4 at 298 K. The selected spectral region shows the signals corresponding to the η^6-bound arene protons (■, *ortho*-; ●, *meta*-; and ▲, *para*-). (A) ^{1}H NMR spectrum of open-tether chlorido complex **20Cl** showing the typical short span between the meta- and para- peaks of the η^6-bound arene. (B) Closed-tether complex **38** shows a wider span in the signals corresponding to the η^6-bound arene protons. This feature provides a useful tool to distinguish between open- and closed-tether analogous complexes.

We determined the X-ray crystal structures of dimer [Ru(η^6-$C_6H_5CH_2COOH$)(μ-Cl)Cl]$_2$ (**34dimer**), and monomers [Ru(η^6-$C_6H_5CH_2COOH$)(en)Cl]Cl (**20Cl**), [Ru(η^6-$C_6H_5CH_2COOH$)(phen)Cl]Cl (**36Cl**) and [Ru(η^6-$C_6H_5CH_2COOH$)(oxo)Cl]Na (**37Cl**). X-ray diffraction quality crystals of **38·PF$_6$**, [Ru(η^6:κ^1-$C_6H_5CH_2COO$)(tmen)]PF_6, were obtained by exchanging the chloride counterion in **38** by addition of excess (5 mol equiv) of ammonium hexafluorophosphate. To the best of our knowledge the crystal structures of these complexes, including the Ru^{II}-arene dimer, are the first to be reported with phenylacetic acid η^6-coordinated to ruthenium(II). Selected bond lengths and angles are shown in Table 4.1. Detailed crystallographic data are shown in Annex 1.

Chlorido-bridged complex [Ru(η^6-$C_6H_5CH_2COOH$)(μ-Cl)Cl]$_2$ (**34dimer**) crystallized as shown in Figure 4.2. Two chlorido ligands tie the ruthenium atoms together forming a central Ru_2Cl_2 rhombus. There is a centre of inversion located at the midpoint of the central Ru_2Cl_2 entity and the asymmetric cell contains two half molecules of [Ru(η^6-$C_6H_5CH_2COOH$)(μ-Cl)Cl]$_2$. The bonds between Ru1 and the bridging chloride ligands

are somewhat longer (2.4462(15) and 2.4450(14) Å) than those to the terminal one (2.4146(17) Å), feature usually observed for such dichlorido-bridged dimers, such as $[(\eta^6\text{-}C_6Me_6)RuCl_2]_2$ (Ru–Cl(terminal), 2.394 Å, and Ru–Cl(bridge), 2.460 Å).[1]

Table 4.1. Crystallographic selected bond lengths (Å) and angles (deg) for dimer $[Ru(\eta^6\text{-}C_6H_5CH_2COOH)(\mu\text{-}Cl)Cl]_2$ (**34dimer**), and monomers $[Ru(\eta^6\text{-}C_6H_5CH_2COOH)(en)Cl]Cl$ (**20Cl**), $[Ru(\eta^6\text{-}C_6H_5CH_2COOH)(phen)Cl]Cl$ (**36Cl**), $[Ru(\eta^6\text{-}C_6H_5CH_2COOH)(oxo)Cl]Na$ (**37Cl**), and $[Ru(\eta^6{:}\kappa^1\text{-}C_6H_5CH_2COO)(tmen)]PF_6$ (**38·PF$_6$**).

Bond / angle	34dimer	20Cl	36Cl	37Cl	38·PF$_6$
Ru–C6	2.168(6)	2.1819(19)	2.228(6)	2.170(17)	2.116(4)
Ru–C5	2.162(6)	2.182(2)	2.206(7)	2.146(17)	2.168(5)
Ru–C4	2.148(7)	2.202(2)	2.182(7)	2.161(18)	2.188(5)
Ru–C3	2.169(4)	2.180(2)	2.188(8)	2.182(17)	2.211(5)
Ru–C2	2.152(6)	2.186(2)	2.188(7)	2.170(15)	2.188(5)
Ru–C1	2.163(6)	2.158(2)	2.190(7)	2.170(15)	2.178(5)
Ru–centroid	1.644	1.666	1.688	1.651	1.659
Ru–X	2.4462(15)	2.1255(17)	2.093(5)	2.094(11)	2.164(4)
Ru–Y	2.4450(14)	2.1229(16)	2.090(5)	2.116(10)	2.187(4)
Ru–Cl/O	2.4146(17)	2.4114(5)	2.3917(17)	2.398(5)	2.080(3)
X-Ru-Y	81.24(5)	78.84(7)	77.5(2)	77.8(4)	80.51(16)
X-Ru-Cl/O	87.46(6)	83.95(5)	85.36(16)	84.0(2)	84.58(14)
Y-Ru-Cl/O	86.55(6)	85.10(5)	85.27(16)	84.2(3)	85.84(13)
Ru-C6-C7	127.10	127.71	130.25	126.72	113.48
C7-offset	0.087(+)	0.069(+)	0.018(+)	0.061(+)	0.548(+)

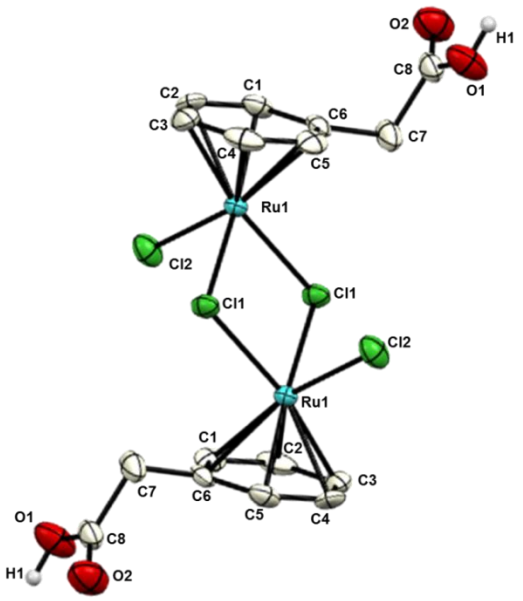

Figure 4.2. ORTEP representation (thermal ellipsoids drawn at 50% probability level), including atom numbering scheme, of the dimer precursor $[Ru(\eta^6\text{-}C_6H_5CH_2COOH)(\mu\text{-}Cl)Cl]_2$ (**34dimer**). Hydrogen atoms have been removed for clarity, except those of the carboxylic-tether group.

Open-tether complexes **20Cl**, **36Cl** and **37Cl** (Figure 4.3) adopted the typical pseudo-octahedral three-legged piano stool geometry, with the metal π-bonded to the phenylacetic acid (the "seat") and σ-bonded to a chlorido ligand and two donor atoms of the chelating ligand (the "legs") common to other Ru^{II} η^6-arene structures.[2, 3] The Ru–C, Ru–centroid, Ru–Cl and Ru–XY bond lengths are in agreement with previously reported Ru^{II}-arene analogues.[2-4]

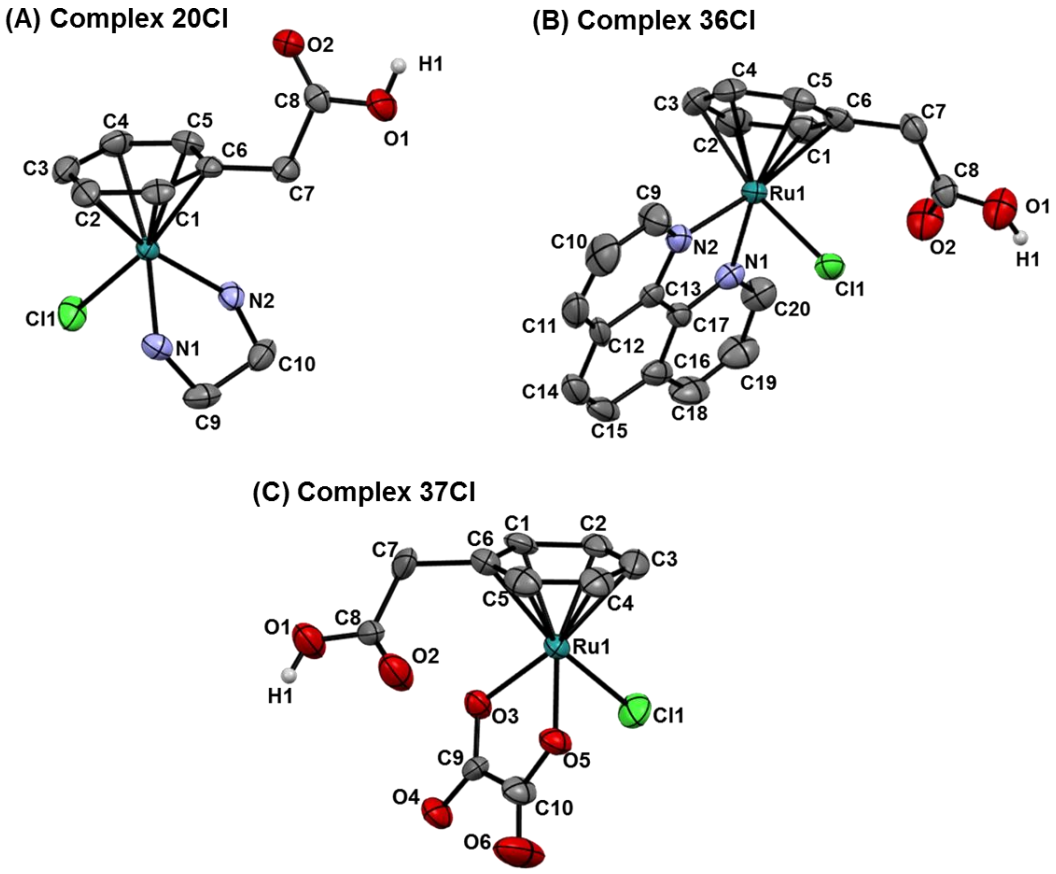

Figure 4.3. X-ray structure and atom numbering schemes of the complexes [Ru(η^6-$C_6H_5CH_2COOH$)(en)Cl]Cl (**20Cl**), [Ru(η^6-$C_6H_5CH_2COOH$)(phen)Cl]Cl (**36Cl**) and [Ru(η^6-$C_6H_5CH_2COOH$)(oxo)Cl]Na (**37Cl**). Thermal ellipsoids show 50% probability. The hydrogen atoms and counter ions have been omitted for clarity (except hydrogen of the carboxylic tether group).

The X-ray crystal structures of complexes **20Cl** and **36Cl** showed extensive H-bonding, as observed before for this type of crystal structures.[5, 6] The crystal structure of complex **36Cl** also shows π-stacking interactions between the central phen ring of two adjacent molecules (centroid-to-centroid distance is 3.504 Å; Figure 4.4).

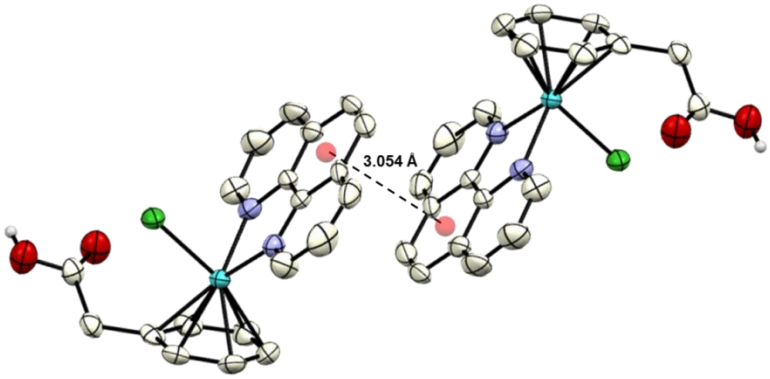

Figure 4.4. Diagram showing π-stacking between the central ring of the phenanthroline ligand of adjacent molecules in the X-ray crystal structure of **36Cl**. The centroids are separated by 3.504 Å. The counter ions and hydrogen atoms (except hydrogens of the carboxylic-tether group) have been omitted for clarity.

The structure of **37Cl** showed dimer formation between equivalent molecules, held together by non-covalent interactions between oxygen atoms of bound oxalate with both sodium (as a counter ion) and solvent water molecules (distances within the range 2.313–2.888 Å). Hydrogen-bond interactions between the hydrogen atom of the OH-tethered group and solvent water molecules were present. Interestingly, hydrogen bonds were observed between arene C–H and O(oxo) of adjacent molecules (C–H···O distance 2.514 Å).

X-ray diffraction data of suitable crystals were collected for the closed-tether complex **38·PF$_6$**, [Ru(η^6:κ^1-$C_6H_5CH_2COO$)(tmen)]PF_6. Here we present the first crystal structure determined by X-ray diffraction of a η^6:κ^1-arene:carboxylate ruthenium(II) complex, and also the first Ru^{II} five-membered η^6:κ^1-arene:O chelate. Its structure and atom numbering scheme are shown in Figure 4.5. Selected bond angles and distances are included in Table 4.1. The complex adopted the expected pseudo-octahedral half-sandwich geometry with the oxygen atom pendant from the η^6-bound arene forming an

additional chelate, or tether ring, in the structure. No H-bonding nor intermolecular π-π stacking interactions were observed.

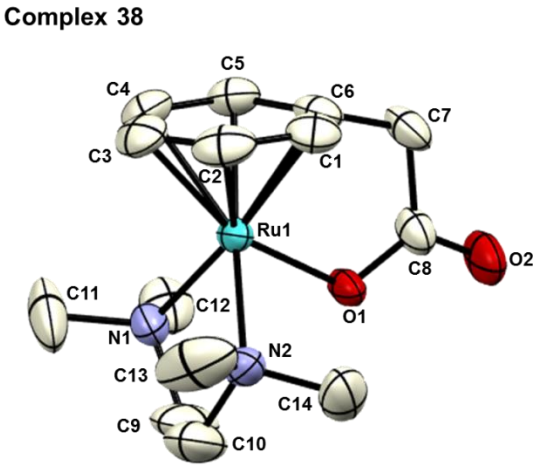

Figure 4.5. X-ray structure and atom numbering scheme of the closed tether complex $[Ru(\eta^6{:}\kappa^1\text{-}C_6H_5CH_2COO)(tmen)]PF_6$ (**38·PF$_6$**). Thermal ellipsoids show 50% probability. The hydrogen atoms and counter ions have been omitted for clarity.

Structural analysis corroborates the strain in the closed-tether structure of complex **38·PF$_6$** compared to its related open complexes **20Cl**, **36Cl** and **37Cl**. Not only a pronounced tilt in the η^6-bound arene is observed (as indicated by the differences in the Ru–C3 versus Ru–C6 bond lengths; 2.211(5) vs 2.116(4) Å, respectively), but also there is a strong offset of C7 toward the Ru^{II} atom with regard to the plane that contains the η^6-bound arene, 0.548 Å versus < 0.069 Å in the open-tether structures. A similar C7-offset in the range 0.460–0.488 Å was found for closed complexes of general structure $[Ru(\eta^6{:}\kappa^1\text{-arene:}NH_2)(XY)]^{2+}$.[7] The Ru-C6-C7 is also an important geometrical parameter discussed in previous Chapters and which correlates with the strain imposed on the arene by the tether arm, indicates that complex **38·PF$_6$** presents a strained angle of 113.48º, while **20Cl**, **36Cl** and **37Cl** have it in the range 126.72–130.25º, very close to the non-strained 130º. These observations are in agreement with others Ru^{II} $\eta^6{:}\kappa^1$-arene:N closed tether complexes where the same angle for a five-member tether ring has been found to range within 113–114º.[7]

In general, we have found that η^6:κ^1-arene:O complexes present a weaker coordination to the ruthenium(II) centre by the O_{tether} in comparison to the analogues investigated in Chapter 3 (N_{tether}),[8, 9] which is particularly true for complexes with two-carbon tether arms.[10] This might explain why there are only few reported complexes with this type of tethered Ru^{II}-arene bearing Ru–O coordination.

4.2.2 Speciation in Water of the Tethered Ru^{II}-arene Complexes and Interconversion of Open and Closed Species in Aqueous Solution

The reactivity of Ru^{II} arene complexes is generally thought to involve aquation. The additional complexity of our systems due to the possibility of association/dissociation of the tether group to the ruthenium(II) centre proves the hydrolysis process rather attractive. To elucidate the aqueous behaviour of these Ru^{II}-tethered complexes a series of experiments in water were carried out.

Figure 4.6 shows the speciation percentage of open-tether-chlorido/open-tether-aqua/closed-tether species) of complexes **20Cl** and **35Cl**–**37Cl** at equilibrium (24 h) in aqueous solution by ^{1}H NMR. Closed-tether complex 38 was included for comparative reasons. After dissolving the complexes the pH of these solutions varied in the range 2.4–2.8 as a result of the deprotonation of the dangling carboxylic acid in the tether.

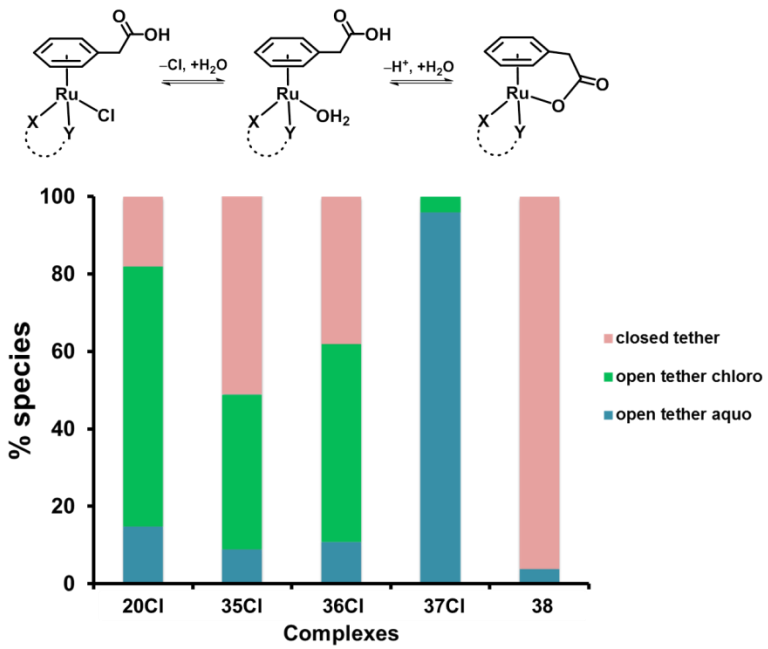

Figure 4.6. Percentage of species (closed-, chlorido- and aqua-) as determined by ^{1}H NMR after 24 h (at equilibrium) when complexes **20Cl** and **35Cl**–**37Cl** and **38** were dissolved in D_2O (pH in the range 2.4–2.8).

For complexes **20Cl**, **35Cl** and **36Cl** in D_2O two major species were observed by ^{1}H NMR immediately after dissolution (ca. 10 min); open-tether-chlorido complexes **20Cl**, **35Cl** and **36Cl**, and closed-tether complexes **20**, **35** and **36**, respectively. Over time, as the solution approaches equilibrium, Ru^{II}-arene speciation evolved and a new species appeared in the ^{1}H NMR spectra, which was attributed to the open-tether aqua complexes **20A**, **35A** and **36A** and confirmed by addition of excess of chloride (Figure 4.7 for aqueous equilibrium of complex **36Cl** as an example). For complex **37Cl**, the spectra show a majority of the open-tether aqua adduct **37A**. The behaviour of **37Cl** can be explained on the basis of an increased electron density at the metal centre due to the dianionic oxalate ligand, as well as stabilising interactions between hydrogen atoms of coordinated water and the oxygen atoms of the oxalato, which may be contributing to the high stabilization of the aqua adduct **37A**. Complex **38** was dissolved in D_2O to show no changes over time.

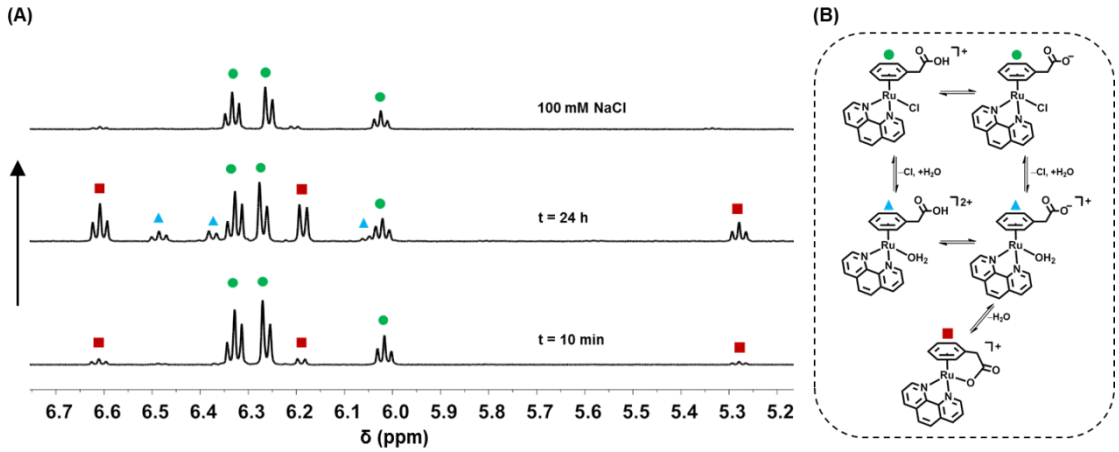

Figure 4.7. (A) ^{1}H NMR spectra showing the different species obtained after dissolving complex **36Cl** in a non-buffered aqueous solution (final pH = 2.7); (bottom spectrum) immediately after dissolving (ca. 10 min), (middle spectrum) at equilibrium after 24 h, (top spectrum) upon addition of 100 mM NaCl to the solution at equilibrium. (B) Scheme of the species that are observed in the ^{1}H NMR regarding the dynamic equilibria of complex **36Cl** resulting from its dissolution in water.

4.2.2.1 pK_a Determination

Both the carboxylic acid group and the water ligand in the aqua adduct have key roles in the chelate ring-opening and closing (switchability) of our system: (i) the carboxylate binds to the Ru^{II} centre when deprotonated, while protonation renders it unable to metal coordination; and (ii) the aqua ligand in Ru–OH_2 can be displaced making the Ru susceptible for nucleophilic attack, while Ru–OH is much less reactive. Given the complexity of our system in aqueous solution, we determined the pK_{a1} (of the pendant carboxylate) and pK_{a2} (of the OH_2 ligand in the aqua adduct) of our complexes in order to understand their aqueous dynamics in the pH scale (0–12).

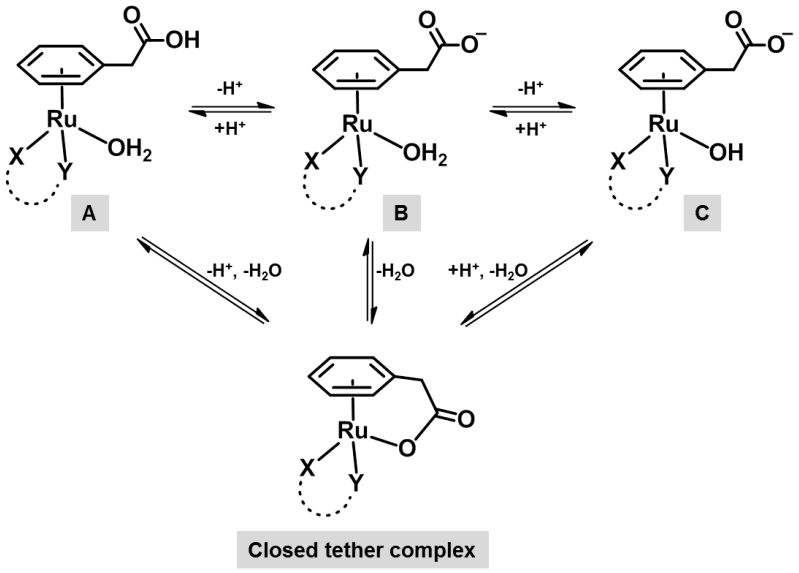

Scheme 4.1.

In order to determine the pK_a values of the OH_2 ligand of the aqua adducts, as well as the deprotonation of the carboxylic group of the complexes under study in this Chapter, aqueous solutions of ca. 10 mM of the deuterated versions of $[Ru(\eta^6\text{-}C_6H_5CH_2COOH)(en)(OD_2)]^{2+}$ (**20A**), $[Ru(\eta^6\text{-}C_6H_5CH_2COOH)(phen)(OD_2)]^{2+}$ (**36A**) and $[Ru(\eta^6\text{-}C_6H_5CH_2COOH)(oxo)(OD_2)]$ (**37A**) were prepared by addition of AgOTf to complexes **20Cl**, **36Cl** and **37Cl** in D_2O, and subsequent removal of the resulting AgCl precipitate. The pH was adjusted to <1. Changes in the ^1H NMR chemical shifts of the H_{meta} η^6-arene protons of **20A**, **36A** and **37A** were recorded at 298 K over the pH range 0–12 by the addition of dilute NaOD (or DNO_3 for adjustment purposes). Scheme 4.1 shows the main species detected in the titration of complexes **20A**, **36A** and **37A**.

Variation of the pH led to interconversion between the species, which was fully reversible as shown by NMR spectroscopy. As an example, selected ^1H NMR spectra for complex **36A** in D_2O are depicted in Figure 4.8A in the pH range 0.5–11.0. The aqua complex $[Ru(\eta^6\text{-}C_6H_5CH_2COOH)(phen)(OH_2)]^{2+}$ (**36A**) predominates at low pH (0.5) and exhibits two deprotonation steps to afford $[Ru(\eta^6\text{-}C_6H_5CH_2COO)(phen)(OH_2)]^{+}$ (**36B**) and subsequently $[Ru(\eta^6\text{-}$

$C_6H_5CH_2COO)(phen)(OH)]$ (**36C**). The chemical shift of the η^6-bound arene protons in meta position were plotted against pH and the data were fitted to the Henderson-Hasselbalch equation, from which the pK_a values of both carboxylic group and coordinated water were determined (Figure 4.8B for complex **36A**). It is worth mentioning that the closed-tether complex **36** is the mayor species in the range of pH ca. 2–8, matching, as expected, the predominant presence of species **36B** (COO^-/H_2O).

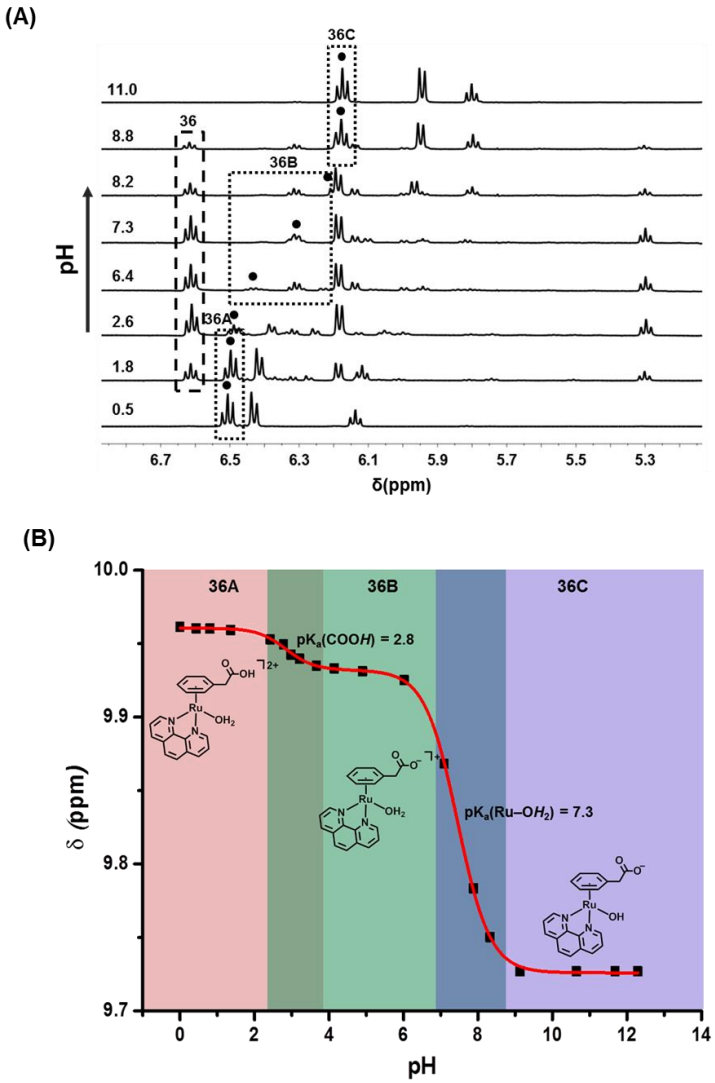

Figure 4.8. (A) pH dependency of the chemical shift of resonances corresponding to the meta η^6-bound arene protons on the ^1H NMR spectra of the different species resulting from the titration of the aqueous solution of complex **36A** in D_2O (**36A**→ **36B** →**36C**). As we go up in the pH scale complex **36** appears, as the major species in the range 2-8 where **36B** is the preferred species in the acid/base equilibria of **36A** (see Scheme 4.1) (B) The curve is a Henderson–Hasselbalch computer-best fit with pK_a values of 2.8 (pK_{a1}; carboxylic acid) and 7.3 (pK_{a2}; aqua adduct) for **36A**.

The pK_{a1} and pK_{a2} values for the aqua adducts **20A**, **36A** and **37A** are listed in Table 2. The pK_{a1} values are ca. 1–1.5 units lower than that of the free arene ligand; 3.3, 2.8 and 3.5, for complexes **20A**, **36A** and **37A**, respectively (versus pK_a 4.31 for the free ligand). This appears to suggest that electron density on the carboxylate pendant arm is more readily delocalized when phenylacetate is η^6-coordinated to Ru^{II}. Since the pK_a decreases in the order **37A** (oxo) > **20A** (en) > **36A** (phen), this may imply that a better π-acceptor chelating ligand (phen) aids such a delocalization. The pK_{a2} values measured for the coordinated water molecule to the ruthenium(II) centre (7.8, 7.3 and 8.5 for **20A**, **36A** and **37A**, respectively) increase in the same fashion, **37A** (oxo) > **20A** (en) > **36A** (phen), which could be explained in a similar manner (coordinated water to ruthenium(II) bound to a π-acceptor group such as phenanthroline is more acidic). The pK_{a2} values found for these complexes are in the same range (ca. 8) than those reported for other Ru^{II} arene complexes of general formula $[Ru(\eta^6\text{-arene})(XY)(OH_2)]^{2+}$.[3, 4]

Table 4.2. pK_a values of the carboxylic group and the aqua ligand in complexes **20A**, **36A** and **37A**.

Complex	C(O)–OH (pK_{a1})	Ru–OH_2 (pK_{a2})
$[Ru(\eta^6\text{-}C_6H_5CH_2COOH)(en)OH_2]^{2+}$ (**20A**)	3.3	7.8
$[Ru(\eta^6\text{-}C_6H_5CH_2COOH)(phen)OH_2]^{2+}$ (**36A**)	2.8	7.3
$[Ru(\eta^6\text{-}C_6H_5CH_2COOH)(oxo)OH_2]$ (**37A**)	3.5	8.5

In the pH range 0–7, the (more reactive) aqua adduct predominates. This reactivity might explain why deprotonation of the carboxylic acid (pH > 2) in **36A** to produce **36B** triggers the formation of the closed-tether complex **36** (via intramolecular re-arrangement), which is susceptible at higher pH values to OH^- attack and eventually converts into **36C**. The latter hydroxido complex predominates in alkaline solution at pH > 9. Closed-tether complex $[Ru(\eta^6{:}\kappa^1\text{-}C_6H_5CH_2COO)(phen)]^+$ (**36**) is present in

solution in the pH range ca. 2–9. The assignment of these signals was confirmed by their pH titration curves. Closed-tether complex **38** remained unaltered in the pH range covered by our experiments; its ^{1}H NMR spectra, as expected, showed no variations.

Additionally, solutions of complexes **20Cl**, **35Cl–37Cl** and **38** were prepared containing 100 mM of NaCl at pH 7.3 using Na_2HPO_3/citric acid buffer (Figure 4.9A) to mimic extracellular conditions. ^{1}H NMR spectra were recorded directly after sample preparation (10 min, 298 K) and after incubation for 24 h. As expected, chemical shifts of complexes **20Cl** and **35Cl–37Cl** showed no changes over 24 h, they did not hydrolyse nor form the closed form under these conditions, with the exception of **36Cl** that exhibited ca. 10% of closed species (**36**). Complex **38** did not exhibit any changes. Finally, we observed the solutions of complexes **20Cl**, **35Cl–37Cl** and **38** upon chloride/chlorido sequestration with AgOTf (and subsequent AgCl removal; Figure 4.9B). As expected, no presence of chlorido species was observed. Complexes bearing *o*-pda and phen favour the closed-tether species **35** and **36** while en and oxalato favour the aqua adduct **20A** and **37A**. No significant changes were observed for **38**. We would have expected that total aquation would render the complexes susceptible towards carboxylate binding and tether-ring closure. However, we found the coexistence of open aqua and closed species at equilibrium. This is in contrast to the aqueous behaviour of analogous complexes of general formula $[Ru\{\eta^6{:}\kappa^1\text{-}C_6H_5(C_6H_4)NH_2\}(XY)]^{2+}$ described in Chapter 3. For the latter, opening of the tether occurred at a pH lower than the pK_a value.[7] For the complexes in this Chapter however, the activation pH is up to one unit higher than the pK_a. This indeed opens up a window for the interaction of the highly reactive Ru^{II}-aqua adduct upon cell and nuclear internalization, where the chloride concentration drops significantly (from 100 mM to 23 mM in the cytosol, to 4 mM in the nucleus).

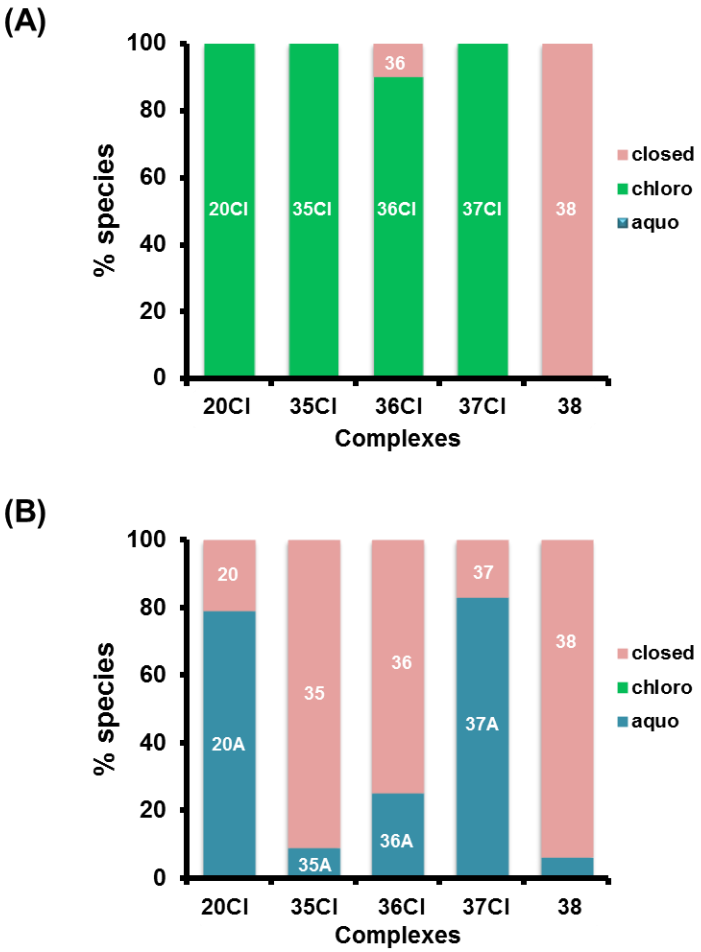

Figure 4.9. Different percentage of species (closed-, chlorido-, and aqua-) observed by ^{1}H NMR after 24 h (at equilibrium) when complexes **20Cl**, **35Cl–37Cl** and **38** were dissolved in: (A) buffered D_2O solution at pH 7.3 and 100 mM NaCl; and (B) D_2O and upon addition of AgOTf (the pH of the solutions ranges between 2.6–3.3) and subsequent removal of AgCl. This bar chart shows that complexes **35** and **36** bearing π-acceptor XY ligands favour the closed tether species, attributable to acidification of the metal centre.

4.2.2.2 pH-Dependent Activation of Closed-Tether Complexes

Following the understanding of the tether-ring closure and its dependence on pH, we wanted to investigate the reversibility of this process aiming at developing organometallics switchable between open and closed forms.

Complex **38** was synthesized and isolated directly in its closed form. Closed tethered complexes **20** and **35**–**37** were isolated in solution state (> 90%) and characterized as described in the Experimental Section.

Acidic activation of closed-tether complexes **20**, **36** and **38** to afford **20B/A**, **36B/A** and **38B/A** was investigated at increasing proton concentration from pH ca. 7 and followed by ^{1}H NMR spectroscopy. A new set of peaks assignable to open-tether aqua adducts (**20A**, **36A** and **38A**) appeared during the acidic titration of complexes over the pH range 7–0. As depicted in Figure 4.10, the three complexes underwent tether-ring opening to different extents following the titration where both $[Ru(\eta^6{:}\kappa^1\text{-}C_6H_5CH_2COO)(XY)]^+$ and $[Ru(\eta^6\text{-}C_6H_5CH_2COOH)(XY)(OH_2)]^{2+}$ species coexisted at different ratios as a response to the concentration of protons in solution.

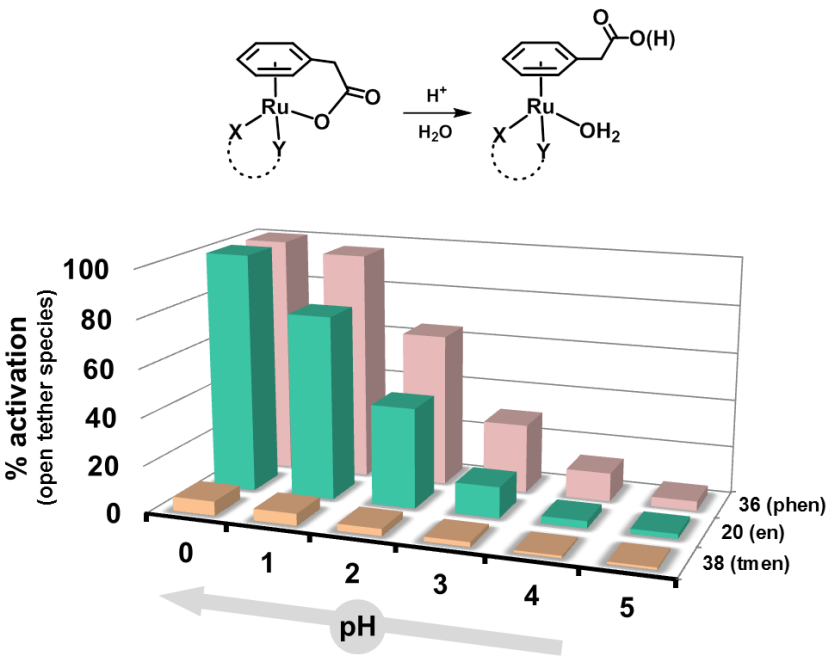

Figure 4.10. Percentages of Ru^{II} open tether species corresponding to the activation of the complexes **20** (en), **36** (phen) and **38** (tmen), in aqueous solutions at different pH values in the acidic range 0–5.

Lowering the pH to 4 resulted in a modest extent of activation of the Ru–O_{tether} bond (ca. 2–12% of open-tether aqua species at equilibrium) for complexes **20** and **36**. At pH 3 the ^{1}H NMR spectra showed some high-intensity peaks assignable to Ru^{II} open-tether complexes (13 and 29%, respectively). At pH 2 the percentages of species **20A** and **36A** are 42 and 64% respectively and below pH 1 the complexes are mostly present in

solution as the open aqua adducts. It is notable that complex **36** exhibited a modestly higher activation than **20**, perhaps related to its capability as π-acceptor that subsequently makes the metal more acidic.

Complex **38** showed the smallest percentage of open species at equilibrium. A similar behaviour was observed in the activation of analogous complex $[Ru\{\eta^6:k^1\text{-}C_6H_5(C_6H_4)NH_2\}(tmen)]^{2+}$ bearing a different hemilabile ligand (2-aminobiphenyl) but the same XY chelating ligand (Chapter 3).[7] The lack of reactivity can be attributed to the absence of H-bond formation capability by tmen, together with the higher steric hindrance in tmen Ru^{II} complexes for incoming nucleophiles.

4.2.3 Cell Viability Studies

Given the aqueous behaviour of our systems, we believed they would have little to no effect in cell growth. The cytotoxicity of complexes **20Cl**, **35Cl–37Cl** and **38** toward the human ovarian A2780 cancer cell line was investigated. Cisplatin was used as positive control, giving an IC_{50} value of 2.2±0.3 μM. Complexes **36Cl**, **37Cl** and **38** did not have any effect on A2780 cancer cells at maximum concentrations of 200 μM (Table 4.2). Complexes **20Cl** and **35Cl**, however, showed IC_{50} values of 130 and 117 μM, respectively. In general, the Ru^{II} complexes studied in this Chapter did not show a cytotoxic activity towards A2780 comparable to those related Ru^{II}-arene complexes of the type developed by Sadler (IC_{50} close to that of cisplatin). Even for complexes **20Cl** and **35Cl**, their IC_{50} values are well above the values of complexes of similar structure.[11, 12] The lack of activity was expected as it is attributable to the Ru^{II} inactivation upon tether-ring closure, and subsequent incapability to bind to DNA. The mild cytotoxic activity shown by **20Cl** and **35Cl** was somewhat surprising.

Table 4.2. Cell viability data for the Ru^{II} complexes studied in this Chapter (**20Cl**, **35Cl**–**37Cl** and **38**) in A2780 human ovarian cancer cells.

Complex	IC_{50} (μM)
20Cl	130.2±1.7
35Cl	116.7±22.5
36Cl	>200
37Cl	>200
38	>200
cisplatin	2.2±0.3

4.2.4 Catalytic Reduction of NAD^+ to NADH and Possible Effect in Cells

In order to gain additional information about the cytotoxicity of complexes **20Cl** and **35Cl**, we looked into the possibility of our systems exerting catalytic activity within cells. Ruthenium(II) half sandwich complexes have previously been reported to catalyse the reduction of pyruvate to lactate, a reduction carried out in vivo by NADH as a cofactor for the enzyme lactate dehydrogenase.[13] Additionally, they have been shown to reduce NAD^+ via transfer hydrogenation using sodium formate ($NaHCO_2$) as a hydride source.[14, 15]

Inspired by these findings, conversion of pyruvate to lactate in the presence of sodium formate by our systems was investigated. Lactate formation mediated by complex **20Cl** was followed by ^1H NMR at a ratio 1:2:200, Ru:pyruvate:formate. ^1H NMR spectra at 310 K were recorded until completion of the reaction (ca. 42 h). Molar ratios of pyruvate and lactate were determined by integrating the signals of pyruvate (3H, singlet, 2.36 ppm) and of lactate (1H, quartet, 4.11 ppm). After recording the initial spectrum (ca. 15 min) conversion to lactate was not identified. However, the percentage of lactate

increased to 67% after 18 h incubation. After 42 h of reaction almost total reduction (95%) of pyruvate to lactate was achieved (Figure 4.11).

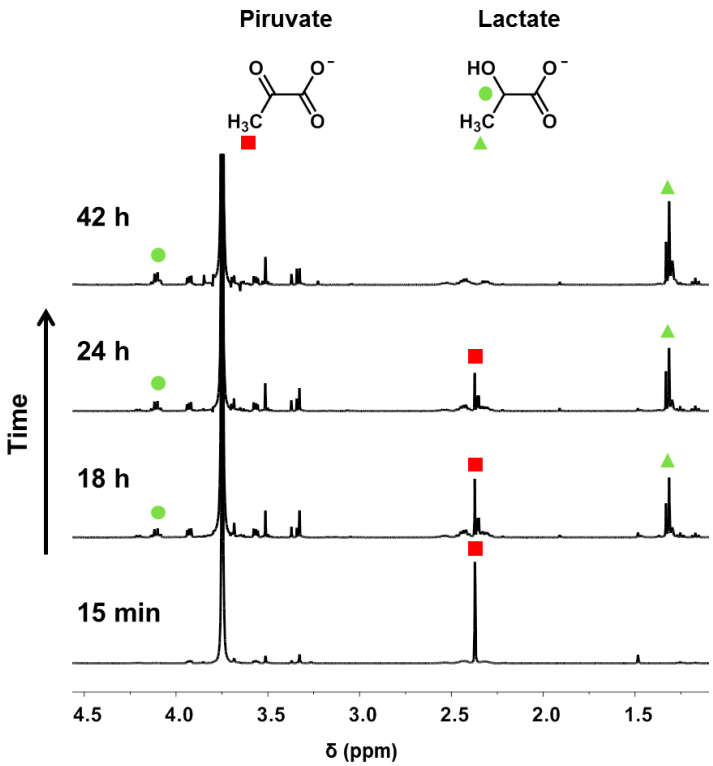

Figure 4.11. ^{1}H NMR spectra showing the conversion of pyruvate to lactate mediated by complex **20Cl** in the presence of $NaHCO_2$ (mol ratio 1:2:200, Ru:pyruvate:formate) in D_2O at 310 K.

We also investigated the catalytic conversion of NAD^+ to NADH using complexes **20Cl** (because of its cytotoxicity) and **38** (because of its stability as a closed tether complex) in the presence of sodium formate as hydride source by ^{1}H NMR spectroscopy in D_2O.

Complex **20Cl** was reacted with AgOTf (2 mol equiv) to ensure full removal of chloride and .chlorido ligands. Subtraction of chloride has been reported to increase the catalytic activity of this class of Ru^{II} arene complexes because chloride may compete to a significant extent with formate for the catalytic binding site.[16] The solution was mixed with NAD^+ (23.2 mM) and sodium formate (2.3 M), final ratio 1:2:200, Ru:NAD^+:formate. The pH of the reaction mixture was adjusted to 7.1 and the sample

incubated at 310 K. ^{1}H NMR spectra were recorded over time for 42 h (Figure 4.12). The spectrum initially contained two major sets of peaks corresponding to the expected aqua-adduct/closed-tether complexes, and a third set of peaks attributed to the formation of the Ru^{II}-formate adduct, $[Ru(\eta^{6}\text{-}C_6H_5CH_2COOH)(en)(HCOO)]^{+}$. This adduct (Ru–OOCH) is generated by the direct substitution of H_2O by formate which binds through the negatively-charged carboxylate oxygen, as has been previously reported for similar metal complexes.[17] The binding of formate to Ru^{II} was confirmed by the appearance of a sharp singlet at 8.20 ppm in the ^{1}H NMR spectrum (free formate appears at 8.46 ppm). The high field shift has been previously observed for analogous Ru^{II} arene formate complexes.[18] Within the first 3 h of reaction some additional changes were observed in the ^{1}H NMR spectrum. These initially suggested the regioselective reduction of NAD^{+} to 1,4-NADH as indicated by a decrease in the intensity of the signals of free NAD^{+} (H2 at 9.31 ppm) and the sole appearance of new peaks assignable to 1,4-NADH (H2' at 6.91 ppm and H4a/H4b at 2.70 ppm). The ^{1}H NMR spectra within 18 h of reaction also revealed the emergence of a second singlet around 7.23 ppm that was assigned to the H2'' of 1,6-NADH. After a total of 24 h, all NAD^{+} had been consumed. Analysis of the percentages of the reduced species at 24 h (52% for 1,4-NADH and 48% of 1,6-NADH) and at 42 h (32% for 1,4-NADH and 68% of 1,6-NADH) indicates the conversion of 1,4-NADH to 1,6-NADH over time. In contrast to the findings by Sadler,[13, 17] who found regioselectivity favouring 1,4- over 1,6-NADH, this result shows no selectivity, in fact 1,6-NADH predominates at longer reaction times, which is unusual. Eventhough the mechanism of the isomerisation favouring the thermodynamic product 1,6-NADH is unknown, it might have an impact inside the cell, whereby sequestration of the biologically active 1,4-NADH isomer might break the NAD^{+}/NADH balance, necessary

for survival. No arene loss and no formation of Ru–H species were detected over this period.

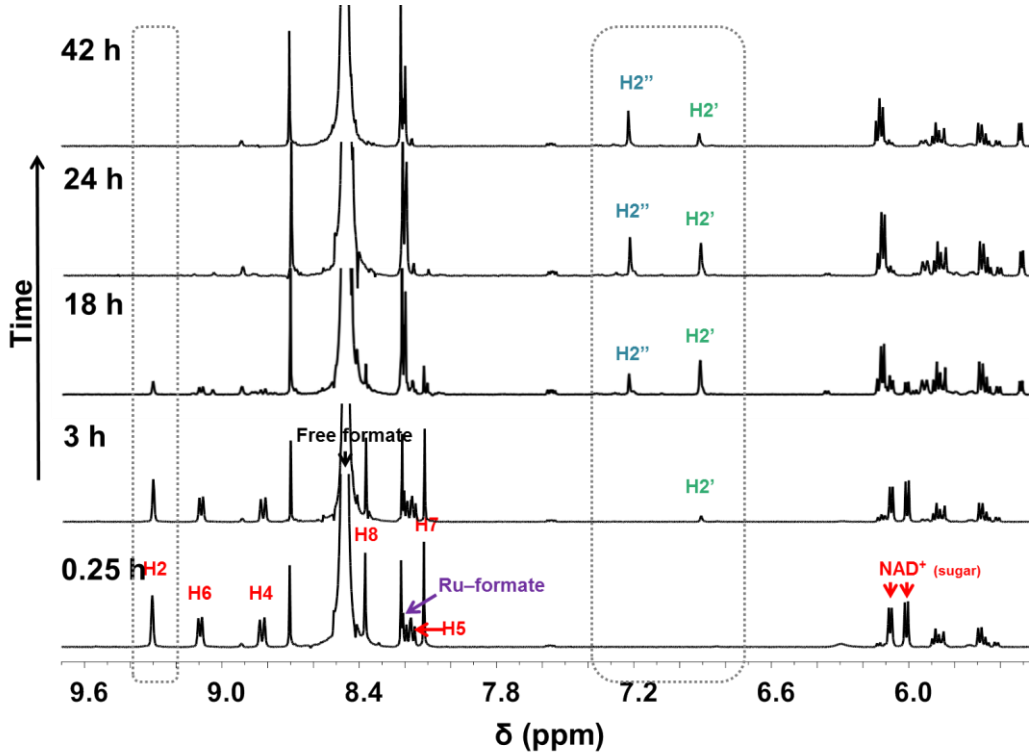

Figure 4.12. ^{1}H NMR spectra recorded during the reaction of a 11.6 mM solution in D_2O of $[Ru(\eta^6\text{-}C_6H_5CH_2COOH)(en)Cl]^+$ (**20Cl**) with NAD^+ and $NaHCO_2$ (molar ratio 1:2:200, respectively) at 310 K and pH ca. 7.1. NAD^+ is labelled in red (H2); 1,4-NADH in green (H2'), and 1,6-NADH in blue (H2'').

In contrast to **20Cl**, the initial spectrum in the analogous experiment with complex **38** contained only a set of signals corresponding to the closed tethered species. Signals attributable to the reduced species NADH appeared at 18 h of reaction (25% NAD^+ consumed). At 24 h only 33% of NAD^+ had been reduced, and 59% at 42 h. As shown in Figure 4.13, the presence of formate appears to trigger ring opening in complex **38** mediating the conversion of NAD^+ to NADH, even though in a much lower percentage than **20Cl**.

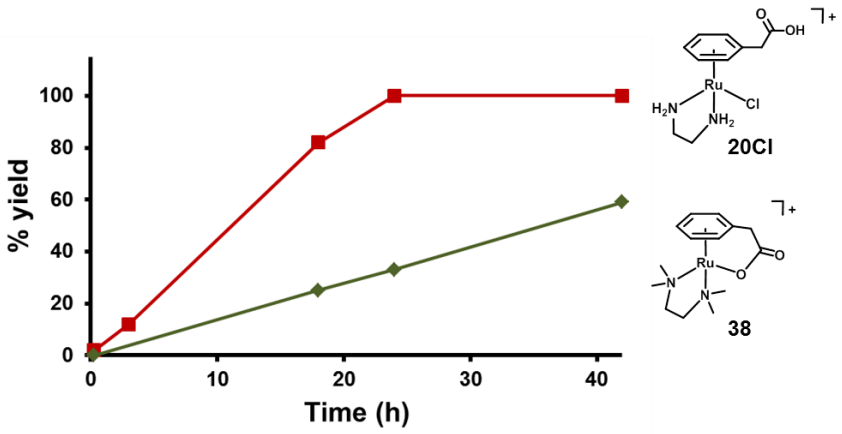

Figure 4.13. Plot showing the conversion of NAD^+ to NADH versus time for the transfer hydrogenation of NAD^+ (23.3 mM) using complexes **20Cl** and **38** in presence of $NaHCO_2$ (2.3 M) in D_2O at 310 K (pH ca. 7.1).

A second series of experiments on the reduction of NAD^+, varying the concentration of sodium formate, was performed for **20Cl** (complex **20Cl**, NAD^+ and sodium formate in the ratio 1:2:X, X = 25, 100, 200 or 500 equiv). A notable increase in the catalytic activity was observed with increase of the hydride source sodium formate (Figure 4.14A). The largest difference can be appreciated after 18 h where NAD^+ has been reduced in a 28, 68, 82 and 100 % for 25, 100, 200 and 500 equiv of formate. A second reduction product was detected in the later stages of the reaction, 1,6-NADH. Strikingly, regioselectivity towards 1,6-NADH was proved to be formate concentration dependent (Figure 4.14B). The percentage of the latter isomer was determined to be as follows: 11, 31, 48 and 87% for 25, 100, 200 and 500 equiv of formate, respectively, after 24 h of reaction. Again, over time the 1,4-isomer seems to evolve to 1,6-NADH. In contrast to reported studies on analogous Ru^{II} arene complexes,[16] the catalytic reduction of NAD^+ in the presence of formate by complex **20Cl** appear not to be regioselctive toward the 1,4-NADH isomer. The ratio of the formation of the hydrogenation products is dependent of the concentration of the hydride-source. Production of up to 25% of 1,6-NADH has been observed for complexes of general formula [Ru(arene)(L-L)Cl] (where

arene = *p*-cymene or benzene and L-L = DPEN, 1,2-diphenyl-1,2-diaminoethane derivates).[19]

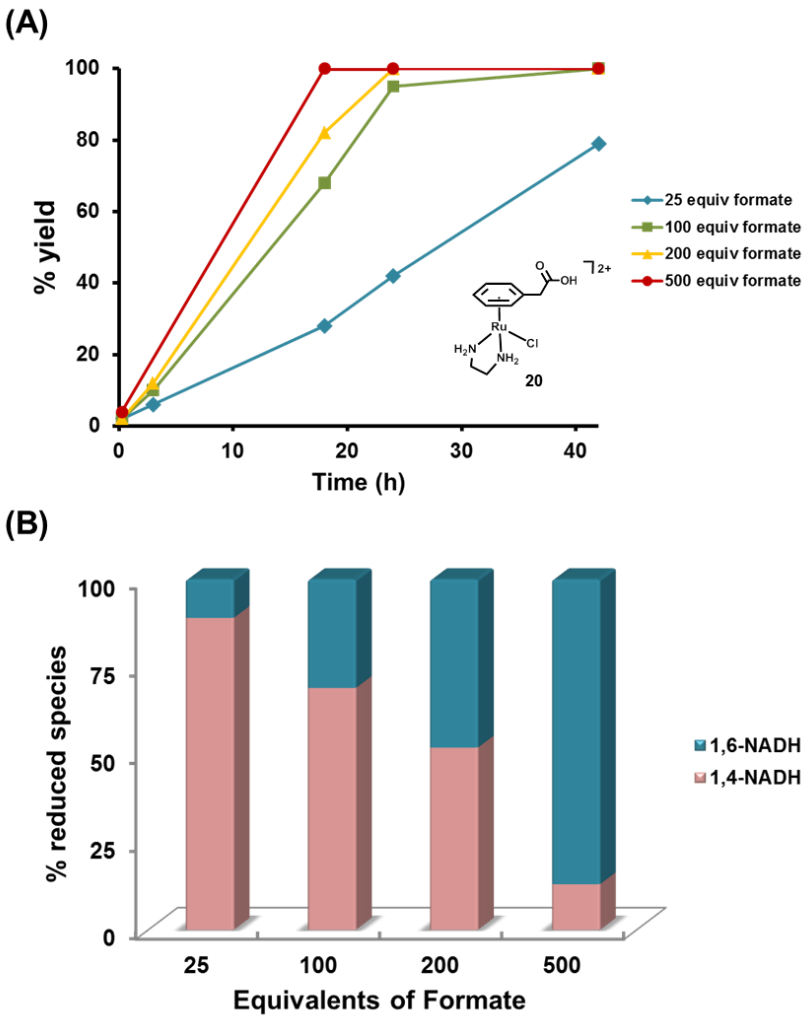

Figure 4.14. (A) Conversion versus time plot for the transfer hydrogenation of NAD^+ to NADH using complex **20Cl** with different $NaHCO_2$ concentrations in D_2O at pH ca. 7 at 310 K. (B) Representation of the different percentages of the reduced species 1,4-NADH and 1,6-NADH as dependent on the formate concentration over 24 h at 310 K.

These results make us think that the capability of undergoing transfer hydrogenation reactions might be responsible for the cell viability effect of **20Cl**. Therefore, we decided to test the cytotoxic activity of **20Cl** in A2780 again, this time in the presence of non-toxic doses of formate. Given the slow reaction of **20Cl** with formate, we tailored the cytotoxicity protocol, avoiding cell washing after 24 h of drug exposure, and leaving the cells for 96 h exposed to the drugs. Cisplatin presented an IC_{50} value of

2.9 μM and formate was completely innocuous at all concentrations tested. Under this protocol, the IC_{50} of **20Cl** alone was determined to be 122 μM. Co-incubation of **20Cl** with 1 mM formate had no significant effect in its IC_{50} (3% decrease), while 2 mM of formate decreased the IC_{50} of **20Cl** by 14% and 4 mM formate decreased the IC_{50} of **20Cl** by 24% (Figure 4.15). These results appear to indicate that the catalytic capabilities of these complexes might have an impact on their cytotoxicity.

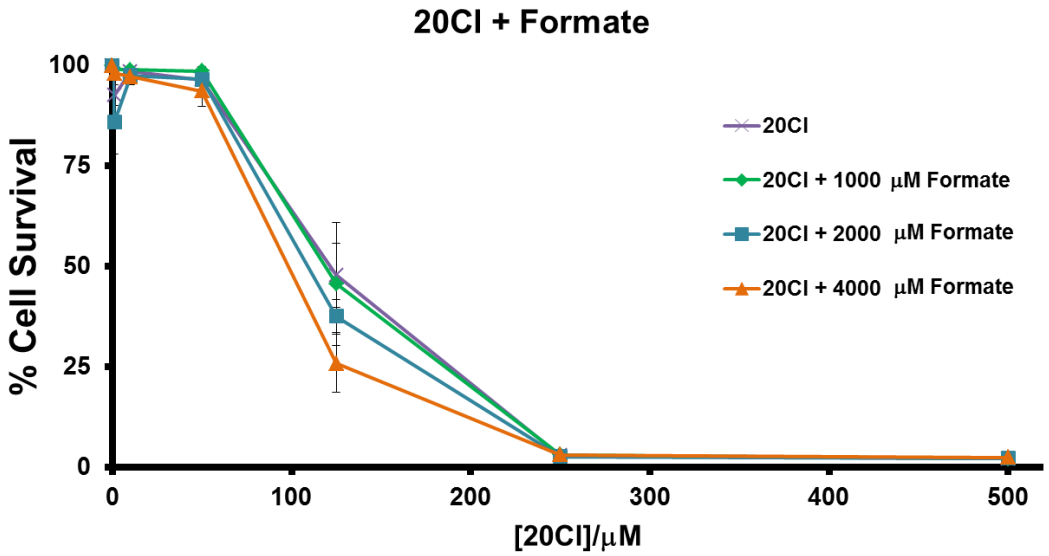

Comp	IC_{50} (μM)
20Cl	122
20Cl + $NaHCO_2$ 1000 μM	118
20Cl + $NaHCO_2$ 2000 μM	105
20Cl + $NaHCO_2$ 4000 μM	93

Figure 4.15. Cell viability – as dose response curves – of complex **20Cl** when co-incubated with different concentrations (μM) of sodium formate.

4.3 Conclusions

In this Chapter we have described the first crystal structure of a 5-member tether ring with a Ru(η^6:κ^1- arene:O) bond, showing the stability of our system.

We pursue to develop reversible pH-triggered activation of complexes. In Chapter 3 we had reported complexes of general formula $[Ru\{\eta^6:\kappa^1\text{-}C_6H_5(C_6H_4)NH_2\}(XY)]^{n+}$, which undergo reversible activation at highly acidic pH (1–2). The complexes presented in this Chapter fulfil the main requirements of our goal, that is, complexes that show reversible pH-dependent responsiveness. Additionally, these complexes represent further advancement toward our aim: (i) the closed tether Ru^{II} complex can be activated (the tether ring opens up) at pH as high as 4 if we introduce the appropriate XY bidentate ligand in the structure (e.g., complex **36Cl**); and (ii) the open-tether chlorido species coexists with its Ru^{II}-aqua adduct counterpart, active toward biomolecule binding. We have studied the complexity of the speciation of this system, finding how to control what species predominates in aqueous solution. Control over the accessibility of a free pendant carboxylate on a ruthenium(II) arene is in fact highly attractive for further functionalization or labelling studies.

Strikingly, complexes **20Cl** and **35Cl**, inactivated (closed tether) in aqueous solution at physiological pH, show micromolar cytotoxicity (range 100 μM). We investigated the possible causes of such activity and found that perhaps intracellular hydrogen-transfer reactions could be implicated, since complex **20Cl** seems to interact with formate to reduce both pyruvate and NAD^+in solution, and co-incubation with non-toxic doses of formate in the cell viability test seemed to increase the cytotoxic activity of **20Cl**. The reduction of NAD^+ appears to produce 1,4-NADH and 1,6-NADH in a non-regioselective manner, yet overtime the non-biologically active 1,6-NADH seems to predominate. The effects of complex **20Cl** at the intracellular level might be related

with a decrease of the concentration of NAD^+ to produce the non-biological active species as 1,6-NADH, disrupting numerous enzymatic processes that require the 1,4-NADH as a cofactor.

4.4 Experimental Section

4.4.1 Instrumentation

NMR Spectroscopy, Mass Spectrometry, Elemental Analysis and **pH Measurements** have been described in Chapter 2.

Single Crystal X-ray diffraction. Suitable crystals of compounds **20Cl**, **34dimer**, **36Cl**, **37Cl** and **38** were coated with mineral oil and mounted on Mitegen MicroMounts. The samples were measured in a Bruker D8 KAPPA APEX II diffractometer with CCD area-detector, equipped with graphite-monochromated Mo Kα radiation (λ = 0.71073 Å). The substantial redundancy in data allowed empirical absorption corrections (SADABS)[20] to be applied using multiple measurements of symmetry-equivalent reflections. Raw intensity data frames were integrated with the SAINT program, which also applied corrections for Lorentz and polarization effects. The Bruker SHELXTL Software Package was used for space group determination, structure solution, and refinement.[21] The space group determination was based on a check of the Laue symmetry, and systematic absences were confirmed using the structure solution. The structures were solved by direct methods (SHELXL-2014/7),[22, 23] completed with different Fourier syntheses, and refined with full-matrix least-squares using SHELXS minimizing $\omega(F_o^2-F_c^2)^2$. Weighted R factors (R_w) and goodness of fit (S) are based on F^2; conventional R factors (R) are based on F. All non-hydrogen atoms were refined with anisotropic displacement parameters. Hydrogen atom positions were geometrically calculated and allowed to ride on their parent carbon or nitrogen atoms with fixed isotropic U. All scattering factors and anomalous dispersion factors are contained in the SHELXTL 6.10 program library.

CCDC identifiers are 1579131 (**20Cl**), 1579130 (**34dimer**), 1579138 (**36Cl**), 1579141 (**37Cl**) and 1579135 (**38**), which contain the supplementary crystallographic data for this Chapter. These data are provided free of charge by the Cambridge Crystallographic Data Centre.

4.4.2 Methods

Calculation of pK_a values. Complexes **20Cl**, **36Cl** and **37Cl** were dissolved in D_2O in the presence of AgOTf, AgCl was filtered off after stiring for 30 min and then the pH was adjusted to ca. 0.5 to afford aqua complexes $[Ru(\eta^6\text{-}C_6H_5CH_2COOH)(en)(OH_2)]^{2+}$ (**20A**), $[Ru(\eta^6\text{-}C_6H_5CH_2COOH)(phen)(OH_2)]^{2+}$ (**36A**), and $[Ru(\eta^6\text{-}C_6H_5CH_2COOH)(oxo)(OH_2)]$ (**37A**). pH titration curves were traced by plotting the variation of the ^1H NMR chemical shifts of the aqua complexes over the pH range 0–12 by the addition of dilute NaOD or DNO_3. The pH titration curves were fitted to the Henderson–Hasselbalch equation using the OriginPro version 9.0 program (OriginLab, Northampton, MA), with the assumption that the observed chemical shifts are weighted averages according to the populations of the protonated and deprotonated species. The pK_a values of both the pendant carboxylic group as well as the aqua ligand of the Ru^{II} complexes **20A**, **36A** and **37A** were determined from these plots.

Hydrolysis. Aqueous solutions of the Ru^{II} complexes (ca. 6 mM at 298 K) were prepared by dissolving **20Cl**, **35Cl–37Cl** and **38** in D_2O. ^1H NMR spectra were recorded directly after sample preparation (data collection at ca. 10 min after dissolution) and after 24 h. Speciation of each complex into chlorido, aqua and closed-tether species was quantified by integration of signals of H_m (meta proton of the η^6-arene) in the ^1H NMR spectra. After equilibrium was reached (24 h), an excess of NaCl

(100 mM) was added and ^{1}H NMR spectra were recorded after 24 h incubation. In another set of experiments for the speciation study in the absence of chloride ions, AgOTf (2 mol equiv for **20Cl**, **35Cl** and **36Cl**, and 1 mol equiv for **37Cl** and **38**) was added to D_2O solutions of **20Cl**, **35Cl–37Cl** and **38**, which were left to stir for 30 min. After removal of AgCl precipitate by filtration the ^{1}H NMR spectra were acquired, and again after 24 h. Finally, Na_2HPO_4/citric acid buffer was used to prepare pH 7.3 D_2O solutions containing 100 mM of NaCl. Complexes **20Cl**, **35Cl–37Cl** and **38** were dissolved (ca. 6 mM) in the buffered solution and the ^{1}H NMR spectra were acquired after dissolution and at 24 h at 298 K.

Cell culture and cytotoxicity toward A2780 human ovarian cancer cell line. The A2780 ovarian cell line was obtained from Sigma-Aldrich. The cells were maintained in RPMI 1640 media, which was supplemented with 10% foetal calf serum, 1% L-glutamine, and 1% penicillin/streptomycin. All cells were grown at 310 K in a humidified atmosphere containing 5% CO_2.

After plating, human ovarian A2780 cancer cells were treated with Ru^{II} complexes **20Cl**, **35Cl–37Cl** and **38** on day two at concentrations ranging from 0.5 to 200 μM. Cells were exposed to the complexes for 24 h, washed, supplied with fresh medium, and allowed to grow for three doubling times (72 h). The protein content was then measured (proportional to cell survival) using the sulforhodamine B (SRB) assay.[24] The data were analysed using OriginPro. IC_{50} values were obtained from plots of the percentage survival of cells versus the logarithm of the concentration expressed in micromolar units and fitted to a sigmoidal curve. Cisplatin was used as a positive control (max DMSO concentration to aid metal complex solubility, 0.25%).

The protocol for co-incubation with formate was carried out as described above with the following modification: the incubation time was 96 h, followed by the SRB assay. The IC_{50} values of complex **20Cl** (dose response curves) were determined at fixed concentrations of formate: 1.0, 2.0, and 4.0 mM. Cisplatin was used as a positive control (max DMSO concentration, 0.25%) in all the experiments.

Transfer hydrogenation reactions. Pyruvate (2 mg, 0.018 mmol) was added to 700 μL of a stock solution (12.9 mM) of complex **20A** (prepared by reaction of **20** with of 2 mol equiv of AgOTf at room temperature for 30 min followed by removal of AgCl). $NaHCO_2$ (122 mg, 1.8 mmol) was then added to the mixture. Final concentrations were as follows: **20Cl**, 12.9 mM; pyruvate 25.7 mM; $NaHCO_2$ 2.6 M; molar ratio 1:2:200. The pH of the solution was adjusted to ca. 7.1 by adding dilute solutions of NaOD and finely adjusting with DNO_3. The mixture was stirred to dissolve the sodium formate and transferred into a 5 mm NMR tube. A series of ^{1}H NMR spectra was then recorded at 310 K at different time intervals up to 42 h. Percentages of the different species in solution (remaining substrate and product formed) were determined by integration of signals corresponding to pyruvate (3H, singlet, 2.36 ppm) and to lactate (1H, quartet, 4.11 ppm).

Experiments to investigate the conversion of NAD^+ to NADH by complex **20A** followed the same experimental protocol using pyruvate as substrate and the molar ratios were: 1:2:200 for **20Cl**:NAD^+:formate. Percentages of species of NAD^+ and its reduced forms 1,4-NADH and 1,6-NADH were determined by integrating the signals corresponding to H2 of NAD^+ (9.31 ppm), H2' of 1,4-NADH (6.91 ppm), and H2" of 1,6-NADH (7.23 ppm). Experiments to investigate the reactivity towards transfer hydrogenation reactions by complex **38** followed the same protocol.

4.4.3 Synthesis

Complexes **20Cl** and **35Cl**–**37Cl** were synthesised as described below for the individual reactions. Complex **38** was synthesized and isolated directly in its closed form.

Closed tethered complexes **20** and **35**–**37** were characterized in aqueous solution (vide infra). The complexes had been previously observed as part of a mixture of species by ^{1}H NMR during the pH titrations (see main text), yet rapid total conversion from **20Cl**, **35Cl** and **36Cl** to closed-tether cations **20**, **35** and **36** took place when solutions of hydroxo complexes (**20C**, **35C** and **36C**) at pH 12 were acidified to neutrality (pH ca. 7). The increase in intensity of the proton resonance signals of the closed tether species was accompanied by a concurrent decrease in the intensity of peaks for hydroxo complexes, which disappeared altogether at about pH 6–7. The total conversion of complex **37Cl** to form complex **37** was not achieved by this method (although 60% of **37** was observed at equilibrium with its open-tether counterpart).

[Ru(η^6-C$_6$H$_5$CH$_2$COOH)(μ-Cl)Cl]$_2$ (34dimer). 2,5-Dihydrophenylacetic acid (400 mg, 2.9 mmol) and $RuCl_3 \cdot 3H_2O$ (473 mg, 1.81 mmol) were suspended in 10 mL of 1:4 (v/v) water/acetone in a closed pressure tube. The reaction mixture was heated at 100 ºC for 3 h. The red precipitate was filtered off, washed with cold ethanol and diethyl ether, and dried in vacuum. Yield: 445 mg, 80%. Elemental analysis: Cald. for $C_{16}H_{16}Cl_4O_4Ru_2$ (616.24): C, 31.19; H, 2.62. Found: C, 31.66; H, 2.55. ^{1}H NMR (400 MHz, DMSO-d_6, δ): 12.79 (br s, OH, 1H), 6.01 (t, J = 5.9 Hz, Ar H, 2H), 5.91 (d, J = 6.1 Hz, Ar H, 2H), 5.83 (t, J = 5.6 Hz, Ar H, 1H), 3.49 (s, CH_2, 2H). Suitable red crystals for X-ray diffraction were collected by filtration from the reaction mixture.

[Ru(η^6-C$_6$H$_5$CH$_2$COOH)(en)Cl]Cl (20Cl). [Ru(η^6-C$_6$H$_5$CH$_2$COOH)Cl$_2$]$_2$ (100 mg, 0.162 mmol) was suspended in anhydrous ethanol (5 mL). Ethylenediamine (22 µL, 0.324 mmol) was added, and the mixture was stirred for 2 h under reflux. The resultant yellow solution was filtered through a 0.45 µm syringe filter. The solvent was reduced to ca. 5% of its original volume, and diethyl ether (4 mL) was added. The sticky solid was sonicated to give a yellow precipitate, centrifuged, washed with diethyl ether and dried in vacuum. Yield: 96 mg (80%). Elemental analysis: Cald. for $C_{10}H_{16}Cl_2N_2O_2Ru$ (368.22): C, 31.10; H, 4.70; N, 7.25. Found: C, 32.54; H, 4.87; N, 7.83.^{1}H NMR (400 MHz, MeOD-d_4, δ): 6.43 (br s, NH_2, 2H), 5.75 (t, J = 5.7 Hz, Ar H, 2H), 5.67 (d, J = 5.7 Hz, Ar H, 2H), 5.64 (t, J = 5.5 Hz, Ar H, 1H), 4.04 (br s, NH_2, 2H), 3.57 (s, CH_2, 2H), 2.54–2.50 (m, 2H), 2.46–2.41 (m, 2H). ESI-MS (m/z): $[M–Cl–H]^+$ calcd. for $C_{10}H_{15}N_2O_2Ru$, 297.0; found, 297.0. X-ray diffraction-quality crystals were grown from a methanol solution at ambient temperature over a period of 2 days.

[Ru(η^6:κ^1-C$_6$H$_5$CH$_2$COO)(en)]$^+$ (20). During the aquation experiments carried out on complex **20Cl** in the presence of AgOTf, intramolecular rearrangement afforded cation **20**, which was characterised in solution state. ^{1}H NMR (400 MHz, D_2O, δ): 6.08 (t, J = 5.9 Hz, Ar H, 2H), 5.63 (d, J = 6.1 Hz, Ar H, 2H), 5.12 (t, J = 5.5 Hz, Ar H, 1H), 3.34 (s, CH_2, 2H), 2.56–2.39 (m, 4H).

[Ru(η^6-C$_6$H$_5$CH$_2$COOH)(*o*-pda)Cl]Cl (35Cl). [Ru(η^6-C$_6$H$_5$CH$_2$COOH)Cl$_2$]$_2$ (60 mg, 0.097 mmol) was suspended in 5 mL of 1:1 water/ethanol. *o*-phenylenediamine (22 mg, 0.195 mmol) was added, and the mixture was stirred for 2 h at ambient temperature. The solvent was reduced to dryness and the remaining solid was redissolved in 2 mL of

ethanol. The resultant yellow solution was filtered through a 0.20 μm syringe filter. The solvent was reduced to ca. 5% of its original volume, and diethyl ether (4 mL) was added. The sticky precipitate was sonicated to give a yellow solid, which was separated by centrifugation, washed with diethyl ether and dried in vacuum. Yield: 49 mg (61%). Elemental analysis: Cald. for $C_{14}H_{16}Cl_2N_2O_2Ru$ (416.26): C, 40.40; H, 3.87; N, 6.73. Found: C, 40.84; H, 3.87; N, 6.50.^{1}H NMR (400 MHz, MeOD-d_4, δ): 7.34–7.31 (m, 2H), 7.26–7.23 (m, 2H), 5.84 (t, J = 5.7 Hz, Ar H, 2H), 5.79 (d, J = 5.7 Hz, Ar H, 2H), 5.74 (t, J = 5.5 Hz, Ar H, 1H), 3.64 (s, CH_2, 2H). ESI-MS (m/z): $[M–Cl–H]^+$ calcd. for $C_{14}H_{15}N_2O_2Ru$, 345.0; found, 345.0.

[Ru(η^6:κ^1-$C_6H_5CH_2COO$)(*o*-pda)]$^+$ (35). During the aquation experiments carried out on complex **35Cl** in the presence of AgOTf, intramolecular rearrangement afforded cation **35**, which was characterised in solution state. ^{1}H NMR (400 MHz, D_2O, δ): 7.36–7.27 (m, Ar H, 4H), 6.23 (t, J = 6.0 Hz, Ar H, 2H), 5.75 (d, J = 6.0 Hz, Ar H, 2H), 5.22 (t, J = 5.6 Hz, Ar H, 1H), 3.77 (s, CH_2, 2H).

[Ru(η^6-$C_6H_5CH_2COOH$)(phen)Cl]Cl (36Cl). $[Ru(\eta^6\text{-}C_6H_5CH_2COOH)Cl_2]_2$ (60 mg, 0.097 mmol) was suspended in ethanol (5 mL). 1,10-Phenanthroline (35 mg, 0.195 mmol) was added, and the mixture was stirred for 2 h at ambient temperature. The solvent was reduced to dryness and redissolved in 2 mL of ethanol. The resultant yellow solution was filtered through a 0.20 μm syringe filter. The solvent was reduced to ca. 5% of its original volume, and diethyl ether (4 mL) was added. The sticky precipitate was sonicated to give a pale yellow solid, which was separated by centrifugation, washed with diethyl ether and dried in vacuum. Yield: 86 mg (91%). Elemental analysis: Cald. for $C_{20}H_{16}Cl_2N_2O_2Ru$ (488.33): C, 49.19; H, 3.30; N, 5.74. Found: C,

49.37; H, 3.28; N, 5.71.^{1}H NMR (400 MHz, MeOD-d_4, δ): 9.86 (dd, J = 5.3, 1.2 Hz, Ar H, 2H), 8.83 (dd, J = 8.2, 1.2 Hz, Ar H, 2H), 8.20 (s, Ar H, 2H), 8.09 (dd, J = 8.2, 5.3 Hz, Ar H, 2H), 6.33 (t, J = 6.1 Hz, Ar H, 2H), 6.25 (d, J = 6.1 Hz, Ar H, 2H), 5.94 (t, J = 5.7 Hz, Ar H, 1H), 3.71 (s, CH_2, 2H). ESI-MS (m/z): $[M–Cl–H]^+$ calcd. for $C_{20}H_{15}N_2O_2Ru$, 417.0; found, 417.0. Crystals suitable for X-ray diffraction were obtained by slow evaporation from a methanol/diethyl ether solution of **36Cl** at ambient temperature.

[Ru(η^6:κ^1-C$_6$H$_5$CH$_2$COO)(phen)]$^+$ (36). During the aquation experiments carried out on complex **36Cl** in the presence of AgOTf, intramolecular rearrangement afforded cation **36**, which was characterised in solution state. ^{1}H NMR (400 MHz, D_2O, δ): 9.76 (d, J = 5.0 Hz, Ar H, 2H), 8.73 (d, J = 8.1 Hz, Ar H, 2H), 8.08 (s, Ar H, 2H), 8.01 (m, Ar H, 2H), 6.55 (t, J = 6.0 Hz, Ar H, 2H), 6.13 (d, J = 6.5 Hz, Ar H, 2H), 5.23 (t, J = 5.5 Hz, Ar H, 1H), 3.75 (s, CH_2, 2H).

[Ru(η^6-C$_6$H$_5$CH$_2$COOH)(oxo)Cl]Na (37Cl). $[Ru(\eta^6\text{-}C_6H_5CH_2COOH)Cl_2]_2$ (60 mg, 0.097 mmol) was suspended in ethanol (5 mL). Sodium oxalate (26 mg, 0.195 mmol) was added, and the mixture was stirred for 2 h at ambient temperature. The solvent was reduced to dryness and redissolved in 2 mL of ethanol. The resultant yellow solution was filtered through a 0.20 µm syringe filter. The solvent was reduced to ca. 5% of its original volume, and diethyl ether (4 mL) was added. The sticky precipitate was sonicated to give an orange solid, which was separated by centrifugation, washed with diethyl ether and dried in vacuum. Yield: 44 mg (57%). Elemental analysis: Cald. for $C_{10}H_{10}Cl_3Na_3O_7Ru$ (518.57): C, 23.16; H, 1.94. Found: C, 24.85; H, 1.89. ^{1}H NMR (400 MHz, MeOD-d_4, δ): 5.83 (t, J = 5.8 Hz, Ar H, 2H), 5.68 (t, 5.6 Hz, Ar H, 1H), 5.61

(d, *J* = 6.1 Hz, Ar H, 2H), 3.60 (s, CH_2, 2H). ESI-MS (m/z): $[M–Cl+H]^+$ calcd. for $C_{10}H_9O_6Ru$, 326.9; found, 326.9. Yellow crystals grown from a warm methanol solution were suitable for X-ray diffraction studies.

$[Ru(\eta^6{:}\kappa^1\text{-}C_6H_5CH_2COO)(oxo)]^-$ (37). During the aquation experiments carried out on complex **37Cl** in the presence of AgOTf, intramolecular rearrangement afforded anion **37**, which was characterised in the solution state. ^{1}H NMR (400 MHz, D_2O, δ): 6.01 (t, *J* = 5.6 Hz, Ar H, 2H), 5.53 (d, *J* = 5.7 Hz, Ar H, 2H), 5.39 (t, *J* = 5.5 Hz, Ar H, 1H), 3.87 (s, CH_2, 2H).

$[Ru(\eta^6{:}\kappa^1\text{-}C_6H_5CH_2COO)(tmen)]Cl$ (38). $[Ru(\eta^6\text{-}C_6H_5CH_2COOH)Cl_2]_2$ (60 mg, 0.097 mmol) was suspended in 5 mL of 1:1 (v/v) water/ethanol. *N,N,N´,N´*-Tetramethylethylenediamine (29 µL, 0.195 mmol) was added, and the mixture was stirred for 1 h at ambient temperature. The solvent was reduced to dryness and redissolved in 2 mL of ethanol. The resultant orange solution was filtered through a 0.20 µm syringe filter. The solvent was reduced to ca. 5% of its original volume, and diethyl ether (4 mL) was added. The sticky precipitate was sonicated to give an orange solid, which was separated by centrifugation, washed with diethyl ether and dried in vacuum. Yield: 70 mg (85%). Elemental analysis: Cald for $C_{14}H_{23}ClN_2O_2Ru$ (387.87): C, 39.63; H, 5.70; N, 6.60. Found: C, 39.40; H, 5.98; N, 6.54. ^{1}H NMR (400 MHz, MeOD-d_4, δ): 6.31 (t, *J* = 6.0 Hz, Ar H, 2H), 5.62 (d, *J* = 6.4 Hz, Ar H, 2H), 5.46 (t, *J* = 5.7 Hz, Ar H, 1H), 3.73 (s, CH_2, 2H), 3.41 (s, $2CH_3$, 6H), 2.71 (s, $2CH_3$, 6H), 2.67–2.60 (m, 2H), 2.40–2.33 (m, 2H). ESI-MS (m/z): $[M]^+$ calcd. for $C_{14}H_{23}N_2O_2Ru$, 353.1; found, 353.1. Complex **38·PF_6** with PF_6^- as counterion was obtained by reaction of complex **38** with an excess of NH_4PF_6 in water. Precipitation of a yellow solid afforded

the desired product. Its ^{1}H NMR spectrum was indistinguishable from that of the starting complex **38**, confirming that the cationic complex remained unaltered.

4.5 References

(1) McCormick, F. B.; Gleason, W. B. The Structure of di-u-chloro-bis[chloro(η6-Hexamethylbenzene)ruthenium(II)]-chloroform (1/2). *Acta Crystallogr. Sect. C* **1988**, *44*, 603-605.

(2) Morris, R. E., et al. Inhibition of Cancer Cell Growth by Ruthenium(II) Arene Complexes. *J. Med. Chem.* **2001**, *44*, 3616-3621.

(3) Betanzos-Lara, S.; Novakova, O.; Deeth, R.; Pizarro, A.; Clarkson, G.; Liskova, B.; Brabec, V.; Sadler, P.; Habtemariam, A. Bipyrimidine Ruthenium(II) Arene Complexes: Structure, Reactivity and Cytotoxicity. *J. Biol. Inorg. Chem.* **2012**, *17*, 1033-1051.

(4) Fernández, R.; Melchart, M.; Habtemariam, A.; Parsons, S.; Sadler, P. J. Use of Chelating Ligands to Tune the Reactive Site of Half-Sandwich Ruthenium(II)–Arene Anticancer Complexes. *Chem. Eur. J.* **2004**, *10*, 5173-5179.

(5) Peacock, A. F. A.; Habtemariam, A.; Fernández, R.; Walland, V.; Fabbiani, F. P. A.; Parsons, S.; Aird, R. E.; Jodrell, D. I.; Sadler, P. J. Tuning the Reactivity of Osmium(II) and Ruthenium(II) Arene Complexes under Physiological Conditions. *J. Am. Chem. Soc.* **2006**, *128*, 1739-1748.

(6) Pizarro, A. M.; Melchart, M.; Habtemariam, A.; Salassa, L.; Fabbiani, F. P. A.; Parsons, S.; Sadler, P. J. Controlling the Reactivity of Ruthenium(II) Arene Complexes by Tether Ring-Opening. *Inorg. Chem.* **2010**, *49*, 3310-3319.

(7) Martínez-Peña, F.; Pizarro, A. M. Control of Reversible Activation Dynamics of [Ru(η6:κ1-C6H5(C6H4)NH2)(XY)]n+ and the Effect of Chelate Ligand Variation. *Chem. Eur. J.* **2017**, 10.1002/chem.201703853.

(8) Stodt, R.; Gencaslan, S.; Müller, Iris M.; Sheldrick, William S. Preparation, Reactivity and Peptide Labelling Properties of (η6-Arene)ruthenium(II) Complexes with Pendant Carboxylate Groups. *Eur. J. Inorg. Chem.* **2003**, *2003*, 1873-1882.

(9) Melchart, M.; Habtemariam, A.; Novakova, O.; Moggach, S. A.; Fabbiani, F. P. A.; Parsons, S.; Brabec, V.; Sadler, P. J. Bifunctional Amine-Tethered Ruthenium(II) Arene Complexes Form Monofunctional Adducts on DNA. *Inorg. Chem.* **2007**, *46*, 8950-8962.

(10) Miyaki, Y.; Onishi, T.; Kurosawa, H. Synthesis and Reaction of Ruthenium(II) Complexes Containing Heteroatom Donor (O, N, and P) Tethered to η6-Arene Ring. *Inorg. Chim. Acta* **2000**, *300–302*, 369-377.

(11) Aird, R. E.; Cummings, J.; Ritchie, A. A.; Muir, M.; Morris, R. E.; Chen, H.; Sadler, P. J.; Jodrell, D. I. In Vitro and In Vivo Activity and Cross Resistance Profiles of Novel Ruthenium(II) Organometallic Arene Complexes in Human Ovarian Cancer. *Br. J. Cancer* **2002**, *86*, 1652.

(12) Dougan, S. J.; Melchart, M.; Habtemariam, A.; Parsons, S.; Sadler, P. J. Phenylazo-pyridine and Phenylazo-pyrazole Chlorido Ruthenium(II) Arene

Complexes: Arene Loss, Aquation, and Cancer Cell Cytotoxicity. *Inorg. Chem.* **2006**, *45*, 10882-10894.

(13) Betanzos-Lara, S.; Liu, Z.; Habtemariam, A.; Pizarro, A. M.; Qamar, B.; Sadler, P. J. Organometallic Ruthenium and Iridium Transfer-Hydrogenation Catalysts Using Coenzyme NADH as a Cofactor. *Angew. Chem. Int. Ed.* **2012**, *51*, 3897-3900.

(14) Soldevila-Barreda, J. J.; Romero-Canelón, I.; Habtemariam, A.; Sadler, P. J. Transfer hydrogenation catalysis in cells as a new approach to anticancer drug design. *Nat. Commun.* **2015**, *6*, 6582.

(15) Canivet, J.; Süss-Fink, G.; Štěpnička, P. Water-Soluble Phenanthroline Complexes of Rhodium, Iridium and Ruthenium for the Regeneration of NADH in the Enzymatic Reduction of Ketones. *Eur. J. Inorg. Chem.* **2007**, *2007*, 4736-4742.

(16) Yan, Y. K.; Melchart, M.; Habtemariam, A.; Peacock, A. F. A.; Sadler, P. J. Catalysis of Regioselective Reduction of NAD+ by Ruthenium(II) Arene Complexes Under Biologically Relevant Conditions. *J. Biol. Inorg. Chem.* **2006**, *11*, 483-488.

(17) Betanzos-Lara, S.; Habtemariam, A.; Sadler, P. J. Transfer Hydrogenation Reactions of Photoactivatable N,N'-Chelated Ruthenium(II) Arene Complexes. *J. Mex. Chem. Soc.* **2013**, *57*, 160-168.

(18) Koike, T.; Ikariya, T. Mechanistic Aspects of Formation of Chiral Ruthenium Hydride Complexes from 16-Electron Ruthenium Amide Complexes and Formic Acid: Facile Reversible Decarboxylation and Carboxylation. *Adv. Synth. Catal.* **2004**, *346*, 37-41.

(19) Soldevila-Barreda, J. J.; Bruijnincx, P. C. A.; Habtemariam, A.; Clarkson, G. J.; Deeth, R. J.; Sadler, P. J. Improved Catalytic Activity of Ruthenium–Arene Complexes in the Reduction of NAD+. *Organometallics* **2012**, *31*, 5958-5967.

(20) Bruker. *APEX2,SAINT and SADABS*; Bruker AXS: Madison, WI, 2008.

(21) Bruker. *SHELXTL Version 6.10, Structure Determination Package*; Bruker AXS: Madison, WI, 2000.

(22) Sheldrick, G. M. A Short History of SHELX. *Acta Crystallogr. Sect. A* **2008**, *64*, 112-122.

(23) Sheldrick, G. M. Crystal Structure Refinement with SHELXL. *Acta Crystallogr. Sect. C* **2015**, *71*, 3-8.

(24) Vichai, V.; Kirtikara, K. Sulforhodamine B Colorimetric Assay for Cytotoxicity Screening. *Nat. Protoc.* **2006**, *1*, 1112-1116.

5.

Contrasting activation behaviour of tethered versus un-tethered Ru^{II} arene complexes by pH and light irradiation

5.1 Introduction

In previous chapters, we have discussed the advantages of tethering the monodentate ligand (Z) to the Ru–arene structure. This appears to provide an attractive strategy to create not only pH-dependent complexes but also switchable compounds that turn-on and -off in a reversible manner. In fact, in Chapters 3 and 4 we have demonstrated the reversible activation of the Ru–Z bond in closed tethered complexes of formula $[Ru\{\eta^6{:}\kappa^1\text{-}C_6H_5(C_6H_4)NH_2\}(XY)]^{n+}$ and $[Ru(\eta^6{:}\kappa^1\text{-}C_6H_5CH_2COO)(XY)]^{+}$ under acidic conditions (proton concentration dependent), where the activation dynamics could be modulated by rational variation of both the XY chelating ligand and the hemilabile ligand.

Photochemical metal-ligand bond activation is an attractive approach for achieving the selective bond cleavage by the absorption of light, promoting the release of the leaving group and offering the possibility of controlling the location and timing activity of the metal complex.[1] This requires breaking of the coordination bond by the use of high-energy UV-visible light photons. In addition, light is already used to treat certain cancers by means of the Food and Drug Administration-approved technique of photodynamic therapy (PDT).[2] Some examples of half-sandwich Ru^{II} arene complexes, $[Ru(\eta^6\text{-}p\text{-cym})(N,N')(Z)]^{2+}$ (where N,N' = bidentate chelated ligand, and Z = pyridine or a pyridine derivate) have been proved to be activated by UV-visible light to photo-dissociate selectively the monodentate ligand (Z) in aqueous solution and in the presence of a nucleobase (9-ethylguanine or 9-ethyladenine).[3]

With the aim of searching how structural features related to the tether ring can influence the stability and activation of these Ru^{II} arene complexes, in this Chapter we present the synthesis, spectroscopic data, activation studies at different pH values, and photochemical behaviour of two families of ruthenium(II) complexes containing

ethylenediamine (en) as chelating ligand: tethered Ru^{II} complexes of general formula $[Ru(\eta^6{:}\kappa^1\text{-arene:N})(en)]^{2+}$, with 2-phenylethylamine, 2-benzylpyridine and 2-aminobiphenyl as the arene:N ligand; and two of the corresponding un-tethered analogues with structure $[Ru(\eta^6\text{-bz})(en)(L)]^{2+}$ where bz = benzene and L = 2-picoline or aniline. Additionally, DFT calculations performed by Prof. Luca Salassa (Donostia International Physics Center) have been employed to gain a deeper understanding on the light-mediated activation of such complexes.

5.2 Results and Discussion

5.2.2 Synthesis and Characterization

Five ruthenium(II) arene complexes were prepared in good yields (Figure 5.1). Closed-tether complexes **7·PF$_6$**, **9·PF$_6$** and **13·PF$_6$** (as hexafluorophosphate salts of the corresponding cationic complexes **7**, **9** and **13**, respectively) were synthesised according to previously reported methods,[4, 5] using the benzoate dimer, [Ru(η^6-etb)Cl$_2$]$_2$, as a precursor. As discussed in the previous Chapters, the hemilabile ligand (2-phenylethylamine, 2-benzylpyridine or 2-aminobiphenyl) was added to a dichloroethane solution of [Ru(η^6-etb)Cl$_2$]$_2$ and the reaction mixture was stirred at ambient temperature. The solution was then heated at 120 ºC and arene thermal displacement occurred to afford the precursor complexes of general formula [Ru(η^6:κ^1-arene:N)Cl$_2$] in good yields over short periods of time (4–18 h). Subsequent reaction of the corresponding dichlorido complex with ethylenediamine (en) in methanol afforded complexes **7·PF$_6$**, **9·PF$_6$** and **13·PF$_6$**.

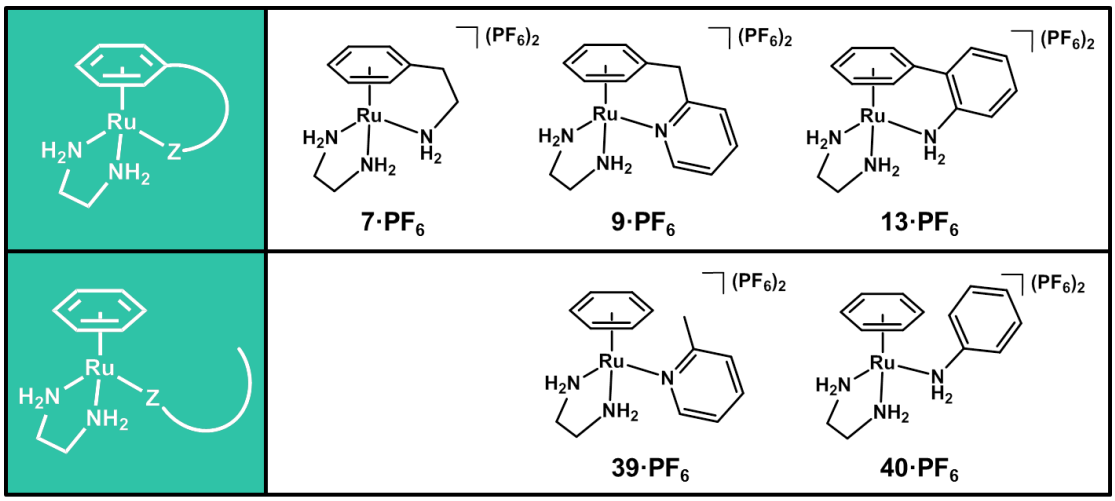

Figure 5.1. Structure of the complexes studied in this Chapter. Complexes **7·PF$_6$**, **9·PF$_6$** and **13·PF$_6$** are closed-tether complexes. Complexes **39·PF$_6$** and **40·PF$_6$** are the un-tethered versions of **9·PF$_6$** and **13·PF$_6$**, respectively.

The ^{1}H NMR spectra of closed tether complexes **7·PF$_6$**, **9·PF$_6$** and **13·PF$_6$** in D_2O at 298 K confirmed η^6-coordination of the corresponding arene ligand to the metal by the observation of a typical NMR pattern of the η^6-bound arene resonances containing three characteristic peaks (triplet:doublet:triplet in a ratio 2:2:1), which are upfield-shifted (ca. 1.8 ppm) in all cases in comparison to those of the free ligands.

The large distance between the most deshielded and most shielded η^6-bound arene signals (ca. 0.8 ppm) demonstrated coordination of the tethering nitrogen to the metal centre (closed-tether complex), as described in previous Chapters.[4] The X-ray crystal structures of complexes **7** (complex **7** with Cl^- as counterion instead of PF_6^-) and **9·PF$_6$** unequivocally verified the structure of these complexes. The crystal structure of complex **13** was discussed in depth in Chapter 3.[4, 5]

Dimer $[Ru(\eta^6\text{-bz})Cl_2]_2$ was synthesised following the reported synthesis by Heim et al.[6] The synthetic route of complexes **39·PF$_6$** and **40·PF$_6$** involved the reaction of the benzene dimer $[Ru(\eta^6\text{-bz})Cl_2]_2$ with ethylenediamine (en) in methanol to afford complex $[Ru(\eta^6\text{-bz})(en)Cl]Cl$. Following a published procedure,[3] reaction of the latter with $AgPF_6$ in methanol, and in the presence of an excess of the appropriate ligand 2-picoline (pic) or phenylamine (pha), led to the corresponding complexes $[Ru(\eta^6\text{-bz})(en)(pic/pha)](PF_6)_2$ (**39·PF$_6$** /**40·PF$_6$**).

The details for individual reactions are described in the Experimental Section. All complexes were characterised by elemental analysis, ^{1}H NMR spectroscopy and LC/MS spectroscopy.

5.2.3 X-Ray Crystallography and Density Functional Theory Modelling

The molecular and crystalline structures of compounds **7** and **9·PF$_6$** were determined by single crystal X-ray diffraction. The new structures along with their atom numbering schemes are shown in Figure 5.2.

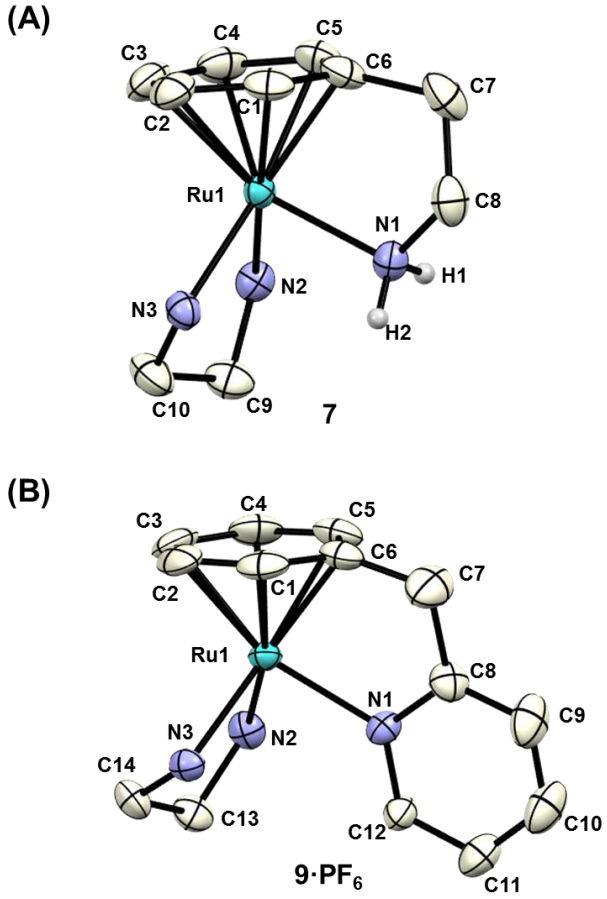

Figure 5.2. ORTEP diagrams and atom numbering schemes for (A) [Ru{η^6:κ^1-$C_6H_5(CH_2)_2NH_2$}(en)]Cl_2 (**7**) and (B) [Ru{η^6:κ^1-$C_6H_5(CH_2)C_5H_4N$}(en)]$(PF_6)_2$ (**9·PF$_6$**). The hydrogen atoms (with the exception of the NH_2-tether protons in **7**), counterions and solvent molecules have been omitted for clarity.

The complexes adopted the typical "piano stool" geometry of ruthenium(II) arene structures.[4, 7, 8] The arene rings displayed the common π-bonded η^6-coordination mode, whereas the ethylenediamine ligand adopted a bidentate-chelate coordination mode, occupying two coordination positions. The remaining site in the coordination sphere was occupied by the nitrogen atom pendant from the tethered arene. The chloride counterions in **7** was extensively involved in H-bonding with the NH_2(tether) hydrogens

(N–H···Cl distances 2.310–2.406 Å) and to the hydrogens of the NH_2(ethylenediamine) ligand (N–H···Cl distances in the range 2.325–2.433 Å). No H-bonding or π-π stacking interactions were presented in the crystal structure of **9·PF$_6$**. Selected bond lengths and angles are given in Table 5.1. This table includes reported X-ray data of complex **13**[5] for comparison purposes. Relevant crystallographic parameters are listed in the Appendix II.

Table 5.1. Selected bond lengths (Å) and angles (deg) for complexes **7**, **9·PF$_6$** and **13**.

Bond / angle	7	9·PF$_6$	13[5]
Ru–C6	2.125(2)	2.117(5)	2.115(13)
Ru–C5	2.175(2)	2.182(5)	2.184(13)
Ru–C4	2.186(2)	2.176(4)	2.207(14)
Ru–C3	2.203(2)	2.195(5)	2.221(15)
Ru–C2	2.183(2)	2.175(5)	2.198(13)
Ru–C1	2.176(2)	2.163(5)	2.191(13)
Ru–centroid	1.651	1.636	1.659
Ru–N1	2.1269(17)	2.121(4)	2.144(11)
Ru–N2	2.1238(17)	2.143(3)	2.148(11)
Ru–N3	2.1258(19)	2.116(3)	2.161(11)
N2-Ru-N3	79.85(7)	78.83(13)	80.4(4)
N2-Ru-N1	89.87(6)	91.65(13)	88.2(4)
N3-Ru-N1	86.63(7)	90.19(14)	88.0(4)
Propeller twist	82.91	89.93	89.7
Ru-C6-C7	114.49	114.44	112.99
Offset C7[a]	0.444(+)	0.436(+)	0.488 (+)
Sigma	1.78	5.95	0.75

[a] Offset of C7 with respect to the plane formed by the bound arene (carbons C1–C6); (+) toward ruthenium

All complexes crystallized with four independent molecules in the unit cell. The Ru–C(arene) bond lengths were in the range of 2.113(2)–2.206(2) Å. The Ru–centroid distances for the different complexes fell into a narrow interval (1.636–1.654 Å) and were similar to reported tethered complexes, such as [Ru{η^6:κ^1-$C_6H_5(CH_2)_2NH_2$}Cl_2],[9] [Ru{η^6:κ^1-$C_6Me_5(CH_2)C_5H_4N$}Cl_2][10] and [Ru{η^6:κ^1-$C_6H_5(C_6H_4)NH_2$}(dach)]Cl_2,[4] with distances 1.631, 1.656, and 1.641 Å, for comparison with complex **7**, **9·PF$_6$** and **13·PF$_6$**, respectively. The Ru–N(en) distances were in the range 2.116(3)–2.1368(17) Å, and the

Ru–N1(tether) distances varied from 2.121(4) to 2.1481(17) Å, also comparable to reported analogues.

No major differences were observed between the structures of complexes **7**, **9·PF$_6$** and **13**. However, a smaller Ru-C6-C7 angle was observed in **13** versus **7** and **9·PF$_6$** (112.9 vs ca. 114.5º). The Ru-C6-C7 angle, where C6 is the arene carbon connected to the tether and C7 is the first carbon atom in the tether arm, is an important parameter which correlates with the strain imposed on the tether ring by the 5-member tether ring. It is interesting to note that while the non-strained Ru-C6-C7 angle lies around 130º,[5, 11] for complexes **7**, **9·PF$_6$** and **13** such an angle is significantly smaller (112.9–114.5º). This suggests that complex **13**, with the smallest angle 112.9º, bears the highest strain of the series. Further evidence of the ring strain in the three closed-tether complexes can be observed by the offset of C7 with respect to the plane containing the bound arene, ranging 0.436–0.488 Å toward ruthenium (with again the longest offset for **13**, 0.488 Å), as well as by the tilt of the η^6-bound arene, whereby the Ru–C3 distance was consistently longer than the Ru–C6 one throughout the series.

Table 5.2 lists relevant bond lengths and structural parameters obtained for cations **7**, **9** and **13** using Density Functional Theory (DFT) calculations at the LC-WPBE/SDD/6-31G** level. This method was selected after benchmarking the performance of five functional and five basis sets combinations against the X-ray structure of **9·PF$_6$** (Appendix III, Section A). We found a good agreement between the computed and X-ray structures with differences in bond lengths smaller than 0.03 Å. The LC-WPBE/SDD/6-31G** method was used for additional computational studies aimed at elucidating the photochemical behaviour of **7**, **9** and **13** (vide infra).

Table 5.2. Calculated bond lengths (Å) and angles (deg) for complexes **7, 9 and 13** (ground state) using DFT at the LC-WPBE_SDD/6-31G** level.

Bond / angle	7	9	13
Ru–centroid	1.654	1.650	1.653
Ru–N1	2.145	2.157	2.133
Ru–N2	2.131	2.132	2.114
Ru–N3	2.128	2.128	2.143
N2-Ru-N3	79.48	79.44	78.91
N2-Ru-N1	89.86	89.51	89.31
N3-Ru-N1	88.20	88.74	93.82
Propeller twist	74.42	88.11	79.22

5.2.4 Aqueous Solution Chemistry of Non-Irradiated Ru^{II} Complexes

5.2.4.1 Activation at Neutral pH

We investigated how structural features (tethered versus un-tethered) influence the stability and activation profile of the Ru–N(tether) bond of Ru^{II} complexes.

The aqueous solution chemistry of the complexes was studied by means of ^{1}H NMR spectroscopy of the corresponding aqueous solutions (6 mM) at 298 K over 24 h at pH 7 (Figure 5.3). The spectra of complexes **7·PF_6**, **9·PF_6** and **13·PF_6** initially contained one major set of peaks corresponding to cations $[Ru\{\eta^6{:}\kappa^1\text{-}C_6H_5(CH_2)_2NH_2\}(en)]^{2+}$, $[Ru\{\eta^6{:}\kappa^1\text{-}C_6H_5(CH_2)C_5H_4N\}(en)]^{2+}$ and $[Ru\{\eta^6{:}\kappa^1\text{-}C_6H_5(C_6H_4)NH_2\}(en)]^{2+}$, respectively. No changes were observed over 24 h, therefore no activation of the Ru–Z bond at this pH was observed (Figure 5.3A). The lack of changes in the ^{1}H NMR also demonstrates the high stability of this type of compounds against hemilabile ligand loss under these conditions, contrary to analogous ruthenium(II) complexes,[12] such as complex $[Ru\{\eta^6{:}\kappa^1\text{-}C_6H_5(CH_2)_2NH_2\}Cl_2]$ that was reported to decompose in approximately 20% after 40 min in solution.

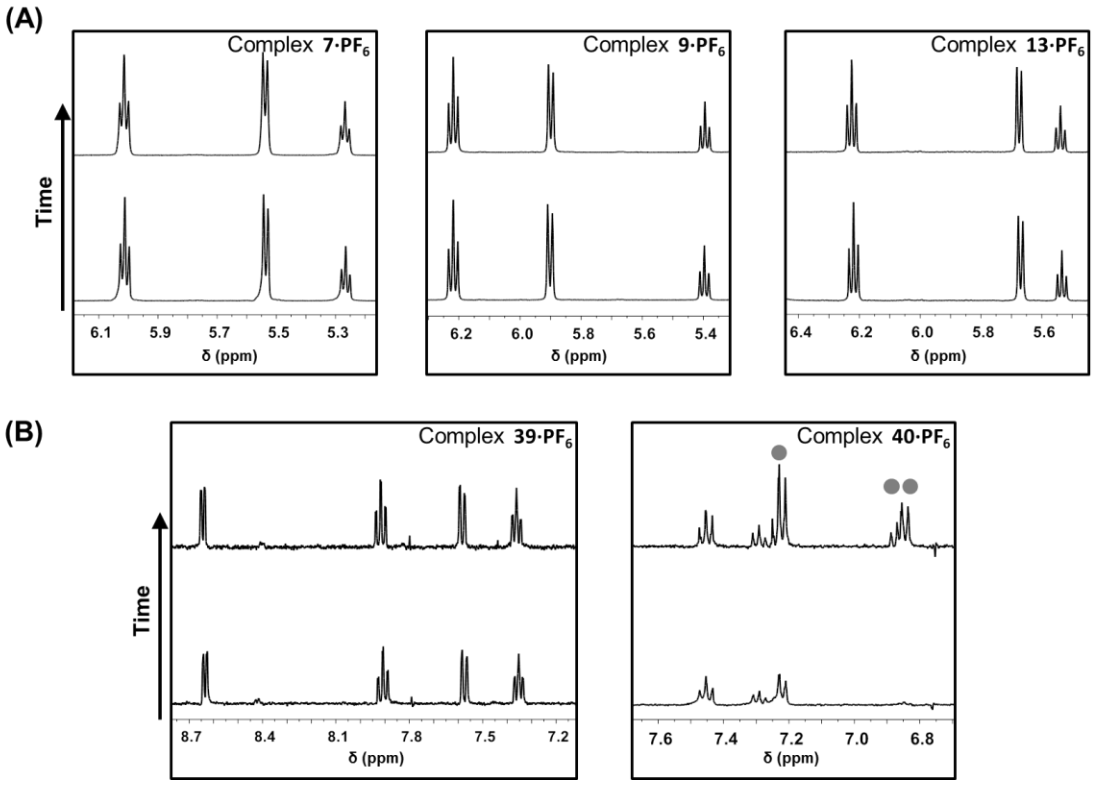

Figure 5.3. ^{1}H NMR at t=15 min (bottom) and t=24 h (up) of (A) complexes **7·PF$_6$**, **9·PF$_6$** and **13·PF$_6$**, and (B) complexes **39·PF$_6$** and **40·PF$_6$**; at pH 7 at 298 K. In (A) we show the NMR region corresponding to the η^6-bound arene protons; while in (B) the NMR area corresponds to the bound/free aniline (for complex **39·PF$_6$**) and 2-picoline (for complex **40·PF$_6$**). Only complex **40·PF$_6$** (bottom right) shows loss of monodentate ligand aniline (grey dots) over time.

We also studied complexes **39·PF$_6$** and **40·PF$_6$** in aqueous solution by ^{1}H NMR at 298 K (Figure 5.3B). Complex **39·PF$_6$**, $[Ru(\eta^6\text{-bz})(en)(pic)]^{2+}$, showed high stability over time towards aquation, comparable to its analogue closed-tether complex **9·PF$_6$**. Similar stability of related complexes containing pyridine derivatives, such as $[Ru(\eta^6\text{-}p\text{-cymene})(2,2'\text{-bipyrimidine})(py)]^{2+}$, has been described in aqueous solution.[13] Aquation of the Ru–Z bond was only observed for complex **40·PF$_6$**, and monodentate ligand aniline was released to afford the corresponding aqua complex $[Ru(\eta^6\text{-bz})(en)OH_2]^{2+}$ (52% of aqua adduct was formed over 24 h). Reactivity toward aquation in complexes **13·PF$_6$** vs **40·PF$_6$** supports the stability induced by tethering the monodentate ligand to the arene.

5.2.4.2 Activation at Acidic pH

Acidic activation of the Ru–N(tether) bond was investigated at pH 0 over 24 h. Complexes **7·PF$_6$**, **9·PF$_6$** and **13·PF$_6$** were dissolved in D_2O, the pH of their solutions was adjusted to 0. The ^{1}H NMR spectra were recorded at 298 K immediately after pH adjustment (ca. 15 min) and after 24 h. Figure 5.4 shows the different extents of complex activation (percentage of open-tether versus closed-tether ring) as determined by integration of the meta proton of the η^6-bound arene in the NMR spectra of both species.

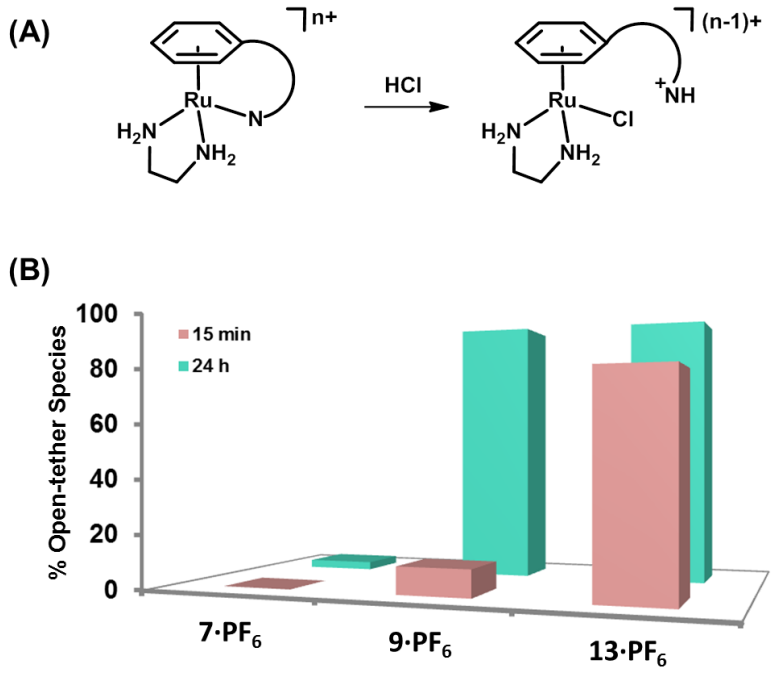

Figure 5.4. (A) Activation (tether-ring opening) of the Ru–N(tether) bond in complexes **7·PF$_6$**, **9·PF$_6$** and **13·PF$_6$** upon acidification. (B) Percentage of conversion of closed-tether to open-tether species at 15 min and 24 h at 298 K in water at pH 0.

The resultant activated species were characterised as protonated open-tether species, of formula $[Ru(\eta^6\text{-arene:}NH_3)(en)Cl]^{2+}$.[4] After 15 min of acidification, the extent of activated (protonated open-tether) species followed the trend **13·PF$_6$** > **9·PF$_6$** >> **7·PF$_6$** (79, 10, 0%, respectively). However, when the equilibrium was reached at 24 h both complexes had fully converted to their activated counterparts, [Ru{η^6-

$C_6H_5(CH_2)C_5H_4NH\}(en)Cl]^{2+}$ and $[Ru\{\eta^6\text{-}C_6H_5(C_6H_4)NH_3\}(en)Cl]^{2+}$, and only 3% of the activated complex, $[Ru\{\eta^6\text{-}C_6H_5(CH_2)_2NH_3\}(en)Cl]^{2+}$, was observed for **7·PF$_6$**. The total conversion of closed tethered species into the protonated open tether Ru^{II} for complexes **9·PF$_6$** and **13·PF$_6$** led to determine the half-life time for the ring opening reaction by monitoring 0.2 mM solutions of the Ru^{II} complexes over 24 h by UV-visible spectroscopy (Figure 5.5). Data were fitted to a pseudo-first-order kinetic equation which yielded a half-life value of 208 min for **9·PF$_6$** (44 min for complex **13** as determined in Chapter 3). The data revealed that activation (ring opening) of the Ru^{II} complex **13·PF$_6$** is much faster at acidic pH.

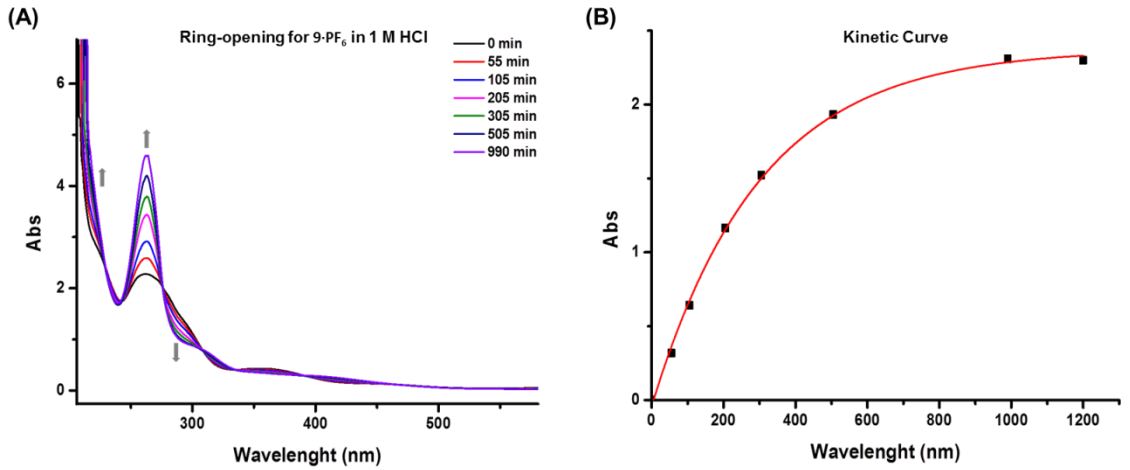

Figure 5.5. (A) UV-visible spectra showing that the largest change in absorbance occurs at 263 nm. (B) Change in absorbance at 263 nm over 20 h during the opening of complex **9·PF$_6$**, from which the kinetic data ($t_{1/2}$ = 208 min) was determined.

According to the results we can highlight the importance of two features affecting the ring-opening process: i) the nature of the donor tether atom, and ii) the ring structural constrain, including flexibility along the tethering arm. Total activation of complexes **13·PF$_6$** and **9·PF$_6$** (aromatic amine) versus poor activation of **7·PF$_6$** (aliphatic amine) may be indicative of the importance of the hybridization on the tethering nitrogen (sp^3 in **7·PF$_6$**, sp^2 in **9·PF$_6$**, and between sp^2 and sp^3, in **13·PF$_6$**),[14] which subsequently affects the basicity of the resulting amine derivative (**7·PF$_6$** being the most basic of the

series). Additionally, the tether arm in **9·PF$_6$** and **13·PF$_6$** is less flexible than that of complex **7·PF$_6$**, supporting that rigidity of the tether chain plays an important role in promoting the activation of the Ru–Z bond. Consistently, the significant difference on the activation rate in **9·PF$_6$** and **13·PF$_6$** (10 vs 79% after 15 min, respectively) and the half-lives values (208 vs 44 min, respectively) correlate with a higher ring constrain imposed by a sp^2-hybridization on the C7 atom in complex **13·PF$_6$** versus a more flexible tether ring by the sp^3-hybridization on C7 in complex **9·PF$_6$**.

5.2.5 Aqueous Solution Chemistry of Light Irradiated Ru^{II} Complexes

5.2.5.1 Activation at Neutral pH

Given the extraordinary stability of the Ru–Z bond at neutral pH, we explored the possibility of using light to photo-trigger Ru–Z bond activation for complexes **7·PF$_6$**, **9·PF$_6$** and **13·PF$_6$**. Additionally, we compared such activation to complexes **39·PF$_6$** and **40·PF$_6$** (un-tethered analogues of **9·PF$_6$** and **13·PF$_6$**, respectively), in order to identify the importance of the tether chelate in the light-mediated process. Solutions of 0.4 mM of freshly dissolved complexes in D_2O at 298 K were prepared. The pH of the solutions varied within the range 6.5–7.1. The activation dynamics under light irradiation were explored by means of UV-visible and ^{1}H NMR spectroscopy.

Before irradiation all complexes displayed transitions in the visible region assignable to MLCT (metal-ligand charge transfer) from the filled 4d orbitals of Ru^{II} to the empty π^* ligand orbitals ($4d^6$ Ru$\rightarrow \pi^*$). TD-DFT calculations of singlet-singlet transitions are in qualitative agreement with this assignment although they fail to predict the lowest-energy transitions responsible for the absorption bands at > 425 nm (Figure 5.6 and Appendix III, Section B).

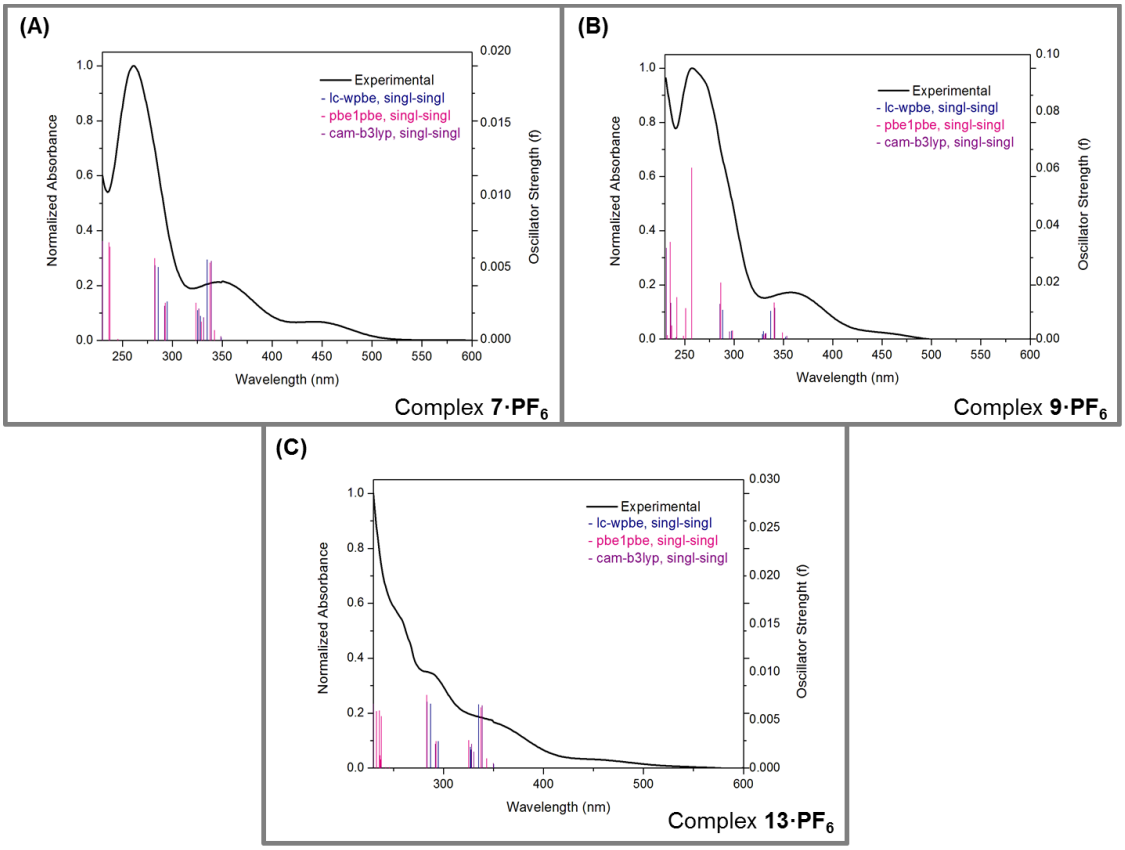

Figure 5.6. Comparison between DFT functionals for the TD-DFT calculation of the singlet-singlet transitions of complexes **7·PF$_6$**, **9·PF$_6$** and **13·PF$_6$** (A–C) and their theoretical UV-visible absorption spectra. Calculated singlet-singlet electronic transitions are shown as vertical bars with heights equal to their oscillator strength. Normalized experimental spectra for the complexes are depicted with a black line.

Upon irradiation changes appeared in the electronic absorption spectra for all complexes. When complex **7·PF$_6$** was irradiated for 53 min overall (see irradiation protocol in the Experimental Section), the spectra showed an increase of the absorption features at 200–230 nm and 292 nm, Figure 5.7A. The free ligand 2-phenylethylamine shows a strong absorption bands at 258 nm (Figure 5.7B), which is not observed upon irradiation of **7·PF$_6$**. When the effects of irradiation on the solution were checked by ^{1}H NMR, no changes were observed in the spectrum.

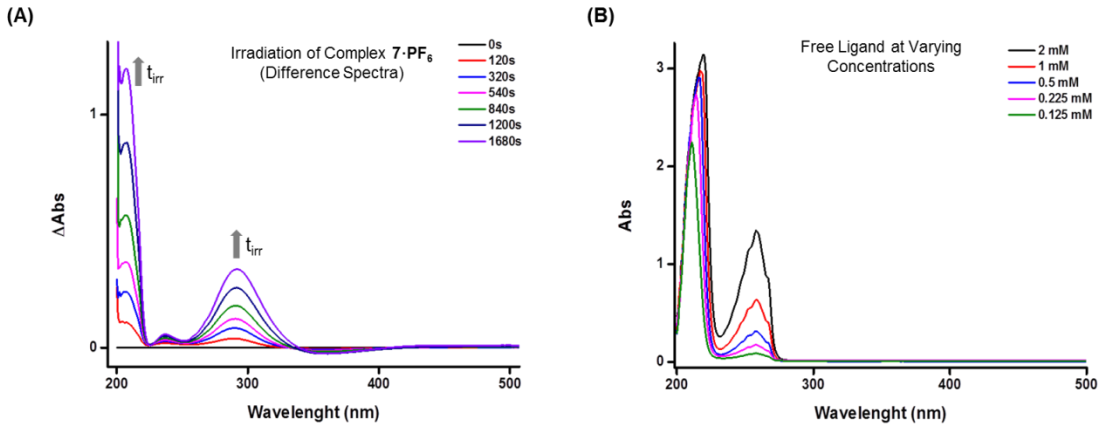

Figure 5.7. (A) Corresponding UV-visible difference spectra showing increase of the bands at < 240 and 292 nm of a solution of complex **7·PF$_6$** (0.4 mM) in D_2O upon irradiation at 365 nm at pH 7. (B) UV-visible spectra of the hemilabile ligand 2-phenylethylamine recorded at different concentrations. It presents a strong absorption band at 258 nm.

The electronic absorption spectrum in aqueous solution of **9·PF$_6$** exhibited an increase in intensity of the bands at 210–240 nm and 333 nm, and a decrease at 270 nm, as indicated in Figure 5.8A, when the solution was irradiated at 365 nm (36 min overall light exposure). The free ligand 2-benzylpyridine shows a strong absorption bands at 263 nm. This is not observed upon irradiation of **9·PF$_6$**. The changes were also followed by ^{1}H NMR (Figure 5.8B). The spectra showed a number of new peaks of small intensity, which we could not assign to any known species. Some of the signals seem to appear in the π-bound ligand-to-metal arene region. We could not assign any of these signals to free 2-benzylpyridine. When a new ^{1}H NMR spectrum was acquired after leaving the sample in the dark overnight, total disappearance of these peaks was observed. Additionally, peaks corresponding to the free tether ligand (2-benzylpyridine) appeared accounting for about a ca. 30% of hemilabile ligand loss.

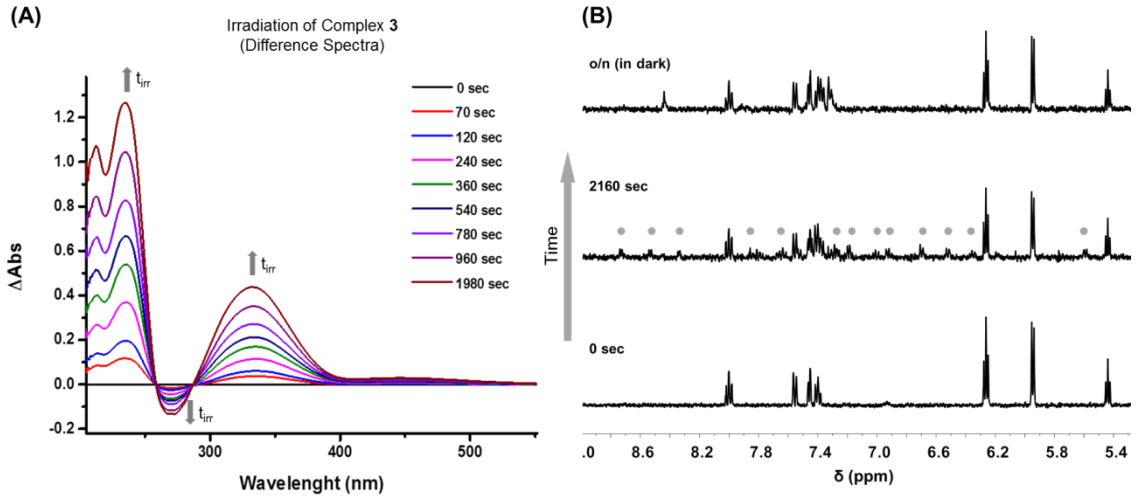

Figure 5.8. (A) UV-visible difference spectra showing increase of the bands at 210–240 and 333 nm, and a decrease at 270 nm, of a solution of complex **9·PF$_6$** (0.4 mM) in D_2O upon irradiation at 365 nm at pH 7. (B) ^{1}H NMR spectra recorded at different stages of photoirradiation at 365 nm of the aqueous solution of **9·PF$_6$** at 298 K. After irradiation (2160 sec), appearance of (a) new species (●) could be observed.

When the aqueous solution of **13·PF$_6$** was photo-irradiated at different time intervals (40 min overall) at 365 nm, the electronic absorption spectra presented some changes (Figure 5.9A). Bands at 220–230 nm and 283 nm showed a high increase with time-irradiation evolution. The UV-visible spectra of the free ligand 2-aminobiphenyl presented similar bands at 224 and 283 nm (Figure 5.9B). The release of the hemilabile ligand (2-aminobiphenyl) was confirmed following different stages of photo-irradiation at 365 nm by ^{1}H NMR (Figure 5.10). Upon 27 min of irradiation 35% of initial complex **13·PF$_6$** had lost its tether ligand.

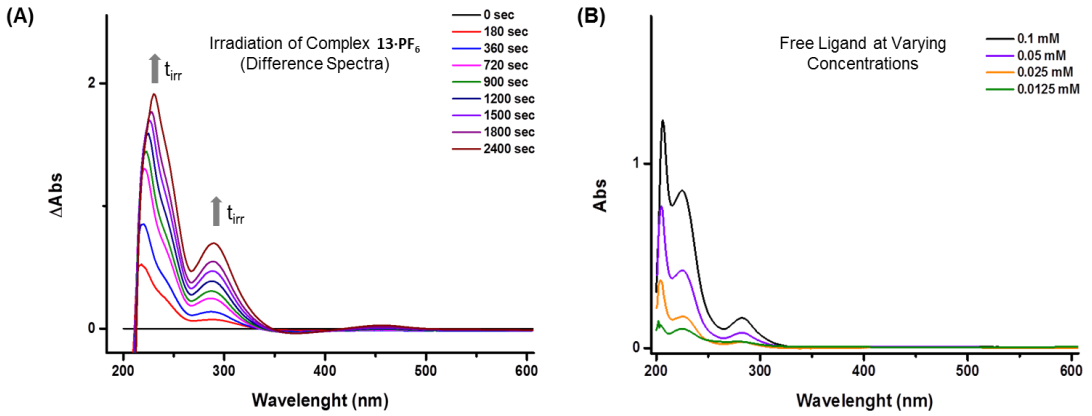

Figure 5.9. (A) Corresponding UV-visible difference spectra of a solution of complex **13·PF$_6$** (0.4 mM) in D_2O upon irradiation at 365 nm at pH 7 showing increase of the bands at 220–230 and 283 nm. (B) UV-visible spectra of the hemilabile ligand 2-aminobiphenyl recorded at different concentrations. It presents bands at 224 and 283 nm.

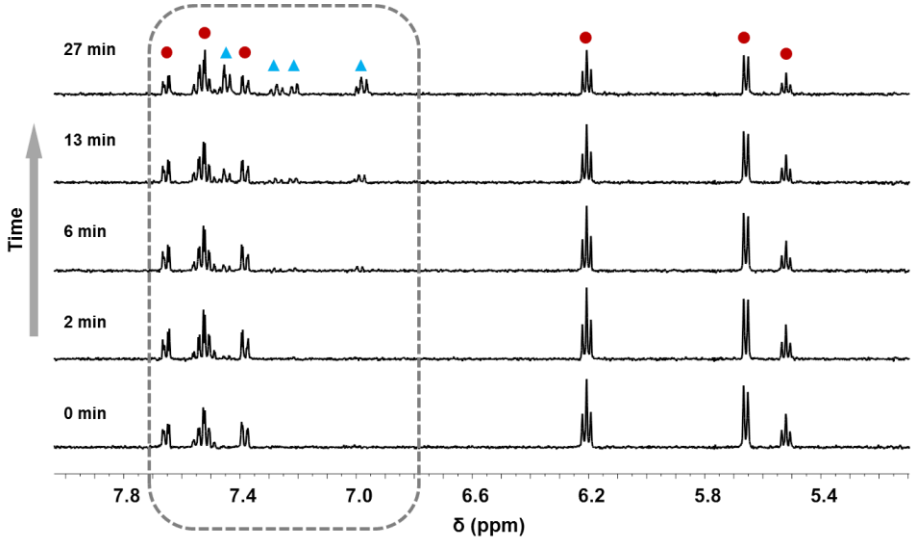

Figure 5.10. ^{1}H NMR spectra recorded during the photoirradiation protocol at 365 nm of an aqueous solution of **13·PF$_6$** at 298 K: (●) [Ru{η^6:κ^1-$C_6H_5(C_6H_4)NH_2$}(en)]$^{2+}$, (▲) free hemilabile tether ligand (2-aminobiphenyl).

Results obtained from irradiation of complex **7·PF$_6$** are in accordance with the acidic activation experiments concluding that this type of tethered Ru–arene complex bearing an aliphatic amine is the most stable of this series of compounds. Irradiation experiments performed for complex **9·PF$_6$** suggest formation of new ruthenium(II)

meta-stable π-bonded arene species which appear to reverse to **9·PF$_6$** with time and/or afford the free ligand, once the irradiation has stopped. On the other hand, complex **13·PF$_6$** appears to not only activate the Ru–Z ligand but also the Ru–arene bonding, resulting in the loss the hemilabile ligand, perhaps affording in situ the corresponding aqua adduct $[Ru(en)(OH_2)_4]^{2+}$.[15] As observed for (non-irradiated) acidic activation at pH 0, complex **13·PF$_6$** seems more reactive than **9·PF$_6$** upon irradiation.

Next, we also compared the photochemistry of complex **9·PF$_6$** with its analogous un-tethered complex **39·PF$_6$**. A solution of **39·PF$_6$** was irradiated for 52 min at 365 nm. The UV-visible spectra revealed an increase of the band at 298 nm and a decrease in bands at 210–220 and 269 nm (Figure 5.11A). ^{1}H NMR spectra was recorded after irradiation (Figure 5.11B), showing three sets of benzene signals corresponding to complex **39·PF$_6$** (80%), the aqua complex $[Ru(\eta^6\text{-benzene})(en)(H_2O)]^{2+}$ (17%; identified by the singlet at ca. 5.9 ppm), and free benzene (arene loss identified by the appearance of a singlet at 7.4 ppm; 3%). In comparison to its non-irradiated analogue experiment, the aquation process occurred only upon irradiation (it did not aquate in the dark). This finding shows that irradiation of complex **39·PF$_6$** results in a Ru–Z bond activation.

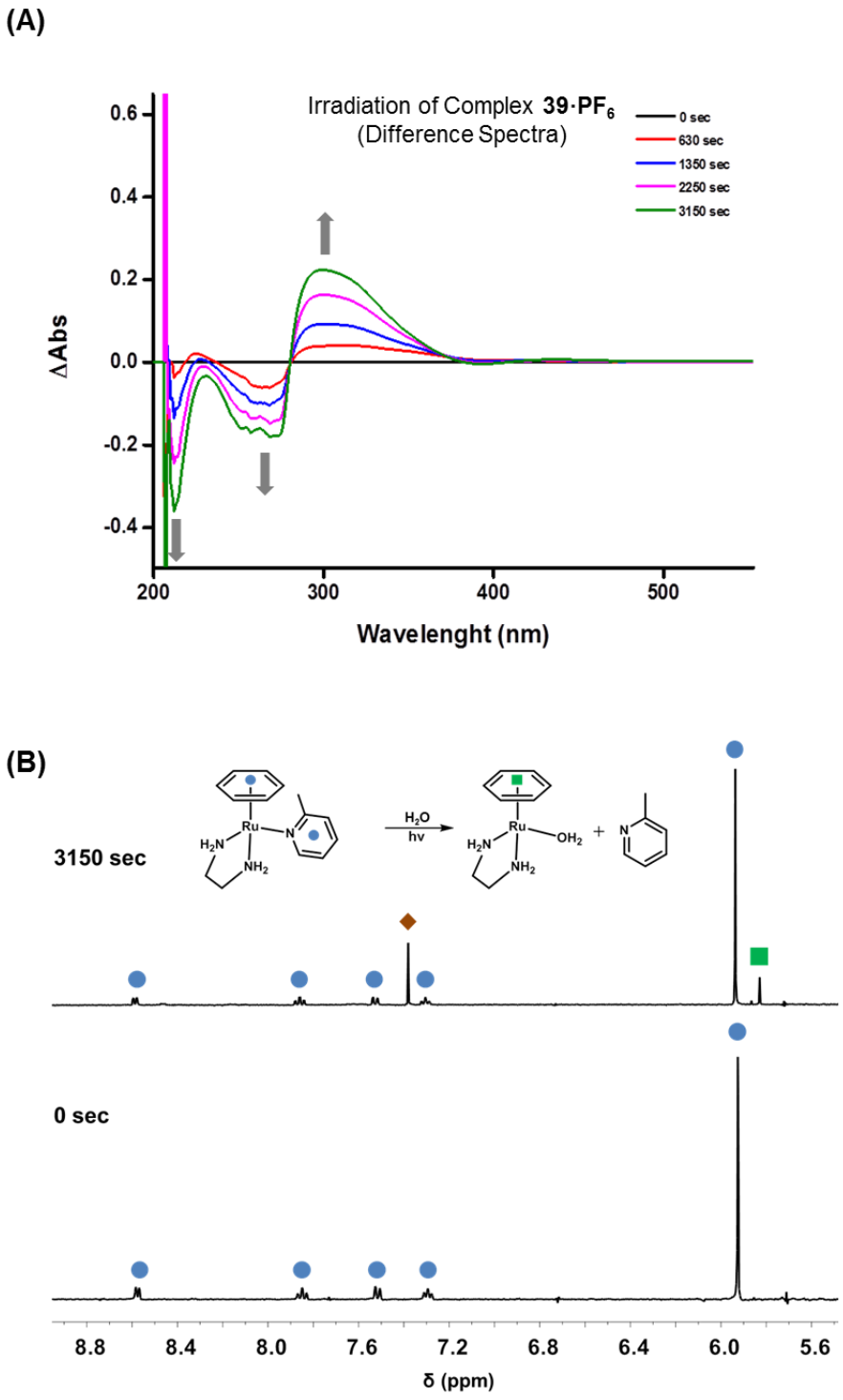

Figure 5.11. (A) Corresponding UV-visible difference spectra of complex **39·PF$_6$** (0.4 mM) in D_2O upon irradiation at 365 nm at pH 7 showing increase of the band at 298 nm and a decrease in bands at 210–220 and 269 nm. (B) ^{1}H NMR spectra of solution for complex **39·PF$_6$** before and after irradiation: (●) intact complex **39·PF$_6$**, (■) aqua adduct [Ru(η^6-benzene)(en)(H_2O)]$^{2+}$, (♦) free benzene.

We also compared the photochemistry of complex **13·PF$_6$** with its analogous un-tethered complex **40·PF$_6$**. The UV-visible spectra of complex **40·PF$_6$** showed an increase of bands at 229 and 286 nm, and decrease at 254 and 309 nm (Figure 5.12A) when the solution was irradiated at 365 nm (total of 57 min). As determined by the ^{1}H NMR analysis, when **40·PF$_6$** was photo-irradiated, it aquated within 57 min up to 37% (Figure 5.12B). Arene loss was observed but not accounting for more than 1%. In comparison to its non-irradiated analogue experiment, the aquation process was more efficient upon irradiation (it aquated only 13% in 3 h in the dark). These results show that while in complex **13·PF$_6$** light-mediated activation occurs in two positions of the Ru^{II} coordination sphere (the arene and the monodentate ligand, i.e. hemilabile ligand loss), for its non-tethered analogue **40·PF$_6$** virtually all activation occurred in the Ru–Z bond. This fact shows how tethering (or un-tethering) can influence on the selectivity towards activation sites on organometallic complexes.

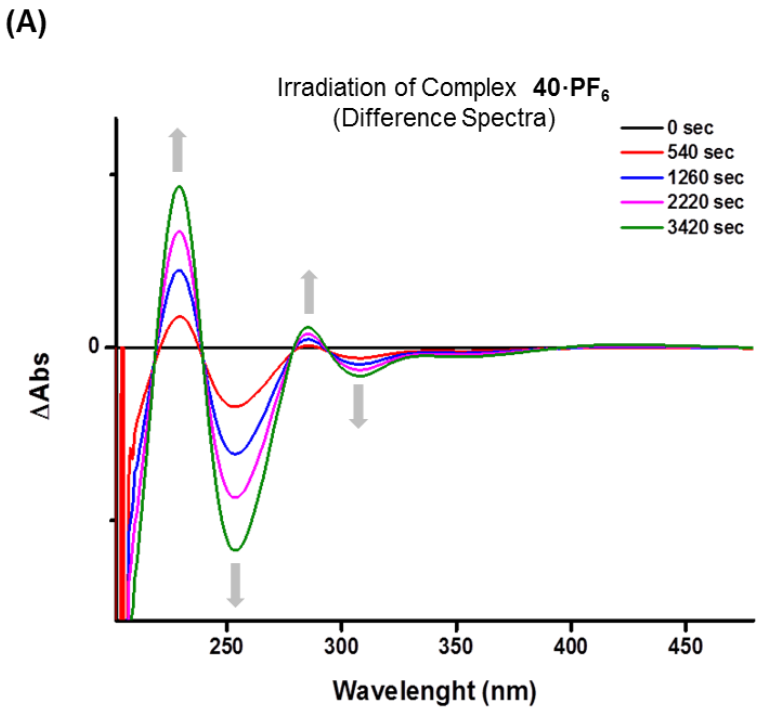

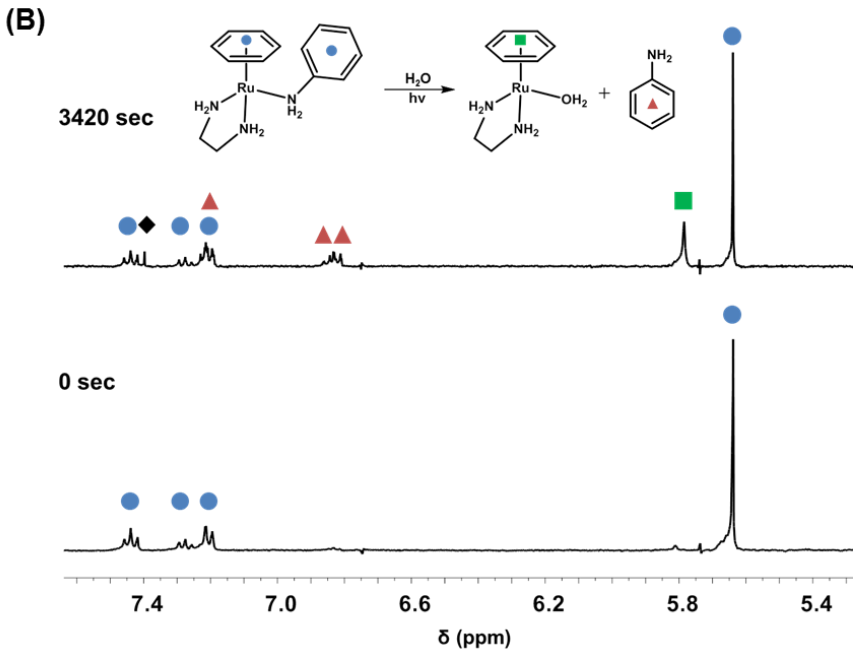

Figure 5.12. (A) Corresponding UV-visible difference spectra of complex **40·PF$_6$** (0.4 mM) in heavy water upon irradiation at 365 nm at pH 7 showing increase in bands at 229 and 286 nm, and decrease at 254 and 309 nm. (B) ^{1}H NMR spectra of solution for complex **40·PF$_6$** before and after irradiation: (●) intact complex **40·PF$_6$**, (■) aqua adduct [Ru(η^6-benzene)(en)(H_2O)]$^{2+}$, (▲) free phenylamine, (♦) free benzene.

5.2.5.2 Activation of Complex 9·PF$_6$ at pH 2

In order to investigate the phenomena observed when complex **9·PF$_6$** was irradiated at pH 7.0, i.e. the increase of bands at 210–240 nm and 333 nm in the electronic absorption spectra and the appearance of unknown photo-products by ^{1}H NMR, we proceeded to photo-irradiate complex **9·PF$_6$** at pH 2.0. Given that the pK_a of the hemilabile ligand is 4.9 we thought that following photo-activation of the Ru–Z bond of complex **9·PF$_6$** at pH < pK_a (i.e., pH 2.0), could perhaps block the reversible coordination of Z toward the metal centre.

An aqueous solution of complex **9·PF$_6$** (0.4 mM) at pH 2.0 was photo-irradiated for 34 min at 365 nm at 298 K. The UV-visible absorption spectrum indicated an increase in intensity of the band 333 nm (Figure 5.13A). The ^{1}H NMR spectra showed no significant changes, while the UV-visible absorption spectrum recorded after the NMR

showed some regression of the band at 333 nm. These results are in accordance with those observed after irradiation at pH 7.0.

Further irradiation (additional 70 min) resulted in a great increase of the band at 265 nm, which matches that of free 2-benzylpyridine. The ^{1}H NMR data recorded afterwards showed clear presence of the free ligand (Figure 5.13B). Strikingly, the UV-visible absorption spectrum recorded after the NMR, again shows a slight decrease of the bands at 234 and 333 nm, yet the strong band at 265 nm, attributed to the free ligand, remains unaffected.

Activation by light of **9·PF$_6$** in acidic conditions confirms that a two-step process occurs, the reversible formation of non-characterised photoproducts, followed by hemilabile ligand loss if irradiation persists.

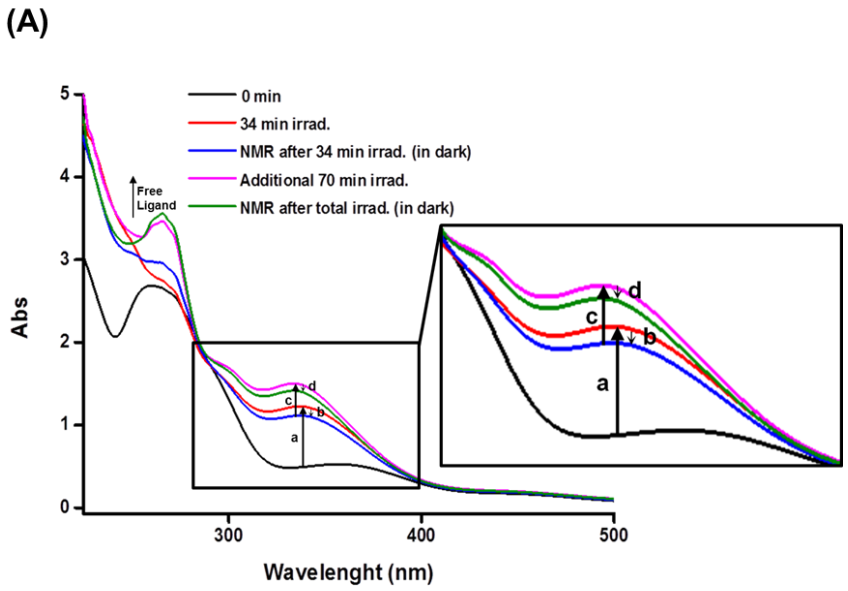

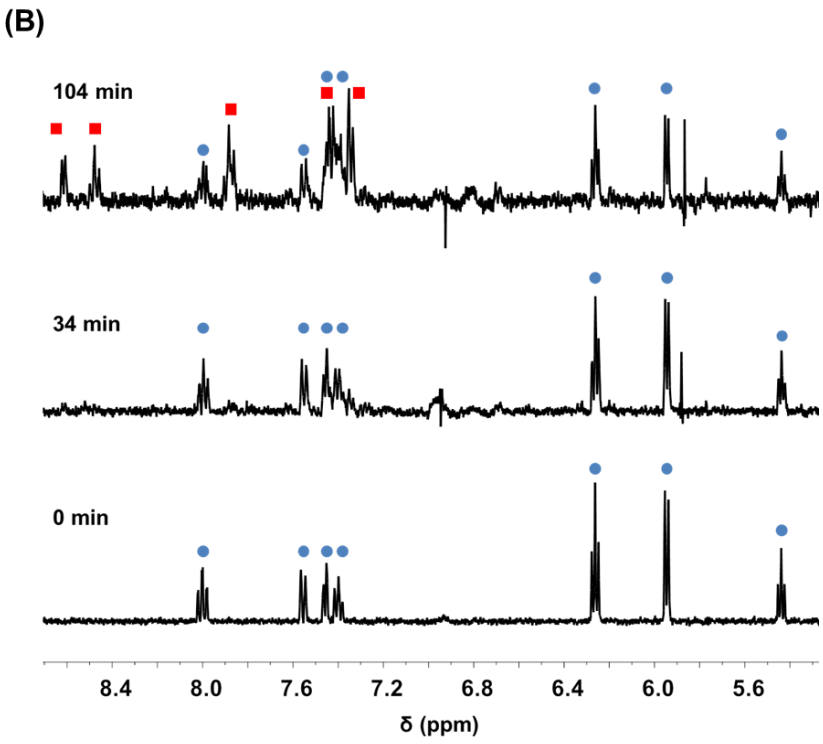

Figure 5.13. (A) Time evolution of the electronic absorption spectra of a solution of complex **9·PF$_6$** (0.4 mM) upon irradiation at 365 nm at pH 2.0. (B) ^{1}H NMR spectra of complex **9·PF$_6$** (●) at different stages of irradiation indicating the appearance of free hemilabile ligand 2-benzylpyridine (■).

5.2.6 Computational Studies

Light irradiation experiments show that tether complexes **7·PF$_6$**, **9·PF$_6$** and **13·PF$_6$** have different photochemical features with respect to their un-tethered analogues. Complexes **39·PF$_6$** and **40·PF$_6$** undergo preferential photo-dissociation of the monodentate ligand and minimal arene loss over prolonged irradiation. Conversely, complexes **7·PF$_6$**, **9·PF$_6$** and **13·PF$_6$** are subject to a more intricate photochemical process, which appear to involve a multistep dissociation of the hemilabile tether ligands. Nevertheless, the photo-stability of these tether derivatives is ultimately remarkable, considering that their decomposition into photoproducts upon prolonged irradiation at 365 nm is overall moderate.

We have employed DFT to gain insights in the excited state chemistry of complexes **7**, **9** and **13** with the aim of guiding future ultrafast spectroscopy studies and the design of new tether complexes. For this reason, we determined the two lowest-lying triplet excited states for these complexes and compared their geometries with their ground-state structures (LC-WPBE/SDD/6-31G**). The interplay between these low energy excited states generally determines the photochemical behaviour of transition metal complexes.[16] Table 5.3 reports selected bond distances for the excited states of **7**, **9** and **13**, while Figure 5.14 shows the geometries of the complexes and spin density surfaces in the case of triplets. For **7**, **9** and **13**, both triplet states (LL1 and LL2) are of metal-centred nature. LL1 has the lowest energy and corresponds to a distorted structure in which the π-bonded region of the arene ligand displays strongly elongated Ru–C distances compared to the ground state (GS) geometry, which may suggest a hapticity interconversion.[17] Ru–N1(Z) distances in LL1 are shorter than 2.15 Å, indicating a strong interaction between the metal centre and the tether arm. Although the distorted coordination of the arene may hint that LL1 is dissociative, the tight coordination of N1 rather suggests that this is not the case. The second optimized triplet geometry, LL2, shows elongated Ru–N1(Z) distances for **7**, **9** and **13** (> 2.57 Å). This finding is consistent with a dissociative excited state capable of promoting the tether ring-opening.

Table 5.3. Selected bond lengths (Å) for the DFT-optimized structures of **7**, **9** and **13** in the ground state (GS) and the two lowest-lying triplet states (LL1 and LL2).

Complex		Bond			
		Ru–centroid	**Ru–N1**	**Ru–N2**	**Ru–N3**
7	**GS**	1.654	2.145	2.131	2.128
	LL1	2.759	2.137	2.145	2.117
	LL2	1.842	2.571	2.121	2.123
9	**GS**	1.653	2.133	2.114	2.143
	LL1	2.734	2.112	2.141	2.141
	LL2	1.837	2.607	2.112	2.131
13	**GS**	1.650	2.157	2.132	2.128
	LL1	2.745	2.147	2.130	2.124
	LL2	1.831	2.622	2.117	2.125

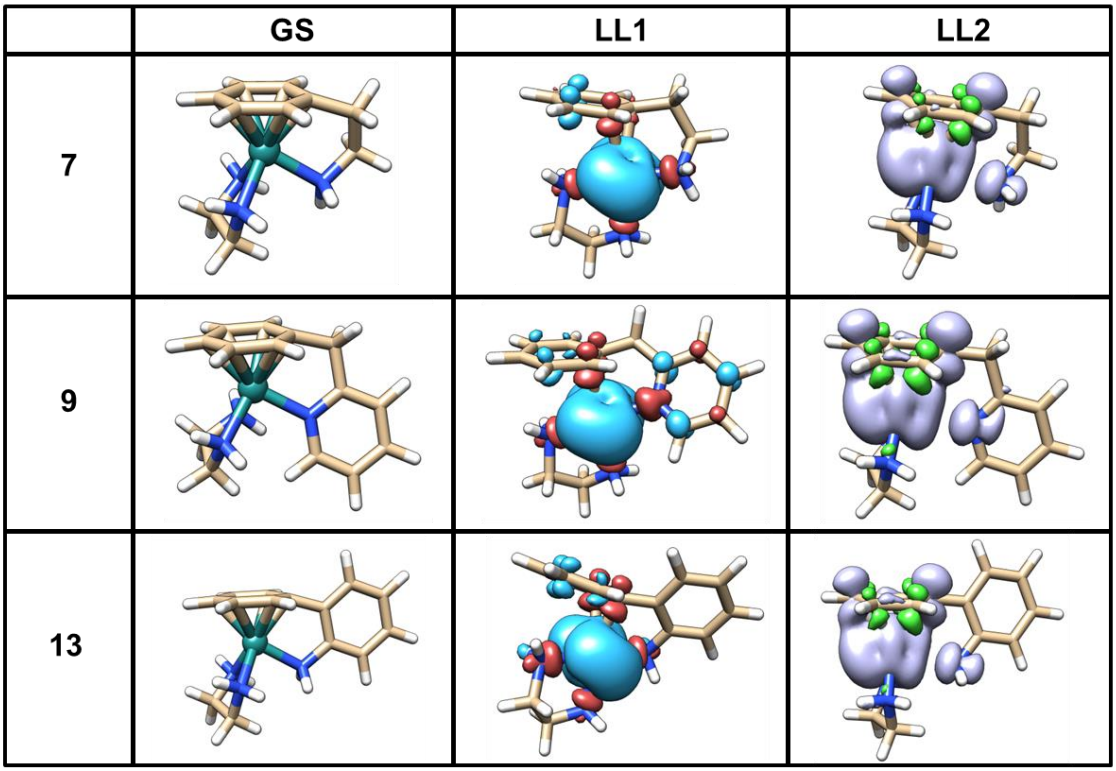

Figure 5.14. DFT-optimized structures for the ground state and the two lowest-lying triplet states of **7**, **9** and **13·** (LC-WPBE/SDD/6-31G**).

5.3 Conclusions

Three different hemilabile ligands were used to prepare closed tethered complexes **7·PF$_6$**, **9·PF$_6$** and **13·PF$_6$**, aiming to fine-tune the activation of the Ru–Z bond of these types of promising switchable organoruthenium compounds. Also, we synthesised the un-tethered complexes **39·PF$_6$** and **40·PF$_6$**, analogues to **9·PF$_6$** and **13·PF$_6$**, respectively. The crystal structures of **7** and **9·PF$_6$** have been elucidated by X-ray diffraction. Subsequent crystallographic analysis has provided critical information about geometrical parameters which are closely related with their activation capability. The activation studies have shown that tethered complexes **7·PF$_6$**, **9·PF$_6$** and **13·PF$_6$** can only be activated in acid environments, i.e.; they are stable at neutral pH but they afford the corresponding open chlorido protonated species in 1 M HCl solutions. The observed differences between the percentage of the activated forms (**13·PF$_6$** > **9·PF$_6$** >> **7·PF$_6$**) has been attributed to the structural variation concerning the hemilabile ligands, demonstrating that aromatic amines (**9·PF$_6$** and **13·PF$_6$**) are more prone to trigger the dissociation from the ruthenium(II) centre than aliphatic amines (**7·PF$_6$**). We have also shown that the rigidity of the tether arm provides an important feature for the ring opening process, making the process faster.

Photo-irradiation of complexes **7·PF$_6$**, **9·PF$_6$** and **13·PF$_6$** was performed to attempt the activation of these tethered complexes at pH 7.0. Complex **7·PF$_6$** was too stable to be activated by light as determined by ^{1}H NMR. Irradiation for **9·PF$_6$** showed the appearance of unidentified photoproducts which maintained the Ru–arene bond, and which reversed to the original complex after irradiation stopped, and/or triggered hemilabile ligand loss over time in the dark. Irradiation of complex **9·PF$_6$** at pH 2.0 was conclusive to suggest a two-step activation process whereby the hemilabile ligand is eventually lost upon persistan irradiation. Upon irradiation of complex **13·PF$_6$**,

hemilabile ligand loss (Ru–Z and Ru–arene cleavage) was observed by UV-visible and ^{1}H NMR.

Regarding the comparison between the reactivity observed for tethered versus un-tethered complexes a summary follows (Figure 5.15). In the dark, complexes **9·PF$_6$** and **39·PF$_6$** showed that none of them was activated at pH 7.0. However, after irradiation the un-tethered complex **39·PF$_6$** showed cleavage of the Ru–Z bond, while **9·PF$_6$** showed formation of uncharacterised species in a little extent (only extensive irradiation ultimately triggered loss of the hemilabile ligand). On other hand, closed tethered complex **13·PF$_6$** was not activated while its un-tethered analogue **40·PF$_6$** hydrolysed at neutral pH in the dark. Upon irradiation, complex **13·PF$_6$** lost the hemilabile ligand (cleavage of Ru–Z and Ru–arene bonds) and **40·PF$_6$** also hydrolysed (Ru–Z bond) yet much faster than without light.

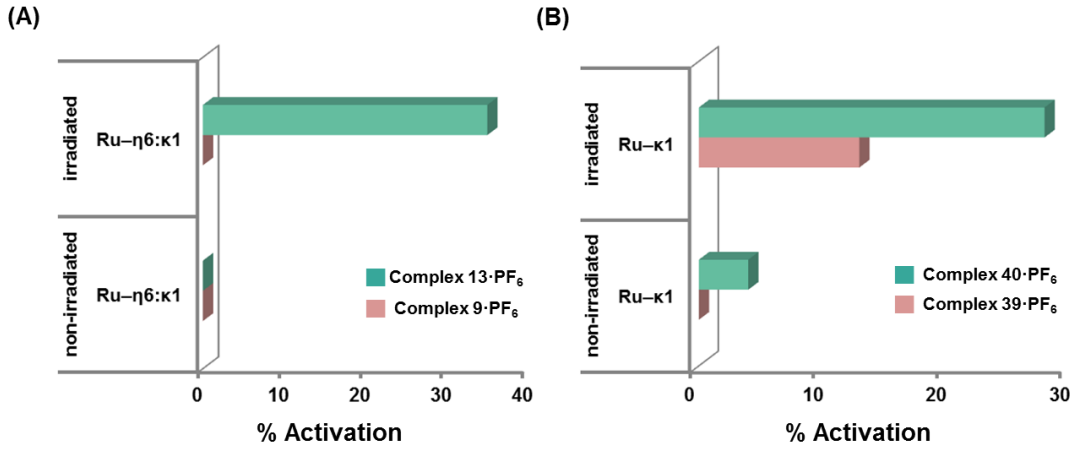

Figure 5.15. (A) Hemilabile ligand loss percentages for complexes **9·PF$_6$** and **13·PF$_6$** under photoactivation at 365 nm and in the dark at 298 K. (B) Activation of the Ru–Z bond of complexes **39·PF$_6$** and **40·PF$_6$** in dark and under light irradiation after ca. 30 min followed by ^{1}H NMR

The preliminary DFT work reported here highlights that the photochemistry of **7**, **9** and **13** is likely driven by two metal-centred excited states, which are (i) capable of inducing a change in the arene coordination mode of the Ru centre (LL1) and (ii) cause ring opening of the tether (LL2). Additional computational studies and ultrafast

spectroscopy are required to have a full understanding of the interplay between these two states, and ultimately control the photochemistry of these complexes.

.

5.4 Experimental Section

5.4.2 Instrumentation

NMR Spectroscopy, Mass Spectrometry, Elemental Analysis and **pH Measurements** have been described in Chapter 2.

X-Ray Crystallography. Suitable crystals of compounds **7** and **9·PF$_6$**, were coated with mineral oil and mounted on Mitegen MicroMounts. The samples were measured in a Bruker D8 KAPPA APEX II diffractometer with CCD area-detector, equipped with graphite-monochromated Mo Kα radiation (λ = 0.71073 Å). The substantial redundancy in data allowed empirical absorption corrections (SADABS)[18] to be applied using multiple measurements of symmetry-equivalent reflections. Raw intensity data frames were integrated with the SAINT program, which also applied corrections for Lorentz and polarization effects. The Bruker SHELXTL Software Package was used for space group determination, structure solution, and refinement.[19] The space group determination was based on a check of the Laue symmetry, and systematic absences were confirmed using the structure solution. The structures were solved by direct methods (SHELXL-2014/7),[20, 21] completed with different Fourier syntheses, and refined with full-matrix least-squares using SHELXS minimizing $\omega(F_o^2 - F_c^2)^2$. Weighted R factors (R_w) and goodness of fit (S) are based on F^2; conventional R factors (R) are based on F. All non-hydrogen atoms were refined with anisotropic displacement parameters. Hydrogen atom positions were geometrically calculated and allowed to ride on their parent carbon or nitrogen atoms with fixed isotropic U. All scattering factors and anomalous dispersion factors are contained in the SHELXTL 6.10 program library. The data were processed by the modelling program Mercury version 3.9 (CSD System). The crystal structures of compounds **7**, and **9·PF$_6$**, have been deposited at the

Cambridge Crystallographic Data Centre with deposition numbers CCDC 1534181 and 1579152, respectively.

UV-visible Spectroscopy. UV-visible absorption spectra were recorded on a Cary 5000 UV-Vis-NIR spectrophotometer (Agilent Technologies, CA) using 1 cm path length quartz cuvettes (800 μL) provided with a Temperature Controller. Spectra were recorded at 298 K in heavy water from 800 to 200 nm. The data were processed using OriginPro version 9.0 (OriginLab, Northampton, MA).

5.4.3 Methods

Acidic Activation of Ru^{II} Complexes. The ring-opening process (via the Ru–Z bond) of tethered complexes **7·PF_6**, **9·PF_6**, and **13·PF_6** was monitored by ^{1}H NMR in aqueous solutions at 298 K. After dissolving complexes (6–7 mM) in D_2O at pH 7.1, DCl was used to adjust the pH close to 0. The relative percentages of closed- versus open-tether species were quantified by integration of peaks in the ^{1}H NMR spectra.

Photoirradiation of Ru^{II} Complexes. Aqueous solutions of Ru^{II} complexes (0.4 mM) were photo-irradiated at 298 K using a UVA lamp (λ_{irr} = 365 nm providing an average light power of 3 J cm^{-2} h^{-1}) placed 20 cm from the cuvette or NMR tube. Light-irradiated solutions were stored in the dark between measurements to minimize unwanted photoreactions.

Computational Methods. Calculations were performed with the Gaussian 09 (G09) program package,[22] employing the DFT and TD-DFT methods.[23, 24]Solvent effects were included using the polarizable continuum model (PCM method),[25, 26] with water as

solvent. The LC-WPBE[27] functional together with the SDD pseudopotential (Ru)[28] and 6-31G** basis set (C H N)[29] were selected after benchmarking their performance as reported in the Appendix III, Section A.

Geometry optimizations were carried out without any symmetry constraints, the nature of all stationary points was confirmed by normal-mode analysis and no imaginary frequencies were found.

The UV-Visible electronic absorption spectra were simulated by TD-DFT computing a total of 32 singlet excited states. The electronic distribution and the localization of the singlet and triplet excited states were visualized using electron density difference maps (EDDMs). GaussSum 2.2.5[30] was used to simulate the theoretical UV-Visible spectra and for EDDMs calculations (Appendix III, Section B). Molecular graphics images were produced using the UCSF Chimera package from the Resource for Biocomputing, Visualization, and Informatics at the University of California, San Francisco (supported by NIH P41 RR001081).[31]

5.4.4 Synthesis

MATERIALS

$RuCl_3 \cdot 3H_2O$ was acquired from Precious Metals Online. Benzoic acid, ethylenediamine, 2-phenylethylamine, 2-benzylpydirine, phenylamine, 2-picoline and 1,4-cyclohexadiene were purchased from Sigma-Aldrich. Dichloroethane and magnesium were acquired from Acros Organics, and 2-aminobiphenyl, iodine, molecular sieves of 3 Å and silver hexafluorophosphate from Fisher. Ethanol, dry methanol, diethyl ether, tetrahydrofuran, sodium metal, hydrochloric acid 37% and sodium chloride were purchased from Sharlau. For NMR spectroscopy, the solvents used were MeOD-d_4, dimethyl-d_6

sulfoxide, deuterium oxide (D_2O), deuterium chloride (DCl) and 1, 4-dioxane obtained from VWR International.

PREPARATION OF COMPLEXES

Complexes $[Ru(\eta^6\text{-bz})Cl_2]_2$[6] and $[Ru(\eta^6\text{-bz})(en)Cl]Cl$[32] were prepared according to previously reported procedures. Complexes $[Ru(\eta^6\text{-etb})Cl_2]_2$,[33] $[Ru\{\eta^6{:}\kappa^1\text{-}C_6H_5(C_2H_4)NH_2\}Cl_2]$, $[Ru\{\eta^6{:}\kappa^1\text{-}C_6H_5(C_6H_4)NH_2\}Cl_2]$[5], $[Ru\{\eta^6{:}\kappa^1\text{-}C_6H_5(CH_2)C_5H_4N\}Cl_2]$ and $[Ru\{\eta^6{:}\kappa^1\text{-}C_6H_5(C_6H_4)NH_2\}(en)]Cl_2$[4] (**13**) have been described in Chapter 2.

$[Ru\{\eta^6{:}\kappa^1\text{-}C_6H_5(CH_2)_2NH_2\}(en)](PF_6)_2$ (7·PF_6). Ethylenediamine (17 μL, 0.260 mmol) was added to a suspension of $[Ru(\eta^6{:}\kappa^1\text{-}C_6H_5(C_2H_4)NH_2)Cl_2]$ (64 mg, 0.220 mmol) in dry methanol (2 mL). The reaction mixture was stirred at ambient temperature for 2 h. The solvent was removed in the rotary evaporator to give a yellow solid, which was redissolved in the minimum volume of ethanol. A small amount of suitable crystals of X-ray diffraction appeared (complex **7**). Addition of an excess of NH_4PF_6 to the remaining ethanolic solution led precipitation of a yellow solid. Yield: 65 mg (52%). Elemental analysis: Cald for $C_{10}H_{19}F_{12}N_3P_2Ru$ (572,28): C, 20.99; H, 3.35; N, 7.34. Found: C, 20.35; H, 3.59; N, 7.12. ^{1}H NMR (400 MHz, D_2O, δ): 6.31 (br s, NH_2, 2H), 6.07 (t, *J* = 6.0 Hz, Ar H, 2H), 5.60 (d, *J* = 6.1 Hz, Ar H, 2H), 5.32 (t, *J* = 6.0 Hz, Ar H, 1H), 3.84-3.70 (m, 2H), 2.73 (t, *J* = 6.7 Hz, Ar H, 2H), 2.65-2.55 (m, 2H), 2.44-2.33 (m, 2H). ESI-MS (m/z): $[M–H]^+$ calcd. for $C_{10}H_{18}N_3Ru$, 282.0; found, 282.1.

$[Ru\{\eta^6{:}\kappa^1\text{-}C_6H_5(CH_2)C_5H_4N\}(en)](PF_6)_2$ (9·PF_6). $AgPF_6$ (51 mg, 0.201 mmol) was added to a solution of $[Ru\{\eta^6{:}\kappa^1\text{-}C_6H_5(CH_2)C_4H_4N\}Cl_2]$ (33 mg, 0.096 mmol) in

anhydrous methanol. The reaction mixture was stirred for 2 h. Then, the precipitated AgCl was removed by filtration, and ethylenediamine (7 μL, 0.106 mmol) was added to the remaining solution. The solvent was removed in the rotary evaporator after 2 h of reaction to give a yellow solid, which was re-dissolved in the minimum volume of ethanol, which was washed with ethanol and diethyl ether, and dried in vacuum. Yield: 55 mg (83%). Elemental analysis: Cald for $C_{14}H_{19}F_{12}N_3P_2Ru$ (620.33): C, 27.11; H, 3.09; N, 6.77. Found: C, 27.32; H, 3.09; N, 7.03. ^{1}H NMR (400 MHz, D_2O, δ): 8.00 (td, *J* = 7.8, 1.6 Hz, Ar H, 1H), 7.56 (d, *J* = 8.0 Hz, Ar H, 1H), 7.46 (d, *J* = 4.8 Hz, Ar H, 1H), 7.41 (t, *J* = 7.0 Hz, Ar H, 1H), 6.27 (t, *J* = 6.0 Hz, Ar H, 2H), 5.95 (d, *J* = 6.2 Hz, Ar H, 2H), 5.45 (t, *J* = 5.7 Hz, Ar H, 1H), 4.44 (s, 2H), 2.90-2.81 (m, 4H). ESI-MS (m/z): $[M–H]^+$ calcd. for $C_{14}H_{19}N_3Ru$, 330.0; found, 330.1.

[Ru{η^6:κ^1-$C_6H_5(C_6H_4)NH_2$}(en)]$(PF_6)_2$ (13·PF_6). Complex **13**, containing PF_6 as counter anions, was obtained by dissolving [Ru{η^6:κ^1-$C_6H_5(C_6H_4)NH_2$}(en)]Cl_2[4] with an excess of NH_4PF_6 in water. Precipitation of a yellow solid afforded the desire product. Its ^{1}H NMR spectrum was indistinguishable from that of the starting complex, confirming that the cation $[Ru\{\eta^6:\kappa^1\text{-}C_6H_5(C_6H_4)NH_2\}(en)]^{2+}$ remained unaltered.

Ru(η^6-bz)(en)(C_6H_7N)]$(PF_6)_2$ (39·PF_6). Using an aluminium foil-covered flask, complex [Ru(η^6-bz)(en)Cl]Cl (37 mg, 0.118 mmol) and $AgPF_6$ (61 mg, 0.236 mmol) in 2 mL of methanol were stirred for 2 h at room temperature. Precipitated AgCl was then removed by filtration. A large excess of 2-picoline (119 μL, 1.2 mmol) was added, and the mixture was left stirring at reflux for 16 h. The volume was reduced by rotary evaporation to ca. 5% of its original volume. Addition of diethyl ether (1 mL) afforded a precipitate that was collected by filtration and washed with portions of ethanol and

diethyl ether, and dried overnight in vacuum. Yield: 42 mg (57%). Elemental analysis: Cald for $C_{14}H_{21}F_{12}N_3P_2Ru$ (622,34): C, 27.02; H, 3.40; N, 6.75. Found: C, 26.70; H, 3.72; N, 6.80. ^{1}H NMR (400 MHz, D_2O, δ): 8.64 (d, *J* = 5.9 Hz, Ar H, 1H), 7.91 (t, *J* = 7.6 Hz, Ar H, 1H), 7.58 (d, *J* = 8.2 Hz, Ar H, 1H), 7.35 (t, *J* = 6.4 Hz, Ar H, 1H), 5.99 (s, 6H), 2.80 (s, 3H), 2.76-2.47 (m, 4H). $[M–L–H]^+$ calcd. for $C_8H_{14}N_2Ru$, 239.0; found, 239.0.

[Ru(η^6-bz)(en)($C_6H_5NH_2$)](PF_6)$_2$ (40·PF_6). Using an aluminium foil-covered flask, a mixture containing complex [Ru(η^6-bz)(en)Cl]Cl (37 mg, 0.118 mmol) and $AgPF_6$ (61 mg, 0.236 mmol) in 2 mL of methanol was stirred for 2 h at room temperature. Precipitated AgCl was then removed by filtration. A large excess of phenylamine (109 μL, 1.200 mmol) was added, and the mixture was left stirring at reflux for 16 h. The volume was reduced by rotary evaporation to ca. 5% of its original volume. Addition of diethyl ether (1 mL) afforded a precipitate that was collected by filtration and washed with ethanol and diethyl ether, and dried overnight in vacuum. Yield: 34 mg (46%). Elemental analysis: Cald for $C_{14}H_{21}F_{12}N_3P_2Ru$ (622,34): C, 27.02; H, 3.40; N, 6.75. Found: C, 26.26; H, 3.62; N, 6.56. ^{1}H NMR (400 MHz, D_2O, δ): 7.47 (t, *J* = 8.2 Hz, Ar H, 2H), 7.31 (t, *J* = 7.4 Hz, Ar H, 1H), 7.46 (d, *J* = 8.7 Hz, Ar H, 2H), 5.67 (s, 6H), 2.64-2.57 (m, 2H), 2.46-2.38 (m, 2H). $[M–L–H]^+$ calcd. for $C_8H_{14}N_2Ru$, 238.9; found, 239.0.

5.4 References

(1) Mari, C.; Pierroz, V.; Ferrari, S.; Gasser, G. Combination of Ru(II) Complexes and Light: New Frontiers in Cancer Therapy. *Chem. Sci.* **2015**, *6*, 2660-2686.

(2) Dolmans, D. E. J. G. J.; Fukumura, D.; Jain, R. K. Photodynamic Therapy for Cancer. *Nat. Rev. Cancer* **2003**, *3*, 380-387.

(3) Betanzos-Lara, S.; Salassa, L.; Habtemariam, A.; Novakova, O.; Pizarro, A. M.; Clarkson, G. J.; Liskova, B.; Brabec, V.; Sadler, P. J. Photoactivatable Organometallic Pyridyl Ruthenium(II) Arene Complexes. *Organometallics* **2012**, *31*, 3466-3479.

(4) Martínez-Peña, F.; Pizarro, A. M. Control of Reversible Activation Dynamics of [Ru{η6:κ1-C6H5(C6H4)NH2}(XY)]n+ and the Effect of Chelating-Ligand Variation. *Chem. Eur. J.* **2017**, *23*, 16231-16241.

(5) Pizarro, A. M.; Melchart, M.; Habtemariam, A.; Salassa, L.; Fabbiani, F. P. A.; Parsons, S.; Sadler, P. J. Controlling the Reactivity of Ruthenium(II) Arene Complexes by Tether Ring-Opening. *Inorg. Chem.* **2010**, *49*, 3310-3319.

(6) Heim, L. E.; Vallazza, S.; van der Waals, D.; Prechtl, M. H. G. Water Decontamination With Hydrogen Production Using Microwave-Formed Minute-Made Ruthenium Catalysts. *Green Chem.* **2016**, *18*, 1469-1474.

(7) Wang, F.; Chen, H.; Parsons, S.; Oswald, I. D. H.; Davidson, J. E.; Sadler, P. J. Kinetics of Aquation and Anation of Ruthenium(II) Arene Anticancer Complexes, Acidity and X-ray Structures of Aqua Adducts. *Chem. Eur. J.* **2003**, *9*, 5810-5820.

(8) Martínez-Alonso, M.; Busto, N.; Jalón, F. A.; Manzano, B. R.; Leal, J. M.; Rodríguez, A. M.; García, B.; Espino, G. Derivation of Structure–Activity Relationships from the Anticancer Properties of Ruthenium(II) Arene Complexes with 2-Aryldiazole Ligands. *Inorg. Chem.* **2014**, *53*, 11274-11288.

(9) Melchart, M.; Habtemariam, A.; Novakova, O.; Moggach, S. A.; Fabbiani, F. P. A.; Parsons, S.; Brabec, V.; Sadler, P. J. Bifunctional Amine-Tethered Ruthenium(II) Arene Complexes Form Monofunctional Adducts on DNA. *Inorg. Chem.* **2007**, *46*, 8950-8962.

(10) Zheng, C.; Kim, K.; Matsumoto, T.; Ogo, S. The Useful Properties of H2O as a Ligand of a Hydrogenase Mimic. *Dalton Trans.* **2010**, *39*, 2218-2225.

(11) Takahiro, M.; Koji, Y.; Chunbai, Z.; Yasuhito, S.; Yoshiki, H.; Hidetaka, N.; Seiji, O. Synthesis and Reactivity of a Water-soluble NiRu Monohydride Complex with a Tethered Pyridine Moiety. *Chem. Lett.* **2016**, *45*, 197-199.

(12) Reiner, T.; Jantke, D.; Miao, X.-H.; Marziale, A. N.; Kiefer, F. J.; Eppinger, J. Phenylalanine - a Biogenic Ligand with Flexible η- and η6:κ1-Coordination at Ruthenium(II) Centres. *Dalton Trans.* **2013**, *42*, 8692-8703.

(13) Betanzos-Lara, S.; Salassa, L.; Habtemariam, A.; Sadler, P. J. Photocontrolled Nucleobase Binding to an Organometallic RuII Arene Complex. *Chem. Commun.* **2009**, *0*, 6622-6624.

(14) Brown, W. H.; Iverson, B. L.; Anslyn, E.; Foote, C. S. *Organic Chemistry*; Cengage Learning: Boston, MA, 2017.

(15) Magennis, S. W.; Habtemariam, A.; Novakova, O.; Henry, J. B.; Meier, S.; Parsons, S.; Oswald, I. D. H.; Brabec, V.; Sadler, P. J. Dual Triggering of DNA Binding and Fluorescence via Photoactivation of a Dinuclear Ruthenium(II) Arene Complex. *Inorg. Chem.* **2007**, *46*, 5059-5068.

(16) Garino, C.; Salassa, L. The Photochemistry of Transition Metal Complexes Using Density Functional Theory. *Philos. Trans. A Math. Phys. Eng. Sci.* **2013**, *371*,

(17) Yang, H. Syntheses, Characterizations and Applications of π-bonded Bis Arene Ruthenium Complexes and Electrochemical Properties of Heterobimetallic Chromium - Manganese Arene Complexes. Brown University, Rhode Island, 2012.

(18) Bruker. *APEX2,SAINT and SADABS*; Bruker AXS: Madison, WI, 2008.

(19) Bruker. *SHELXTL Version 6.10, Structure Determination Package*; Bruker AXS: Madison, WI, 2000.

(20) Sheldrick, G. M. A Short History of SHELX. *Acta Crystallogr. Sect. A* **2008**, *64*, 112-122.

(21) Sheldrick, G. M. Crystal Structure Refinement with SHELXL. *Acta Crystallogr. Sect. C* **2015**, *71*, 3-8.

(22) M.J. Frisch, et al. *Gaussian 09, Revision C.01*; Gaussian Inc: Wallingford, CT, USA, 2009.

(23) Casida, M. E.; Jamorski, C.; Casida, K. C.; Salahub, D. R. Molecular Excitation Energies to High-Lying Bound States from Time-Dependent Density-Functional Response Theory: Characterization and Correction of the Time-Dependent Local Density Approximation Ionization Threshold. *J. Chem. Phys.* **1998**, *108*, 4439-4449.

(24) Stratmann, R. E.; Scuseria, G. E.; Frisch, M. J. An Efficient Implementation of Time-Dependent Density-Functional Theory for the Calculation of Excitation Energies of Large Molecules. *J. Chem. Phys.* **1998**, *109*, 8218-8224.

(25) Cossi, M.; Scalmani, G.; Rega, N.; Barone, V. New Developments in the Polarizable Continuum Model for Quantum Mechanical and Classical Calculations on Molecules in Solution. *J. Chem. Phys.* **2002**, *117*, 43-54.

(26) Miertuš, S.; Scrocco, E.; Tomasi, J. Electrostatic Interaction of a Solute with a Continuum. A Direct Utilizaion of AB Initio Molecular Potentials for the Prevision of Solvent Effects. *Chem. Phys.* **1981**, *55*, 117-129.

(27) Vydrov, O. A.; Scuseria, G. E.; Perdew, J. P. Tests of Functionals for Systems With Fractional Electron Number. *J. Chem. Phys.* **2007**, *126*, 154109.

(28) Dunning, T. H.; Hay, P. J. In *Methods of Electronic Structure Theory*; Schaefer, H. F., Eds; Springer US: Boston, MA, 1977; pp 1-27.

(29) Rassolov, V. A.; Ratner, M. A.; Pople, J. A.; Redfern, P. C.; Curtiss, L. A. 6-31G* Basis Set for Third-Row Atoms. *J. Comput. Chem.* **2001**, *22*, 976-984.

(30) O'Boyle, N. M.; Tenderholt, A. L.; Langner, K. M. cclib: A Library for Package-Independent Computational Chemistry Algorithms. *J. Comput. Chem.* **2008**, *29*, 839-845.

(31) Pettersen, E. F.; Goddard, T. D.; Huang, C. C.; Couch, G. S.; Greenblatt, D. M.; Meng, E. C.; Ferrin, T. E. UCSF Chimera—A Visualization System for Exploratory Research and Analysis. *J. Comput. Chem.* **2004**, *25*, 1605-1612.

(32) Morris, R. E., et al. Inhibition of Cancer Cell Growth by Ruthenium(II) Arene Complexes. *J. Med. Chem.* **2001**, *44*, 3616-3621.

(33) Habtemarian, A.; Betanzos-Lara, S.; Sadler, P. J. *Ruthenium Complexes, in Inorganic Syntheses*; John Wiley & Sons: 2010.

6.

Vapour-Induced Crystalline State Reversible Reactions of Ruthenium(II) Complexes Containing Hemilabile Tethered-Arene Ligands

6.1 Introduction

There is a continuous interest in crystalline materials able to reversibly incorporate small molecules into the crystal lattice due to the potential impact they can have on several applications, such as gas storage/separation, heterogeneous catalysis, and development of sensors.[1] Solid state reactions with vapours, a different type of solvent-free reactions where there has been much effort toward the design of materials capable of interacting with a range of gases, including O_2, N_2, H_2, NO, and CO, are uncommon in the field of organometallic chemistry.

A very early example of solid state organometallic synthesis using solid-gas techniques was reported in the 1960s when the oxidative addition of various HX gases (HF, HCl, HBr, HI and H_2S) to Vaska-type complexes $IrX'(CO)(PPh_3)_2$ (X' = Cl, Br, I, SCN) was reported to form *trans*-$Ir(PPh_3)_2(X')(CO)(H)(X)$.[2] Similarly, addition of I_2 to $Pt(acac)_2$ (acac = acetylacetonate) formed the oxidative addition product *trans*-$PtI_2(acac)_2$.[3] More recently, an interesting example was reported in this area by van Koten for the uptake and release of SO_2 by an organoplatinum complex involving the corresponding formation and cleavage of a coordination bond (Pt–S).[4] Also, Brammer and co-workers[5-7] have shown that the conversion of *trans*-$[CuCl_2(n\text{-}X\text{-}C_5H_4N)_2]$ (n = 3, 4; X = Cl, Br) with HCl gas to form $[n\text{-}X\text{-}C_5H_4NH]_2[CuCl_4]$ can take place under solid-state conditions. These reactions have been monitored by powder diffraction, including in situ powder synchrotron diffraction.

Solid-state reactions reported for ruthenium(II) complexes have been scarce. Werner and co-workers published that addition of CO to a Ru^{II} complex that contains a hemilabile phosphine ether ligand[8, 9] (P,O) results in the dissociation of the oxygen atom from the Ru^{II} centre,[10] while McGee et al. have investigated crystalline solid reactions of ruthenium(II) complexes as potential benzene and oxygen sensors. [11, 12]

Nowadays, the detection of volatile organic compounds (VOCs) by simple means requiring only a low-cost technology is an attractive research target.[13] In this context platinum(II)- and gold(I)-containing compounds are the two largest families of vapochromic substances, i.e. substances which change colour upon exposure to certain vapors,[14] and whose transformation can be often detect even by the naked eye.

With these findings in mind, in this Chapter, we describe the solid state reaction of the crystalline closed complexes of formula [Ru(η^6:κ^1-arene:N)Cl_2], bearing as hemilabile ligands 2-aminobiphenyl and 2-benzylpyridine, with hydrated HCl vapour, which led to the dissociation of the nitrogen atom from the ruthenium(II) centre to afford the corresponding open tether complexes, [Ru(η^6:κ^1-arene:NH)Cl_3], as characterized by powder X-ray diffraction. We examined the reversibility of the solid-vapour reaction in presence of a HCl capture agent such as $AgPF_6$. Finally, we further investigated the possibility of closing the open species upon heat-mediated loss of HCl gas at different temperatures. The reversibility of the tether-ring opening and closure in the solid state of ruthenium(II) complexes of formula [Ru(η^6:κ^1-arene:N)Cl_2] (where arene:N is 2-aminobiphenyl and 2-benzylpyridine) was examined in detail using powder X-ray diffraction and thermogravimetric analysis, and the kinetic parameters of the tether ring closure were also determined.

6.2 Results and Discussion

6.2.1 Synthesis of the Ru^{II} Complexes

Dichlorido closed-tether complexes **41** and **42** of general formula [Ru(η^6:κ^1-arene:N)Cl_2] and their corresponding open-tether complexes, **41HCl** and **42HCl**, with formula [Ru(η^6-arene:NH)Cl_3] (Figure 6.1), were prepared by previously reported procedures.[15, 16]

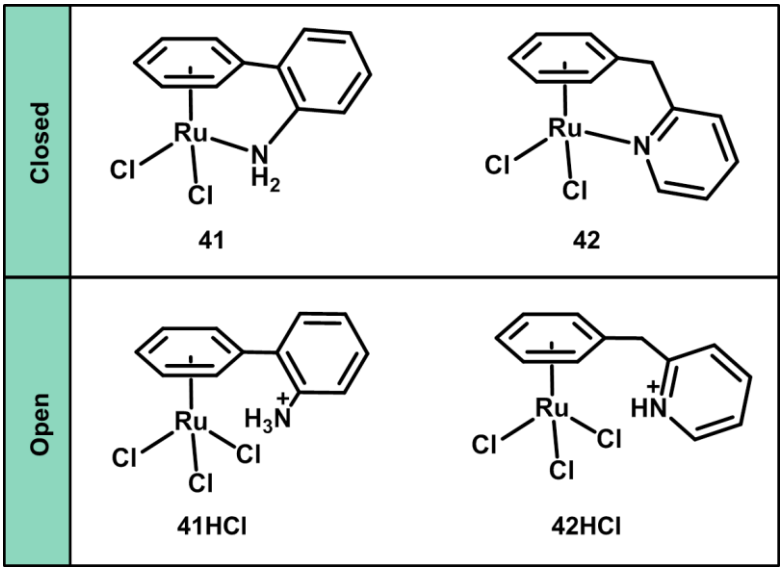

Figure 6.1. Structures of complexes synthesized in this Chapter. Complexes **41** and **42** were synthesised as closed-tether complexes while **41HCl** and **42HCl** are the related protonated open-tether complexes.

Typically, dimer [$RuCl_2(\eta^6$-etb)]$_2$ and the corresponding hemilabile ligand (2-aminobiphenyl or 2-benzylpyridine, respectively) were suspended in 1,2-dichloroethane. The mixture was stirred for 45 min at ambient temperature giving a dark red solution. THF was added, and the mixture degassed with argon for 30 min. The vessel was closed, and the reaction mixture heated under pressure at 393 K (5–16 h). The air-stable microcrystalline material was collected by filtration, washed with chloroform and diethyl ether, and dried in air yielding complexes **41** and **42**. The counterparts open-tether complexes **41HCl** and **42HCl** were obtained when the

corresponding closed complex was suspended in concentrated HCl (37%) and let stir overnight at room temperature. Details of the amounts of reactants, volume of solvents, stirring times, and the nature of the product are described in the Experimental Section for the individual reactions, as well as any variation in the synthetic procedure.

All complexes were insoluble in most common solvents, whereas related complexes, such as [Ru(η^6-biphenyl)(NH_3)Cl_2], [Ru{η^6:κ^1P-(S)-(2-biphenyl)P(OMe)Ph}Cl_2] are reported to be soluble in water, dichloromethane and/or in chloroform.[17,18] After prolonged sonication, dichlorido closed-tether complexes **41** and **42** appeared to dissolve in DMSO-d_6 but detailed examination of the ^{1}H NMR spectra showed a chemical shift pattern consistent with the dmso-adduct [Ru{η^6-$C_6H_5(C_6H_4)NH_2$}(DMSO)Cl_2],[15] where the N(tether) has been displaced by a DMSO molecule. In fact, strongly coordinating solvents such as acetonitrile or DMSO are known to be capable to exchange N-ligands from Ru^{II} complexes such as [Ru (η^6-*p*-cym)(MBZ)Cl_2] where MBZ = non-symmetrical nitrogen-binding benzimidazole ligands or [Ru(η^6:κ^1-PheOH)Cl_2] where PheOH = phenylalanine.[19,20] Because of the ability of some solvents to coordinate to the ruthenium(II) centre and the intrinsic lack of solubility of **41** and **42** in others, all complexes were further characterized by solid state techniques as elemental analysis, powder X-ray diffraction, thermogravimetric analysis and/or single crystal X-ray diffraction to confirm their structures.

6.2.2 Single Crystal X-Ray Diffraction

X-ray diffraction data of suitable crystals corresponding to closed-tether complexes were collected for [Ru{η^6:κ^1-$C_6H_5(C_6H_4)NH_2$}Cl_2] (**41**) and [Ru{η^6:κ^1-$C_6H_5(CH_2)C_5H_4N$}Cl_2] (**42**). The crystallographic analyses revealed that both complexes crystallized in the monoclinic P 2_1/n space group with four molecules in the

unit cell. ORTEP diagrams and atom numbering of **41** and **42** are shown in Figure 6.2. In these complexes, the coordination environment of the Ru^{II} atom retains the half-sandwich geometry in which the η^6-arene ligand occupies half of the coordination sphere (Ru–centroid distances of 1.631 Å for **41** and **42**) using the typical hexahapto coordination mode. Two chlorides and a nitrogen atom from the pendant arm occupy the three remaining coordination sites. Selected bond lengths and angles are shown in Table 6.1, and detailed crystallographic data in Appendix II. Data of **41HCl**,[15] already reported, has been included for comparison purposes.

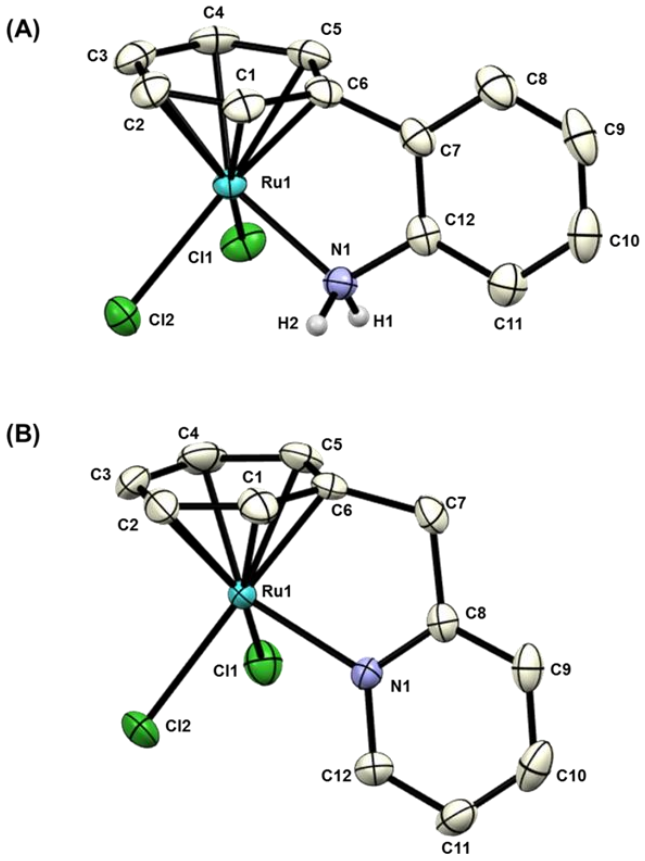

Figure 6.2. Molecular structures and atom numbering of closed tether complexes (A) $[Ru\{\eta^6{:}\kappa^1\text{-}C_6H_5(C_6H_4)NH_2\}Cl_2]$ (**41**) and (B) $[Ru\{\eta^6{:}\kappa^1\text{-}C_6H_5(CH_2)C_5H_4N\}Cl_2]$ (**42**). The hydrogen atoms have been ommited for clarity (except on Nt_{ether} in **41**).

Table 6.1. Crystallographic selected bond lengths (Å) and angles (deg) for complexes $[Ru\{\eta^6:\kappa^1\text{-}C_6H_5(C_6H_4)NH_2\}Cl_2]$ (**41**), $[Ru\{\eta^6:\kappa^1\text{-}C_6H_5(C_6H_4)NH_3\}Cl_3]$ (**41HCl**)[15] and $[Ru\{\eta^6:\kappa^1\text{-}C_6H_5(CH_2)C_5H_4N\}Cl_2]$ (**42**).

Bond / angle	41	42	41HCl[15]
Ru–C6	2.090(3)	2.093(3)	2.1970(18)
Ru–C5	2.142(3)	2.146(4)	2.1798(18)
Ru–C4	2.169(3)	2.165(3)	2.1799(18)
Ru–C3	2.211(3)	2.189(3)	2.1591(18)
Ru–C2	2.180(3)	2.174(4)	2.1707(18)
Ru–C1	2.158(3)	2.164(4)	2.1721(19)
Ru–centroid	1.631	1.631	1.647
Ru–Cl1	2.4193(7)	2.4056(9)	2.4053(5)
Ru–Cl2	2.4126(7)	2.4224(8)	2.4367(4)
Ru–N1	2.140(2)	2.127(3)	2.4175(5)
Cl1-Ru-Cl2	88.20(3)	88.32(3)	87.049(16)
Cl1-Ru-N1	88.20(6)	86.08(8)	87.532(17)
Cl2-Ru-N1	84.77(6)	91.00(8)	86.288(17)
C7–offset[a]	0.497 (+)	0.498 (+)	0.014 (-)
Ru-C6-C7	113.43	115.18	132.05

[a] Offset of C7 with respect to the plane formed by the bound arene (carbons C1–C6); (+) toward ruthenium, (-) away from ruthenium

The Ru–Cl bonds in complexes **41** [2.4193(7), 2.4126(7) Å] and **42** [2.4056(9), 2.4224(8)] are within the range found for other ruthenium(II) arene complexes.[21] The Ru–N bond in complex **41** is longer than that found in complex **42** where de N atom belongs to an aromatic pyridine ring [2.140(2) vs 2.127(3) Å, respectively]. This observation has been reported in related Ru^{II} structures.[22, 23] The Ru–C(arene) bond lengths are in the range 2.090(3)–2.211(3) Å. A tilt in the η^6-bound arene carbon is evidenced by the differences in the Ru–C3 versus Ru–C6 bond lengths [2.211(3) vs 2.090(3) Å, and 2.189(3) vs 2.093(3) Å, for complexes **41** and **42**, respectively]. A strong offset of C7 toward the Ru^{II} atom with regard to the plane that contains the η^6-bound arene, ca. 0.498 Å was observed for both complexes. A similar C7-offset in the range 0.460–0.488 Å was found for closed complexes of general structure $[Ru(\eta^6:\kappa^1\text{-arene:}NH_2)(XY)]^{2+}$.[16] The Ru-C6-C7 angle, where C7 is the first carbon atom of the tether arm, is 113.43 and 115.18º for complexes **41** and **42**, respectively. These

observations are in agreement with others Ru^{II} η^6:κ^1-arene:N closed tether complexes where the same angle for a five-member tether ring has been found to range within 113–115º.[16, 20, 21, 24] The structural analysis comparison between the closed tethered complex **41** and the crystal structure of its related open complex **41HCl**[15] shows a significant difference in the Ru-C6-C7 angle (ca. 114º for **41** and 132.05º for **41HCl**). This angle is an important geometrical parameter which correlates with the strain imposed on the arene by the tether arm. This suggests that the higher the Ru-C6-C7 angle, less strain is imposed, as indicated by the similarity between this angle in **41HCl** and the angle observed for non-strained complexes (ca. 130º).

6.1.1 Solid-state Reaction to Open Closed-Tethered Complexes

Processes in the crystalline phase that involve substrate binding and release, and thus a change in the overall atom content within the unit cell are not very common in the organometallic field. Closed-tether complexes **41** and **42** were chosen to explore the possibility of activating ruthenium(II) organometallic compounds through a solid-state reaction consisting in tether-ring opening. This choice was based on the aqueous chemistry of their derivatives of formula $[Ru(\eta^6:\kappa^1\text{-arene:}NH_2)(XY)]^{2+}$ (where XY is a variety of bidentate ligands), since they showed tuneable reversible pH- and pCl-dependent activation of the Ru–N(tether) bond.[16] We believed they were good candidates as activatable molecules due to the lability of the Ru–N(tether) bond and the relative readiness to form single crystals. Since we had already observed this reaction in the solution state, HCl vapours were thought to be useful in order to promote inclusion of HCl and cleavage of the Ru–N bond to ultimately transform the complexes in their related open-tether species **41HCl** and **42HCl** (Figure 6.3).

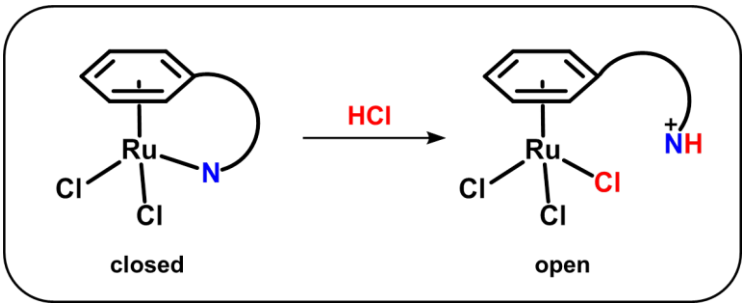

Figure 6.3. Structural re-arrangement of closed complexes **41** or **42** after exposure to HCl vapours to afford open tether complexes (**41HCl** or **42HCl**, respectively). Ru–N bond is cleaved while Ru–Cl and N–H bonds are formed.

For this purpose, crystals of **41** and **42** were exposed to an atmosphere of concentrated aqueous HCl vapours in a sealed vessel at 298 K. The reaction was monitored by powder X-ray diffraction after 2 and 6 days of exposure to the acidic vapours. A colour change of the material (from yellow to red in both cases) seemed to indicate re-arrangement of the ligands around the ruthenium(II) sphere (Figure 6.4). Analogous experiments using H_2SO_4 or HBr as inorganic acids did not result in a change in colour, so they were not used for further investigation.

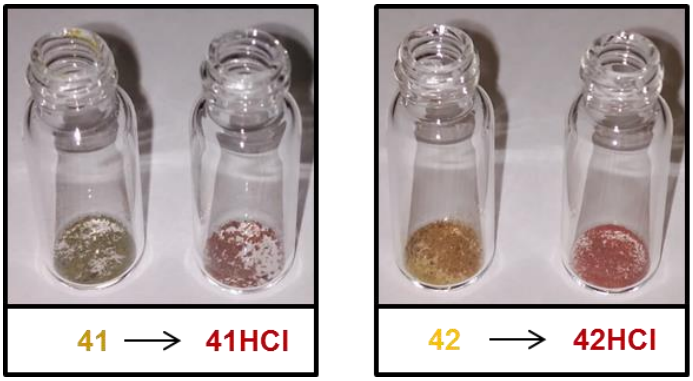

Figure 6.4. Solid-state reactions **41**→ **41HCl** and **42**→ **42HCl** led to a change in colour from yellow (closed-tether complex) to red (open-tether complex) after 6 days of exposure to HCl vapours.

The powder X-ray diffraction analysis of the product obtained by the solid-gas reaction of **41** with HCl vapours is depicted in Figure 6.5. The patterns showed peaks

belonging to the starting complex which decreased significantly, while new signals corresponding to another crystalline phase appeared. The reaction had not reached completion within 2 days (ca. 30%), and 100% conversion could not be obtained by extending the period of reaction with the HCl vapours for 6 days (ca. 60% of conversion). Exposure of HCl vapours even during 27 days for complex **1** did still not show the full conversion (ca. 70%).

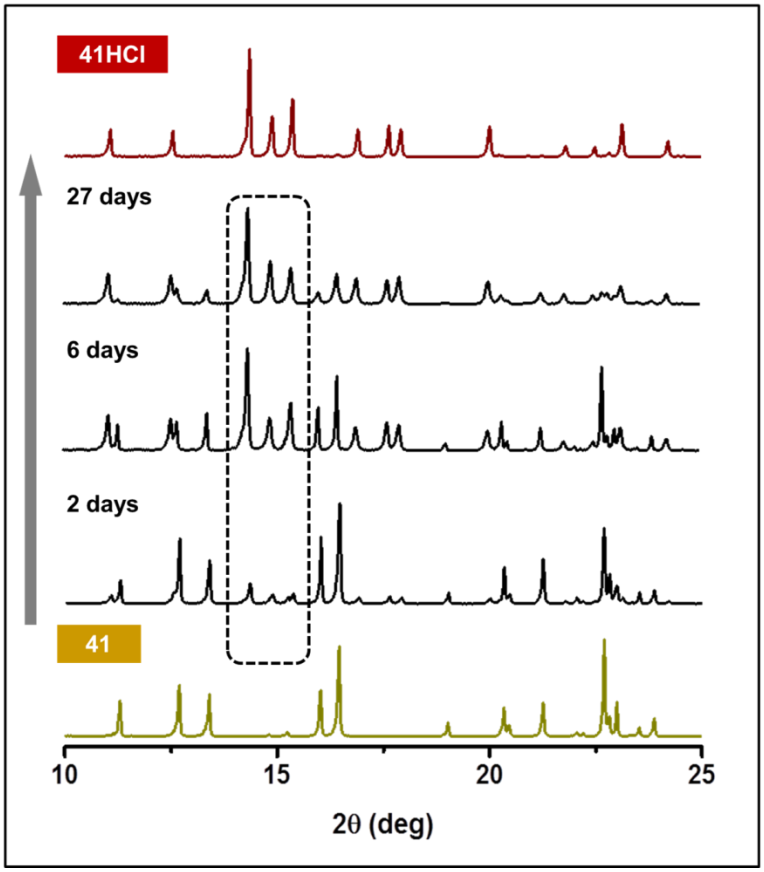

Figure 6.5. Powder X-ray diffraction patterns monitoring the solid-gas reaction of **41** with HCl vapours over time, to afford a mixture that contains remaining **41** and a product identified as **41HCl** (dotted lines). Powder X-ray diffraction patterns for **41** (bottom) and **41HCl** (top) correspond to the complexes synthesised in bulk (and are in accordance with the patterns calculated from their single crystal X-ray structures).

The identity of the new products was attributed to the open-tether species **41HCl**. The powder diffraction pattern calculated on the basis of the crystal structure of **41HCl**[15] was compared with that obtained by the solid-gas reaction and both corresponded to the

same crystalline structure, confirming that partial conversion of **41** to **41HCl** under exposure of HCl vapours took place, as shown in Figure 6.5. The structural features of **41** and **41HCl** are known from single crystal X-ray analyses (Figure 6.6A–B). The powder diffraction diagram of the mixture could be used to determine the ratio of open and closed complexes because their patterns are very different. The precise composition of these mixtures was strongly dependent on the exposure time.

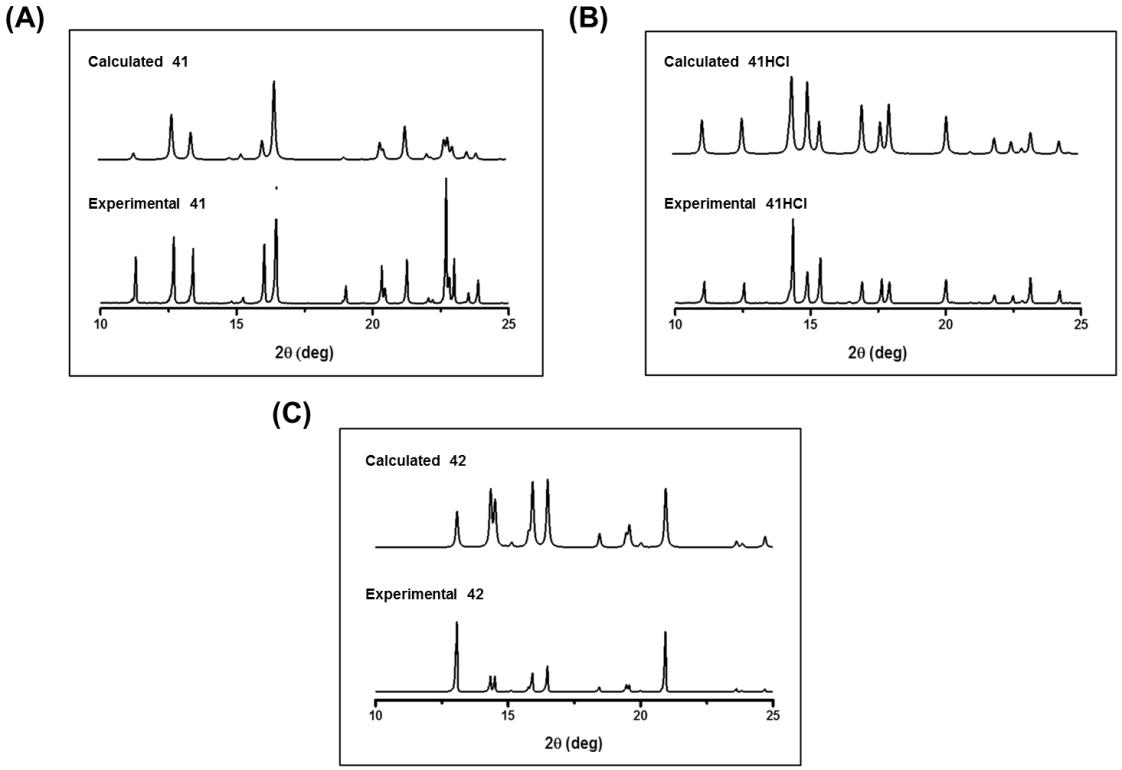

Figure 6.6. Comparison between the powder pattern calculated on the basis of the single crystal structure of **41** (A), **41HCl** (B) and **42** (C) and those determined experimentally on the powder of the complexes synthesized in bulk showing 10–25º 2θ intervals, where the signals of the two involved phases are well distinguishable.

Figure 6.7 shows the powder X-ray diffraction patterns obtained by solid-gas reaction of complex **42** with HCl vapours. Contrary to complex **41**, total consumption of **42** occurred after 6 days of exposure to HCl vapours. The structural feature of **42** is also known from single crystal X-ray analyses (Figure 6.6C), yet not for **42HCl**. A number

of attempts to grow X-ray quality single crystals of **42HCl** were performed unsuccessfully. The pattern resulting for exposure of **42** for 6 days matched to that obtained for **42HCl** synthesised in bulk, as shown in Figure 6.7, although traces of an additional phase was suggested by the appearance of some diffraction peaks of little intensity which are not present in the pattern of **42HCl**. It is worth mentioning that these extra peaks disappeared when the tether-ring opening was reversed to the original closed-tether complex **42** (vide infra).

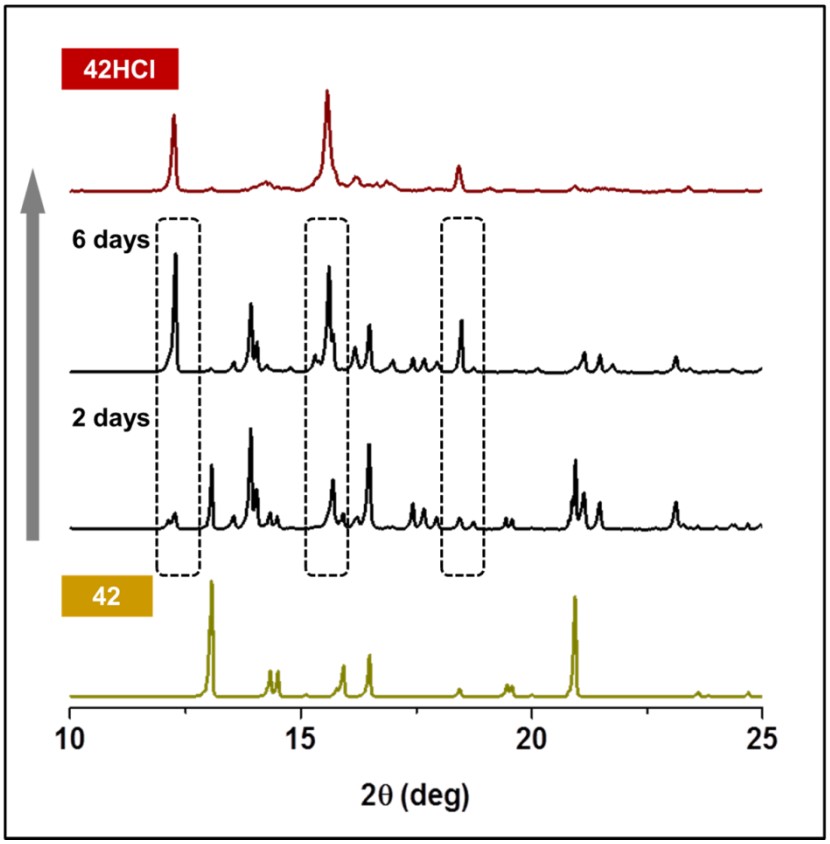

Figure 6.7. Powder X-ray diffraction patterns monitoring of the solid-gas reaction of **42** with HCl vapours overtime. The patterns of **42** (bottom) and **42HCl** (top) correspond to the complexes synthesised in bulk (pattern of **42** is in accordance with the patterns calculated from their single crystal X-ray structures). Dotted lines highlight the prsence of the major product in the mixture, **42HCl**, at 2 and 6 days.

Once the single crystals of **41** and **42** were exposed to acid vapours, transformation to **41HCl** and **42HCl** implied formation of red crystalline powders that were no longer

suitable for a full single crystal X-ray analysis. The geometrical modification around ruthenium(II) was expected to affect the crystallinity. In fact, the loss of crystallinity is a typical event in solid state reactions because most chemical reactions cause considerable stress and intermolecular re-organization.[4] The processes here explained involve multiple changes in covalent and coordinative bonding. Specifically, a HCl molecule is inserted into Ru–N bond requiring rupture of that coordinative bond and formation of coordination Ru–Cl and covalent N–H bonds. The crystalline products, **41HCl** and **42HCl**, now contain three Ru–Cl bonds in an open-ring arrangement rather than two Ru–Cl and one Ru–N bonds in the closed tether-ring geometry of **41** and **42**, consistent with the change in colour. Dissociation of the nitrogen atom from the ruthenium(II) centre is faster for complex **42**. This finding is contrary to our previous results obtained in solution state for analogues complexes described in Chapter 5, where the Ru–N(tether) bond cleavage was faster for the complex containing 2-aminobiphenyl as hemilabile ligand. This is consistent with previous reports that claim that solid-state reactions can promote different reactivity than that observed in the solution phase.[10]

6.1.2 Solid-State Reaction to Close Open-Tether Complexes

In order to explore the possibility of our system to undergo the reversed process, vials containing the red crystalline products obtained after treatment of **41** and **42** with HCl vapours for 6 days were exposed to a mixture 1:1 methanol/water solution of $AgPF_6$ at 298 K for 24 h. A significant colour change back to yellow was observed under microscope examination (Figure 6.8), suggesting the reversible formation of **41** and **42**.

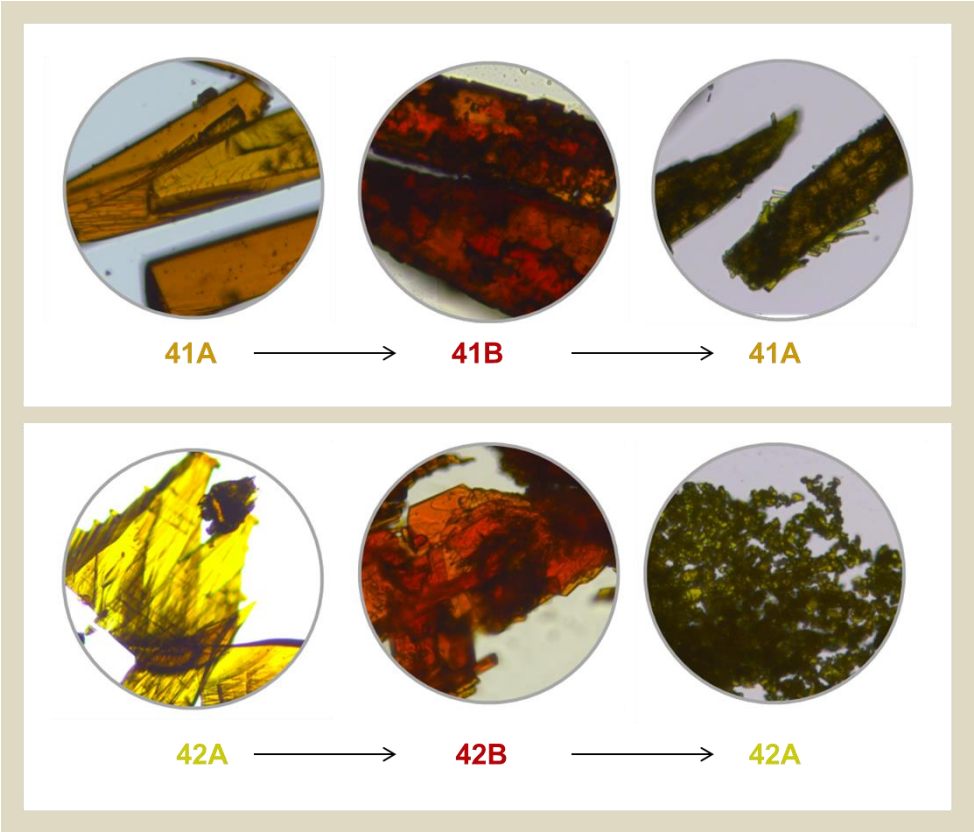

Figure 6.8. Microscopic images obtained for the solid-state reaction of single crystals of **41** and **42** (yellow) with hydrated HCl vapours to afford complexes **41HCl** and **42HCl** (red), and reversible formation to **41** and **42** after exposure with hydrated $AgPF_6$ (yellow; loss of crystallinity).

Remarkably, structural determination of powder X-ray diffraction confirmed unequivocally the total reversibility of the process, reverting back to the original closed complexes **41** and **42**, as depicted in Figure 6.9 and 6.10 for complex **41** and **42**, respectively. Therefore, sequestration of proton and Cl^- ions by the $AgPF_6$ vapours had promoted the extrusion of HCl from the open-tether complexes **41HCl** and **42HCl**. Elemental analysis also confirmed this finding. In the absence of a HCl capturing agent, no apparent reaction occurs in a sealed vessel.

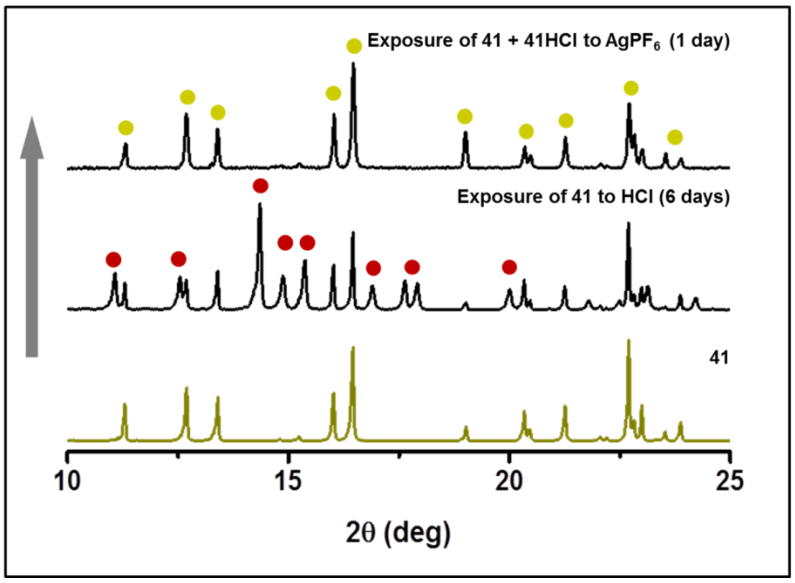

Figure 6.9. Powder X-ray diffraction patterns demonstrating the capture and release of a chlorido ligand by complex **41**. Complex **41** was exposed to HCl vapours for 6 days and new peaks corresponding to **41HCl** appeared, affording a mixture containing both **41** and **41HCl**. When this mixture was exposed to $AgPF_6$ as a HCl capturing agent, peaks corresponding to **41HCl** disappeared completely, demonstrating reversibility of the solid-vapour reaction.

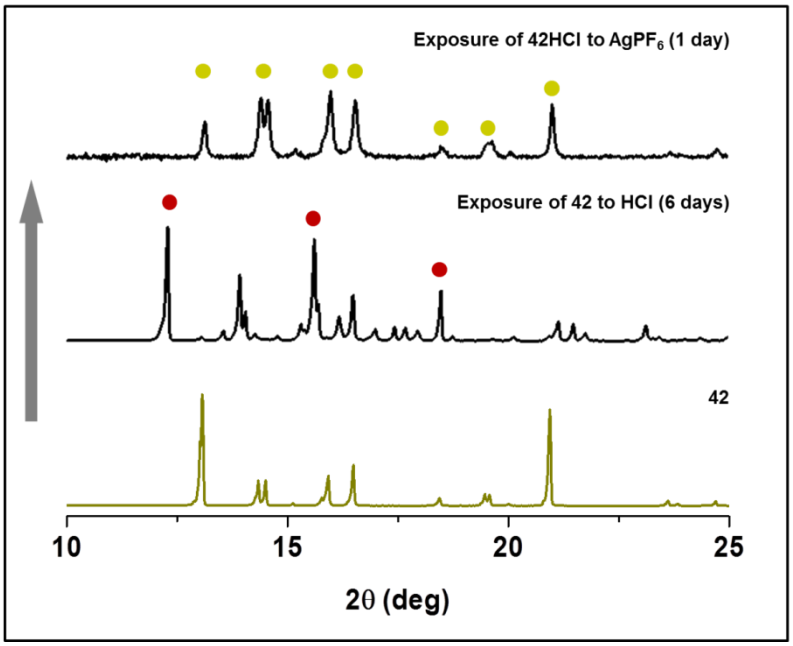

Figure 6.10. Powder X-ray diffraction patterns demonstrating the capture and release of a chlorido ligand by complex **42**. Complex **42** was totally consumed after exposure to HCl vapours for 6 days and new peaks corresponding to **42HCl** appeared (traces of an intermediate phase were also observed). When this mixture was exposed to $AgPF_6$ as a HCl capturing agent, all peaks disappeared completely to afford only peaks corresponding to complex **42**, demonstrating reversibility of the solid-vapour reaction.

We were also interested in verifying the possibility of transforming open complexes **41HCl** and **42HCl** into their counterparts closed complexes **41** and **42** by HCl extrusion by other means than using a HCl scavenger, but vacuum alone was not sufficient even if applied overnight. However, complete de-hydrochlorination could be achieved by heating the complexes for 16 h (at 373 and 423 K, for **41HCl** and **42HCl**, respectively) as suggested by a change in colour (Figure 6.11) and confirmed by the elemental analysis of the resulting crystalline powder. Powder X-ray diffraction patterns unequivocally demonstrated that the heating process led to complete regeneration of the original complexes **41** and **42**.

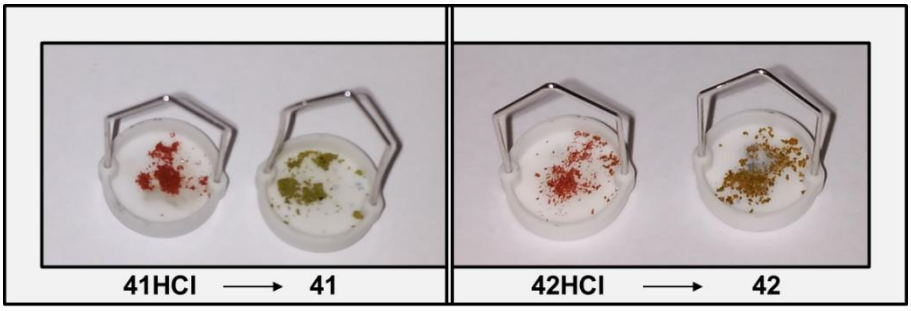

Figure 6.11. Colour changes observed after heating the open complexes **41HCl** and **42HCl** (red) at 373 K and 423 K, respectively, to afford closed tether complexes **41** and **42** (yellow).

Interestingly, when complex **41HCl** was introduced in a sealed vessel close to a pH strip and then heated, the paper indicator changed to red, illustrating the loss of HCl molecules (Figure 6.12). These observations led us to investigate the reversibility of the reaction in depth, to examine the elimination of HCl more closely. In order to do that, the reversibility and kinetics of these crystalline-state reactions were further investigated by thermogravimetric analysis (TGA).

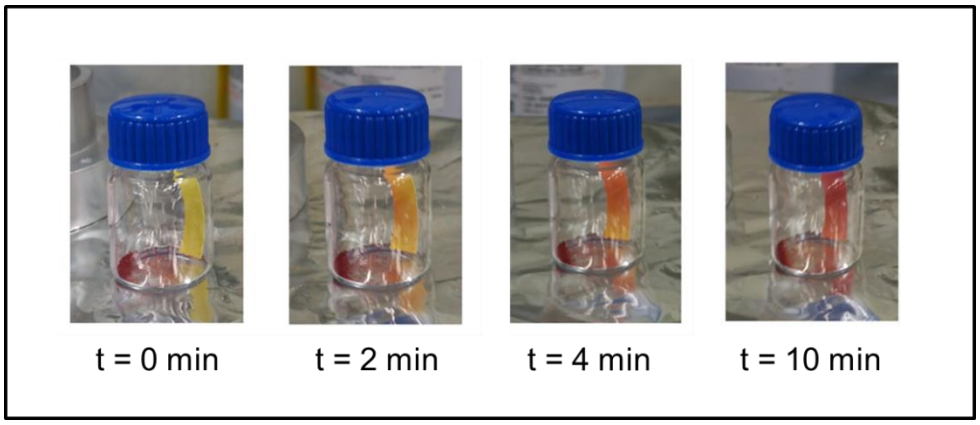

Figure 6.12. Images show complex **41HCl** in a closed vial with a pH strip at 423 K. HCl elimination is indicated by coloration of the pH strip overtime.

The loss of the corresponding HCl molecules to promote the conversion to the closed complexes and the kinetic parameters of the process were investigated by means of TGA for complexes **41HCl** and **42HCl** at different temperatures under a nitrogen atmosphere. The isothermal extrusion of HCl was carried out at 373, 378, 383 and 398 K for **41HCl**, and at 423, 433, 443 and 453 K for complex **42HCl** over 400 min. The temperature dependency of the complete removal of HCl (and hence the re-generation of Ru–N(tether) bonds) for **41HCl** and **42HCl** is shown in Figure 6.13 and 6.14, respectively. Within all temperatures, a weight loss of 9.3% and 9.9% was recorded for **41HCl** and **42HCl**, respectively, corresponding to the elimination of one molecule of HCl per formula unit. At temperatures lower than 348 K for **41HCl** and 398 K for **42HCl**, almost no mass loss occurred.

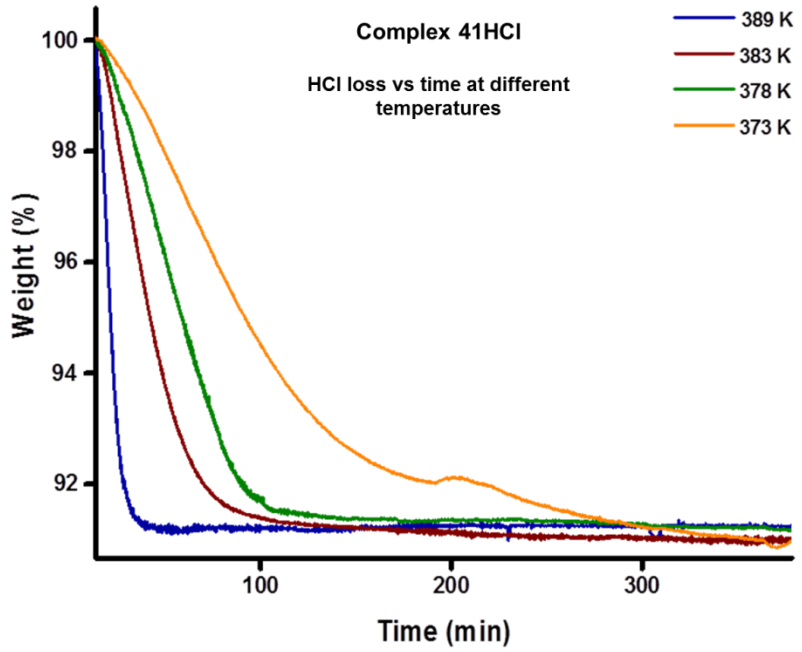

Figure 6.13. Isothermal extrusion of HCl in complex **41HCl** carried out at 373, 378, 383 and 398 K. The graphic shows the weight loss with time, corresponding to one HCl molecule per formula unit.

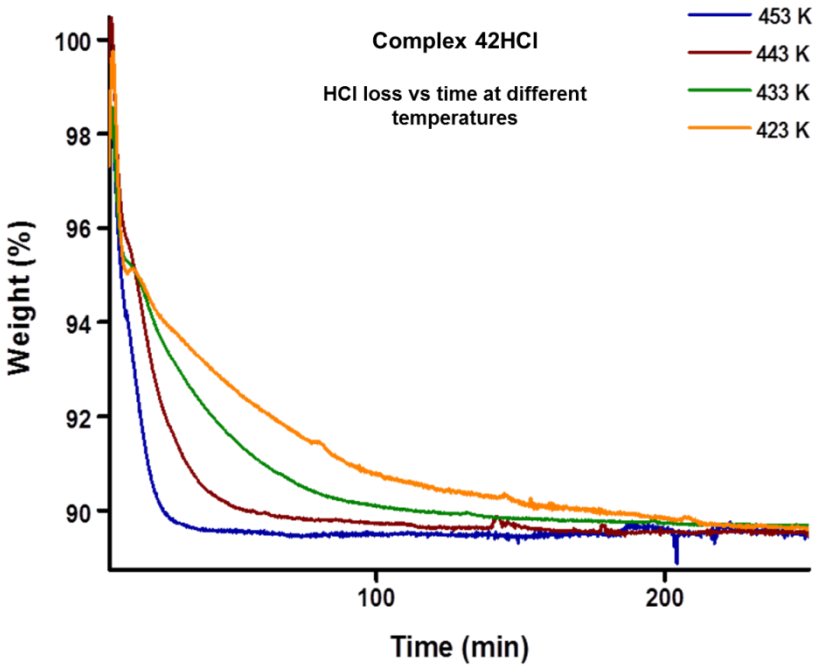

Figure 6.14. Isothermal extrusion of HCl in complex **42HCl** carried out at 423, 433, 443 and 453 K. The graphic shows the weight loss with time, corresponding to one HCl molecule per formula unit.

In each case the temperature dependency of the HCl loss followed first-order kinetics, corresponding to the rate constant k_{-HCl} and half-lives listed in Table 6.2. The rate of conversion toward closed-tether complexes was found to be markedly temperature-dependent, increasing with an increase in temperature. The rate constants varied one order of magnitude with increasing temperature from 373 K to 398 K for **41HCl** ($1.84 \cdot 10^{-4}$ vs $3.34 \cdot 10^{-3}$ s^{-1}, respectively), and from 423 K to 453 K for **42HCl** ($2.66 \cdot 10^{-4}$ and $2.30 \cdot 10^{-3}$ s^{-1}, respectively). Moreover, these results show that the closure of the complex by extruding HCl molecules by heating is faster for **41HCl** than for **42HCl**.

Table 6.2. Rate constants and half-lives obtained for the heat-mediated HCl elimination reaction for complexes **41HCl** and **42HCl**.

41HCl	**398 K**	**383 K**	**378 K**	**373 K**
k(s^{-1})	3.34E-03	5.61E-04	4.75E-04	1.84E-04
$t_{1/2}$(s)	207.31	1235.91	1457.75	3769.08
r^2	0.9944	0.9906	0.9813	0.9886

42HCl	**453 K**	**443 K**	**433 K**	**423 K**
k(s^{-1})	0.0023	0.0012	5.161E-4	2.661E-4
$t_{1/2}$(s)	301.87	579.58	1342.99	2604.83
r^2	0.99211	0.99309	0.99508	0.99265

Contrary to **42**, which was fully converted to its corresponding open complex **42HCl** in 6 days, complex **41** could not be fully converted to **41HCl** even after exposure of 27 days. This is in accordance with the high rate constant obtained for the closure reaction to afford complex **41**, showing a preference of complex **41** to be maintained in its closed form.

Determination of the rate constants at different temperatures allowed for determination of the activation energy (E_a), activation enthalpy ($\Delta H^{\dagger}$) and activation entropy ($\Delta S^{\dagger}$). The activation parameters resulting from the Arrhenius and Eyring plots for the de-hydrochlorination are listed in Table 6.3. The $\Delta S^{\dagger}$ term is very informative, since the activation entropies for **41HCl** and **42HCl** (41.76 and -49.72 J K^{-1} mol^{-1}, respectively) can help determine whether the reaction occurs through an associative or dissociative mechanism.[25, 26] The positive value obtained for **41HCl** indicates that the closure reaction to afford closed complex **41** takes places via a dissociative mechanism, which shows an increase in the randomness when the complex reaches its transition state. Conversely, complex **42HCl** appears to eliminate its HCl molecule via an associative mechanism due to the negative value obtained for the activated entropy, implicating that there are less molecules/ions present in the transition state than in the reactants, where the metal increases its coordination number in the activated complex.

Table 6.3. Kinetics parameters obtained from the Arrhenius and Eyring plots for the HCl elimination reaction for complexes **41HCl** and **42HCl**.

	E_a (KJ mol^{-1})	**$\Delta H^{\dagger}$(KJ mol^{-1})**	**$\Delta S^{\dagger}$ (J K^{-1} mol^{-1})**
41HCl	137.18	133.95	41.76
42HCl	116.49	112.86	-49.72

6.3 Conclusions

We have described the synthesis of closed-tether complexes **41** and **42**, and their counterparts open-tether complexes **41HCl** and **42HCl**. The crystallographic structures for **41** and **42** have been elucidated and discussed. The solid-state reaction of **41** and **42** with vaporous HCl triggered the activation of the Ru–N(tether) bond to afford **41HCl** and **42HCl**, accompanied by a change in colour from yellow to red. Total activation for complex **41** was not achieved after 27 days (ca. 70%), contrary to **42** which after 6 days of exposure to HCl underwent total conversion. This suggests that complex **42** promotes the ring opening process more efficient than **41**, contrary to studies in solution-state for investigated analogues previously inthis dissertation. Interestingly, the reaction in the solid state of open-tether complexes **41HCl** and **42HCl** with vaporous $AgPF_6$ as a HCl-capture agent promoted the completely reversible reaction toward the closed-tether analogues **41** and **42**. Similar results were obtained through a heat-mediated reaction at 373 K for **41HCl** and 423 K for **42HCl**, where the expected change in colour red to yellow also occurred. The loss of the corresponding HCl molecules to promote the conversion to the closed complexes and the kinetic parameters of the process showed that complex **42HCl** requires a higher range of temperatures than that for **41HCl**, to carried out the closure of the complex. In other words, **42HCl** needed more energy to convert into **42**, than **41HCl** to convert into **41**.The activation entropies for **41HCl** and **42HCl** (41.76 and -49.72 J K^{-1} mol^{-1}, respectively) seem to indicate that a dissociative mechanism occurs for the closure reaction of **41HCl**, but an associative mechanism occurs for the elimination of the HCl molecule in **42HCl**. This highlights how isostructural hemilabile ligands (but with different rigidity in the tether arm and different functional group coordinated to the metal centre, i.e. NH_2 vs N_{pyr}) can afford complexes with different mechanism for ring-closure reactions. These results describe

unprecedented HCl capturing and realising behaviour for ruthenium(II) complexes, phenomena that can be tuned via hemilabile ligand variation. Extensive investigations are planned in our laboratory to extend this study and clarify our understanding of the reaction mechanisms for the bond-breaking and bond-making steps in the described solid-state reactions.

6.4 Experimental Section

6.4.1 Instrumentation

NMR Spectroscopy and **Elemental Analysis** have been described in Chapter 2.

Single Crystal X-ray Diffraction. Suitable crystals of compounds **41** and **42** were coated with mineral oil and mounted on Mitegen MicroMounts. The samples were measured in a Bruker D8 KAPPA APEX II diffractometer with CCD area-detector, equipped with graphite-monochromated Mo Kα radiation (λ = 0.71073 Å). The substantial redundancy in data allowed empirical absorption corrections (SADABS)[27] to be applied using multiple measurements of symmetry-equivalent reflections. Raw intensity data frames were integrated with the SAINT program, which also applied corrections for Lorentz and polarization effects. The Bruker SHELXTL Software Package was used for space group determination, structure solution, and refinement.[28] The space group determination was based on a check of the Laue symmetry, and systematic absences were confirmed using the structure solution. The structures were solved by direct methods (SHELXL-2014/7),[29, 30] completed with different Fourier syntheses, and refined with full-matrix least-squares using SHELXS minimizing $\omega(F_o^2 - F_c^2)^2$. Weighted R factors (R_w) and goodness of fit (S) are based on F^2; conventional R factors (R) are based on F. All non-hydrogen atoms were refined with anisotropic displacement parameters. Hydrogen atom positions were geometrically calculated and allowed to ride on their parent carbon or nitrogen atoms with fixed isotropic U. All scattering factors and anomalous dispersion factors are contained in the SHELXTL 6.10 program library.

CCDC identifiers are 1812917 and 1523006 for **41** and **42**, respectively. These data are provided free of charge by The Cambridge Crystallographic Data Centre.

Powder X-ray diffraction. All of the samples were lightly ground in an agate mortar. Powder X-ray diffractograms were collected at ambient temperature on a Panalytical X'Pert PRO diffractometer (Cu-Kα_1 X-radiation, λ_1 = 1.5406 Å) equipped with a X'Celerator detector and a flat-plate sample holder Bragg-Brentano para-focusing optics configuration (45 kV, 40 mA). Intensity data were collected by the step-counting method (step 0.0167º), in continuous mode, in the $10 \leq 2\theta \leq 60º$ range. The program Mercury was used for calculation of powder X-ray patterns.

Thermogravimetric analysis. TGA studies were carried out using a TA Instruments TGAQ500 system under nitrogen atmosphere with a flow rate of 10 mL/min. The sample size used for each isothermal TG run was kept small and relatively constant (0.5–1.1 mg) for each experiment. The material was evenly spread at the bottom of the pan before being placed in the TG instrument to ensure consistent and reproducible results.

Solid-state reactions. Exposure to the hydrated HCl vapours was carried out by placing a small vial, containing the powder sample of complexes **41** or **42**, in a cylindrical bottle containing 5 mL of the acid aqueous solution (HCl, 37%) at room temperature for the days described for each particular experiment. The powder and the solution were not in contact. The reaction took place in a closed system. A change of colour of the powder from yellow to orange occurred within hours, yet the samples were allowed to react for 6 days, time during which the powder became red in colour.

Solid-state reactions with $AgPF_6$ were carried out as follows. A vial containing powder Ru^{II} complex **41HCl** or **42HCl** was introduced in a cylindrical bottle with 130 mg of $AgPF_6$ dissolved in a 1:1 mixture water/methanol solution (5 mL). The powder and the solution were not in contact. The reaction took place over 24 h inside a closed system, showing a change in colour over time.

Heat-mediated reactions of complex **41HCl** at 373 K and **42HCl** at 423 K in the solid state were carried out as follows. The crystalline powder was spread over a glass holder which was placed on a heating plate at the desire temperature overnight. The reaction took place in an open system and the solids changed colour from red to yellow.

6.4.2 Synthesis

MATERIALS

$RuCl_3 \cdot 3H_2O$ was acquired from Precious Metals Online and Johnson Matthey Fine Chemicals. Ethyl benzoate was adquired from Sigma Aldrich. Dichloroethane, 2-aminobiphenyl, 2-benzylpyridine, silver hexafluorophosphate and hydrochloride acid 37% were purchased from Acros Organics, and iodine from Fisher. Ethanol, dry methanol, diethyl ether, tetrahydrofuran and sodium metal were purchased from Sharlau. For NMR spectroscopy, the solvent used was DMSO-d_6 from VWR International.

PREPARATION OF COMPLEXES

The Ru^{II} dimer $[Ru(\eta^6\text{-etb})Cl_2]_2$ where etb is ethyl benzoate was synthesized following the reported synthesis by Habtemariam et al..[31] and is described in Chapter 2. The dichlorido complexes $[Ru\{\eta^6{:}\kappa^1\text{-}C_6H_5(C_6H_4)NH_2\}Cl_2]$ (**41**) and $[Ru\{\eta^6{:}\kappa^1\text{-}C_6H_5(CH_2)C_5H_4N\}Cl_2]$ (**42**) were synthesized via thermal displacement of ethyl

benzoate in the Ru^{II} dimer $[Ru(\eta^6\text{-etb})Cl_2]_2$ by the hemilabile ligand (2-aminobiphenyl or 2-benzylpyridine) in 1,2-dichloroethane under pressure overnight as reported by Pizarro et al.[16, 32] Subsequent reaction of the corresponding dichlorido complex with HCl aqueous solution overnight, afforded the open-tether complexes $[Ru\{\eta^6\text{-}C_6H_5(C_6H_4)NH_3\}Cl_3]$ (**41HCl**) and $[Ru\{\eta^6\text{-}C_6H_5(CH_2)C_5H_4NH\}Cl_3]$ (**42HCl**).

$[Ru\{\eta^6\text{:}\kappa^1\text{-}C_6H_5(C_6H_4)NH_2\}Cl_2]$ (41). $[RuCl_2(\eta^6\text{-etb})]_2$ (200 mg, 0.310 mmol) and 2-aminobiphenyl (105 mg, 0.620 mmol) were suspended in 1,2-dichloroethane (25 mL). The reaction mixture was heated under pressure at 393 K for 5 h. The red crystals were collected by filtration, washed with acetone and diethyl ether, and dried in air. Yield: 202 mg (95%). Elemental analysis: Cald for $C_{12}H_{11}Cl_2NRu$ (341.20): C, 42.24; H, 3.25; N, 4.11. Found: C, 42.11; H, 3.22; N, 3.97. TGA (isotherm at 150 ºC for 300 min): observed loss <1%. Suitable crystals for X-ray diffraction were obtained from the reaction mixture. Formation of **41A** and phase purity were confirmed by powder X-ray diffraction.

$[Ru\{\eta^6\text{:}\kappa^1\text{-}C_6H_5(C_6H_4)NH_2\}Cl_2]$ (41HCl). Complex $[Ru\{\eta^6\text{:}\kappa^1\text{-}C_6H_5(C_6H_4)NH_2\}Cl_2]$ (**1**) (71 mg, 0.211 mmol) was suspended in 37% HCl and left stirring at ambient temperature for 18 h. The solvent was removed and the red powder was collected by filtration, washed with ethanol and diethyl ether, and dried in vacuum. Yield: 62 mg (78%). Elemental analysis: Cald for $C_{12}H_{12}Cl_3NRu$ (377.66): C, 38.16; H, 3.20; N, 3.71. Found: C, 38.82; H, 3.45; N, 3.57. ^{1}H NMR (400 MHz, DMSO-d_6, δ): 7.38 (d, J = 7.7 Hz, Ar H, 1H), 7.16 (t, J = 7.4 Hz, Ar H, 1H), 6.80 (d, J = 8.0 Hz, Ar H, 1H), 6.67 (t, J = 7.4 Hz, Ar H, 1H), 6.22 (d, J = 6.0 Hz, Ar H, 2H), 6.13 (t, J = 5.5 Hz, Ar H, 1H), 5.95 (t, J = 5.9 Hz, Ar H, 2H). TGA (isotherm at 150 ºC for 300 min): observed loss: 9.3%;

calculated loss for 1 molecule of HCl: 9.7%. The crystal structure of this complex has been previously reported.[15] Formation of **41HCl** and phase purity were confirmed by powder X-ray diffraction.

[Ru{η^6:κ^1-C$_6$H$_5$(CH$_2$)C$_5$H$_4$N}Cl$_2$] (42). [RuCl$_2$(η^6-etb)]$_2$ (117 mg, 0.182 mmol) and 2-benzylpyridine (58 μL, 0.364 mmol) were suspended in 1,2-dichloroethane (12 mL). The reaction mixture was heated under pressure at 393 K for 16 h. A pale yellow powder was collected by filtration, washed with acetone and diethyl ether, and dried in air. Yield: 92 mg (75%). Elemental analysis: Cald for $C_{12}H_{11}Cl_2NRu$ (341.20): C, 42.24; H, 3.25; N, 4.11. Found: C, 42.45; H, 3.26; N, 3.95. TGA (isotherm at 150 ºC for 300 min): observed loss <1%. Single crystals suitable for X-ray diffraction were obtained from the reaction mixture. Formation of **2** and phase purity were confirmed by powder X-ray diffraction.

[Ru{η^6:κ^1-C$_6$H$_5$(CH$_2$)C$_5$H$_4$N}Cl$_2$] (42HCl). Complex [Ru{η^6:κ^1-C$_6$H$_5$(CH$_2$)C$_5$H$_4$N}Cl$_2$] (**42**) (59 mg, 0.175 mmol) was suspended in aqueous 37% HCl and left stirring at ambient temperature for 18 h. Solvent was removed until dryness. The red powder was collected by filtration, washed with ethanol and diethyl ether, and dried in vacuum. Yield: 46 mg (70%). Elemental analysis: Cald for $C_{12}H_{12}Cl_3NRu$ (377.66): C, 38.16; H, 3.20; N, 3.71. Found: C, 38.07; H, 3.35; N, 3.61. ^{1}H NMR (400 MHz, DMSO-d_6, δ): 7.95 (td, *J* = 7.7, 1.7 Hz, Ar H, 1H), 7.76 (dd, *J* = 5.8, 1.4 Hz, Ar H, 1H), 7.50 (d, *J* = 7.9 Hz, Ar H, 1H), 7.36 (t, *J* = 6.7 Hz, Ar H, 1H), 5.99 (t, *J* = 5.8 Hz, Ar H, 2H), 5.79 (d, *J* = 5.8 Hz, Ar H, 2H), 5.56 (t, *J* = 5.6 Hz, Ar H, 1H), 4.43 (s, –C*H*$_2$–, 2H). TGA (isotherm at 150 ºC for 300 min): observed loss: 9.9%; calculated loss

for 1 molecule of HCl: 9.7%. The phase purity was established by X-ray powder diffraction.

6.5 References

(1) Bacchi, A.; Bourne, S.; Cantoni, G.; Cavallone, S. A. M.; Mazza, S.; Mehlana, G.; Pelagatti, P.; Righi, L. Reversible Guest Removal and Selective Guest Exchange with a Covalent Dinuclear Wheel-and-Axle Metallorganic Host Constituted by Half-Sandwich Ru(II) Wheels Connected by a Linear Diphosphine Axle. *Cryst. Growth Des.* **2015**, *15*, 1876-1888.

(2) Vaska, L. Stereospecific Addition of Hydrogen Halides to Tetragonal d8 Complexes. *J. Am. Chem. Soc.* **1966**, *88*, 5325-5327.

(3) Cook, P. M.; Dahl, L. F.; Hopgood, D.; Jenkins, R. A. Oxidative-Addition Reaction of Platinum Acetylacetonate with Iodine in Solid State and Solution. Crystal Structure and Equilibrium Studies of trans-bis(acetylacetonato)di-iodoplatinum(IV). *J. Chem. Soc., Dalton Trans.* **1973**, 10.1039/DT9730000294.294-301.

(4) Albrecht, M.; Lutz, M.; Spek, A. L.; van Koten, G. Organoplatinum Crystals for Gas-Triggered Switches. *Nature* **2000**, *406*, 970-974.

(5) Vitorica-Yrezabal, I. J.; Sullivan, R. A.; Purver, S. L.; Curfs, C.; Tang, C. C.; Brammer, L. Synthesis and Polymorphism of (4-ClpyH)2[CuCl4]: Solid-Gas and Solid-Solid Reactions. *CrystEngComm* **2011**, *13*, 3189-3196.

(6) Minguez Espallargas, G.; Florence, A. J.; van de Streek, J.; Brammer, L. Different Structural Destinations: Comparing Reactions of [CuBr2(3-Brpy)2] Crystals with HBr and HCl Gas. *CrystEngComm* **2011**, *13*, 4400-4404.

(7) Mínguez Espallargas, G.; van de Streek, J.; Fernandes, P.; Florence, A. J.; Brunelli, M.; Shankland, K.; Brammer, L. Mechanistic Insights into a Gas–Solid Reaction in Molecular Crystals: The Role of Hydrogen Bonding. *Angew. Chem. Int. Ed.* **2010**, *49*, 8892-8896.

(8) Jeffrey, J. C.; Rauchfuss, T. B. Metal Complexes of Hemilabile Ligands. Reactivity and Structure of Dichlorobis(o-(diphenylphosphino)anisole)Ruthenium(II). *Inorg. Chem.* **1979**, *18*, 2658-2666.

(9) Braunstein, P.; Naud, F. Hemilability of Hybrid Ligands and the Coordination Chemistry of Oxazoline-Based Systems. *Angew. Chem. Int. Ed.* **2001**, *40*, 680-699.

(10) Werner, H.; Rappert, T.; Baum, M.; Stark, A. Metallorganische Chemie in Fester Phase: Umlagerungs-, eEiminierungs-und Additionsreaktionen von Organometallverbindungen Ohne Solvens. *J. Organomet. Chem.* **1993**, *459*, 319-323.

(11) McGee, K. A.; Veltkamp, D. J.; Marquardt, B. J.; Mann, K. R. Porous Crystalline Ruthenium Complexes Are Oxygen Sensors. *J. Am. Chem. Soc.* **2007**, *129*, 15092-15093.

(12) McGee, K. A.; Marquardt, B. J.; Mann, K. R. Concurrent Sensing of Benzene and Oxygen by a Crystalline Salt of Tris(5,6-dimethyl-1,10-phenanthroline)ruthenium(II). *Inorg. Chem.* **2008**, *47*, 9143-9145.

(13) Wenger, O. S. Vapochromism in Organometallic and Coordination Complexes: Chemical Sensors for Volatile Organic Compounds. *Chem. Rev.* **2013**, *113*, 3686-3733.

(14) Nagel, C. C. Thermochromic Double-Complex Salts 1989.

(15) Pizarro, A. M.; Melchart, M.; Habtemariam, A.; Salassa, L.; Fabbiani, F. P. A.; Parsons, S.; Sadler, P. J. Controlling the Reactivity of Ruthenium(II) Arene Complexes by Tether Ring-Opening. *Inorg. Chem.* **2010**, *49*, 3310-3319.

(16) Martínez-Peña, F.; Pizarro, A. M. Control of Reversible Activation Dynamics of [Ru(η6:κ1-C6H5(C6H4)NH2)(XY)]n+ and the Effect of Chelate Ligand Variation. *Chem. Eur. J.* **2017**, 10.1002/chem.201703853.

(17) Betanzos-Lara, S.; Habtemariam, A.; Clarkson, G. J.; Sadler, P. J. Organometallic cis-Dichlorido Ruthenium(II) Ammine Complexes. *Eur. J. Inorg. Chem.* **2011**, *2011*, 3257-3264.

(18) Navarro, M.; Vidal, D.; Clavero, P.; Grabulosa, A.; Muller, G. Mild Photochemical Tethering of [RuCl2(η6-arene)P*] Complexes with P-Stereogenic 2-Biphenylylphosphines. *Organometallics* **2015**, *34*, 973-994.

(19) Patra, M.; Joshi, T.; Pierroz, V.; Ingram, K.; Kaiser, M.; Ferrari, S.; Spingler, B.; Keiser, J.; Gasser, G. DMSO-Mediated Ligand Dissociation: Renaissance for Biological Activity of N-Heterocyclic-[Ru(η6-arene)Cl2] Drug Candidates. *Chem. Eur. J.* **2013**, *19*, 14768-14772.

(20) Reiner, T.; Jantke, D.; Miao, X.-H.; Marziale, A. N.; Kiefer, F. J.; Eppinger, J. Phenylalanine - a Biogenic Ligand with Flexible η6- and η6:κ1-Coordination at Ruthenium(II) Centres. *Dalton Trans.* **2013**, *42*, 8692-8703.

(21) Melchart, M.; Habtemariam, A.; Novakova, O.; Moggach, S. A.; Fabbiani, F. P. A.; Parsons, S.; Brabec, V.; Sadler, P. J. Bifunctional Amine-Tethered Ruthenium(II) Arene Complexes Form Monofunctional Adducts on DNA. *Inorg. Chem.* **2007**, *46*, 8950-8962.

(22) Tyagi, D.; Binnani, C.; Rai, R. K.; Dwivedi, A. D.; Gupta, K.; Li, P.-Z.; Zhao, Y.; Singh, S. K. Ruthenium-Catalyzed Oxidative Homocoupling of Arylboronic Acids in Water: Ligand Tuned Reactivity and Mechanistic Study. *Inorg. Chem.* **2016**, *55*, 6332-6343.

(23) Gupta, D. K.; Sahay, A. N.; Pandey, D. S.; Jha, N. K.; Sharma, P.; Espinosa, G.; Cabrera, A.; Puerta, M. C.; Valerga, P. Synthesis, Characterization, Reactivity and Structure of Some Mono and Binuclear (η6-p-cymene)ruthenium(II) Complexes. *J. Organomet. Chem.* **1998**, *568*, 13-20.

(24) Ito, M.; Endo, Y.; Ikariya, T. Well-Defined Triflylamide-Tethered Arene−Ru(Tsdpen) Complexes for Catalytic Asymmetric Hydrogenation of Ketones. *Organometallics* **2008**, *27*, 6053-6055.

(25) Porterfield, W. W. *Inorganic Chemistry*; Elsevier Science: 2013.

(26) Williams, A. F. *A Theoretical Approach to Inorganic Chemistry*; Springer Berlin Heidelberg: 2013.

(27) Bruker. *APEX2,SAINT and SADABS*; Bruker AXS: Madison, WI, 2008.

(28) Bruker. *SHELXTL Version 6.10, Structure Determination Package*; Bruker AXS: Madison, WI, 2000.

(29) Sheldrick, G. M. A Short History of SHELX. *Acta Crystallogr. Sect. A* **2008**, *64*, 112-122.

(30) Sheldrick, G. M. Crystal Structure Refinement with SHELXL. *Acta Crystallogr. Sect. C* **2015**, *71*, 3-8.

(31) Abraha Habtemarian, S. B.-L., and Peter J. Sadler. *Ruthenium Complexes, in Inorganic Syntheses*; John Wiley & Sons: 2010.

(32) Pizarro, A. M.; Melchart, M.; Habtemariam, A.; Salassa, L.; Fabbiani, F. P. A.; Parsons, S.; Sadler, P. J. Controlling the Reactivity of Ruthenium(II) Arene Complexes by Tether Ring-Opening. *Inorg. Chem.* **2010**, *49*, 3310-3319.

General Conclusions

In this dissertation a family of ruthenium-based metallodrugs, which are design to target the disrupted metabolism in the cancer cell, has been developed. For this purpose, a tethered ruthenium(II) arene scaffold was selected and the activation of the Ru–Z bond was extensively explored by following different strategies. Structural modifications have been performed both on the hemilabile ligand and on the chelating ligand with the aim of finely tuning the activation of the κ^1Z bond under different conditions.

The results obtained in this Thesis allows us to conclude that:

The novel structure-activation relationship established between the new tethered complexes of formula $[Ru(\eta^6{:}\kappa^1\text{-arene:Z})(en)]^{n+}$ in which only a building block is varied (tether hemilabile ligand), is a useful method to gain information about the hemilabile ligand structural features and how they affect the susceptibility of Ru–Z activation. Both length and rigidity of the spacer, and the nature of the donor atom that closes the tether appear to play a key role in the activation of the Ru–Z bond. We demonstrate that complexes with κ^1N-coordination bearing aromatic amines are more prone to activation than those containing aliphatic amines as donor group. Also, we determine that κ^1O-coordination is weaker than κ^1N-coordination.

Complexes containing 2-aminobiphenyl as hemilabile ligand, $[Ru(\eta^6{:}\kappa^1\text{-}C_6H_5(C_6H_4)NH_2)(XY)]Cl_n$, were excellent scaffolds to understand the ring-opening and ring-closing processes in view of the development of new pH-activatable metallodrugs. Our complexes showed activation, to different extents and at different rates, of the Ru–Z bond in different solvents. We determine that the activation under acidic conditions is

fully reversible and it can be modulated by the electronic and steric effects provided by varying the chelating ligand (XY). Moreover, only open-tether complexes were susceptible to interact with nucleobases, validating the pro-drug approach in this new family of complexes.

The complexes containing phenylacetic acid as hemilabile ligand (κ^1O-coordination) are promising structures to build reversible pH-dependent systems. The activation of the Ru–Z bond was finely tuned by changing the chelating ligand. The extensive study about their speciation in aqueous solution demonstrates how these species can be pH controlled. Also, we determine that these complexes can undergo selective hydrogen-transfer reactions, proving that ring-opening is involved in the catalytic cycle. More importantly, we demonstrate that these complexes can reduce NAD^+ to NADH and this might have an effect inside the cell in presence of formate, decreasing the IC_{50} value compared to that in absence of formate.

We demonstrate that the rigidity of the tether arm provides an important feature for the ring-opening process, making the process faster. Preliminary photo-irradiation experiments helped us to start to understand the behaviour of these complexes under light excitation. However, we determine that irradiation of these tether complexes does not provide a useful methodology to activate the Ru–Z bond, demonstrating that the tethering feature in the structure of the Ru-arene (i) provides the complex with extraordinary structural stability, (ii) affords complexes with different reactivity when compared with their un-tether counterparts under light irradiation, and (iii) the photo-reactivity of the tether complexes within a series differs from that in the dark.

The solid-state reaction of closed tether complexes with vaporous HCl triggers the activation of the Ru–N(tether) bond accompanied by a change in colour. The novelty in this area lies on (i) the selectivity of dissociating the donor atom from the ruthenium centre only when the vapour is HCl (but not when it comes from HBr or H_2SO_4 solutions), (ii) different activation rates depending on the hemilabile ligand (influenced by the rigidity and the donor atom), and (iii) the reversibility to the original complex using a HCl scavenger and upon heating. Therefore, these complexes could serve as gas sensors.

In summary, the results reported in this dissertation describe a novel family of tethered ruthenium(II) arene complexes as a unique scaffold in cancer drug discovery. They can serve as new pharmacological tools to exploit the particular pericellular environment of the cancer cell.

Appendix I

NMR Spectra

Appendix I

^{1}H NMR Complex **1**

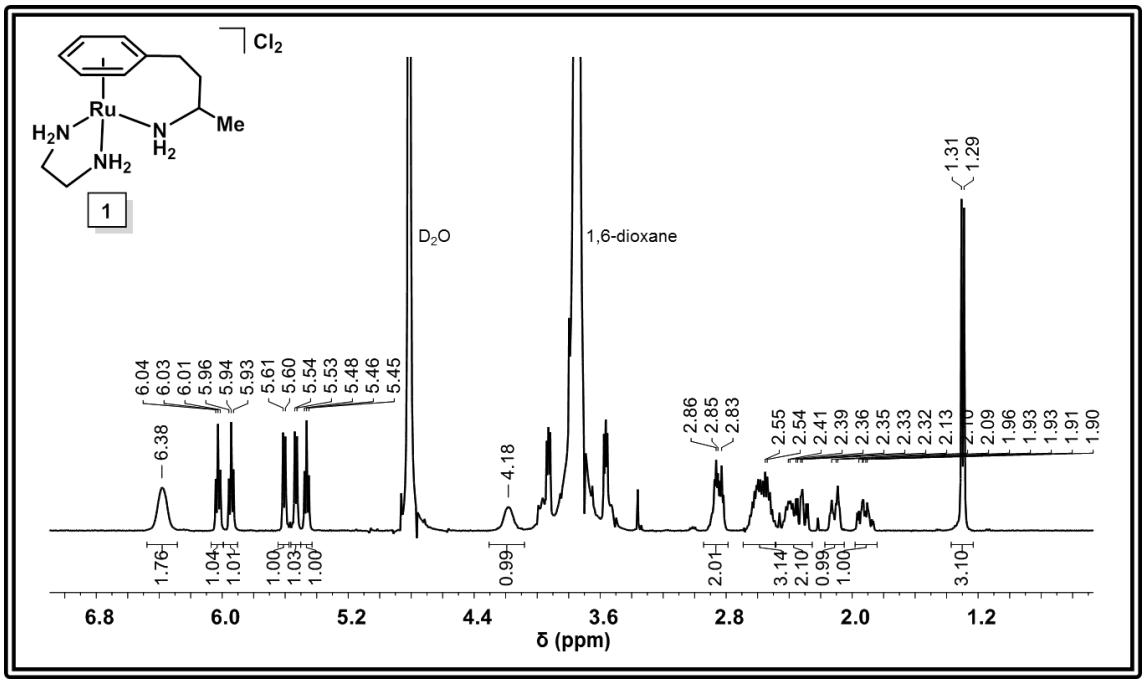

^{1}H NMR Complex **2**

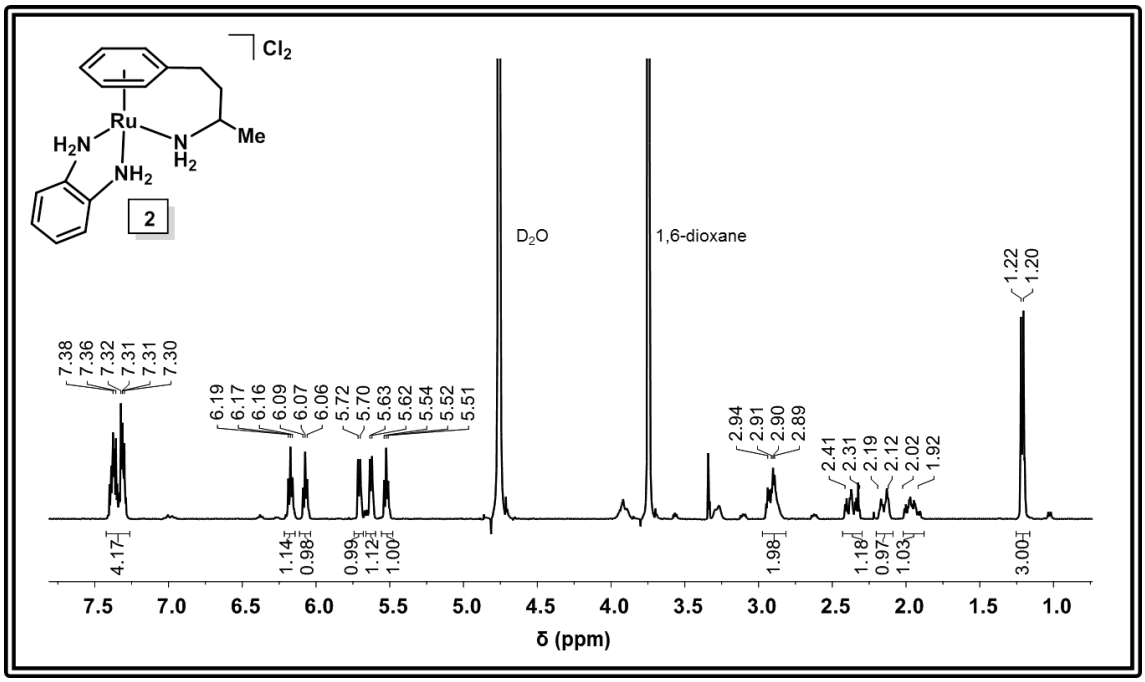

^{1}H NMR Complex **3**

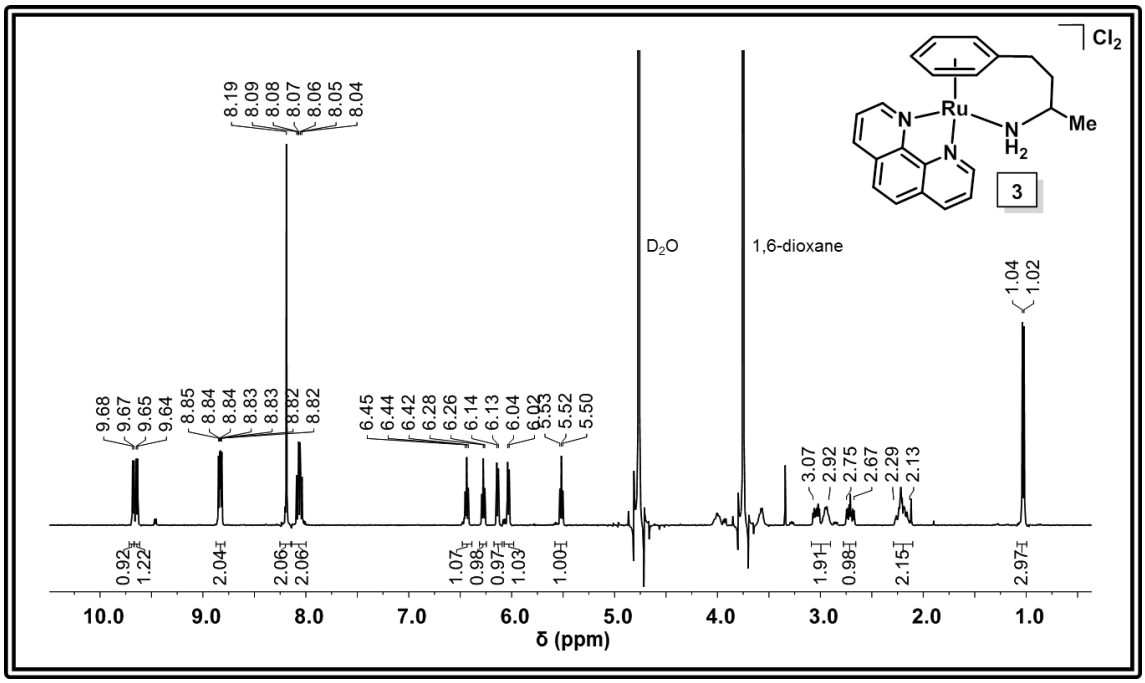

^{1}H NMR Complex **4**

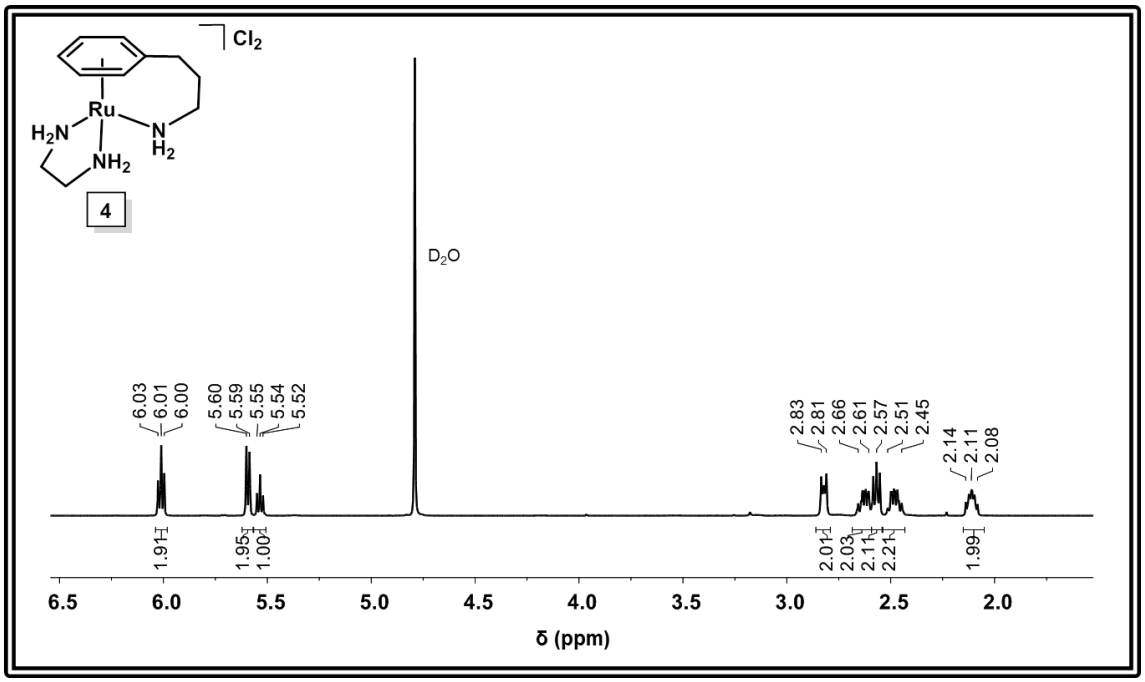

Appendix I

^{1}H NMR Complex **5**

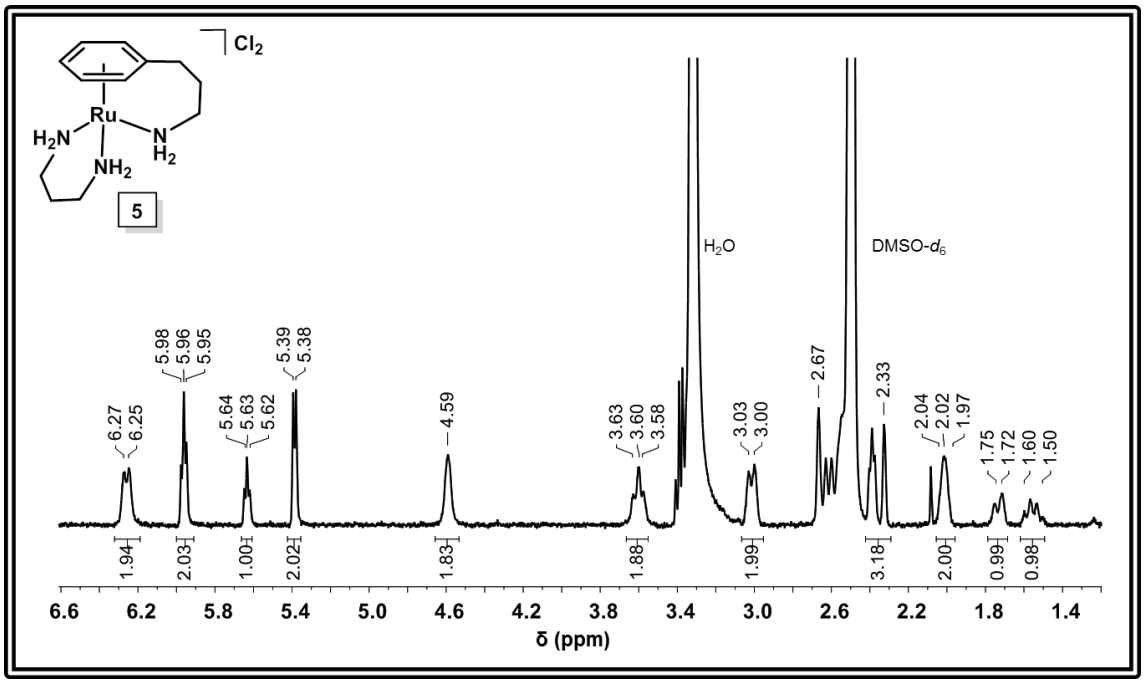

^{1}H NMR Complex **6**

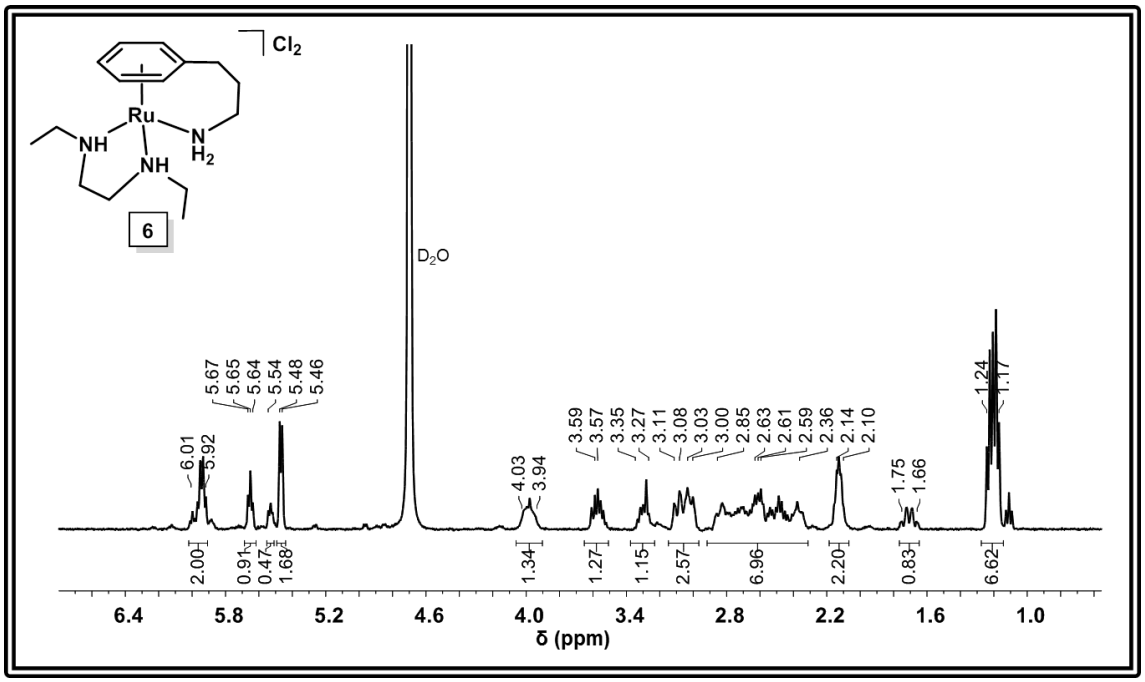

^{1}H NMR Complex **7**

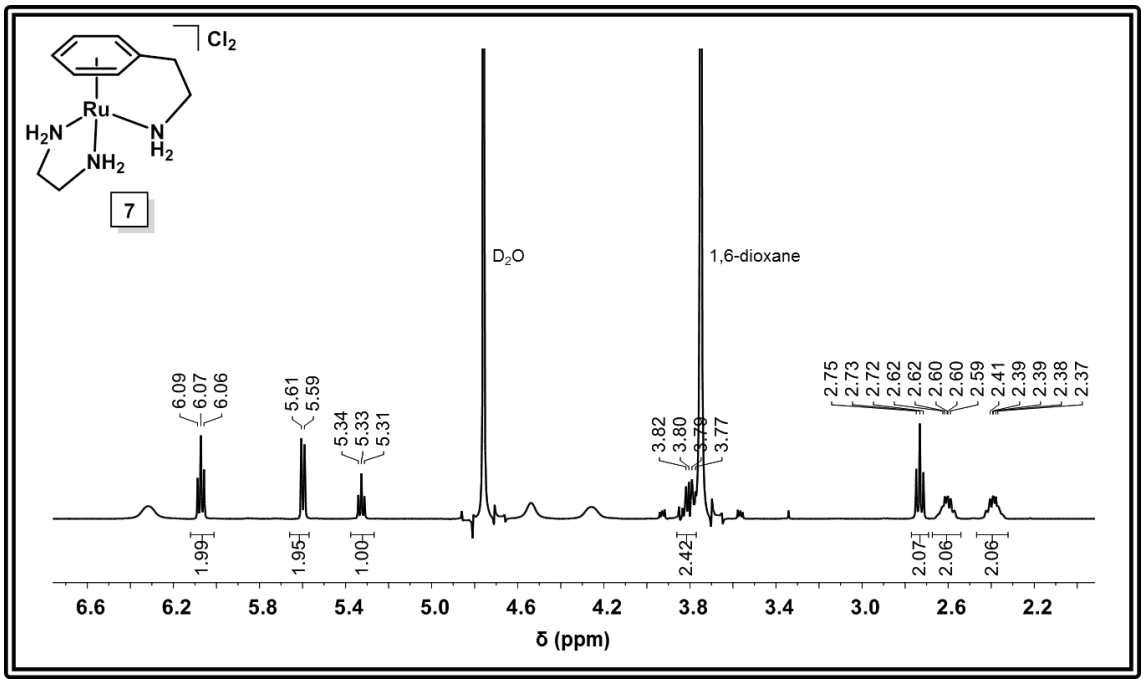

^{1}H NMR Complex **8**

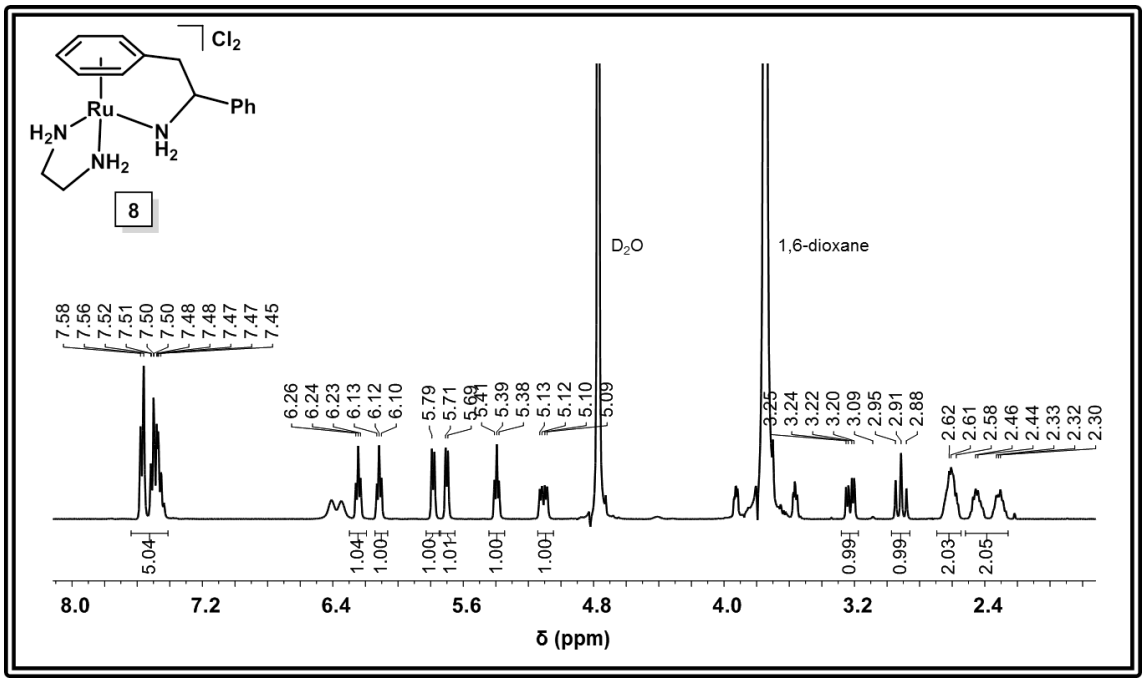

^{1}H NMR Complex **9**

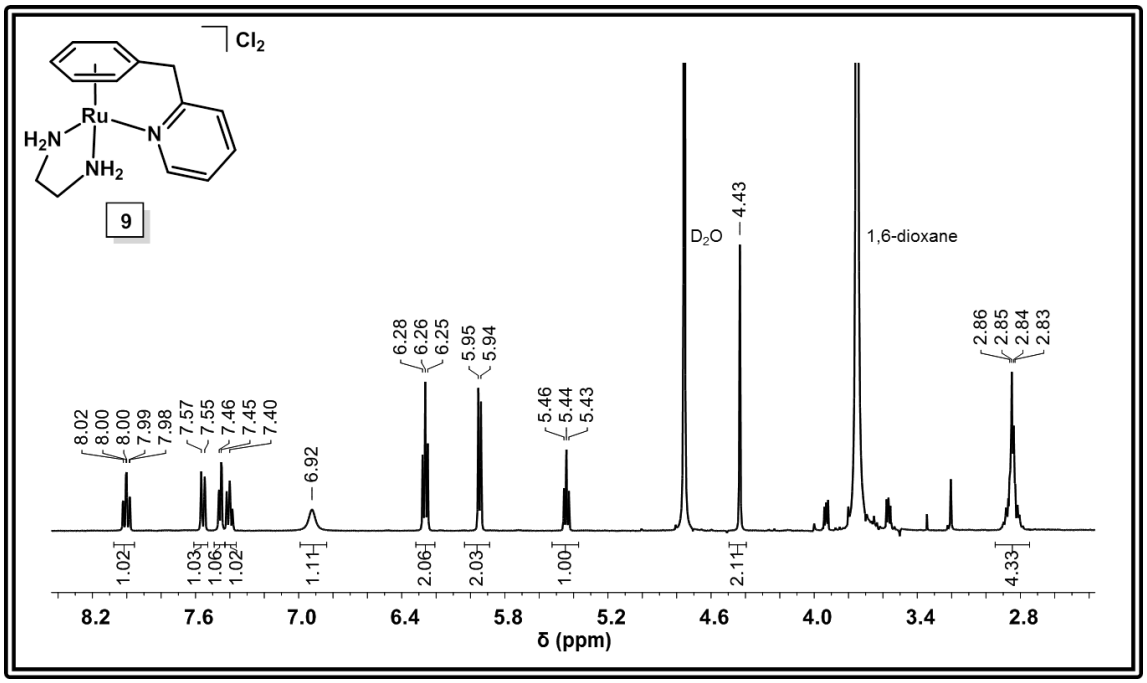

^{13}C NMR Complex **9**

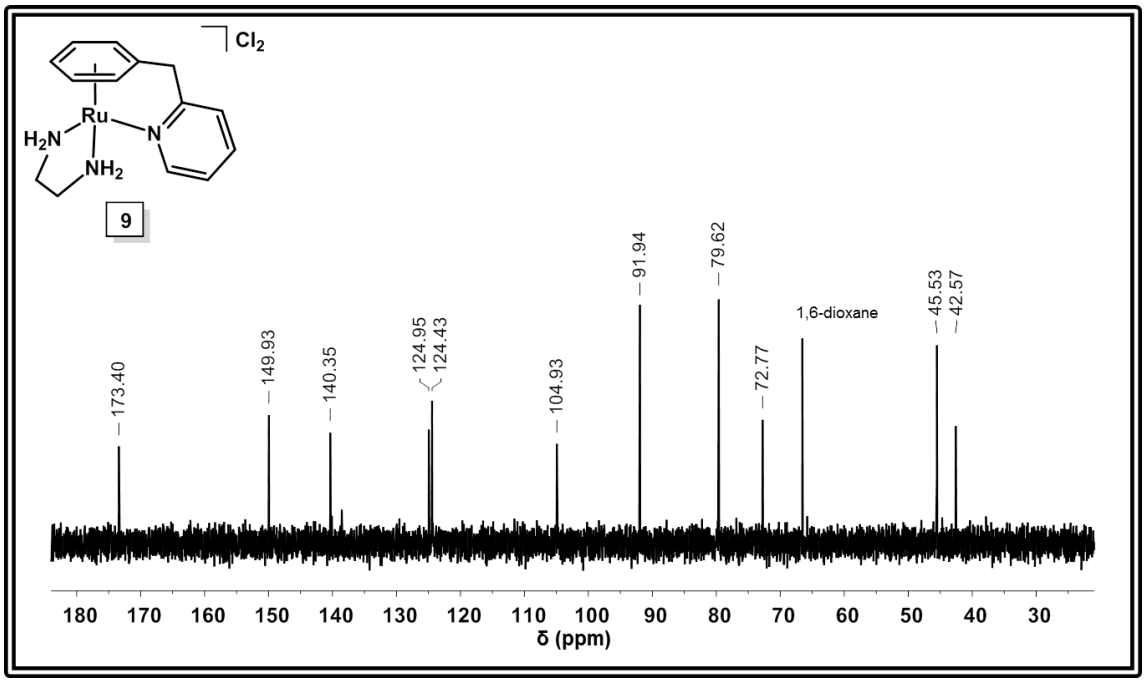

COSY NMR Complex **9**

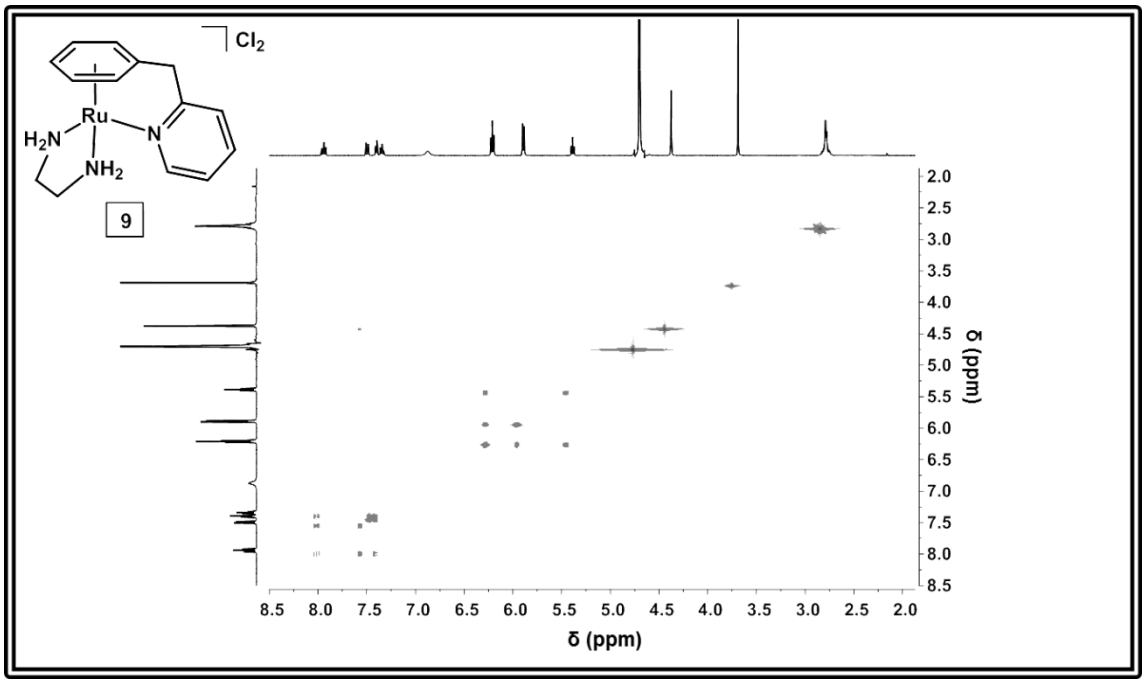

HMQC NMR Complex **9**

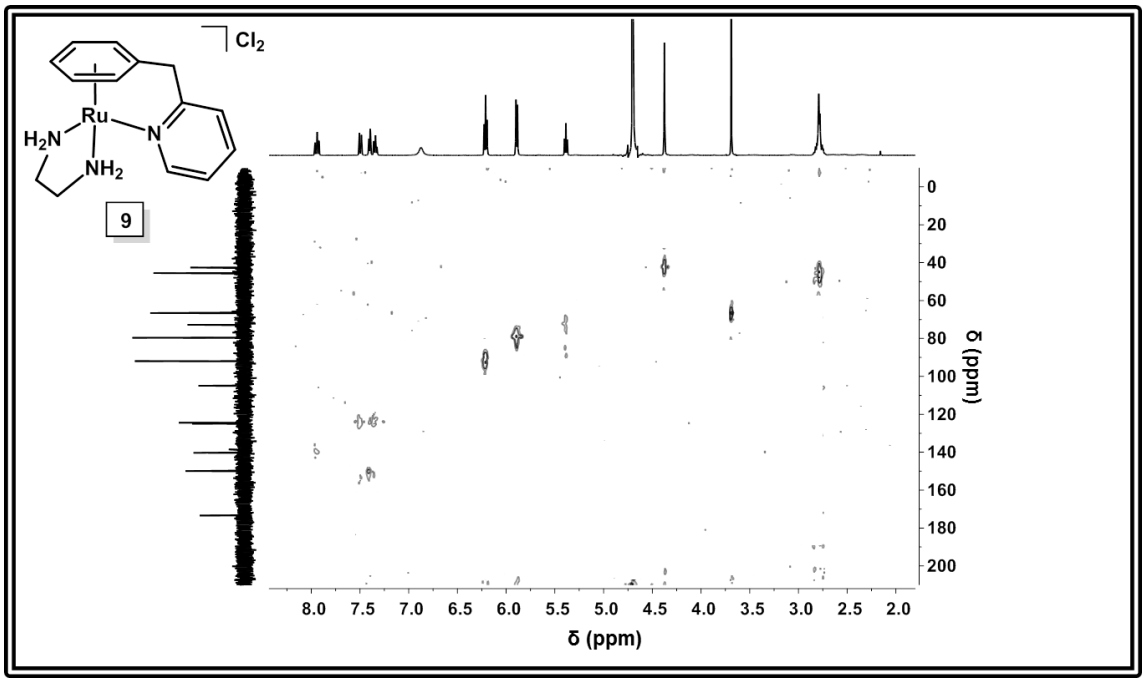

^{1}H NMR Complex **10**

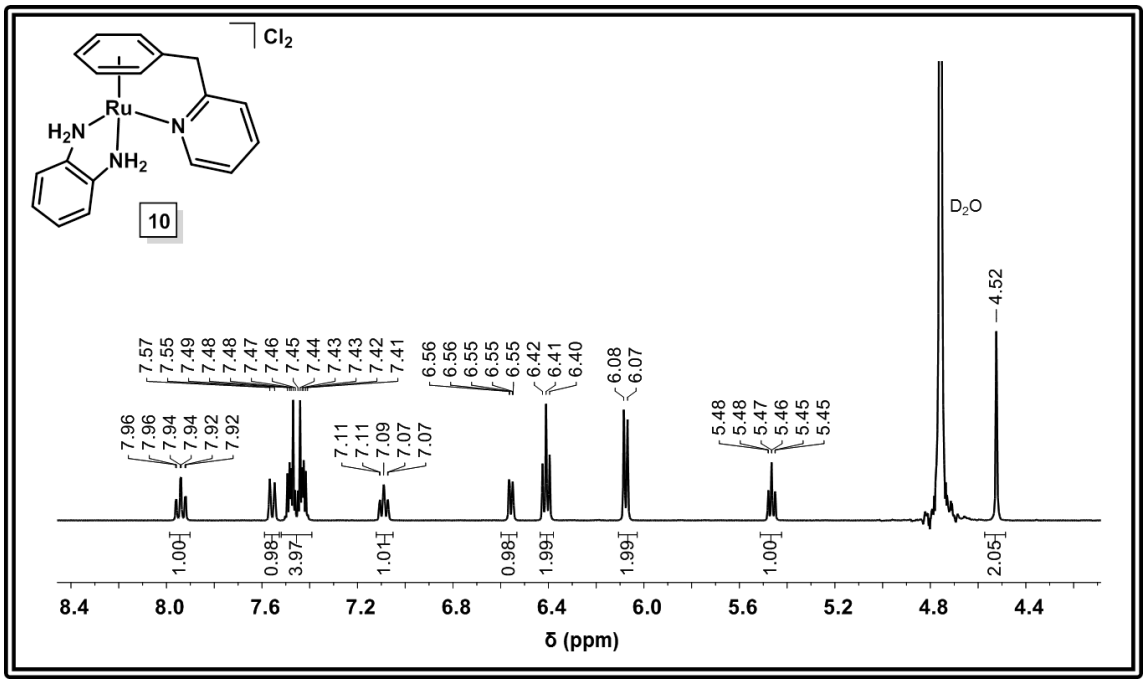

^{1}H NMR Complex **11**

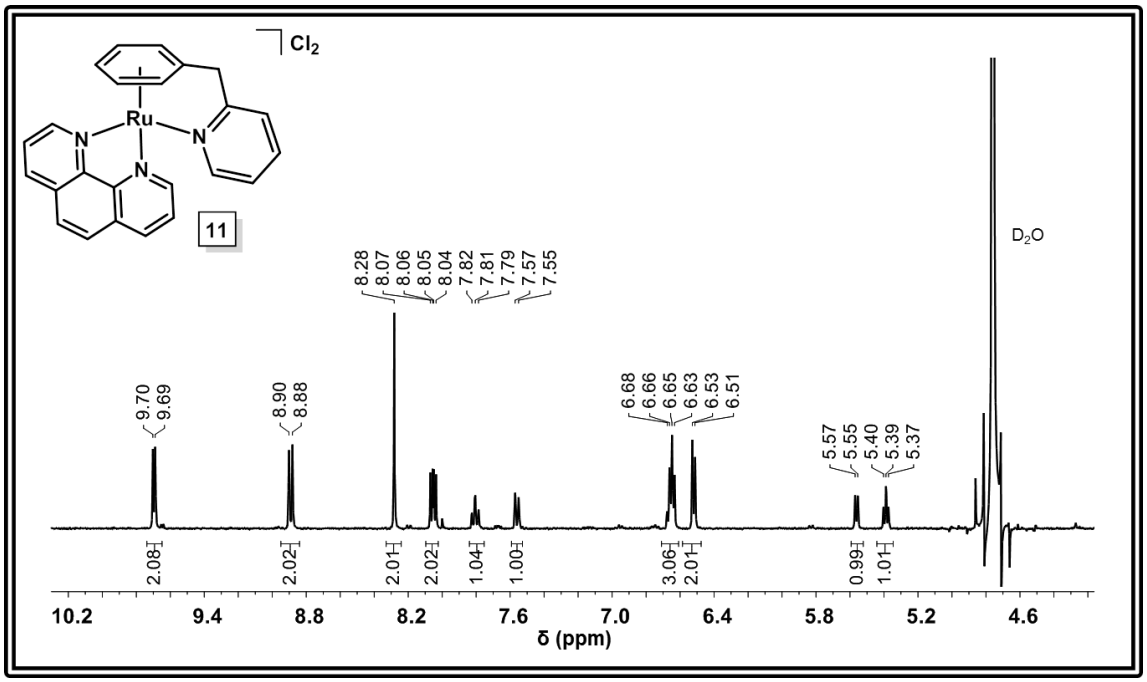

^{1}H NMR Complex **12**

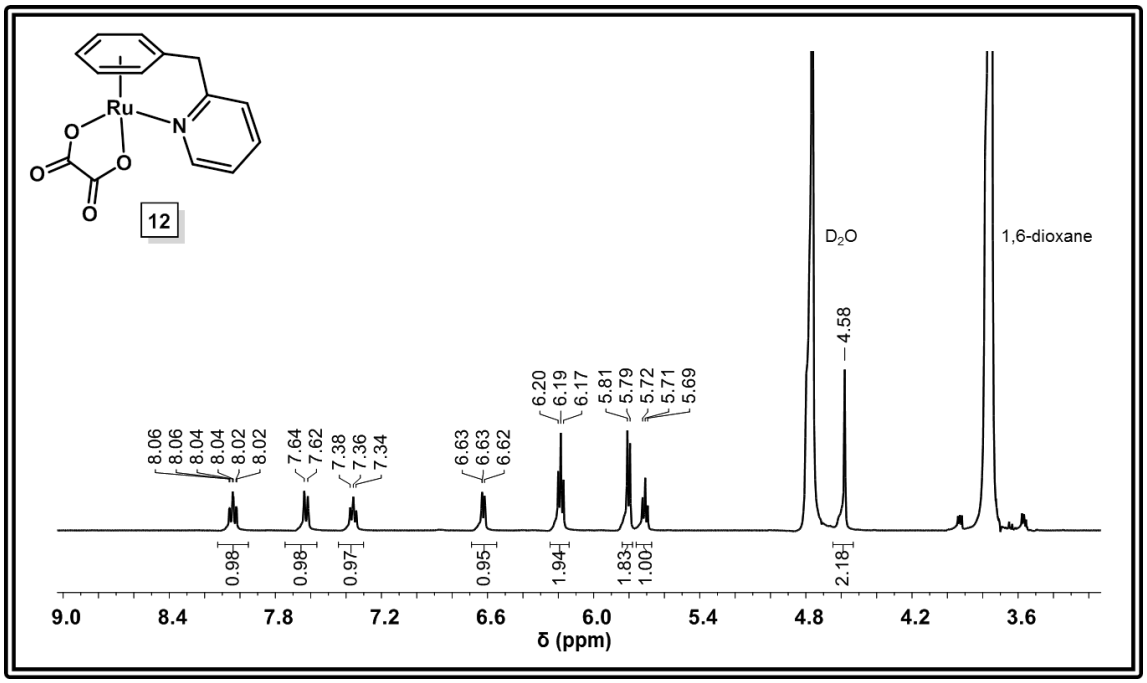

^{1}H NMR Complex **13**

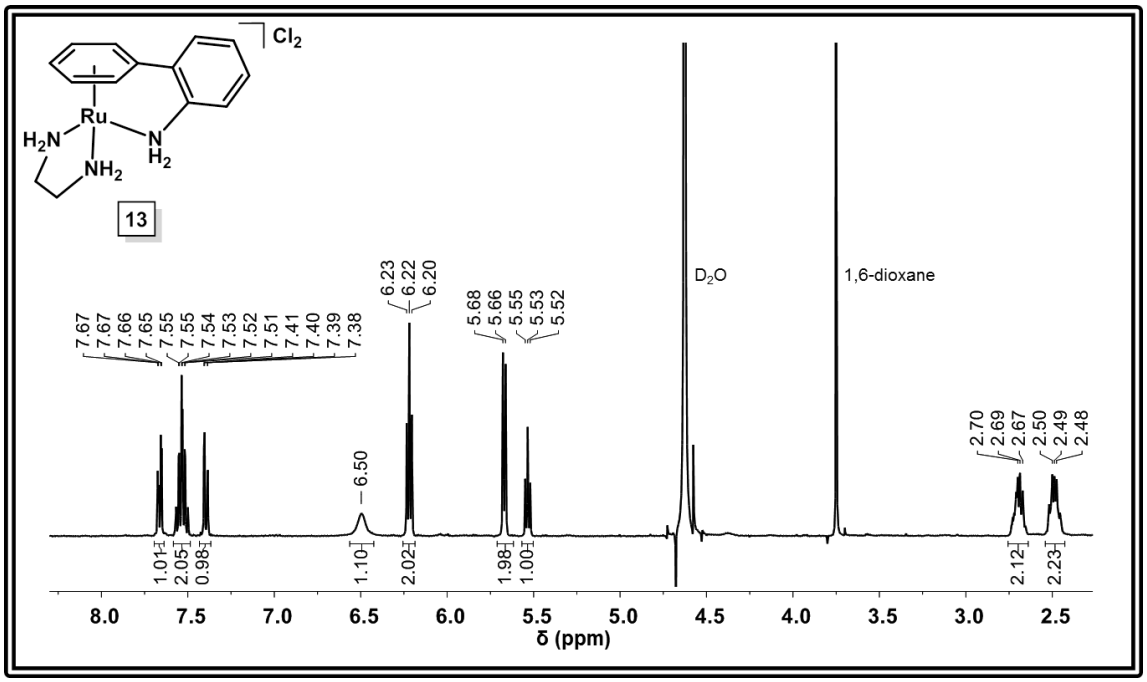

^{13}C NMR Complex **13**

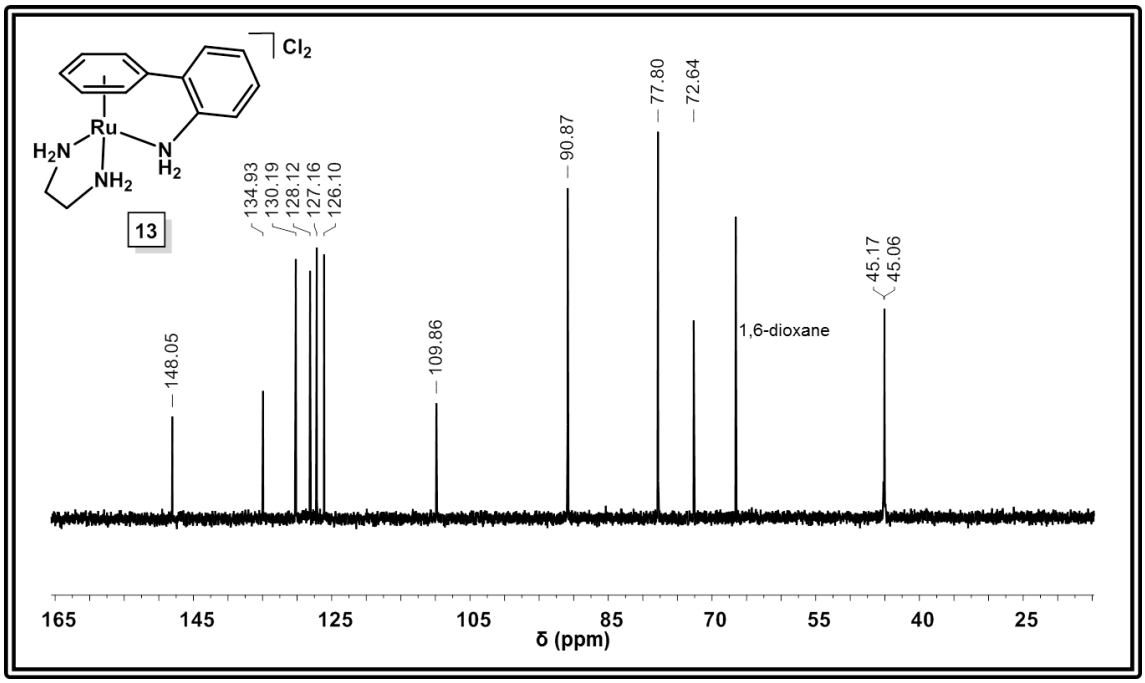

COSY Complex **13**

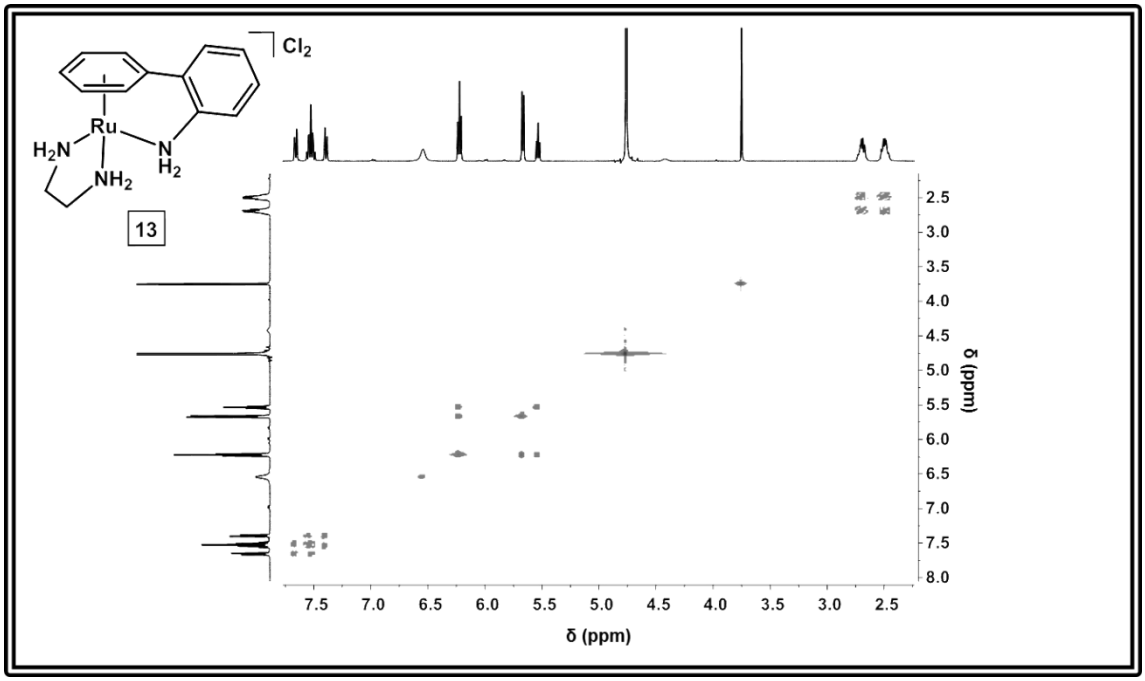

HMQC Complex **13**

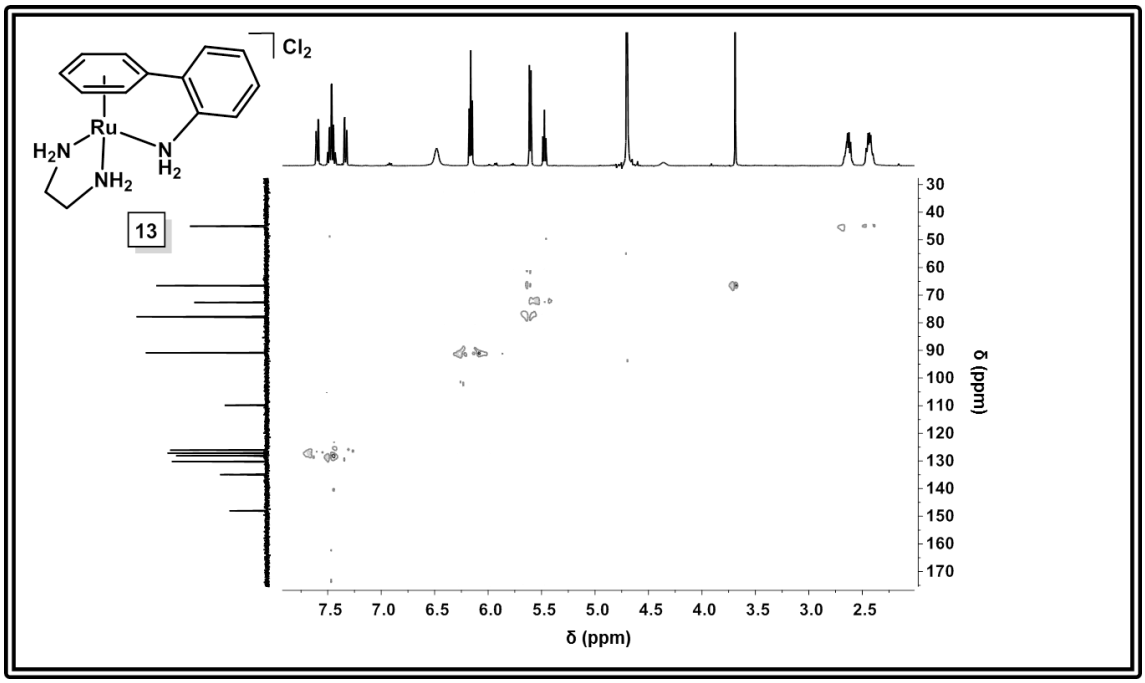

^{1}H NMR Complex **14**

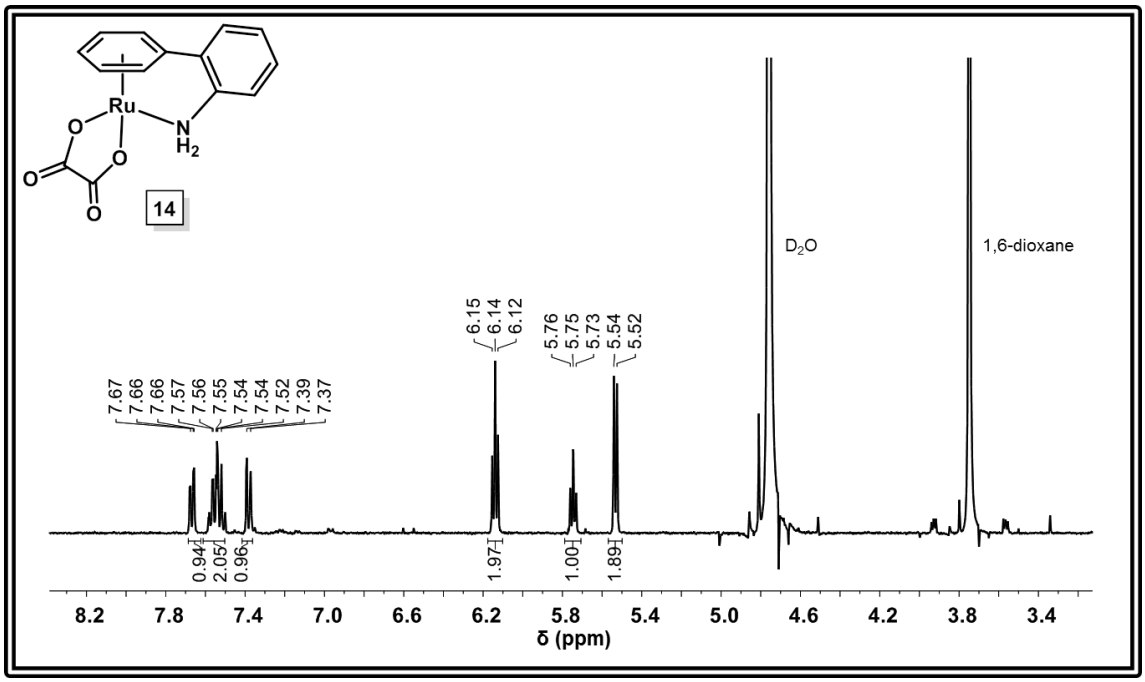

^{1}H NMR Complex **15Cl**

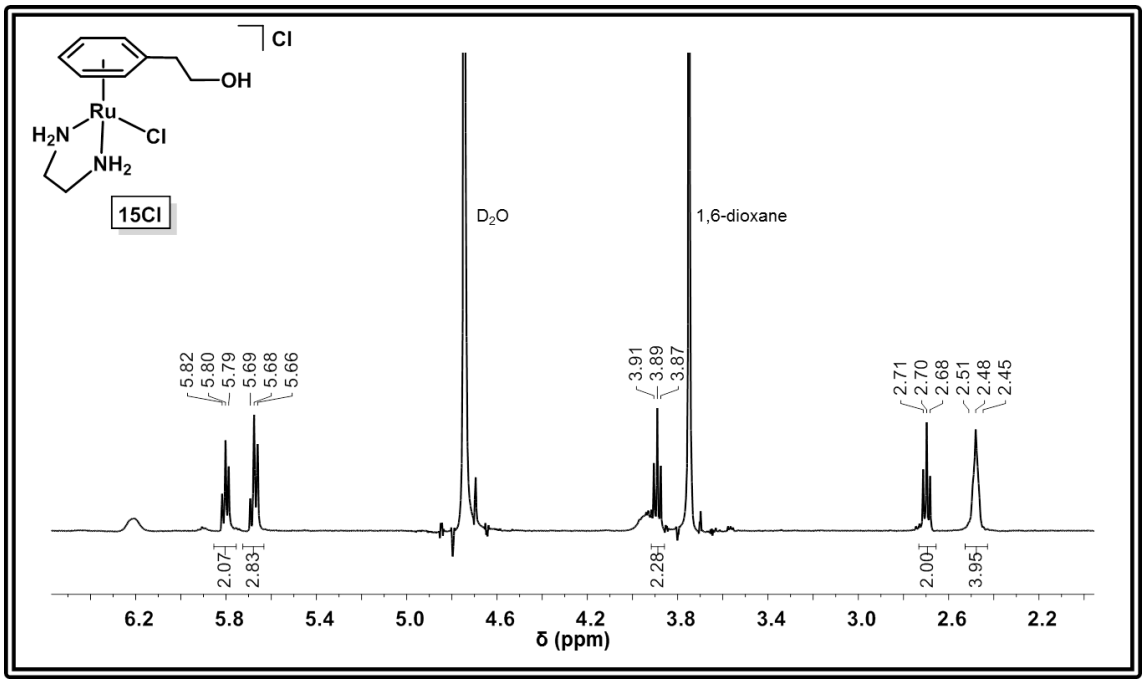

^{1}H NMR Complex **16Cl**

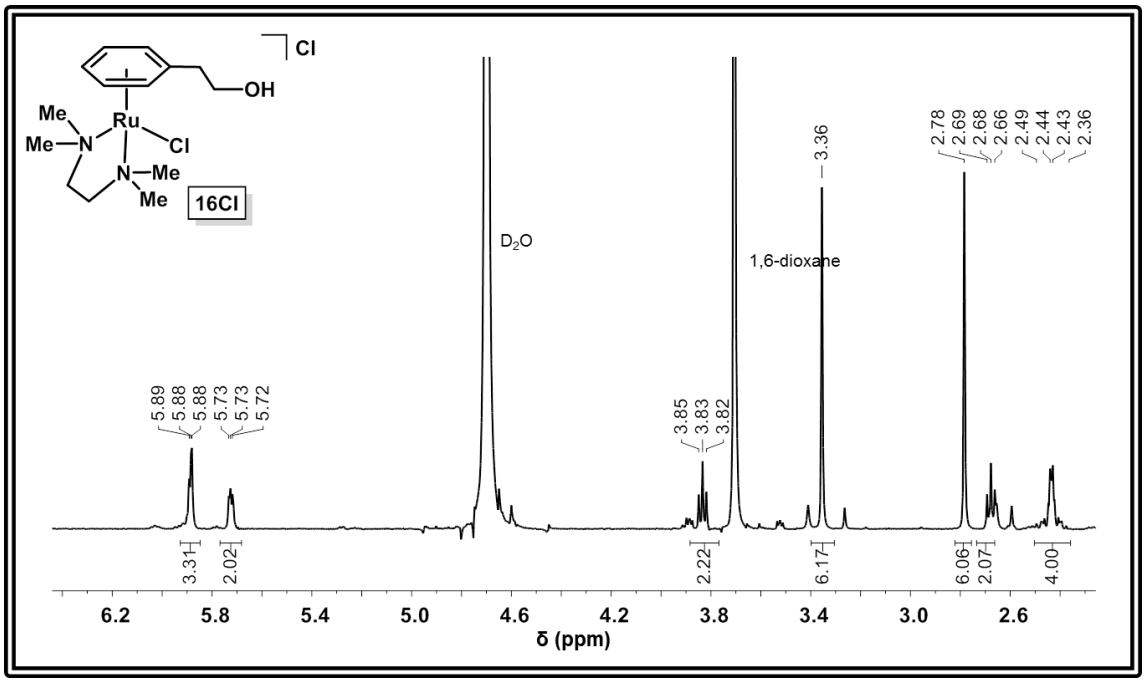

^{1}H NMR Complex **17Cl**

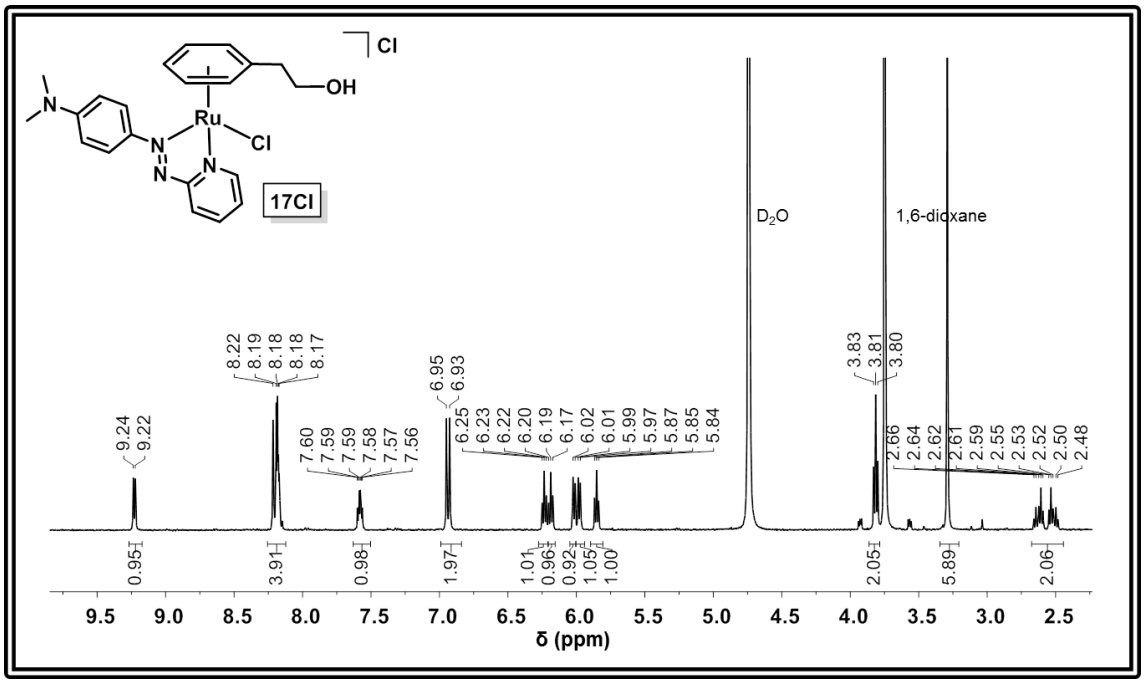

^{1}H NMR Complex **18Cl**

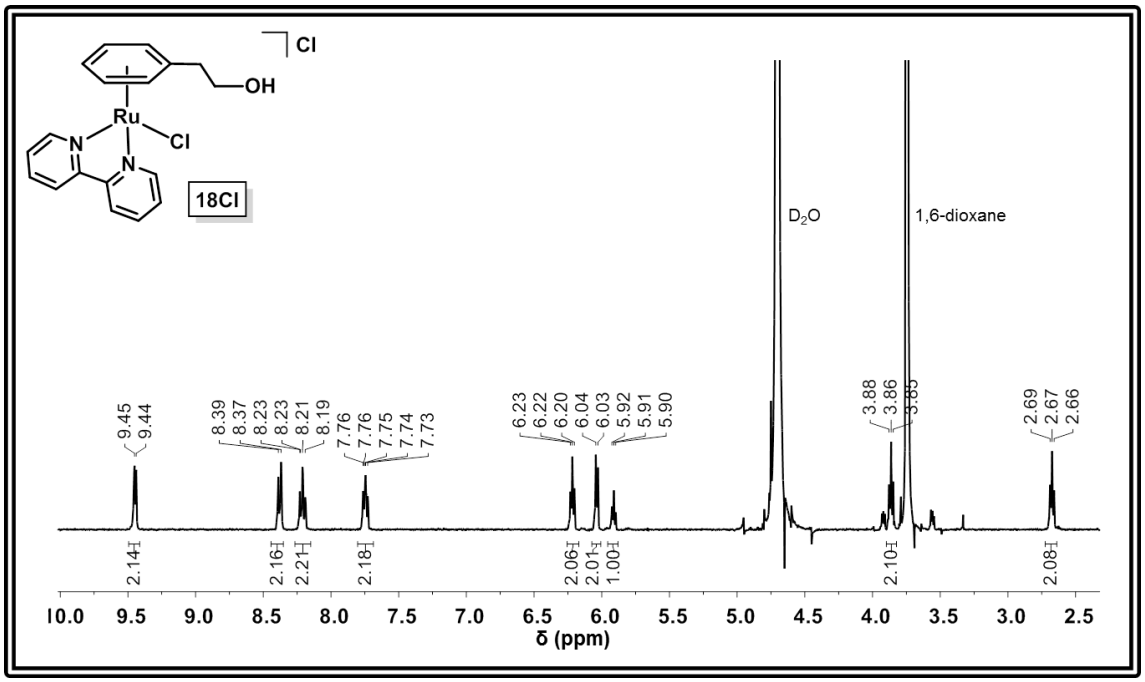

^{1}H NMR Complex **19Cl**

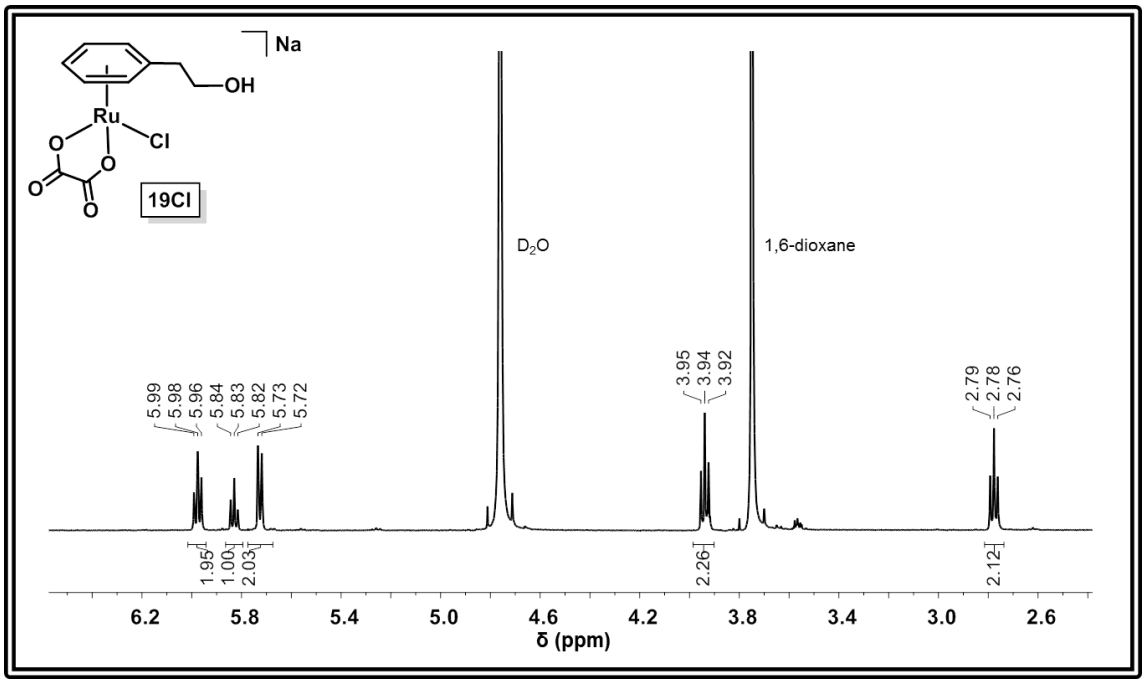

^{1}H NMR Complex **20Cl**

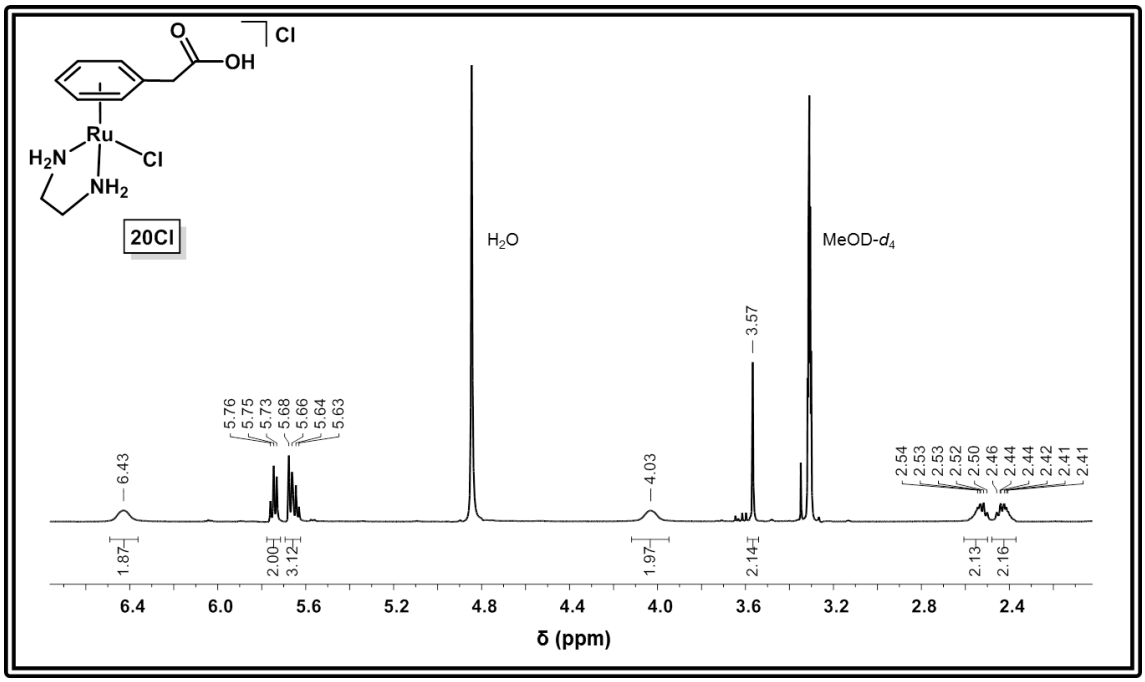

^{1}H NMR Complex **21**

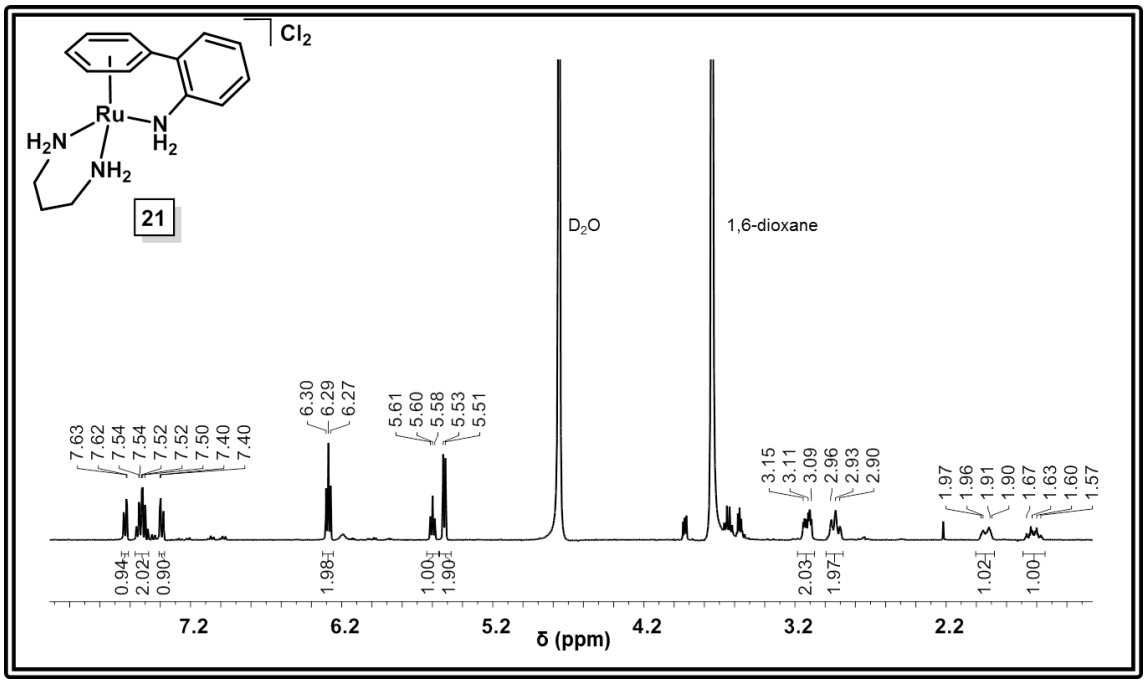

^{1}H NMR Complex **22**

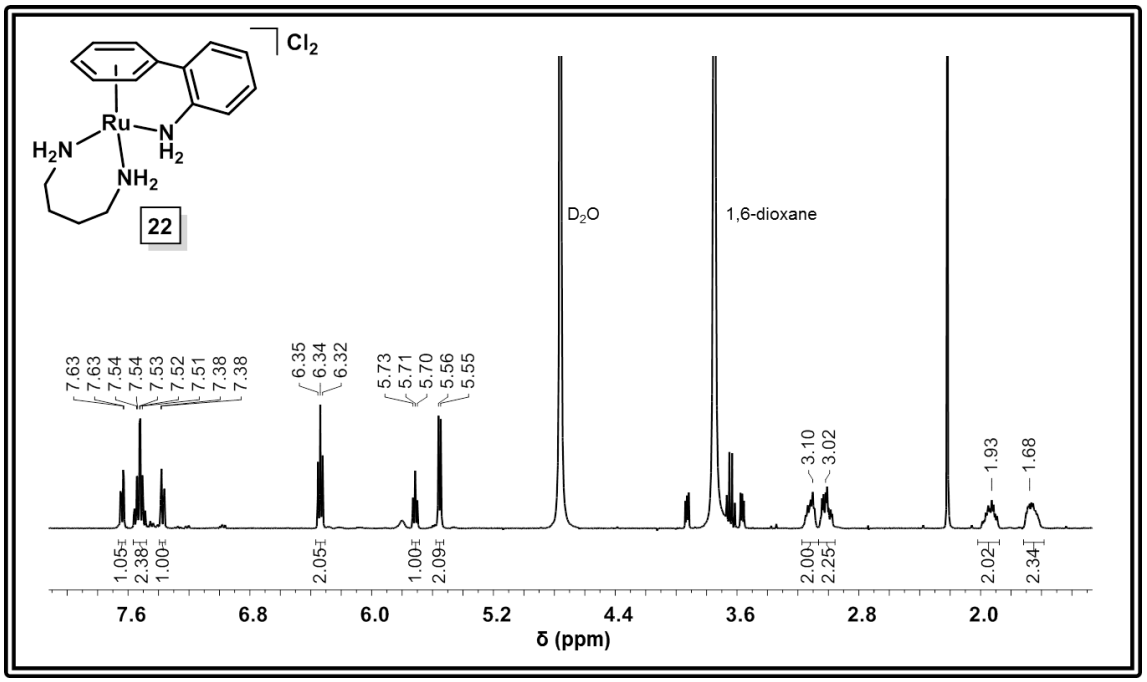

^{1}H NMR Complex **23**

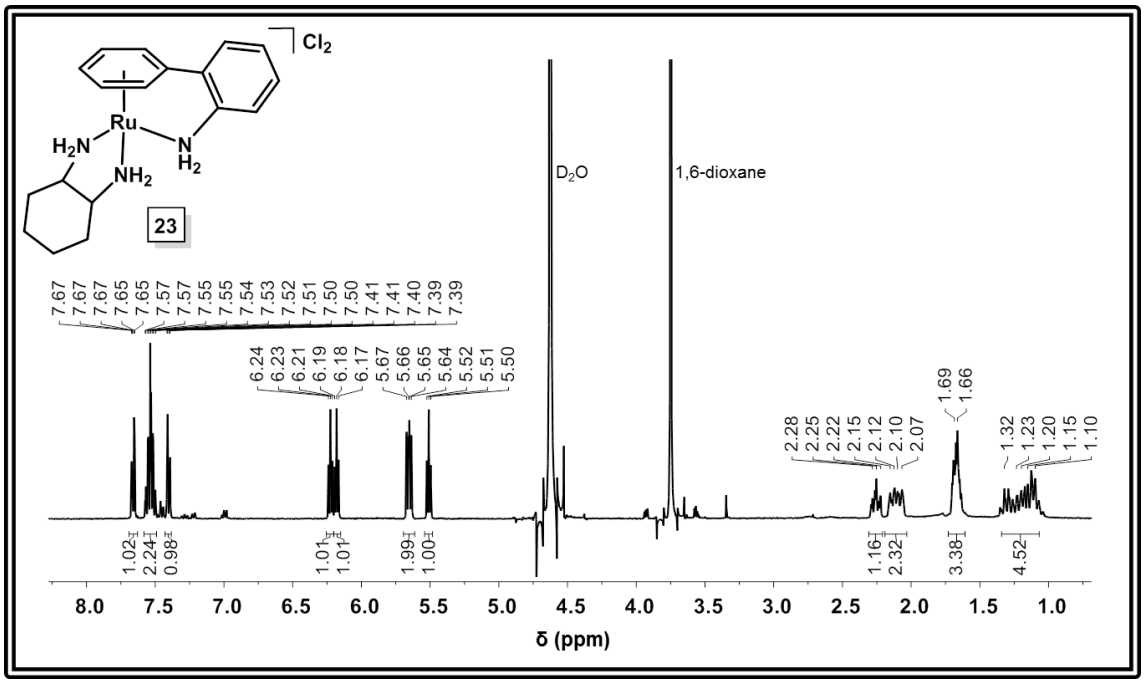

^{1}H NMR Complex **24**

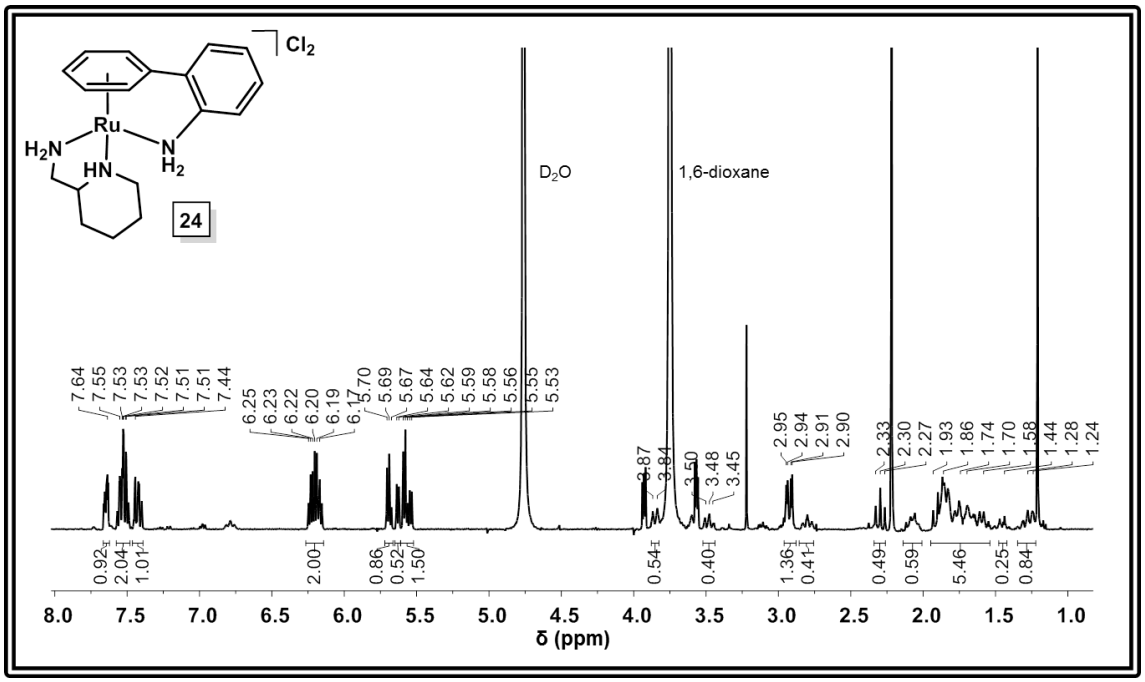

^{1}H NMR Complex **25**

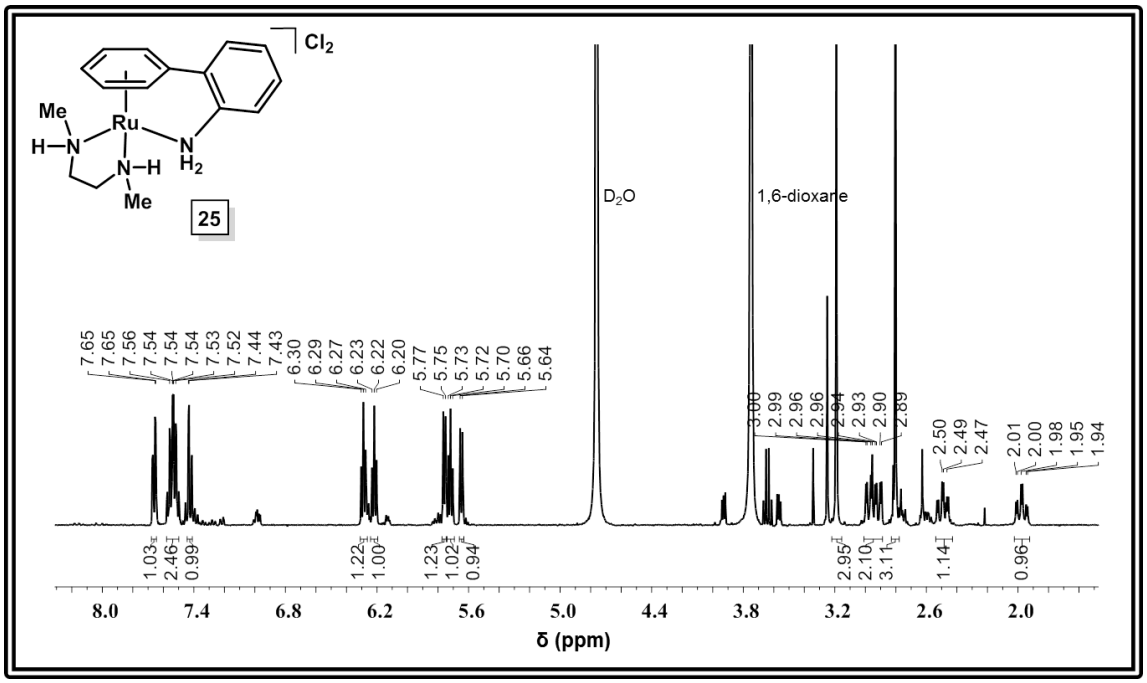

^{1}H NMR Complex **26**

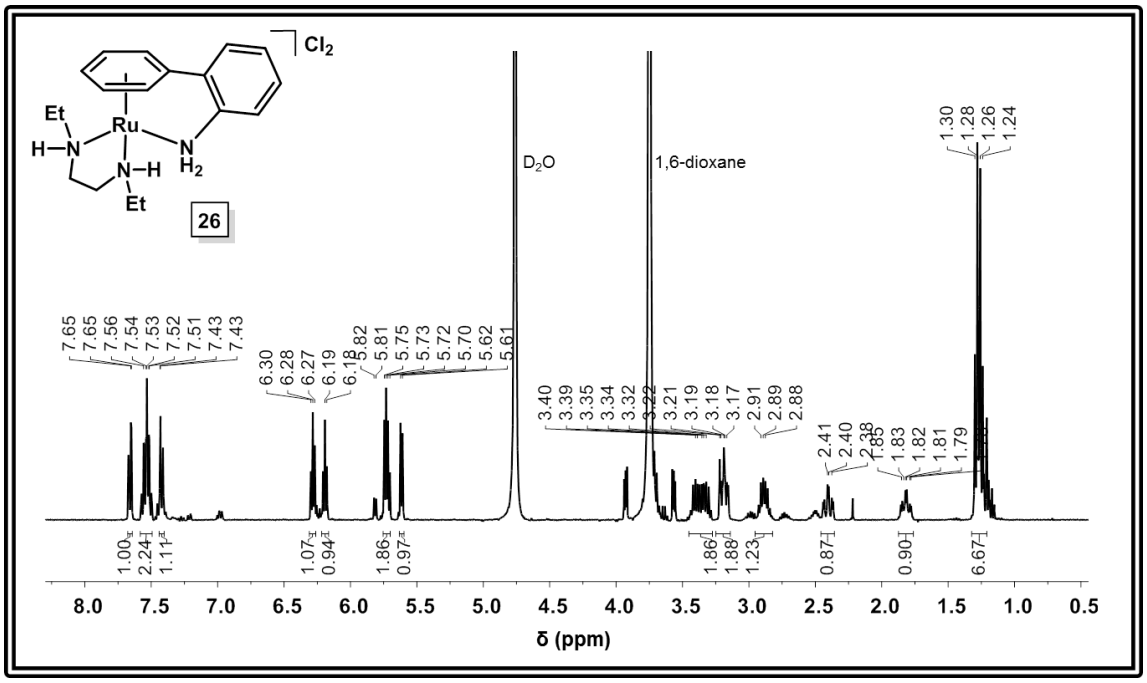

^{1}H NMR Complex **27**

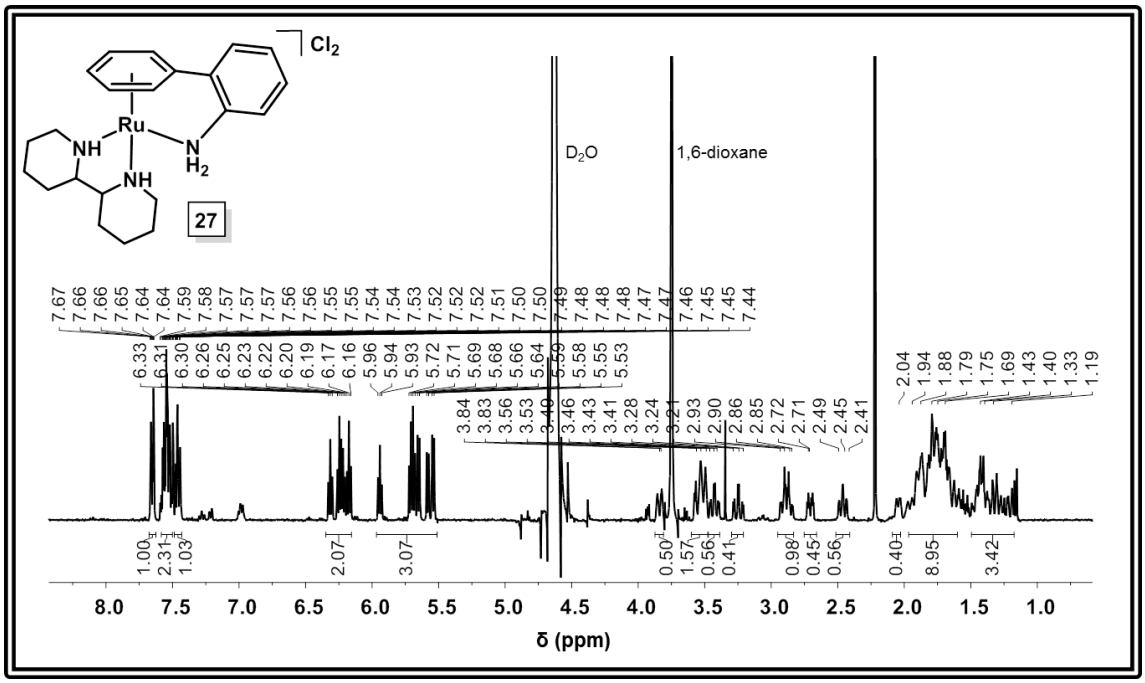

^{1}H NMR Complex **28**

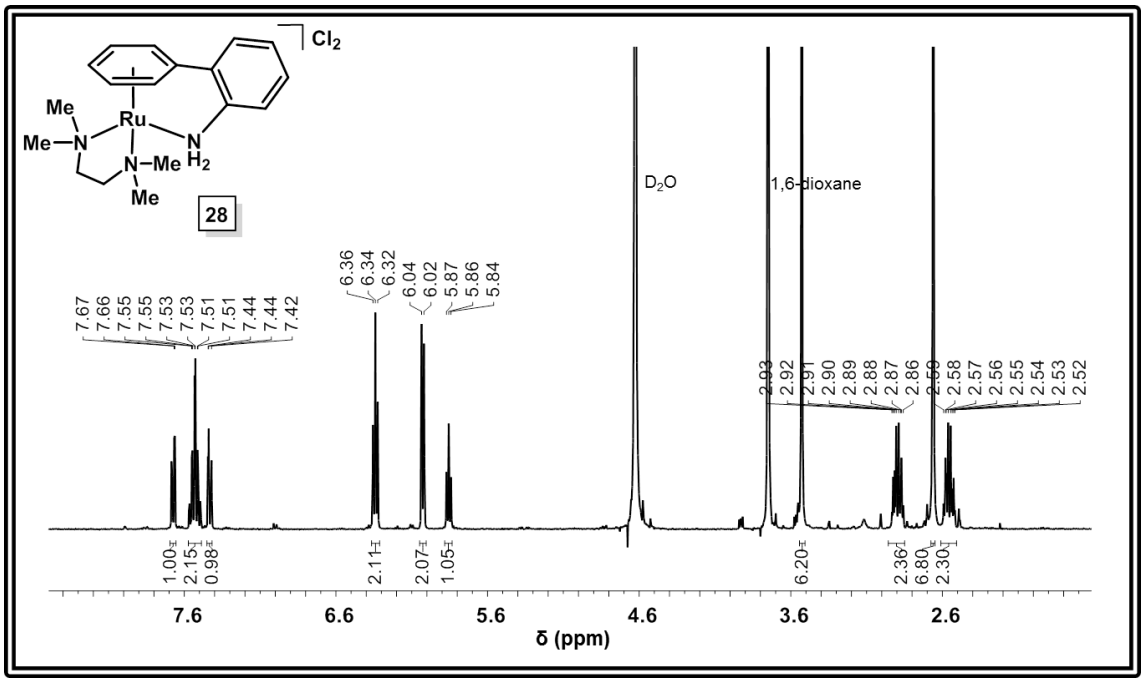

^{1}H NMR Complex **29**

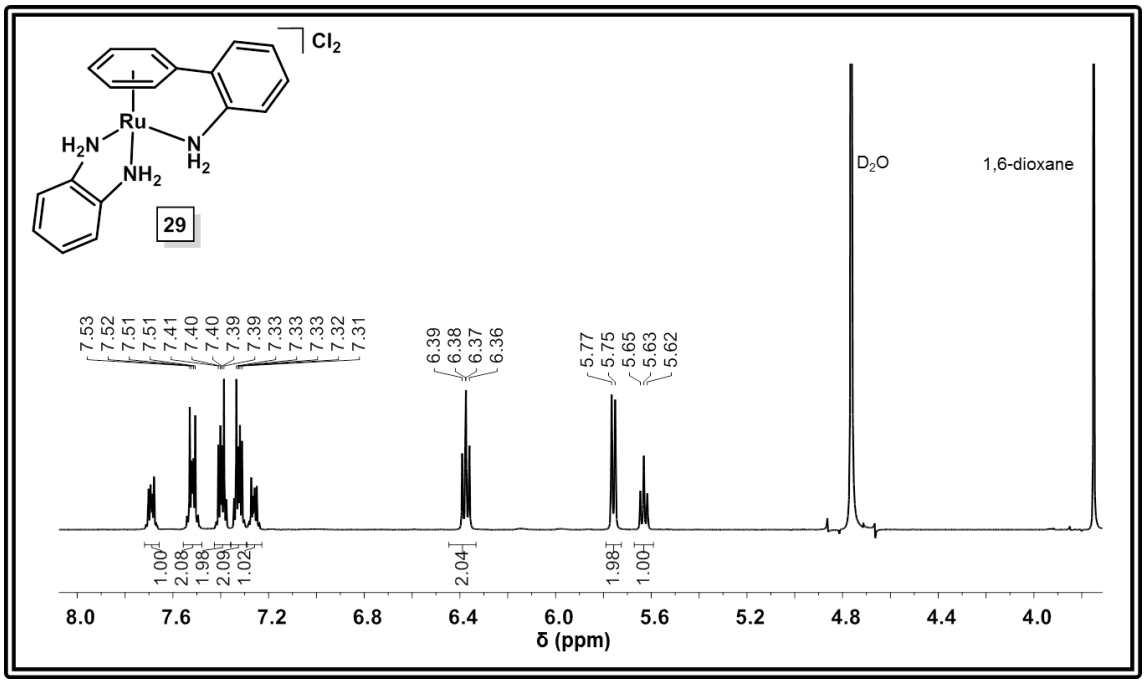

^{1}H NMR Complex **30**

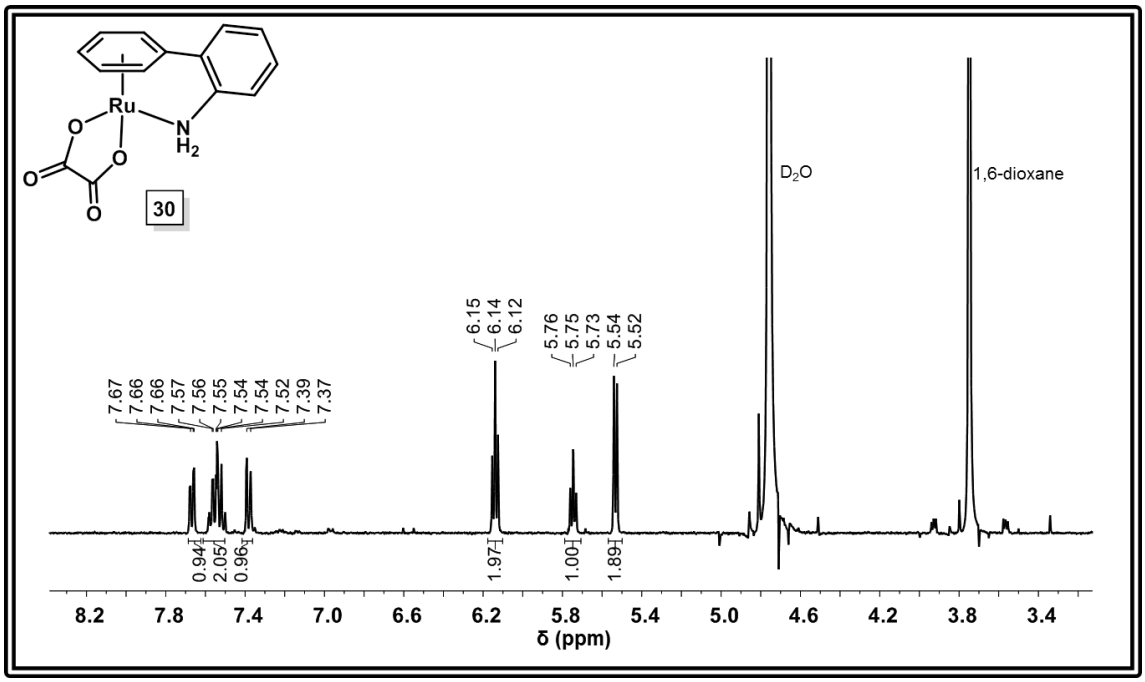

Appendix I

^{1}H NMR Complex **31Cl**

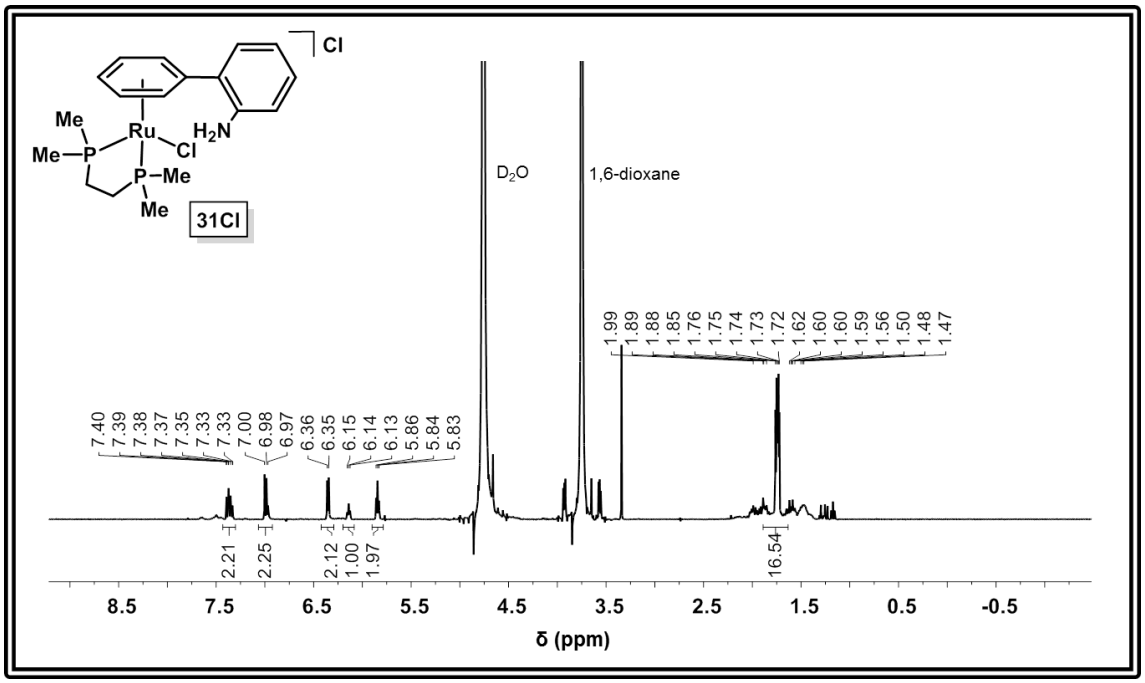

^{1}H NMR Complex **32Cl**

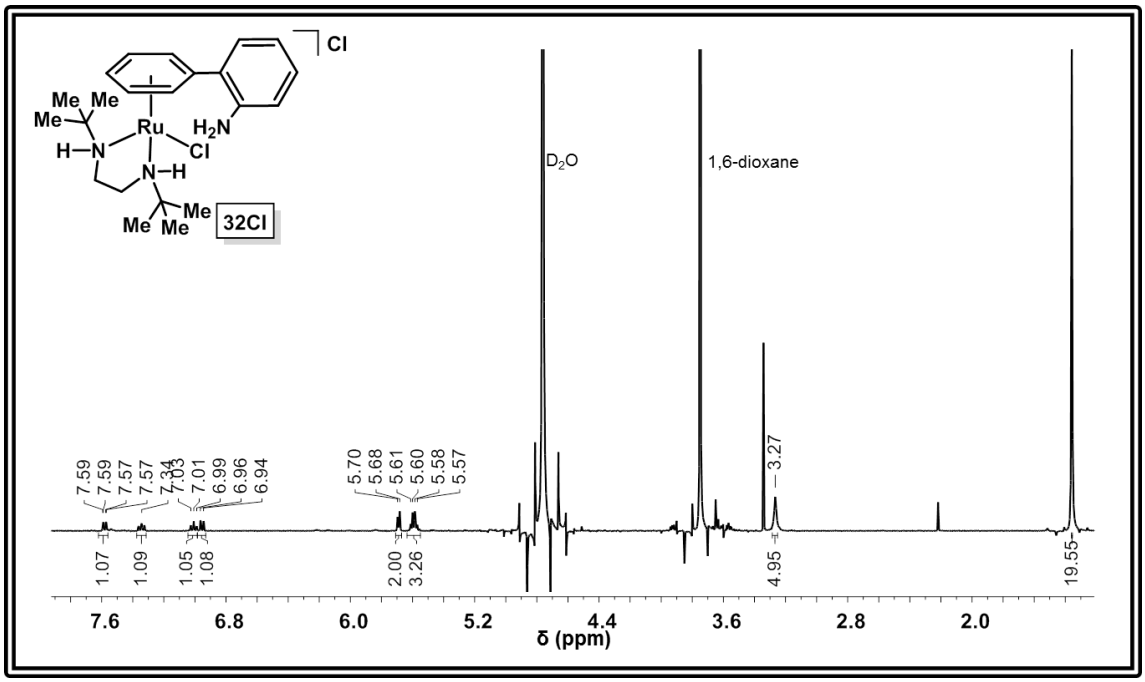

^{1}H NMR Complex **33Cl**

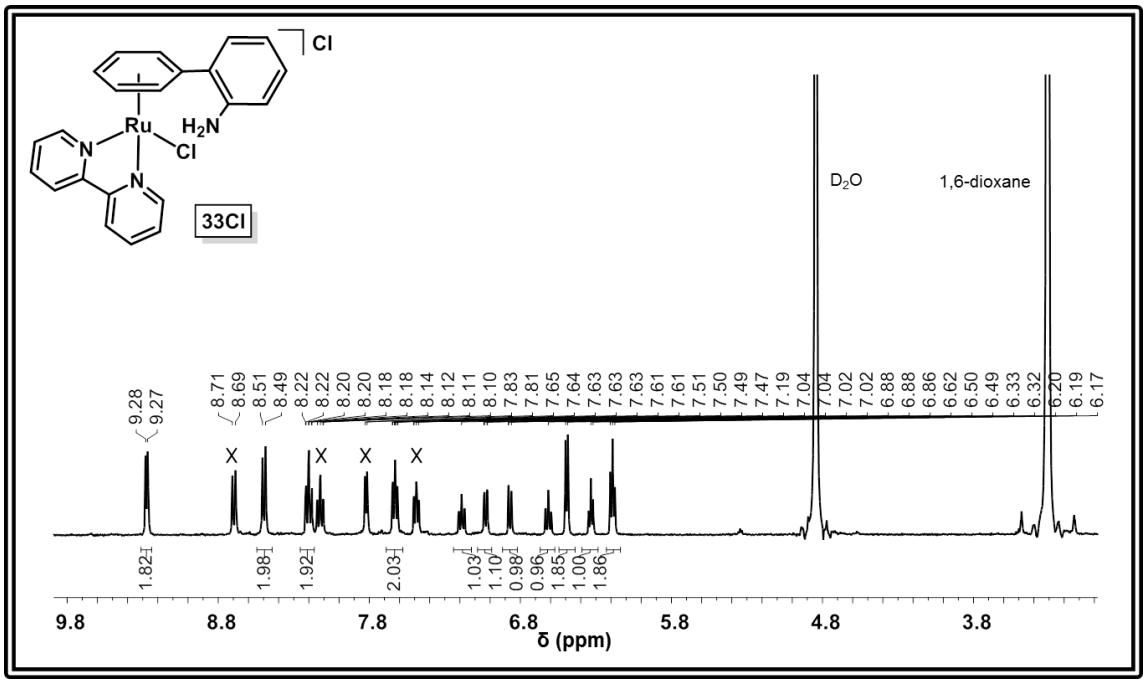

^{1}H NMR Complex **34dimer**

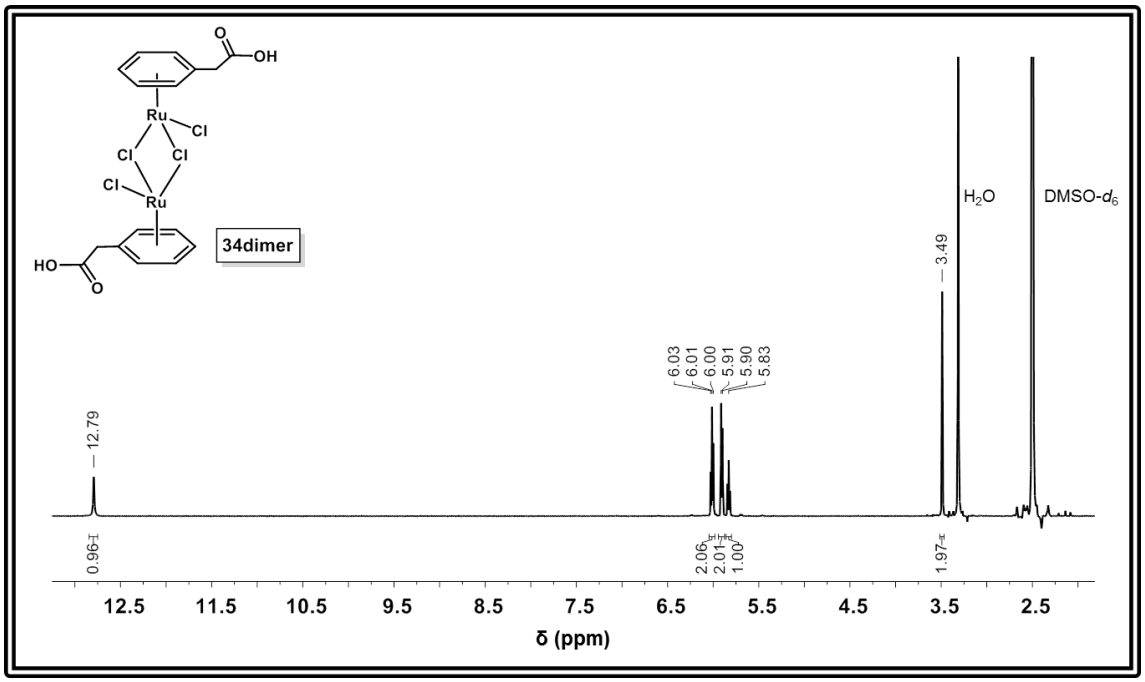

^{1}H NMR Complex **35Cl**

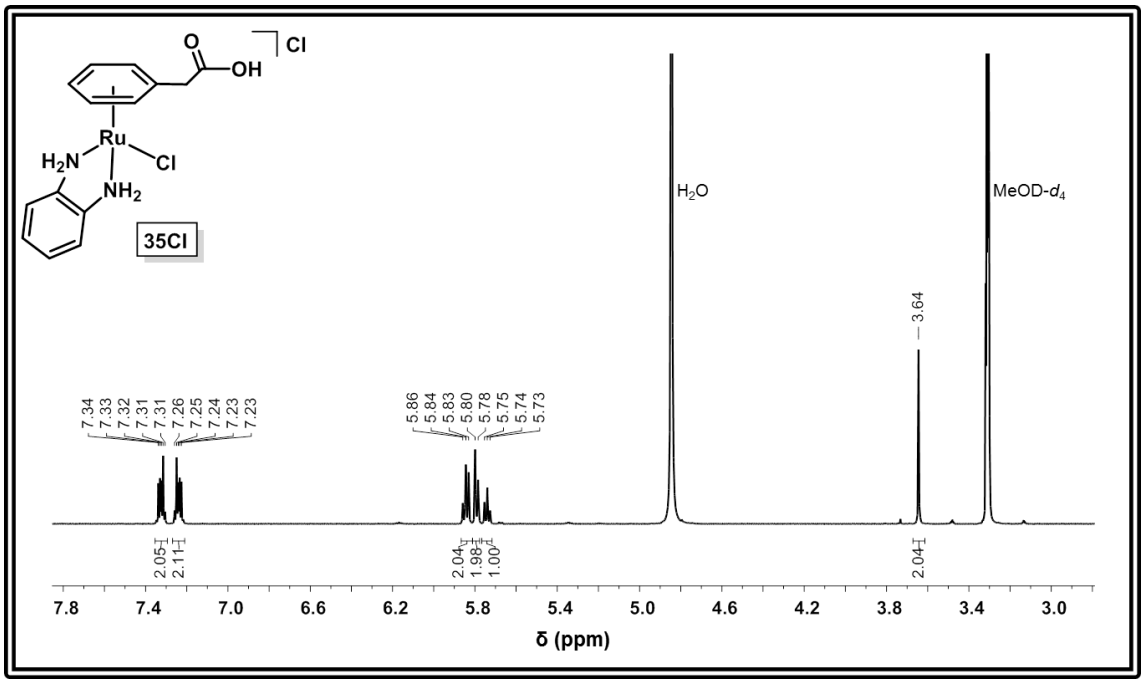

^{1}H NMR Complex **36Cl**

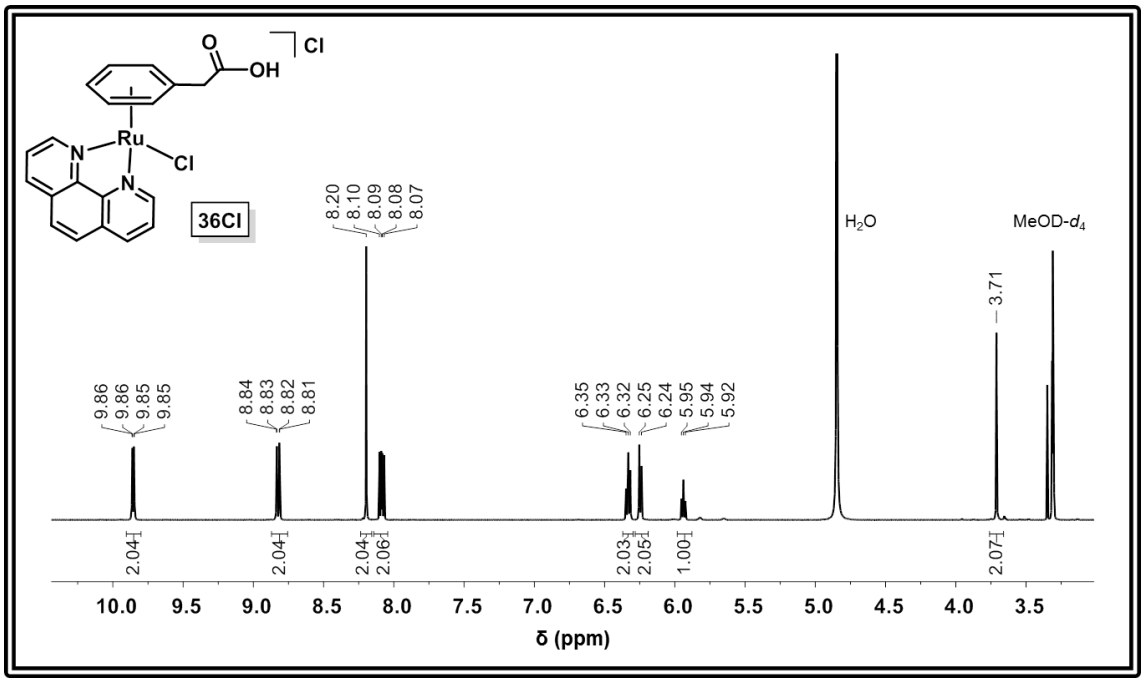

^{1}H NMR Complex **37Cl**

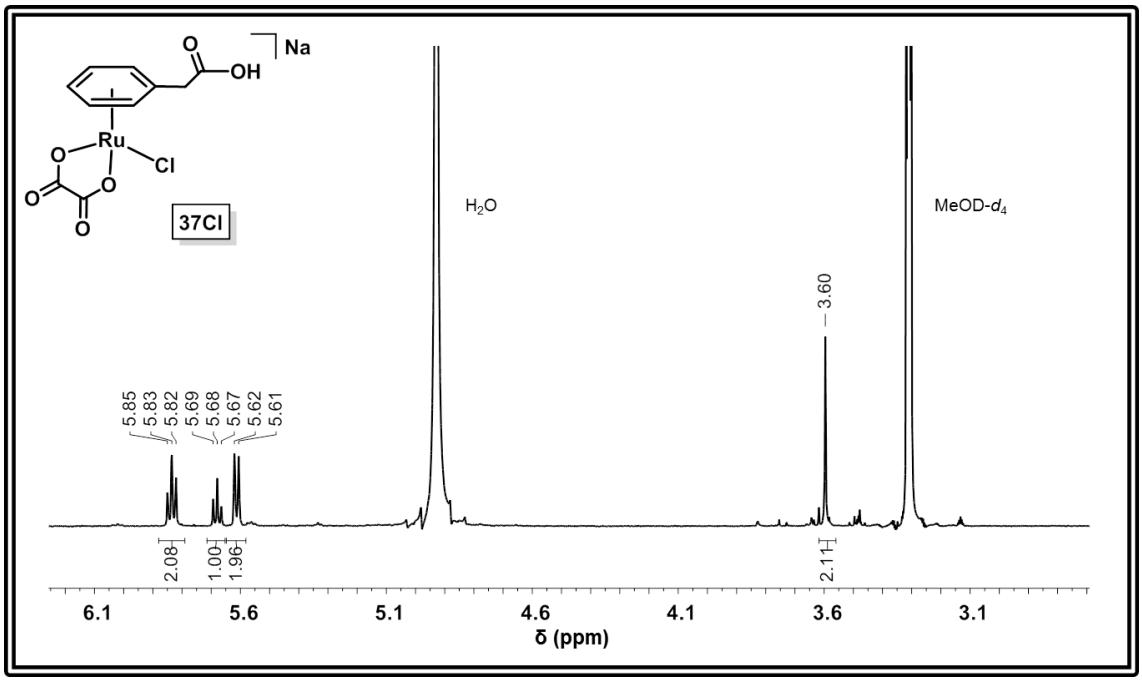

^{1}H NMR Complex **38**

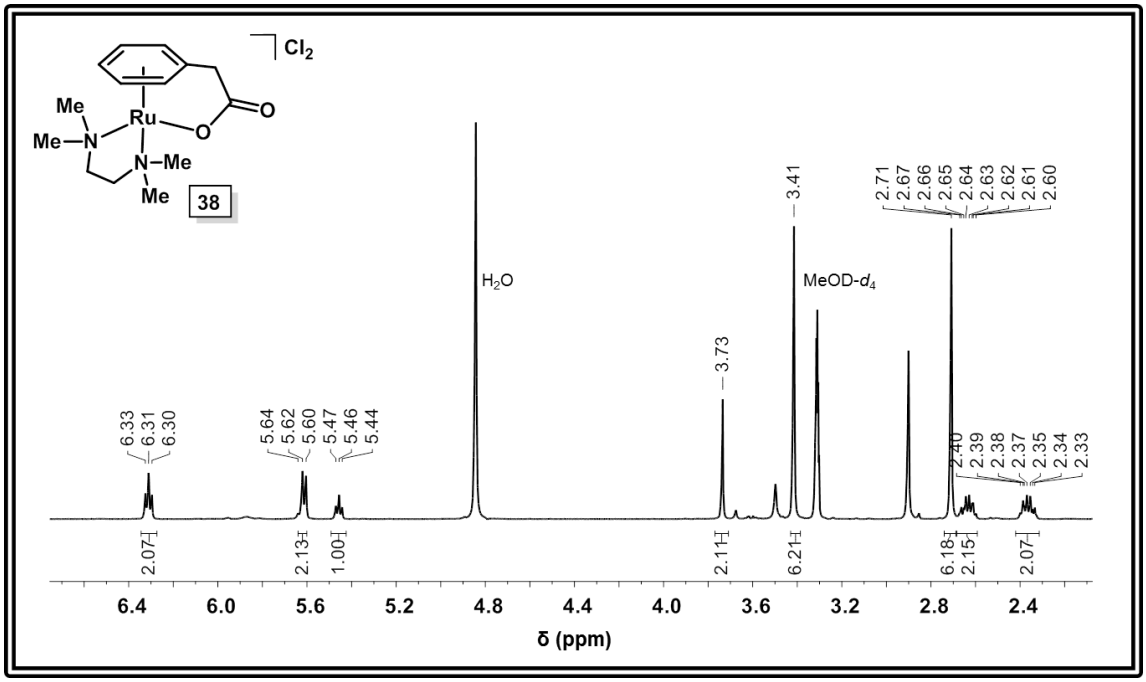

Appendix II

Crystallographic Data

Crystallographic data for closed tethered complexes included in Chapter 2.

Complex	**5**	**6**	**7**
Formula	$C_{15}H_{33}Cl_2N_3O_2Ru$	$C_{12}H_{23}Cl_2N_3ORu$	$C_{10}H_{23}Cl_2N_3ORu$
MW	459.41	397.30	373.28
Crystal description	yellow prismatic	yellow prismatic	yellow-orange plate
Crystal size (mm)	0.08 x 0.14 x 0.16	0.02 x 0.04 x 0.08	0.12 x 0.47 x 0.56
λ (Å)	0.71073	0.71073	0.71073
T (K)	200(2)	296(2)	296(2)
Crystal system	monoclinic	monoclinic	orthorhombic
Space group	P 1 21/c 1	P 1 21/n 1	P 21 21 21
***a* (Å)**	13.8329(5)	8.8098(4)	8.2419(6)
***b* (Å)**	8.7529(3)	14.4814(5)	11.6210(5)
***c* (Å)**	16.8436(5)	13.4656(5)	16.3156(13)
α (deg)	90	90	90
β (deg)	94.273(2)	104.596(2)	90
γ (deg)	90	90	90
Vol (Å^3)	2033.72(12)	1662.47(11)	1562.69(18)
Z	4	4	4
R [F > 4α(F)] (%)	2.02	4.81	1.68
R_w (%)	5.58	14.93	4.09
GOF	1.167	1.079	1.052
Δρ max and min (e Å^{-3})	0.370 and -0.489	2.060 and -1.349	0.301 and -0.406
RMS (e Å^{-3})	0.085	0.187	0.045
Complex	**9**	**12**	**13**
Formula	$C_{14}H_{19}F_{12}N_3P_2Ru$	$C_{14}H_{11}F_6NNaO_6PRu$	$C_{14}H_{13}Cl_2N_3O_2Ru$
MW	620.33	558.27	427.24
Crystal description	yellow prismatic	yellow prismatic	colourless prismatic
Crystal size (mm)	0.114 x 0.168 x 0.170	0.05 x 0.09 x 0.10	0.02 x 0.04 x 0.06
λ (Å)	0.71073	0.71073	0.71073
T (K)	200(2)	200(2)	200(2)
Crystal system	orthorhombic	monoclinic	monoclinic
Space group	P n a 21	C 1 2/c 1	I 1 2/m 1
***a* (Å)**	12.8394(6)	26.2903(12)	7.800(4)
***b* (Å)**	14.8390(8)	14.6155(6)	9.812(4)
***c* (Å)**	10.7448(6)	10.0480(4)	23.048(14)
α (deg)	90	90	90
β (deg)	90	107.757(2)	92.57(5)
γ (deg)	90	90	90
Vol (Å^3)	2047.14(19)	3677.0(3)	1762.2(15)
Z	4	8	4
R [F > 4α(F)] (%)	2.16	3.51	7.78
R_w (%)	4.84	9.77	23.10
GOF	1.009	1.093	1.094
Δρ max and min (e Å^{-3})	0.299 and -0.243	0.630 and -0.740	0.956 and -1.118
RMS (e Å^{-3})	0.047	0.115	0.239

Crystallographic data for open tether complexes included in Chapter 2.

Complex	**15Cl**	**16Cl**	**17Cl**
Formula	$C_{10}H_{18}Cl_2N_2ORu$	$C_{14}H_{25}Cl_2N_2ORu$	$C_{21}H_{25}Cl_2N_4O_{2.25}Ru$
MW	354.23	409.33	541.42
Crystal description	brown-green plate	clear yellow plate	dark purple prismatic
Crystal size (mm)	0.03 x 0.22 x 0.38	0.01 x 0.08 x 0.14	0.12 x 0.20 x 0.20
λ (Å)	0.71073	0.71073	0.71073
T (K)	296(2)	296(2)	200(2)
Crystal system	orthorhombic	monoclinic	orthorhombic
Space group	P n m a	P 1 21 1	P b c a
***a* (Å)**	9.0990(2)	8.2545(3)	13.5363(15)
***b* (Å)**	7.2049(2)	10.8769(4)	16.5216(17)
***c* (Å)**	20.2635(6)	9.5166(4)	21.902(3)
α (deg)	90	90	90
β (deg)	90	90.276(3)	90
γ (deg)	90	90	90
Vol ($Å^3$)	1328.42(6)	854.42(6)	4898.2(10)
Z	4	2	8
R [F > 4α(F)] (%)	2.26	6.61	6.93
R_w (%)	9.07	16.97	28.48
GOF	1.025	1.087	1.028
Δρ max and min (e $Å^{-3}$)	0.509 and -0.249	1.137 and -0.818	2.695 and -0.999
RMS (e $Å^{-3}$)	0.086	0.134	0.320
Complex	**18Cl**		**20Cl**
Formula	$C_{39}H_{48}Cl_4N_4O_5Ru_2$		$C_{10}H_{16}Cl_2N_2O_2Ru$
MW	996.75		368.22
Crystal description	light orange prismatic		yellow prismatic
Crystal size (mm)	0.06 x 0.06 x 0.38		0.080 x 0.180 x 0.200
λ (Å)	0.71073		0.71073
T (K)	296(2)		296(2)
Crystal system	Monoclinic		monoclinic
Space group	C 1 c 1		P 1 21/c 1
***a* (Å)**	7.0923(16)		7.51280(10)
***b* (Å)**	20.307(5)		13.6076(3)
***c* (Å)**	29.055(5)		13.1434(3)
α (deg)	90		90
β (deg)	91.815(11)		92.3830(10)
γ (deg)	90		90
Vol ($Å^3$)	4182.5(15)		1342.50(5)
Z	4		4
R [F > 4α(F)] (%)	8.27		1.74
R_w (%)	24.29		4.46
GOF	1.002		1.011
Δρ max and min (e $Å^{-3}$)	1.315 and -1.945		0.485 and -0.420
RMS (e $Å^{-3}$)	0.180		0.053

Crystallographic data for closed tethered complexes included in Chapter 3.

Complex	**23**	**27**	**29**
Formula	$C_{18}H_{25}Cl_2N_3O_{1.16}Ru$	$C_{23}H_{35}Cl_2N_3ORu$	$C_{19}H_{19}Cl_2N_3ORu$
MW	473.94	541.51	477.34
Crystal description	yellow prismatic	yellow prismatic	yellow prismatic
Crystal size (mm)	0.18 x 0.35 x 0.42	0.19 x 0.38 x 0.41	0.03 x 0.05 x 0.21
λ (Å)	0.71073	0.71073	0.71073
***T* (K)**	200(2)	200(2)	200(2)
Crystal system	Monoclinic	triclinic	orthorhombic
Space group	C 1 2/c 1	P -1	P 21 21 2
***a* (Å)**	25.0917(14)	9.3207(3)	12.6688(16)
***b* (Å)**	8.9754(4)	10.1655(4)	14.2715(14)
***c* (Å)**	19.1582(10)	13.1494(5)	11.4437(15)
α (deg)	90	106.958(2)	90
β (deg)	96.994(2)	101.054(2)	90
γ (deg)	90	90.749(2)	90
Vol (Å^3)	4282.5(4)	1166.45(7)	2069.1(4)
Z	8	2	4
R [F > 4α(F)] (%)	4.8	4.15	4.21
R_w (%)	17.24	12.95	13.55
GOF	1.103	1.084	1.187
Δρ max and min (e Å^{-3})	1.870 and -0.598	3.144 and -0.987	1.558 and -0.657
RMS (e Å^{-3})	0.219	0.129	0.217
Complex	**26Cl**	**28Cl**	**28HCl**
Formula	$C_{23}H_{39}Cl_2N_3ORu$	$C_{18}H_{29}Cl_2N_3ORu$	$C_{18}H_{28}Cl_3N_3O_{0.50}Ru$
MW	545.54	475.41	501.85
Crystal description	orange prismatic	yellow prismatic	orange prismatic
Crystal size (mm)	0.09 x 0.12 x 0.14	0.06 x 0.08 x 0.10	0.08 x 0.14 x 0.20
λ (Å)	0.71073	0.71073	0.71073
T (K)	200(2)	296(2)	296(2)
Crystal system	monoclinic	triclinic	monoclinic
Space group	P 1 21/c 1	P -1	P 1 21/n 1
***a* (Å)**	12.675(4)	7.6786(2)	9.1375(2)
***b* (Å)**	19.0058(5)	9.7149(3)	24.7797(7)
***c* (Å)**	11.0177(3)	14.7107(5)	9.8170(2)
α (deg)	90	108.527(2)	90
β (deg)	106.2210(10)	100.957(2)	103.0430(10)
γ (deg)	90	96.9360(10)	90
Vol (Å^3)	2548.49(13)	1002.00(5)	2165.46(9)
Z	4	2	4
R [F > 4α(F)] (%)	3.37	2.44	2.68
R_w (%)	11.8	5.1	9.74
GOF	1.165	1.001	1.163
Δρ max and min (e Å^{-3})	1.081 and -0.572	0.450 and -0.442	0.572 and -0.469
RMS (e Å^{-3})	0.171	0.074	0.102

Crystallographic data for complexes included in Chapter 4.

Complex	**34dimer**	**35Cl**
Formula	$C_{16}H_{16}Cl_4O_4Ru_2$	$C_{21}H_{20}Cl_2N_2O_3Ru$
MW	616.23	520.36
Crystal description	orange plate	orange prismatic
Crystal size (mm)	0.020 x 0.070 x 0.080	0.040 x 0.050 x 0.050
λ (Å)	071073	0.71073
T (K)	296(2)	296(2)
Crystal system	Triclinic	orthorhombic
Space group	P -1	P b c a
***a* (Å)**	7.1124(3)	13.6426(5)
***b* (Å)**	10.0188(4)	15.1243(5)
***c* (Å)**	14.6863(6)	19.7624(5)
α (deg)	70.587(2)	90
β (deg)	77.652(2)	90
γ (deg)	71.649(2)	90
Vol ($Å^3$)	929.82(7)	4077.7(2)
Z	2	8
R [F > 4α(F)] (%)	4.01	4.21
R_w (%)	10.03	15.50
GOF	1.070	1.122
Δρ max and min (e $Å^{-3}$)	0.726 and -0.788	0.717 and -0.937
RMS (e $Å^{-3}$)	0.176	0.267
Complex	**37Cl**	**38·PF_6**
Formula	$C_{10}H_8ClNaO_{7.75}Ru$	$C_{14}H_{23}F_6N_2O_2PRu$
MW	411.67	513.38
Crystal description	yellow plate	yellow prismatic
Crystal size (mm)	0.040 x 0.122 x 0.134	0.120 x 0.120 x 0.350
λ (Å)	0.71073	0.71073
T (K)	296(2)	293(2)
Crystal system	orthorhombic	monoclinic
Space group	P n a 21	P 1 21/n 1
***a* (Å)**	15.5647(7)	9.1170(6)
***b* (Å)**	25.9037(15)	16.9924(10)
***c* (Å)**	7.3193(3)	12.3649(7)
α (deg)	90	90
β (deg)	90	95.196(3)
γ (deg)	90	90
Vol ($Å^3$)	2951.0(2)	1907.7(2)
Z	8	4
R [F > 4α(F)] (%)	6.23	4.38
R_w (%)	17.99	12.44
GOF	1.070	1.027
Δρ max and min (e $Å^{-3}$)	1.514 and -1.220	1.128 and -0.578
RMS (e $Å^{-3}$)	0.188	0.102

Crystallographic data for complexes included in Chapter 5 and Chapter 6.

Complex	**7**	**9·PF$_6$**
Formula	$C_{10}H_{23}Cl_2N_3ORu$	$C_{14}H_{19}F_{12}N_3P_2Ru$
MW	373.28	620.33
Crystal description	yellow-orange plate	brown-yellow prismatic
Crystal size (mm)	0.12 x 0.47 x 0.56	0.114 x 0.168 x 0.170
λ (Å)	0.71073	0.71073
T (K)	296(2)	200(2)
Crystal system	orthorhombic	orthorhombic
Space group	P 2_1 2_1 2_1	P n a 2_1
***a* (Å)**	8.2419(6)	12.8394(6)
***b* (Å)**	11.6210(5)	14.8390(8)
***c* (Å)**	16.3156(13)	10.7448(6)
α (deg)	90	90
β (deg)	90	90
γ (deg)	90	90
Vol (Å^3)	1562.69(18)	2047.14(19)
Z	4	4
R [F > 4α(F)] (%)	1.68	2.16
R_w (%)	4.09	4.84
GOF	1.052	1.009
Δρ max and min (e Å^{-3})	0.301 and -0.406	0.299 and -0.243
RMS (e Å^{-3})	0.045	0.047
Complex	**41**	**42**
Formula	C18H19Cl2N3Ru	C12H11Cl2NRu
MW	449.34	341.19
Crystal description	clear orange plate	orange prismatic
Crystal size (mm)	0.03 x 0.08 x 0.26	0.08 x 0.08 x 0.19
λ (Å)	0.71073	0.71073
T (K)	296(2)	296(2)
Crystal system	monoclinic	Monoclinic
Space group	P 21/n	P 21/n
***a* (Å)**	9.4741(2)	6.8305(2)
***b* (Å)**	7.7849(2)	13.5339(3)
***c* (Å)**	15.9151(4)	12.3545(2)
α (deg)	90	90
β (deg)	100.2770(10)	92.8240(10)
γ (deg)	90	90
Vol (Å^3)	1154.99(5)	1140.70(5)
Z	4	4
R [F > 4α(F)] (%)	2.05	2.17
R_w (%)	5.73	8.27
GOF	1.052	1.216
Δρ max and min (e Å^{-3})	0.387 and -0.331	0.592 and -0.693
RMS (e Å^{-3})	0.095	0.259

Appendix III

DFT Calculations

Section A

Benchmarking of the computational methods. Calculated bond lengths (Å) and angles (deg) for complex **9** using different DFT functional and basis sets.

Bond / angle	X-ray Structure	PBE1PBE/ CEP-31G	B3LYP/ CEP-31G	LC-WPBE/ CEP-31G	M062X/ CEP-31G	WB97XD/ CEP-31G
Ru-centroid	1.651	1.741	1.805	1.724	1.839	1.753
Ru-N1	2.157	2.124	2.151	2.128	2.139	2.142
Ru-N2	2.138	2.121	2.147	2.115	2.138	2.135
Ru-N3	2.130	2.150	2.177	2.142	2.176	2.163
N2-Ru-N3	79.26	79.84	79.73	80.04	79.78	79.76
N2-Ru-N1	88.40	89.66	89.99	89.95	89.64	89.95
N3-Ru-N1	90.39	94.2	94.78	93.93	94.68	94.05
N2-Ru-Centroid	133.36	130.9	131.12	130.78	131.32	130.85
N3-Ru-Centroid	130.11	110.02	130.18	130.01	130.93	130.08
N1-Ru-Centroid	121.00	119.62	118.79	119.64	118.13	119.62
ΔTd*	**21.80**	**18.57**	**20.27**	**20.28**	**20.44**	**20.36**

Bond / angle	LC-WPBE/ CEP-31G	LC-WPBE/ LANL08/ 6-31G**	LC-WPBE/ SDD/ 6-31G**	LC-WPBE/ SDD/ 6-311G**	LC-WPBE/ SDD/ 6-31G**+
Ru-centroid	1.724	1.672	1.653	1.649	1.653
Ru-N1	2.128	2.123	2.133	2.136	2.133
Ru-N2	2.115	2.151	2.114	2.118	2.114
Ru-N3	2.142	2.140	2.143	2.146	2.143
N2-Ru-N3	80.04	78.81	78.91	78.74	78.91
N2-Ru-N1	89.95	89.61	89.31	89.37	89.31
N3-Ru-N1	93.93	94.03	93.82	93.63	93.82
N2-Ru-Centroid	130.78	131.46	131.49	131.57	131.49
N3-Ru-Centroid	130.01	130.6	130.48	130.67	130.48
N1-Ru-Centroid	119.64	119.44	119.8	119.75	119.8
ΔTd*	**20.28**	**20.83**	**20.89**	**20.99**	**20.89**

The LC-WPBE/SDD/6-31G** level was selected for all geometry calculations. Together with the LC-WPBE/SDD/6-311G**, this method provided the best agreement between computed geometry and X-ray structure of **3**. However, the 6-31G** basis set required half the computational cost of the 6-311G** analogue.

Section B

Selected singlet-singlet transition and corresponding Electron density difference maps (EDDMs) for complex **7** calculated at the LC-WPBE/SDD/6-31G** level. In the EDDMs electron density migrates from grey to green areas.

Transition	Energy / eV (nm)	f*	Major Contributions
1	3.55 (349)	0.0020	H-1→L+1 (42%) HOMO→LUMO (35%)
2	3.70 (335)	0.0056	H-2→L+1 (32%) HOMO→L+1 (36%)
3	3.78 (328)	0.0017	H-2→LUMO (61%)
4	3.81 (325)	0.0021	H-1→LUMO (43%) HOMO→L+1 (20%)
5	4.20 (295)	0.0027	H-2→LUMO (10%) H-1→L+1 (33%) HOMO→LUMO (38%)
6	4.35 (285)	0.0051	H-2→L+1 (46%) H-1→LUMO (18%) HOMO→L+1 (18%)

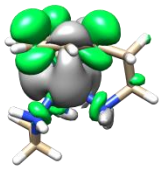

Transition 1

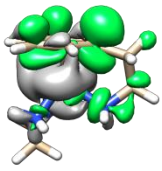

Transition 2

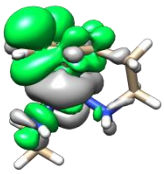

Transition 3

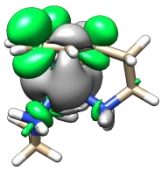

Transition 4

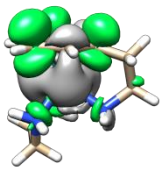

Transition 5

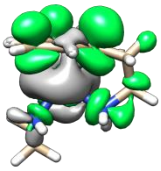

Transition 6

Selected singlet-singlet transition and corresponding Electron density difference maps (EDDMs) for complex **9** calculated at the LC-WPBE/SDD/6-31G** level. In the EDDMs electron density migrates from grey to green areas.

Transition	Energy / eV (nm)	f*	Major Contributions
1	3.50 (352)	0.0008	H-1→LUMO (11%) H-1→L+2 (11%) HOMO→L+1 (49%)
2	3.60 (337)	0.0099	H-3→L+1 (27%), H-1->L+1(10%) HOMO→LUMO (14%) HOMO→L+2 (14%)
3	3.64 (330)	0.0027	H-1→L+1 (45%) HOMO→LUMO (11%) HOMO→L+2 (11%)
4	3.69 (329)	0.0017	H-3→LUMO (28%) H-3→L+2 (31%)
5	4.14 (297)	0.0028	H-1→LUMO (21%) H-1→L+2 (20%) HOMO→L+1 (23%)
6	4.20 (288)	0.0102	H-3→L+1 (44%) H-1→L+1 (18%)
7	5.39 (231)	0.0013	H-1→L+6 (11%) HOMO→L+1 (13%) HOMO→L+5 (53%)

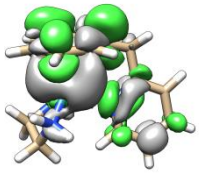

Transition 1

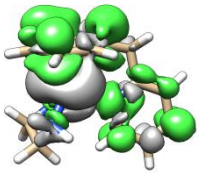

Transition 2

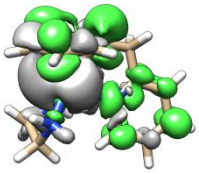

Transition 3

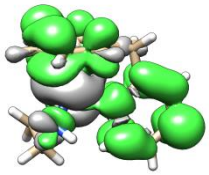

Transition 4

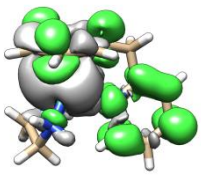

Transition 5

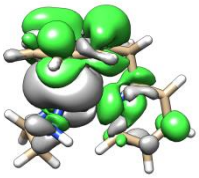

Transition 6

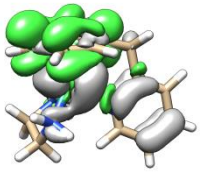

Transition 7

Selected singlet-singlet transition and corresponding Electron density difference maps (EDDMs) for complex **13** calculated at the LC-WPBE/SDD/6-31G** level. In the EDDMs electron density migrates from grey to green areas.

Transition	Energy / eV (nm)	f*	Major Contributions
1	3.54 (350)	0.0004	H-3→L+1 (22%) H-1→LUMO (24%) HOMO->L+1 (24%)
2	3.70 (335)	0.0066	H-4→L+1 (37%) H-2→L+1 (10%) H-1→L+1 (20%)
3	3.78 (328)	0.0019	H-4→LUMO (35%) H-3→LUMO (12%) H-1→L+1 (11%) HOMO→LUMO (13%)
4	3.79 (327)	0.0022	H-4→LUMO (35%) H-1→L+1 (12%)
5	4.20 (295)	0.0028	H-4→LUMO (11%) H-3→L+1 (13%) H-2→LUMO (12%) H-1→LUMO (30%) HOMO→L+1 (15%)
6	4.32 (287)	0.0067	H-4→L+1 (46%) H-1→L+1 (16%)

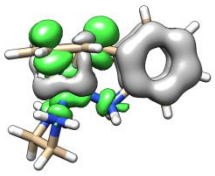

Transition 1

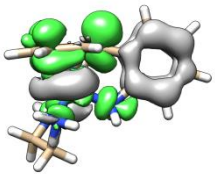

Transition 2

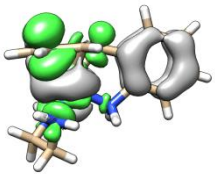

Transition 3

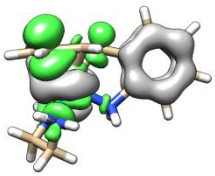

Transition 4

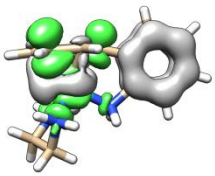

Transition 5

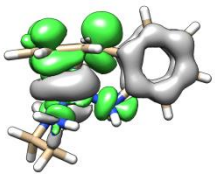

Transition 6

Appendix IV

Table of Complexes

The following table shows the numbering assigned to most of the complexes compiled in this Thesis taking into account its building blocks, i.e. both the hemilabile ligand and the chelating ligand.

In red are represented the complexes which were synthesised in the closed form, while in green are indicated the complexes which were synthesised in the open form.

	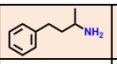	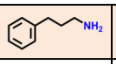	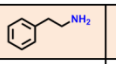	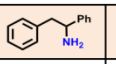	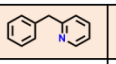	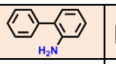	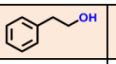	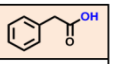
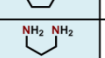	1	4	7	8	9	13	15Cl	20Cl ; 20
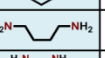		5				21		
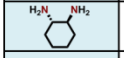						22		
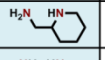						23		
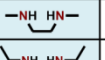						24		
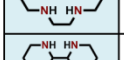						25Cl ; 25		
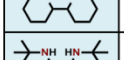		6				26Cl ; 26		
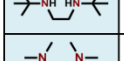						27Cl ; 27		
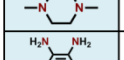						32Cl		
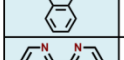						28Cl ; 28	16Cl	38
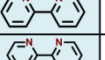	2				10	29		35Cl ; 35
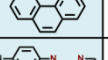							18Cl	
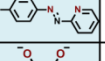	3				11			36Cl ; 36
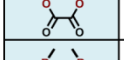							17Cl	
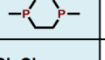					12	30	19Cl	37Cl
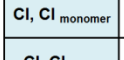						31		
Cl, Cl monomer	✓	✓	✓	✓	42	42		
Cl, Cl dimer							✓	34dimer

Complex synthesised as the open-tether form

Complex synthesised as the closed-tether form